RETINA™

THE JOURNAL OF RETINAL AND VITREOUS DISEASES

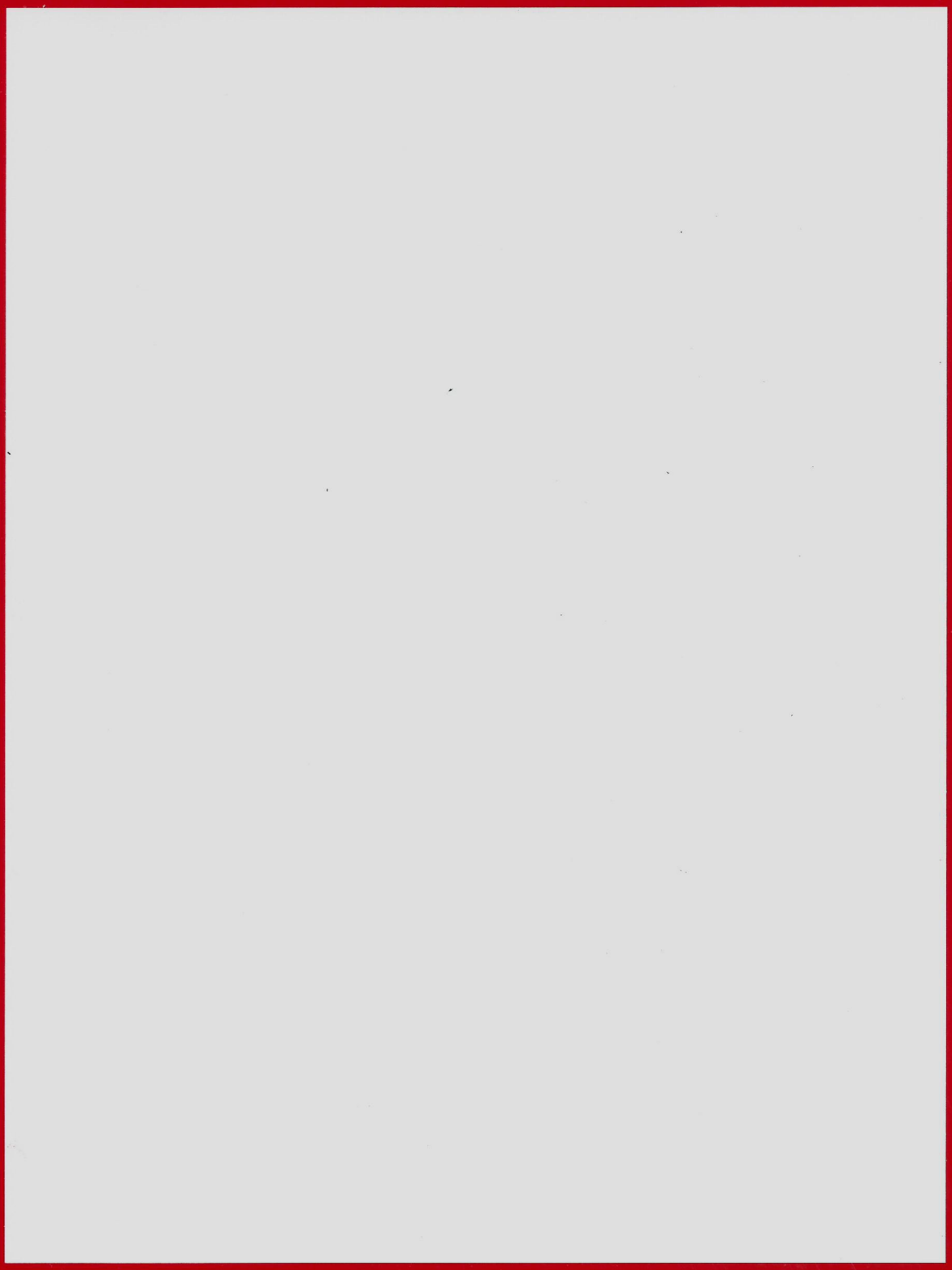

Retina

June 2023 - Volume 43 - Issue 6

Fragiotta, Serena; Parravano, Mariacristina; Costanzo, Eliana; More

Retina. 43(6):913-922, June 2023.

LONG-TERM MICROVASCULAR REMODELING AND CYSTIC CHANGES AFTER RETINAL DETACHMENT TREATED WITH SILICON OIL TAMPONADE

Pfister, Nathalie; Dormegny, Léa; Ballonzoli, Laurent; More

Retina. 43(6):923-931, June 2023.

ULTRA-WIDEFIELD OPTICAL COHERENCE TOMOGRAPHY ANGIOGRAPHY IN MILD FAMILIAL EXUDATIVE VITREORETINOPATHY

Wang, You; Lai, Yanting; Zhou, Xiaodi; More

Retina. 43(6):932-939, June 2023.

IMMEDIATE VITRECTOMY vs TAP AND INJECT IN EYES WITH ACUTE POSTCATARACT ENDOPHTHALMITIS AND VISUAL ACUITY ≥HM: A Randomized Clinical Trial

Sen, Alok C.; Mehta, Sonali M.; Sule, Ashita; More

Retina. 43(6):940-946, June 2023.

CLINICAL OUTCOMES OF ACUTE ENDOPHTHALMITIS AFTER INTRAVITREAL DELIVERY OF VASCULAR ENDOTHELIAL GROWTH FACTOR INHIBITORS VERSUS STEROIDS

Adams, Olufemi E.; Sodhi, Guneet S.; Vagaggini, Tommaso; More

Retina. 43(6):947-954, June 2023.

DO DAILY ACTIVITIES AFFECT GAS TAMPONADE–RETINA CONTACT AFTER PARS PLANA VITRECTOMY?: A Computational Fluid Dynamics Study

Rossi, Tommaso; Badas, Maria Grazia; Angius, Federico; More

Retina. 43(6):955-963, June 2023.

RISK FACTORS FOR PUPILLARY OPTIC CAPTURE FOLLOWING SUTURELESS FLANGED INTRAOCULAR LENS FIXATION FOR INTRAOCULAR LENS DISLOCATION

Do, Jae Rock; Park, Su Jin; Kim, Jin Young; More

Table of Contents Outline | Back to Top

Retina. 43(6):1047-1049, June 2023.

Table of Contents Outline | Back to Top

An Unusual Optical Coherence Tomography Appearance in Coats Disease

Tekin, Kemal; Freund, K. Bailey; Teke, Mehmet Yasin

Retina. 43(6):e35-e36, June 2023.

Editorial

Pathways of Fluid Leakage in Age-Related Macular Degeneration

Neovascular Fluid Pathway

Age-related macular degeneration (AMD) represents a massive burden of vision impairment and blindness in the United States and worldwide,[1] but the management of this devastating disease has remarkably progressed because of the development of advanced retinal imaging tools, especially high-resolution, depth-resolved optical coherence tomography (OCT) and OCT angiography (OCTA). Currently recognized OCT biomarkers for neovascular activity include intraretinal fluid (IRF), subretinal fluid (SRF), subretinal pigment epithelium fluid, and subretinal hyperreflective material (SHRM), which are critical factors guiding therapy.[2–4] Fluid is a major hallmark of exudation and angiogenic activity in eyes with neovascular AMD, indicating the need for treatment with anti–vascular endothelial growth factor (VEGF) injection.[2,3,5]

A long list of pivotal clinical trials essential for the ratification and approval of various anti-VEGF therapies, including aflibercept,[6] brolucizumab,[7] and faricimab,[8] relied on the OCT response of anatomical biomarkers of neovascular activity to corroborate the observed functional efficacy of the investigated agent. In all cases, the study drug was no less effective or was better in resolving fluid markers such as IRF and SRF, and these OCT outcomes were critical factors that were evaluated to determine the treatment effect of the anti-VEGF agent. Fluid as a marker of neovascular activity is a universal concept that is essential for clinical trials, and daily clinical practice and the ubiquitous use of OCT worldwide can be attributed, in large part, to this association.

However, recent studies have provided insight into the various nonneovascular pathways of exudation in eyes with AMD and indicate that fluid can have a much more complex and nuanced etiology and is not always an indicator of neovascular activity in AMD.[9–14] Although some have labelled nonneovascular fluid as a transudate and neovascular fluid as an exudate,[11,13] the mechanisms may be more complicated, and therefore, any form of fluid leakage (neovascular or nonneovascular) is best referred to as exudation. The subsequent sections of this editorial will summarize the various nonneovascular pathways of exudation (examples of exudation include IRF, SRF, and/or vitelliform lesions) in AMD and will provide guidelines for the diagnosis and management of nonneovascular fluid.

Nonneovascular Intraretinal Fluid Associated with Cellular Degeneration

It is important to understand that both IRF and SRF can be the result of nonneovascular pathways in the context of AMD.[9–14] The presence of IRF and SRF with OCT does not always indicate neovascular activity and can be a sign instead of degenerative mechanisms. Pseudocysts were originally described by Cohen et al[15] and represent a form of IRF overlying the areas of retinal pigment epithelium (RPE) atrophy and cRORA (complete RPE and outer retinal atrophy). These cystoid lesions should not be confused with outer retinal tubulations, which are identified exclusively in the outer retina and illustrate hyperreflective rings with OCT unlike pseudocysts.[16,17] The etiology of pseudocysts may be the result of Müller cell atrophy because the Müller cells are a critical component of hydrostasis in the retina.[18] These degenerative cysts are predominantly located in the middle retina (i.e., in the inner nuclear layer) as is the case of degenerative fluid associated with other etiologies such as optic atrophy[19,20] and X-linked juvenile retinoschisis.[21]

E. Bousquet has been a consultant for Bayer and Allergan and received personal fees from Novartis. S.R. Sadda receives personal fees from Amgen, Allergan/Abbvie, Apellis, Iveric, Oxurion, Roche/Genentech, Novartis, Bayer, Regeneron, Jannsen, Nanoscope, Biogen, Boerhinger Ingelheim, Centervue, Heidelberg, Nidek, Optos, and Notal; grants from Carl Zeiss Meditec; nonfinancial support from Topcon, Carl Zeiss Meditec, Centervue, Heidelberg, Nidek, and Optos. D. Sarraf receives grants, personal fees from Amgen, personal fees from Bayer, grants from Boehringer, grants from Genentech, non-financial support from Heidelberg, personal fees from Novartis, personal fees, non-financial support from Optovue/Visionix, grants from Regeneron, nonfinancial support from Topcon, personal fees from Iveric Bio. The remaining authors have no financial disclosures.

Degenerative fluid can be detected in eyes with either nonneovascular and neovascular AMD, but the topographic association with underlying cRORA and RPE atrophy is another important clue to the nonneovascular etiology (Figure 1).

Nonneovascular Subretinal Fluid as a Result of Retinal Pigment Epithelium Dysfunction

Subretinal fluid can also complicate nonneovascular AMD[9,10,12,13] and like IRF can be the result of degenerative mechanisms such as RPE impairment. Hilely et al[10] showed that large drusen and drusenoid pigment epithelial detachment (PED) can be associated with nonneovascular SRF and suggest that RPE pump dysfunction may explain this mechanism of fluid development. The authors described three patterns of fluid over large drusen, including apex fluid, fluid drapes, and fluid pockets in the valleys between adjacent large drusen. Apex fluid may be the most common pattern because this represents the point of greatest RPE displacement from the underlying choroid, which nourishes and oxygenates the RPE. This may explain why taller drusen are more likely to display biomarkers of RPE atrophy, such as intraretinal hyperreflective foci and plumes, especially at the apex, and why larger drusen are at a greater risk of collapse and atrophy.[22] In fact, the presence of nonneovascular SRF associated with large drusen may be a marker for the development of iRORA (incomplete RORA) and cRORA. Hilely et al[10] noted that more than 50% of cases of drusen associated with SRF proceed to iRORA or cRORA. With greater separation of the RPE from the underlying choriocapillaris, there is a significantly higher risk of RPE ischemia leading to RPE dysfunction and impairment and ultimately RPE atrophy and death.

Additional pathways to consider include ischemic RPE migration into the retina (i.e., intraretinal hyperreflective foci), driven by inner choroidal ischemia (as evidenced by choriocapillaris flow deficits with OCTA) and higher levels of intraretinal VEGF leading to increased retinal vascular permeability and leakage of fluid.[14]

OCT angiography is a critical tool to differentiate nonneovascular from neovascular fluid. In an eye with suspected nonneovascular SRF, the absence of macular neovascularization (MNV) with OCTA can prevent unnecessary anti-VEGF injection treatments.[12]

Vitelliform lesions, like nonneovascular fluid, are another example of nonneovascular exudation and can also develop as a result of RPE dysfunction and impaired phagocytic activity, either as a result of inherited susceptibility or as a result of acquired causes such as intermediate AMD or pachychoroid disease. Acquired vitelliform lesions (AVL) can be confused with neovascular SHRM because of Type 2 MNV, and the partial resorption of AVLs may result in hyporeflective cavities that can masquerade as neovascular fluid on OCT.[23–25] Multimodal imaging is essential to differentiate vitelliform lesions from MNV. Acquired vitelliform lesions are round and yellow on color fundus photography and exhibit a typical hyperautofluorescent signal on fundus autofluorescence. On OCT, AVLs are hyperreflective and represent a form of SHRM located between the thickened RPE and the elevated neurosensory retina. They are often associated with focal outer retinal attenuation and typically progress to atrophy after several years of follow-up. OCT angiography is an indispensable tool to exclude MNV in these cases.[24]

Nonneovascular Subretinal Fluid Associated with Pachychoroid Disorder

An additional nonneovascular pathway of SRF leakage to consider in AMD is pachychoroid disease defined by the presence of pachyvessels (dilated outer choroidal veins in Haller layer) and/or focal or diffuse thickening of the choroid according to age. Although most investigators regard a subfoveal choroidal thickness greater than 300 μm on enhanced depth imaging OCT (EDI-OCT) sufficient for the diagnosis of pachychoroid, age and axial length are important factors to consider.[26] However, in the elderly population, a choroidal thickness greater than 250 μm is unusual, and greater than 300 μm is very rare and can be considered pathological.[27] Choroidal morphological alterations are also important criteria for the diagnosis of pachychoroid and include dilated Haller layer vessels with attenuation of Sattler layer and the choriocapillaris and associated overlying RPE disruption.[28] The pachychoroid spectrum includes pachychoroid pigment epitheliopathy,[29] central serous chorioretinopathy,[30] polypoidal choroidal vasculopathy,[31] pachychoroid neovasculopathy,[32] peripapillary pachychoroid syndrome (PPS),[33] and focal choroidal excavation.[34] Pachydrusen and pachyvitelliform maculopathy are additional manifestations of pachychoroid disease that can occur in older patients and may represent variants of nonneovascular AMD.[24,35,36] Choroidal hyperpermeability, as illustrated with indocyanine green angiography (ICGA), is a common denominator of all disorders in the pachychoroid spectrum, and therefore, ICGA can be a resourceful

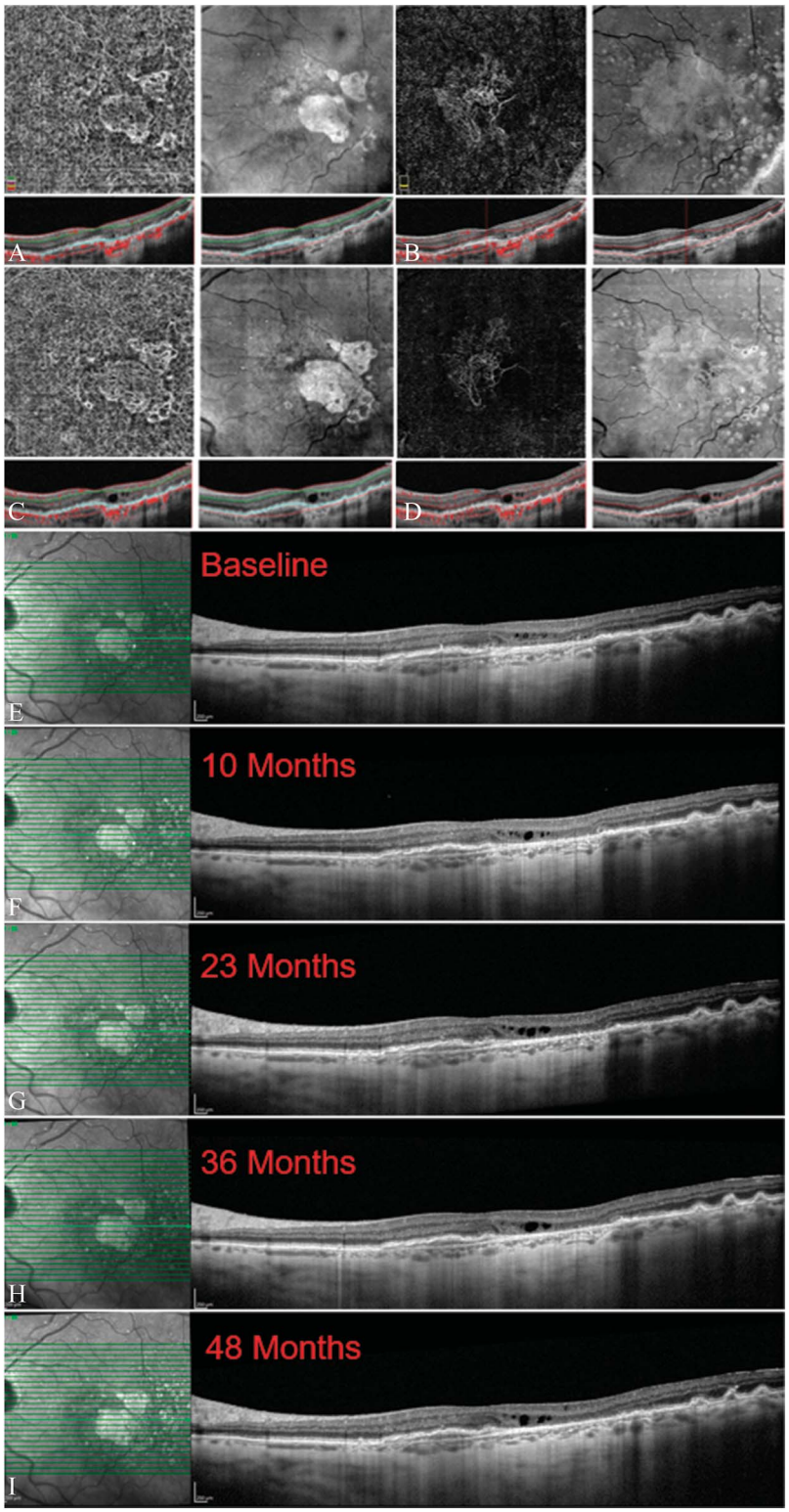

Fig. 1. Multimodal imaging of nonneovascular degenerative intraretinal fluid (IRF) in a patient with neovascular age-related macular degeneration (AMD). The left eye of an 88-year-old man with a history of neovascular AMD and 14 prior injections of anti–vascular endothelial growth factor (anti-VEGF) is shown. En-face optical coherence tomography angiography (OCTA) with choriocapillaris slab segmentation is shown at the baseline visit (**A**) and at the final follow-up 4 years later (**C**). Note the progression of macular atrophy with both the en-face OCTA and the en-face OCT over time. Segmentation at the level of the outer retina in the respective en-face OCTA scans at baseline (**B**) and 4 years later (**D**) show Type 1 macular neovascularization (MNV) adjacent to the expanding area of outer retinal atrophy. OCT B scans at baseline (**E**) demonstrate a fibrovascular pigment epithelial detachment in the nasal macula (corresponding to the type 1 MNV) adjacent to the area of complete retinal pigment epithelium and outer retinal atrophy (cRORA) with overlying cysts of degenerative IRF. This fluid was attributed to nonneovascular pathways, and further anti-VEGF therapy was deferred and an observe-and-extend regimen was initiated. The IRF remained relatively stable with gradual expansion of the area of cRORA noted on the OCT B scans at the subsequent follow-up visits 10 months (**F**), 2 years (**G**), 3 years (**H**), and 4 years (**I**) after baseline.

diagnostic tool in this context.[37,38] The choroid should be evaluated in any eye with IRF or SRF to determine if the fluid is the result of pachychoroid pathways. Choroidal vascular leakage or compression of the choriocapillaris causing RPE stress or pump failure can lead to exudative complications, including serous PED and SRF and IRF accumulation.[28] There may even be a threshold level of choroidal thickening leading to the

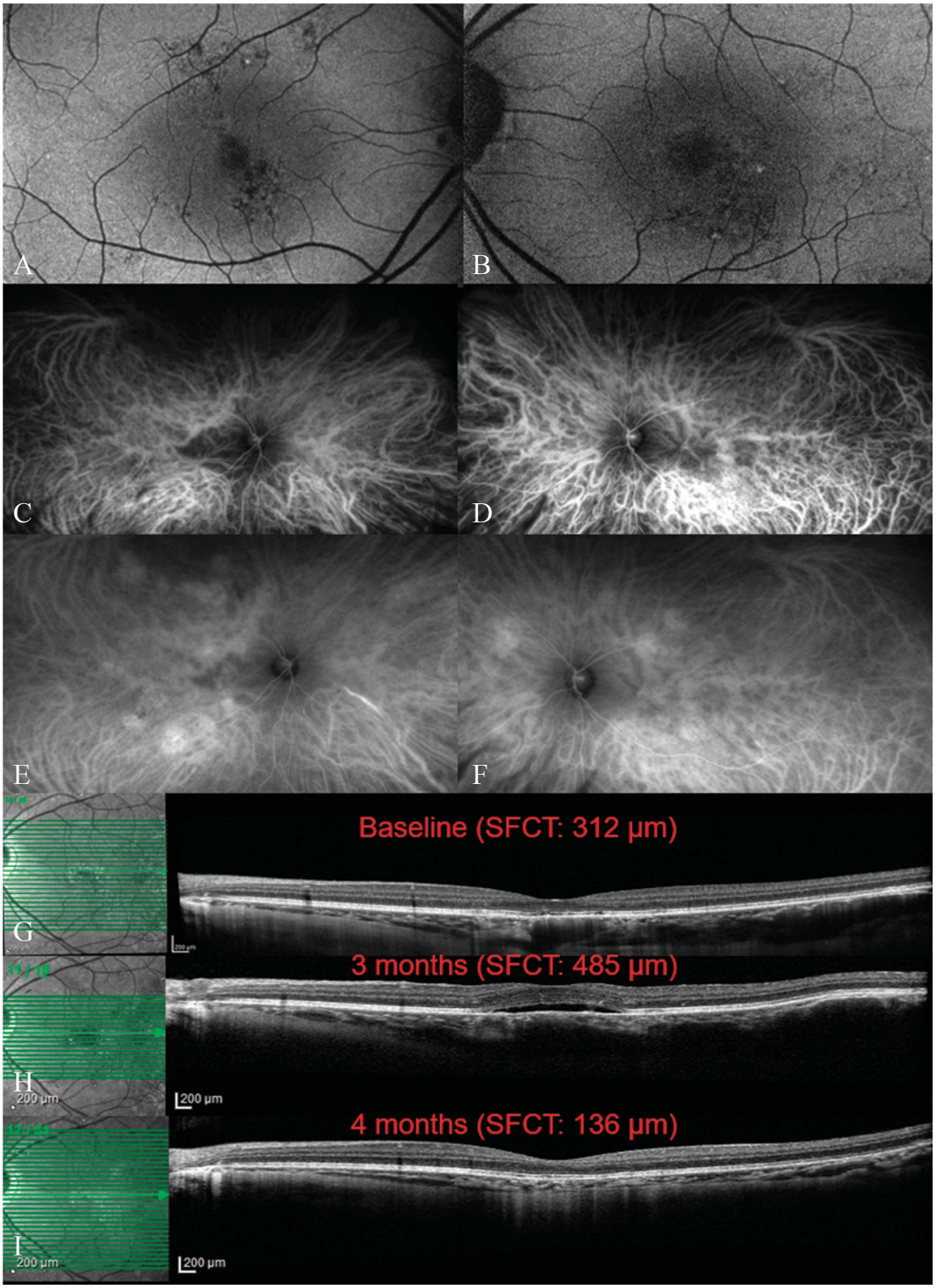

Fig. 2. Multimodal image of a 40-year-old male patient with a history of herpetic anterior uveitis and bilateral pachychoroid disease. Fundus autofluorescence of the right (**A**) and left (**B**) eyes show mottled hypoautofluorescence and hyperautofluorescence of the retinal pigment epithelium (RPE) consistent with pachychoroid pigment epitheliopathy. Early phase indocyanine green angiography of the right (**C**) and left (**D**) eyes show large choroidal vessels and midphase images (**E** and **F**) show multifocal hyperfluorescent areas of choroidal vascular hyperpermeability. Optical coherence tomography (OCT) B scans of the left eye at the first visit (**G**) show large choroidal veins more obvious in the subfoveal region with areas of RPE and ellipsoid zone disruption. Three months later (**H**), subretinal fluid (SRF) develops commensurate with a remarkable increase in choroidal thickness. With steroid treatment of the recurrent uveitis episode and at follow-up 1 month later, the choroidal thickness dramatically decreased with spontaneous resolution of the SRF (**I**).

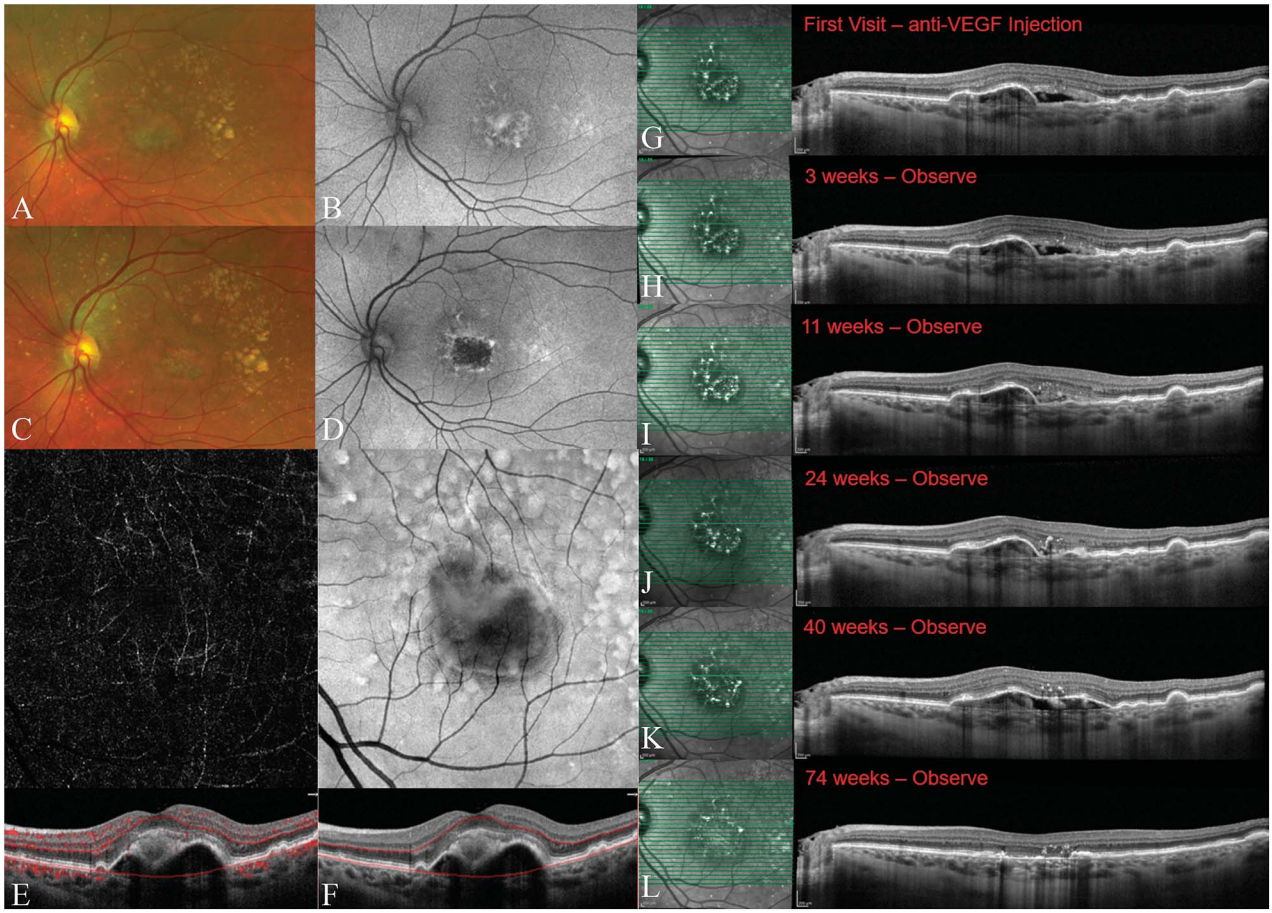

Fig. 3. Multimodal imaging of a case of age-related macular degeneration (AMD) with nonneovascular fluid successfully managed by an observe-and-extend protocol. The left eye of a 64-year-old woman with history of exudative nonneovascular AMD is shown. Fundus photography of the left eye at baseline (**A**) shows confluent macular drusen and corresponding fundus autofluoresecence (**B**) shows hyperautofluorescence of the macular drusen and a central acquired vitelliform lesion. At the final follow-up 17 months later, fundus photography (**C**) and autofluorescence (**D**) of the left eye show the development of central macular atrophy. En-face optical coherence tomography (OCT) angiography at baseline (**E**) with slab segmentation at the outer retina shows no evidence of macular neovascularization and corresponding en-face OCT (**F**) shows the central large drusenoid pigment epithelial detachment (PED) with overlying vitelliform exudation and surrounding drusen. OCT B scan of the left eye at baseline (**G**) shows large macular drusen and drusenoid PED with a temporal drape of subretinal fluid. The patient received a trial of one intravitreal anti-VEGF injection, and follow-up 3 weeks later (**H**) shows no change in the OCT fluid volume. An observe-and-extend protocol was subsequently adopted and at increasing intervals of 11 week (**I**), 24 weeks (**J**), and 40 weeks (**K**). The fluid fails to progress and gradually resolves with OCT without any further injections. The subsequent collapse of the drusenoid PED with the development of complete retinal pigment epithelium and outer retinal atrophy (cRORA) with OCT is noted on the final follow-up at 17 months after baseline (**L**).

development of SRF (Figure 2). OCT angiography can be an extraordinary tool in eyes with pachychoroid disease and fluid accumulation, especially when a shallow PED is identified, to exclude MNV and tailor the therapeutic plan.[39] In AMD cases with suspected nonneovascular fluid, the choroid should be measured to determine if pachychoroid disease may represent a factor contributing to the accumulation of fluid in the intraretinal or subretinal space. Even with the detection of MNV with OCTA in the context of pachychoroid disease, the nonneovascular pathways should be considered as a potential source of the fluid. For the management of nonneovascular fluid in the setting of pachychoroid and AMD, please see the "Evaluation and Management of Non-Neovascular Fluid" section below.

Persistent Fluid in Anti-VEGF Clinical Trials

One of the targeted end points of clinical trials of anti-VEGF agents for neovascular AMD is the achievement of a dry macula with OCT, yet a significant portion (approximately 25%–50%) of study eyes that receive repeated anti-VEGF injection therapy can exhibit persistent fluid at 1 or 2 years from baseline.[4,40–42] In the HARBOR clinical trial that compared monthly versus pro re nata ranibizumab, persistent fluid was noted in 27% of eyes at 12 and

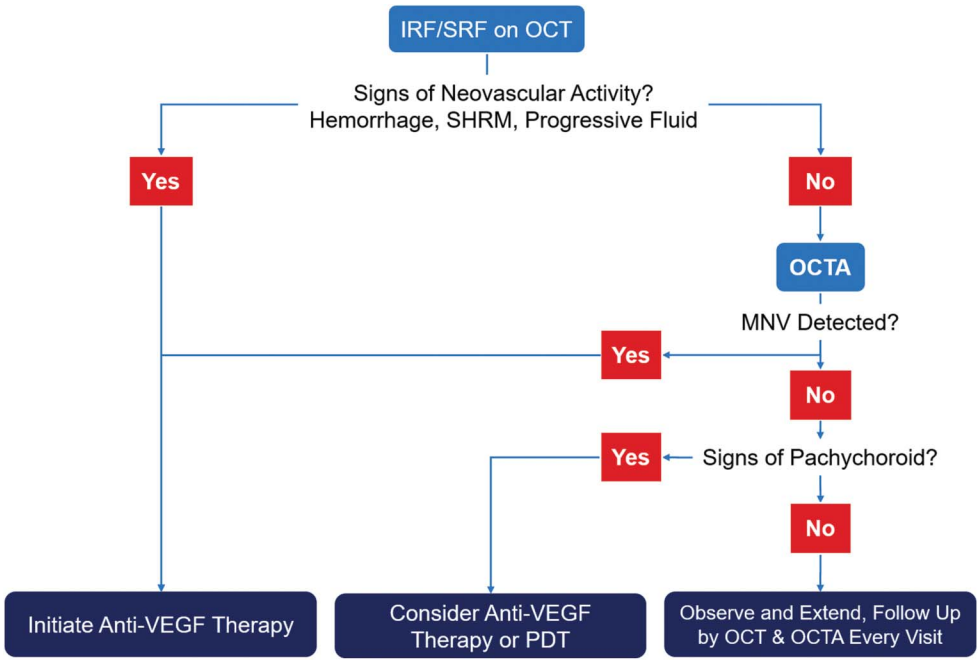

Fig. 4. Management algorithm of fluid detected on optical coherence tomography in eyes with age-related macular degeneration. IRF, intraretinal fluid; MNV, macular neovascularization; OCT, optical coherence tomography; OCTA, optical coherence tomography angiography; PDT, photodynamic therapy; SHRM, subretinal hyperreflective material; SRF, subretinal fluid; VEGF, vascular endothelial growth factor.

24 months.[4] The Comparison of Age-Related Macular Degeneration Treatments Trials (CATT) comparing ranibizumab versus bevacizumab showed that 54.5% of eyes treated with monthly injections (and 77.7% of eyes in the pro re nata group) demonstrated persistent fluid at 24 months.[41] In the VIEW 1 and 2 studies that assessed the efficacy of aflibercept versus ranibizumab, residual fluid was detected in 30% and 48% of eyes at 52 and 96 weeks, respectively.[42] In the HAWK and HARRIER brolucizumab trials, persistent fluid was detected in 31.2% and 25.8% of eyes, respectively, at 48 weeks after the initiation of therapy.[7]

Although persistent fluid can certainly be the result of persistent neovascular activity requiring stronger anti-VEGF agents or more frequent injection intervals,[7] nonneovascular pathways, such as RPE pump impairment or pachychoroid disease, should also be considered. Mild stable SRF may be tolerated, and in the absence of fluid progression or other features of neovascularization such as hemorrhage or SHRM or enlarging PED, observation may represent the most optimal management when further improvement with aggressive therapy is not observed.[4,40] Tolerable SRF is a concept that has emerged from post hoc analyses that demonstrated better visual outcomes in eyes with persistent SRF rather than IRF.[40,43] This counterintuitive observation may be explained on the basis of viable but functionally impaired RPE cells that are capable of supporting the overlying photoreceptors but not capable of completely removing SRF, as opposed to eyes with RPE atrophy in which there is free fluid movement into the choroidal vasculature.[44] This is supported by the observation that nonneovascular fluid typically resolves with the development of cRORA[10,12] and is also validated by clinical trial articles that have identified the association of RPE atrophy with the absence of SRF.[43,45,46] It should be noted, however, that in studies showing positive visual outcomes in the setting of persistent fluid, patients were being consistently treated and monitored for fluid that was deemed to be related to MNV activity. In this regard, it is important to distinguish the management approach for fluid assigned to neovascular activity versus fluid considered the result of nonneovascular mechanisms.

Evaluation and Management of Nonneovascular Fluid

Differentiation of nonneovascular and neovascular fluid is important but can pose a challenge. Associated findings of neovascular activity, such as heme and SHRM, and the presence of a multilayered or fibrovascular PED should be excluded before the diagnosis of nonneovascular fluid.[10,12,13] Progression of fluid or an enlarging PED are additional signs of neovascular activity. Degenerative IRF can be detected in the presence or absence of neovascularization because macular atrophy can occur in either setting.[47] The location of the "pseudocysts" on OCT overlying a region of RPE atrophy and the relative stability of this degenerative IRF over a long duration of follow-up are indicative of

a nonneovascular pathway. Such degenerative IRF can be safely monitored and often exhibits a stable clinical course.[15]

Although OCTA is not 100% sensitive in the identification of MNV, especially in the setting of immature or small MNV or large PED, repeated OCTA testing without MNV detection supports the diagnosis of nonneovascular fluid associated with intermediate or atrophic AMD. Dye-based angiography, including fluorescein (FA) and ICGA previously considered the gold standard for the detection of MNV, is considered inferior to OCTA for the detection of occult MNV.[48–50] The sensitivity of OCTA for the detection of Type 1 MNV when combined with structural OCT reaches 85%, whereas that with FA alone is 66%.[49] Nonspecific or occult leakage patterns on FA can be present because of neovascular or nonneovascular (e.g., RPE pump impairment) mechanisms, and therefore, FA is a poor method to differentiate neovascular and nonneovascular fluid.[50] Moreover, OCTA is a fast, simple, and noninvasive tool that can be repeated each visit for more reliable detection of MNV. Dye-based FA is invasive and time consuming and cannot be repeated visit to visit.

Santina et al[12] recently proposed an "observe-and-extend protocol for the management of nonneovascular SRF in eyes with intermediate AMD and noted stable or improved fluid with progressively longer intervals of observation. In the observe-and-extend protocol, interval extension is increased by 2 to 4 weeks only if fluid remains stable and in the absence of associated features of MNV such as heme or SHRM or progressive PED and without MNV detection with OCTA at every visit. The natural history of nonneovascular fluid in eyes with intermediate AMD is long-term stability, although in the Santina and Hilely studies, fluid did resolve in those eyes that developed iRORA/cRORA with commensurate visual decline (Figure 3). This is in distinct contrast to neovascular fluid, which invariably progresses without anti-VEGF intervention. These findings suggest that observation of nonneovascular fluid in the setting of intermediate AMD may be a valid option, but vigilance is absolutely critical because any progression of fluid, decline in vision, or detection of MNV with OCTA or identification of other signs of neovascularization should all warrant urgent intervention with anti-VEGF therapy. Larger, prospective, controlled studies are needed to validate the observe-and-extend protocol.

Choroidal thickness and morphology should be evaluated in eyes with AMD in which SRF and/or IRF develop, especially in cases with persistent fluid, as the presence of pachychoroid can be a causative or contributory pathway for fluid accumulation in these eyes. Spectral-domain OCT (especially EDI-OCT) or swept-source OCT are effective methods for measuring choroidal thickness and evaluating outer vessel morphology. Dye-based angiography can supplement the diagnosis of pachychoroid disease. The presence of associated choroidal hyperpermeability with ICGA can provide confirmatory diagnostic information. Indocyanine green angiography is also the best tool to detect polyps, which can be a very important finding because polypoidal choroidal vasculopathy (PCV) is another consideration in eyes with recalcitrant fluid, and PCV may respond better to photodynamic therapy (PDT).[51] Indocyanine green angiography and FA may also identify sites of leakage that can be targeted by laser treatment.[28] Anti-VEGF therapy can shrink the choroid and reduce the fluid load in eyes with PPS.[52] Another treatment option for nonneovascular SRF associated with pachychoroid is PDT (full fluence or half fluence),[53] although an observe-and-extend protocol can be considered if the SRF is mild and stable and not visually significant, despite the presence of pachychoroid.

Recently, the Food and Drug Administration approved the treatment of atrophic AMD with a C3 complement inhibitor, which reduced the rate of atrophy based on fundus autofluorescence by 12%–22% after 1 year of monthly intravitreal injection therapy.[54] Although this is a breakthrough in the treatment of nonneovascular AMD, 10% of eyes developed signs of exudation such as SRF or IRF in the preceding Phase 2 clinical trial.[55] The study suggested a possible treatment protocol of these eyes with anti-VEGF therapy concurrent with the complement inhibitor therapy. However, these eyes did not undergo OCTA to determine if the origin of this fluid was neovascular or nonneovascular. This is a key oversight because these eyes all exhibited features of degeneration and atrophy and would therefore be at very high risk of nonneovascular fluid as a result of cellular degeneration and RPE impairment. OCT angiography should be performed in these eyes to assess for MNV. In the absence of MNV with OCTA and other features of neovascularization, an observe-and-extend protocol could be considered while the C3 inhibitor therapy is continued, which could be a major breakthrough for patients, thereby reducing the overall burden of intravitreal therapy.

Conclusion

In summary, the detection of intraretinal or SRF in eyes with AMD should not always trigger a reflex response of intravitreal anti-VEGF injection. Careful

evaluation of the underlying pathway leading to fluid leakage should be performed to determine if the fluid is the result of nonneovascular or neovascular pathways (Figure 4). In the absence of MNV with OCTA and other signs of neovascularization with multimodal retinal imaging and with a stable clinical course, an observe-and-extend approach may be the most effective management strategy of nonneovascular fluid. Persistent fluid in the setting of neovascular AMD is an additional clinical context, where it may be important to differentiate neovascular and nonneovascular origins of fluid.

Yousef A. Fouad, MD*†
Ahmad Santina, MD*
Elodie Bousquet, MD, PHD*‡
Srinivas R. Sadda, MD§
David Sarraf, MD*
*Retinal Disorders and Ophthalmic Genetics Division, Stein Eye Institute, University of California Los Angeles, Los Angeles, CA
†Department of Ophthalmology, Ain Shams University Hospitals, Cairo, Egypt
‡Department of Ophthalmology, Université Paris Cité, Hôpital Lariboisière, Assistance Publique-Hôpitaux de Paris, Paris, France
§Doheny Eye Institute, University of California Los Angeles, Los Angeles, CA

References

1. Mitchell P, Liew G, Gopinath B, Wong TY. Age-related macular degeneration. Lancet 2018;392:1147–1159.
2. Wong DT, Berger AR, Bourgault S, et al. Imaging biomarkers and their impact on therapeutic decision-making in the management of neovascular age-related macular degeneration. Ophthalmologica 2021;244:265–280.
3. Schmidt-Erfurth U, Waldstein SM. A paradigm shift in imaging biomarkers in neovascular age-related macular degeneration. Prog Retin Eye Res 2016;50:1–24.
4. Holekamp NM, Sadda S, Sarraf D, et al. Effect of residual retinal fluid on visual function in ranibizumab-treated neovascular age-related macular degeneration. Am J Ophthalmol 2022;233:8–17.
5. Kodjikian L, Parravano M, Clemens A, et al. Fluid as a critical biomarker in neovascular age-related macular degeneration management: literature review and consensus recommendations. Eye 2021;35:2119–2135.
6. Heier JS, Brown DM, Chong V, et al. Intravitreal aflibercept (VEGF trap-eye) in wet age-related macular degeneration. Ophthalmology 2012;119:2537–2548.
7. Dugel PU, Koh A, Ogura Y, et al. HAWK and HARRIER: phase 3, multicenter, randomized, double-masked trials of brolucizumab for neovascular age-related macular degeneration. Ophthalmology 2020;127:72–84.
8. Heier JS, Khanani AM, Quezada Ruiz C, et al. Efficacy, durability, and safety of intravitreal faricimab up to every 16 weeks for neovascular age-related macular degeneration (TENAYA and LUCERNE): two randomised, double-masked, phase 3, non-inferiority trials. Lancet 2022;399:729–740.
9. Sikorski BL, Bukowska D, Kaluzny JJ, et al. Drusen with accompanying fluid underneath the sensory retina. Ophthalmology 2011;118:82–92.
10. Hilely A, Au A, Freund KB, et al. Non-neovascular age-related macular degeneration with subretinal fluid. Br J Ophthalmol 2021;105:1415–1420.
11. Samanta A, Jhingan M, Arora S, et al. Intraretinal, sub-retinal, and sub-retinal pigmented epithelium fluid in non-exudative age-related macular degeneration: follow-up with OCT imaging. Eur J Ophthalmol 2022;32:2419–2426.
12. Santina A, Romero-Morales V, Abraham N, et al. Non-neovascular fluid in age-related macular degeneration: observe-and-extend regimen in a case-series study. Can J Ophthalmol 2022. (Advance online publication).
13. Lek JJ, Caruso E, Baglin EK, et al. Interpretation of subretinal fluid using OCT in intermediate age-related macular degeneration. Ophthalmol Retina 2018;2:792–802.
14. Bacci T, Essilfie JO, Leong BCS, Freund KB. Exudative non-neovascular age-related macular degeneration. Graefe's Arch Clin Exp Ophthalmol 2021;259:1123–1134.
15. Cohen SY, Dubois L, Nghiem-Buffet S, et al. Retinal pseudocysts in age-related geographic atrophy. Am J Ophthalmol 2010;150:211–217.e1.
16. Zweifel SA. Outer retinal tubulation: a novel optical coherence tomography finding. Arch Ophthalmol 2009;127:1596–1602.
17. Preti RC, Govetto A, Filho RGA, et al. Optical coherence tomography analysis of outer retinal tubulations. Retina 2018;38:1518–1525.
18. Spaide RF. Retinal vascular cystoid macular EDEMA. Retina 2016;36:1823–1842.
19. Abegg M, Dysli M, Wolf S, et al. Microcystic macular edema. Ophthalmology 2014;121:142–149.
20. Chen X, Kuehlewein L, Pineles SL, et al. EN face optical coherence tomography of macular microcysts due to optic neuropathy from neuromyelitis optica. Retin Cases Brief Rep 2015;9:302–306.
21. Han IC, Whitmore SS, Critser DB, et al. Wide-field swept-source OCT and angiography in X-linked retinoschisis. Ophthalmol Retina 2019;3:178–185.
22. Au A, Santina A, Abraham N, et al. Relationship between drusen height and OCT biomarkers of atrophy in non-neovascular AMD. Invest Ophthalmol Vis Sci 2022;63:24.
23. van Dijk EHC, Boon CJF. Serous business: delineating the broad spectrum of diseases with subretinal fluid in the macula. Prog Retin Eye Res 2021;84:100955.
24. Iovino C, Ramtohul P, Au A, et al. Vitelliform maculopathy: diverse etiologies originating from one common pathway. Surv Ophthalmol 2023 . (Advance online publication).
25. Zatreanu L, Freund KB, Leong BCS, et al. Serous macular detachment in best disease. Retina 2020;40:1456–1470.
26. Lin CY, Huang YL, Hsia WP, et al. Correlation of choroidal thickness with age in healthy subjects: automatic detection and segmentation using a deep learning model. Int Ophthalmol 2022;42:3061–3070.
27. Wakatsuki Y, Shinojima A, Kawamura A, Yuzawa M. Correlation of aging and segmental choroidal thickness measurement using swept source optical coherence tomography in healthy eyes. PLoS One 2015;10:e0144156.
28. Cheung CMG, Lee WK, Koizumi H, et al. Pachychoroid disease. Eye 2019;33:14–33.
29. Warrow DJ, Hoang QV, Freund KB. Pachychoroid pigment epitheliopathy. Retina 2013;33:1659–1672.

30. Freund KB, Meyerle CB, Yannuzzi LA. Central serous chorioretinopathy. In: Albert DM, Miller J, Azar DT, Blodi B, eds. Albert & Jakobiec's Principles & Practice of Ophthalmology. Switzerland: Springer Cham. 2008:1871–1880.
31. Kim SW, Oh J, Kwon SS, et al. Comparison of choroidal thickness among patients with healthy eyes, early age-related maculopathy, neovascular age-related macular degeneration, central serous chorioretinopathy, and polypoidal choroidal vasculopathy. Retina 2011;31:1904–1911.
32. Pang CE, Freund KB. Pachychoroid neovasculopathy. Retina 2015;35:1–9.
33. Phasukkijwatana N, Freund KB, Dolz-Marco R, et al. Peripapillary pachychoroid syndrome. Retina 2018;38:1652–1667.
34. Chung H, Byeon SH, Freund KB. Focal choroidal excavation and its association with pachychoroid spectrum disorders. Retina 2017;37:199–221.
35. Spaide RF. Disease expression in nonexudative age-related macular degeneration varies with choroidal thickness. Retina 2018;38:708–716.
36. Barequet D, Iglicki M, Meshi A, et al. Acquired vitelliform lesions: a novel finding in eyes with peripapillary pachychoroid syndrome. Retina 2022;42:949–956.
37. Sakurada Y, Leong BCS, Parikh R, et al. Association between choroidal caverns and choroidal vascular hyperpermeability in eyes with pachychoroid diseases. Retina 2018;38:1977–1983.
38. Spaide RF, Gemmy Cheung CM, Matsumoto H, et al. Venous overload choroidopathy: a hypothetical framework for central serous chorioretinopathy and allied disorders. Prog Retin Eye Res 2022;86:100973.
39. Dansingani KK, Balaratnasingam C, Klufas MA, et al. Optical coherence tomography angiography of shallow irregular pigment epithelial detachments in pachychoroid spectrum disease. Am J Ophthalmol 2015;160:1243–1254.e2.
40. Guymer RH, Markey CM, McAllister IL, et al. Tolerating subretinal fluid in neovascular age-related macular degeneration treated with ranibizumab using a treat-and-extend regimen: FLUID study 24-month results. Ophthalmology 2019;126:723–734.
41. Martin DF, Maguire MG, Fine SL, et al. Ranibizumab and bevacizumab for treatment of neovascular age-related macular degeneration. Ophthalmology 2012;119:1388–1398.
42. Schmidt-Erfurth U, Kaiser PK, Korobelnik JF, et al. Intravitreal aflibercept injection for neovascular age-related macular degeneration. Ophthalmology 2014;121:193–201.
43. Zarbin MA, Hill L, Maunz A, et al. Anti-VEGF-resistant subretinal fluid is associated with better vision and reduced risk of macular atrophy. Br J Ophthalmol 2022;106:1561–1566.
44. Sharma A, Kumar N, Parachuri N, et al. Understanding the mechanisms of fluid development in age-related macular degeneration. Ophthalmol Retina 2021;5:105–107.
45. Grunwald JE, Pistilli M, Daniel E, et al. Incidence and growth of geographic atrophy during 5 years of comparison of age-related macular degeneration treatments trials. Ophthalmology 2017;124:97–104.
46. Sadda SR, Tuomi LL, Ding B, et al. Macular atrophy in the HARBOR study for neovascular age-related macular degeneration. Ophthalmology 2018;125:878–886.
47. Sadda SR, Guymer R, Monés JM, et al. Anti-vascular endothelial growth factor use and atrophy in neovascular age-related macular degeneration. Ophthalmology 2020;127:648–659.
48. Roisman L, Zhang Q, Wang RK, et al. Optical coherence tomography angiography of asymptomatic neovascularization in intermediate age-related macular degeneration. Ophthalmology 2016;123:1309–1319.
49. Inoue M, Jung JJ, Balaratnasingam C, et al. A comparison between optical coherence tomography angiography and fluorescein angiography for the imaging of type 1 neovascularization. Invest Opthalmol Vis Sci 2016;57:OCT314–323.
50. Bansal R, Dogra M, Mulkutkar S, et al. Optical coherence tomography angiography versus fluorescein angiography in diagnosing choroidal neovascularization in chronic central serous chorioretinopathy. Indian J Ophthalmol 2019;67:1095–1100.
51. Koh A, Lee WK, Chen LJ, et al. EVEREST study: efficacy and safety of verteporfin photodynamic therapy in combination with ranibizumab or alone versus ranibizumab monotherapy in patients with symptomatic macular polypoidal choroidal vasculopathy. Retina 2012;32:1453–1464.
52. Abraham N, Bousquet E, Santina A, et al. Successful treatment of severe peripapillary pachychoroid syndrome with anti VEGF therapy. Retin Cases Brief Rep 2023 . (Advance online publication).
53. Iovino C, Peiretti E, Tatti F, et al. Photodynamic therapy as a treatment option for peripapillary pachychoroid syndrome: a pilot study. Eye 2022;36:716–723.
54. Goldberg R, Heier JS, Wykoff CC, et al. Efficacy of intravitreal pegcetacoplan in patients with geographic atrophy (GA): 12-month results from the phase 3 OAKS and DERBY studies. Invest Ophthalmol Vis Sci 2022;63:1500.
55. Wykoff CC, Rosenfeld PJ, Waheed NK, et al. Characterizing new-onset exudation in the randomized phase 2 FILLY trial of complement inhibitor pegcetacoplan for geographic atrophy. Ophthalmology 2021;128:1325–1336.

LONG-TERM PROGNOSIS OF CHOROIDAL NEOVASCULARIZATION COMPLICATING ANGIOID STREAKS

CHARLOTTE ROHART, MD, PHD,*†‡ HOANG-MAI LE, MD,§ JULIANA ESTRADA-WALKER, MD,§ AUDREY GIOCANTI-AUREGAN, MD, PHD,¶ SALOMON Y. COHEN, MD, PHD*§

Purpose: To report the very long-term visual prognosis of choroidal neovascularization complicating angioid streaks in the antivascular endothelial growth factor era.

Methods: Retrospective monocentric study aimed at analyzing patients' demographics, choroidal neovascularization features, angioid streak–associated conditions, and previous and current therapies for choroidal neovascularization. The main outcome measures were the quantitative measurement of central retinal pigment epithelial atrophy enlargement by comparing the ratio of pixels involved on automated infrared images acquired by spectral-domain optical coherence tomography and the changes in best-corrected visual acuity. The secondary outcome measures were the number of intravitreal injections and the changes in central choroidal thickness and central retinal thickness. Subgroup analyzes were performed to compare macular atrophy extent between eyes of patients with or without proven pseudoxanthoma elasticum ("PXE" or "no PXE") and between eyes previously treated or not with photodynamic therapy ("PDT" or "no PDT").

Results: Thirty-three eyes of 23 patients were included. The mean best-corrected visual acuity decreased significantly from 66 ± 19 Early Treatment Diabetic Retinopathy Study letters at the time of the first antivascular endothelial growth factor injection to 52 ± 23 Early Treatment Diabetic Retinopathy Study letters at the end of the follow-up (mean follow-up duration: 109 ± 42 months, range: 47–175 months). The ratio of central retinal pigment epithelial atrophy enlargement was 201%, 110%, 240%, and 111% in the PXE, no PXE, PDT, and no PDT groups, respectively.

Conclusion: Despite the use of antivascular endothelial growth factor agents, the very long-term prognosis appeared relatively poor, especially in patients with PXE. This study also suggests that PDT should be used with caution in the management of choroidal neovascularization in eyes with angioid streaks.

RETINA 43:882–887, 2023

Angioid streaks (ASs) are dehiscences in the Bruch membrane due to the progressive fragmentation and calcification of the elastic lamina in this membrane. They can be idiopathic or associated with a systemic disease such as pseudoxanthoma elasticum (PXE), Ehler–Danlos syndrome, and Paget disease.[1,2] The most common complication of ASs is the development of choroidal neovascularization (CNV) occurring in 42% to 86% of cases.[3–6] Past therapeutic approaches for CNV, including laser photocoagulation and photodynamic therapy (PDT), have been associated with a high recurrence rate, laser scar enlargement, and poor final visual outcomes.[7–12]

Intravitreal antivascular endothelial growth factor (anti-VEGF) agents have been shown to significantly improve the visual prognosis of eyes developing this complication.[13,14] However, the long-term prognosis of eyes with CNV secondary to ASs has rarely been documented. Moreover, it varies from one study to

From the *Ophthalmology Center for Imaging and Laser, Paris; †Department of Ophthalmology, Ophtalmopôle Hôpital Cochin, APHP, and University of Paris, Paris, France; ‡Department of Ophthalmology, Clinique Beausoleil, Montpellier, France; §Department of Ophthalmology, University of Paris-Est Creteil, France; and ¶Department of Ophthalmology, Hôpital Avicenne, APHP, and University of Paris, Paris, France.

Supported by an unrestricted grant from CIL-ASSOC (Paris, France), an association for research and education.

The authors declare no conflicts of interest.

Reprint requests: Salomon Y. Cohen, MD, PhD, Centre Ophtalmologique d'Imagerie et de Laser, 11 Rue Antoine Bourdelle, Paris 75015, France; e-mail: sycsyc75@gmail.com

another.[15–20] Macular atrophy of the retinal pigment epithelium (RPE) has been proposed as one of the possible causes of the long-term visual loss, but its progression rate has never been reported.[20,21] The aims of this study were to assess the very long-term prognosis of eyes with CNV secondary to ASs due to PXE in the anti-VEGF era and to investigate central RPE atrophy enlargement in AS eyes with or without PXE.

Methods

A monocentric retrospective study was conducted in patients with CNV secondary to ASs, diagnosed and treated between July 2007 and January 2022 in a tertiary retinal center located in Paris, France.

Data collected from patients' charts included the age; sex; follow-up duration; BCVA obtained using standard Early Treatment Diabetic Retinopathy Study (ETDRS) charts; CNV type and location, that is, Type 1 or Type 2, and subfoveal, juxtafoveal, or extrafoveal; past treatments with PDT or thermal laser photocoagulation; number of intravitreal injections; and injected drugs.

Spectral-domain optical coherence tomography (SD-OCT) was performed using the Cirrus HD-OCT 4000 and 5000 devices (version 5.0; Carl Zeiss Meditec Dublin, CA). B and C scans were acquired using the Cirrus HD-OCT 5 Line Raster for horizontal and vertical images. The central choroidal thickness (CCT) and central retinal thickness were measured by a trained technician on the B scans passing through the fovea. The automated infrared images allowed delineating central RPE atrophy. Initial and final central RPE atrophy was measured using FIJI software. Two independent graders (H.M.L. and J.E.) evaluated all images. A manual method was used to measure the atrophic area. Measurements were repeated by each grader to determine the intraobserver repeatability. Images were deidentified and all personal data were removed. Because of use of different versions of Zeiss Cirrus OCT during the study period, there was no attempt to obtain absolute values of central RPE atrophy. RPE atrophy frequently started in the peripapillary atrophy. It was decided to keep this area in the analysis. Thus, central RPE atrophy was first delineated in the final image. Readers tried to analyze the same area in the initial image to allow a comparative pixel analysis.

Infrared images were exported and transferred to FIJI (an extension of the image processing software, available at http://fiji.se/; National Institutes of Health, Bethesda, MD). Each grader manually delimited the atrophic area using the region overlay tool and then the atrophic area was measured by the software. For images with multiple atrophic lesions, graders repeated the same selection and subsequent steps to take into account each area. In these cases, all atrophic areas measured were summed to report the final number. Each grader performed the measurements on three consecutive days.

The numbers of pixels presented as percentages, corresponding to the initial number/final number ratios, were compared.

The statistical analysis was performed using a Student's t test, and P values <0.05 were considered statistically significant. All data were collected in an Excel file (Microsoft Excel for Mac).

The main outcome measures were the quantitative measurement of central RPE atrophy enlargement and the changes in BCVA. The secondary outcome measures were the number of intravitreal injections and the changes in CCT and central retinal thickness.

This study was conducted in accordance with the principles of the Declaration of Helsinki and the French bioethics legislation. The study conduct was approved by the Ethics Committee/Independent Review Board of the Fédération France Macula.

Results

Thirty-three eyes of 23 patients were included in this study. Patients' demographics are summarized in Table 1. There were 12 women and 11 men with a mean age of 57 ± 8 years (range: 46–76 years) at the time of the first injection. Fifteen patients (65%) had skin biopsy–proven PXE (Figure 1). Nineteen eyes (58%) presented with occult CNV (Type 1) and 14 (42%) with classic CNV (Type 2). Choroidal neovascularization was bilateral in 10 patients (43%) at the time of initial treatment. Choroidal neovascularization was juxtafoveal in 9 eyes (27%), subfoveal in 13 eyes (40%), and extrafoveal in 11 eyes (33%). Sixteen eyes (48%) were treated with ranibizumab, 1 (3%) with aflibercept, 9 (27%) with ranibizumab and aflibercept, and 7 (22%) with bevacizumab and ranibizumab. Fourteen eyes (42%) had previously been treated with PDT and 3 (9%) with thermal photocoagulation. Patients received a mean number of 21 ± 25 injections, that is, a mean number of 2.4 injections per year. The mean follow-up duration was 109 ± 42 months (4–14 years).

The mean BCVA was 66 ± 19 ETDRS letters at the time of the first anti-VEGF injection and decreased to 52 ± 23 ETDRS letters at the end of the follow-up. The mean change in visual acuity was 14 ± 17 ETDRS letters throughout the follow-up, and this difference was statistically significant (P <0.05). The proportion of patients with a visual acuity loss >20 ETDRS letters, >15 ETDRS letters, >10 ETDRS letters, and >5 ETDRS letters was 33%, 42%, 57%, and 67%, respectively. One patient was considered blind (visual acuity

Table 1. Demographics and Treatment Details

Patients	23
Men, n	11
Women, n	12
Eyes, n	33
Proven PXE, n (%)	15 (65%)
Mean age at the time of the first injection, years	57 ± 8
Mean follow-up duration, months	109 ± 42
Mean treatment duration, months	79 ± 53
CNV type	
1, n (%)	19 (58%)
2, n (%)	14 (42%)
CNV bilaterality, n (%)	10 (43%)
CNV location	
Extrafoveal, n (%)	11 (33%)
Juxtafoveal, n (%)	9 (27%)
Subfoveal, n (%)	13 (40%)
Mean number of intravitreal injections	21 ± 25
Mean of number of injections per year	2.4
Injected drugs	
Ranibizumab, n (%)	16 (48%)
Aflibercept, n (%)	1 (3%)
Ranibizumab and aflibercept, n (%)	9 (27%)
Ranibizumab and bevacizumab, n (%)	7 (22%)
Previous therapy	
Photodynamic therapy, n (%)	14 (42%)
Thermal photocoagulation, n (%)	3 (9%)

<1/20 in both eyes) at the end of the follow-up (Figure 2).

The changes in BCVA were assessed depending on AS etiology and the presence or the absence of a history of CNV therapy. In the PXE-related AS group, the proportion of patients with a visual acuity loss >20 ETDRS letters, >15 ETDRS letters, >10 ETDRS letters, and >5 ETDRS letters was 38%, 38%, 57%, and 71%, respectively. In the PXE group, the mean initial BCVA was 65 ± 20 ETDRS letters and the final BCVA was 51 ± 25 ETDRS letters. In the no PXE group, the mean initial BCVA was 67 ± 18 ETDRS letters and the final BCVA was 55 ± 19 ETDRS letters. The number of patients in both groups was too small to perform a statistical analysis.

In the PDT group, the mean initial BCVA was 61 ± 24 ETDRS letters and the final BCVA was 46 ± 26 ETDRS letters. In the no PDT group, the mean initial BCVA was 70 ± 15 ETDRS letters and the final BCVA was 57 ± 20 ETDRS letters. The number of patients in both groups was too small to perform a statistical analysis (Table 2).

The mean central retinal thickness decreased from 264 ± 55 μm at baseline to 226 ± 53 μm at the end of the follow-up (P <0.05). The mean CCT decreased from 188 ± 85 μm at baseline to 155 ± 84 μm at the end of the follow-up (P <0.05).

At the end of the follow-up, an enlargement of macular RPE atrophy was found in all eyes, with a mean increase by 187 ± 185%. The increase was <25% in 8 eyes (24%), between 25% and 50% in 2 eyes (6%), between 50% and 100% in 4 eyes (12%), and >100% in 19 eyes (58%). Two eyes of one patient showed virtually no increase in atrophy (<2%). The visual acuity impairment was of 19 ± 17 ETDRS letters in the group with an enlargement >100%.

The ratio of macular atrophy enlargement strongly depended on the presence of PXE and previous treatment with PDT. The increase in macular atrophy was of 210% in the PXE group (21 eyes), of 303% in the PXE and PDT group (9 eyes), and of 143% in the PXE and no PDT group (12 eyes) (Table 3). More precisely, the enlargement of RPE atrophy was of 110% in the no PXE group (12 eyes), of 81% in the no PXE and no PDT group (5 eyes), and of 140% in the no PXE and PDT group (7 eyes). The extent of atrophy was of 240% in the PDT group and of 111% in no PDT group. In the 7 eyes with major atrophy extent, 100% had PXE.

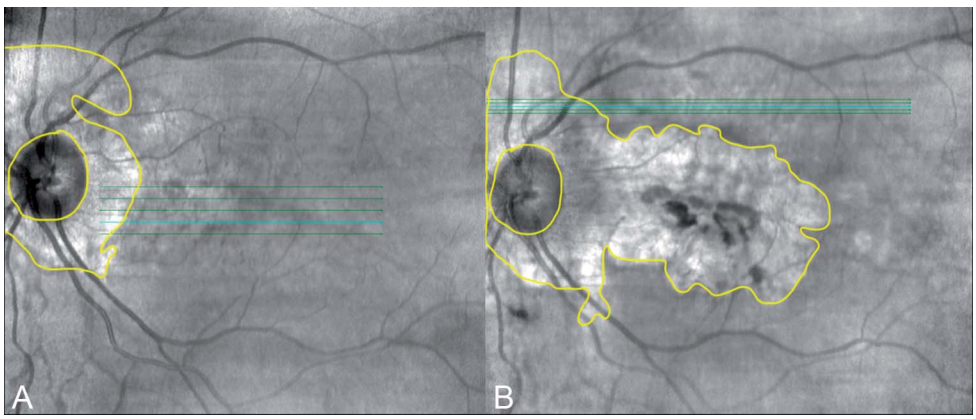

Fig. 1. Infrared imaging of a 62-year-old patient presenting with angioid streaks showing the progression of atrophy measured with Fiji from 2009 (**A**) to 2020 (**B**) (from 90,306 pixels to 117,258 pixels). An enlargement of the atrophy area can be seen.

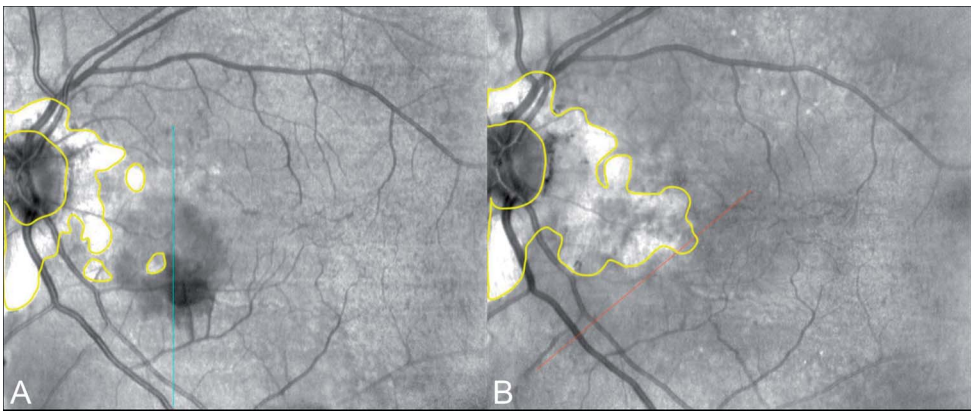

Fig. 2. Infrared imaging of a 50-year-old patient presenting with angioid streaks showing the progression of atrophy measured with Fiji from 2011 (**A**) to 2015 (**B**) (from 54,550 pixels to 223,077). An enlargement of the atrophy area can be seen.

Discussion

Choroidal neovascularization is considered the main complication of ASs. The natural history of CNV associated with ASs is poor, most of the eyes progressing toward legal blindness.[22] Before the advent of intravitreal anti-VEGFs, patients underwent laser photocoagulation, transpupillary thermotherapy, PDT, and surgical removal.[8,9,11,12,23–26] Conventional laser photocoagulation was used to treat juxtafoveal and extrafoveal CNV to stabilize the visual acuity. However, the recurrence rate was high, and the laser induced scar enlargement. Photodynamic therapy allowed managing subfoveal CNV and the outcomes were slightly better with VA stabilization over a limited period. Despite these treatments, CNV was a major source of visual impairment.[10]

Many studies have confirmed the efficacy of intravitreal anti-VEGF therapy on CNV secondary to ASs.[13–20,27] Intravitreal injections have improved the functional outcome of these patients by controlling CNV activity. The French PIXEL study has shown that the mean VA was maintained at one year with treatment with 0.5 mg of ranibizumab and it remained stable for up to four years.[28] However, in this previous study, the mean follow-up was limited to 36.5 months. Only a few studies have shown that, despite the control of CNV secondary to ASs, the long-term visual prognosis could be poor. To the best of our knowledge, our study is the first to report a mean follow-up longer than 100 months (109 months, range: 48–175 months). Mori et al[20] reported the outcomes of a cohort after a mean follow-up of 91 months. The median BCVA was significantly deteriorated at the end of the follow-up. In our study, the mean final BCVA was 52 ETDRS letters. The decrease in BCVA was statistically significant, with a lower final VA than previously reported. Moreover, in our study, the mean final BCVA tended to be poorer in the PXE group and PDT group compared, respectively, with the no PXE group and no PDT group. However, the limited number of cases prevented any statistical confirmation. Some factors have been shown to contribute to the visual prognosis. Mori et al also reported that two major factors contribute to a poor visual outcome in CNV secondary to ASs: CCT thinning and RPE atrophy enlargement. Our study supported their result for the CCT and atrophy progression. Indeed, we found a thin CCT at baseline and a significantly thinner CCT at the end of the follow-up. The very long follow-up duration with macular atrophy enlargement could also explain the poor visual prognosis. Indeed, we observed a significant progression of macular atrophy in the long term with a large geographic atrophic lesion in eyes with CNV secondary to ASs. We performed a quantitative assessment with a mean atrophy progression of 187%. This enlargement corresponded to a rate of atrophy progression of 19.7% per year.

Our study is the first to have quantitatively compared CNV secondary to ASs between patients with and without PXE. In our patients with PXE, atrophy progression was greater than 100% and the VA impairment was of 19 ETDRS letters. The poor visual prognosis could be explained by the progression of atrophy with foveal involvement, whereas CNV was controlled by anti-VEGF intravitreal injections.

Table 2. Mean Initial and Final BCVA

	Mean Initial BCVA (in ETDRS Letters)	Mean Final BCVA (in ETDRS Letters)
All eyes	66 ± 19 letters	52 ± 23 letters
Yes	65 ± 20 letters	51 ± 25 letters
PXE		
No	67 ± 18 letters	55 ± 19 letters
Yes	61 ± 24 letters	46 ± 26 letters
PDT		
No	70 ± 15 letters	57 ± 20 letters

Table 3. Ratio of Macular Retinal Pigment Epithelium Atrophy Enlargement Depending on the Presence or the Absence of Pseudoxanthoma Elasticum (PXE) and Previous Treatment With Photodynamic Therapy (PDT) or Not

All eyes	187 ± 185%
PXE	210%
No PXE	110%
PDT	240%
No PDT	111%

Macular atrophy was increased by 210% in the PXE group versus 110% in the no PXE group. Schoenberger et al[21] investigated the progression of macular atrophy in PXE regardless of the presence of CNV and they have identified risk factors for atrophy. They have found geographic atrophy in 20% of eyes and the growth rate was 1.7 mm^2 per year. In PXE, the RPE–Bruch membrane complex is the pathologic site. The authors have identified pattern dystrophy and linear pigment deposits as high-risk factors for geographic atrophy in PXE. In our study, the number of eyes with macular atrophy was twice as high in patients with PXE as in patients with no PXE, suggesting that the presence of lesions in PXE such as pattern dystrophy and linear pigment deposits could predispose to macular atrophy.

However, previous treatment with PDT could also contribute to atrophy extent. In the PDT group, macular atrophy was enlarged by 240%, more than twice compared with the no PDT group (111%). Studies conducted in eyes with age-related macular degeneration have concluded that PDT could be associated with adverse effects on normal tissue due to choroidal hypoperfusion and severe RPE alterations in the treated area after PDT.[29] They have suggested different reasons to explain RPE atrophy such as a collateral damage to the choriocapillaris with subsequent secondary RPE atrophy. In our study, the strongest progression of atrophy was observed in the PXE and PDT group with an atrophy extent of 303%. The association of PXE and PDT seemed to be the major factor for atrophy in our study, likely explained by the addition of their risk factors. However, we should keep in mind that PDT may have been proposed to patients who presented with the most aggressive CNV, more at risk to develop RPE atrophy secondary to the progression of CNV. The combination of anti-VEGF and PDT may also lead to more severe RPE atrophy than each treatment alone. These elements could constitute potential biases in association with the relatively low number of included eyes in each subgroup.

Several studies have reported the control of CNV in ASs with 1 to 2 intravitreal injections per year, which is a relatively low number. These studies have reported a mean number of 4.1 ± 4.0 and 5.4 ± 3.2 intravitreal injections for CNV secondary to ASs during a follow-up of 36.5 months and 53.8 months, respectively.[14,30] In our study, a mean number of 21.5 ± 25 intravitreal injections were received during a mean follow-up of 109 months. The higher number of total injections and injections per year found in our study could be explained by the use of a proactive treatment regimen in some patients.

In summary, the advent of anti-VEGF intravitreal therapy has radically improved treatment and the short-term prognosis of patients with CNV secondary to ASs. However, based on our findings, the long-term visual prognosis remains relatively poor. Despite its limitations, that is, its retrospective design and the inclusion of eyes previously treated with other modalities than anti-VEGFs, this study showed that central RPE atrophy progression is the major factor for the long-term prognosis, despite a good response of CNV to anti-VEGF agents. Moreover, this study also suggests that PDT should be used with caution in the management of CNV in eyes with ASs, especially in patients with PXE.

Key words: angioid streaks, pseudoxanthoma elasticum, choroidal neovascularization, anti-VEGF, photodynamic therapy.

References

1. Clarkson JG, Altman RD. Angioid streaks. Surv Ophthalmol 1982;26:235–246.
2. Connor PJ, Juergens JL, Perry HO, et al. Pseudoxanthoma elasticum and angioid streaks. Am J Med 1961;30:537–543.
3. Chatziralli I, Saitakis G, Dimitriou E, et al. Angioid streaks: a comprehensive review from pathophysiology to treatment. Retina 2019;39:1–11.
4. Cohen SY, Laroche A, Leguen Y, et al. Etiology of choroidal neovascularization in young patients. Ophthalmology 1996; 103:1241–1244.
5. Spaide RF. Choroidal neovascularization in younger patients. Curr Opin Opthalmology 1999;10:177–181.
6. Gliem M, Finger RP, Fimmers R, et al. Treatment of choroidal neovascularization due to angioid streaks: a comprehensive review. Retina 2013;33:1300–1314.
7. Singerman LJ. Current management of choroidal neovascularization. Ann Ophthalmol 1988;20:415–420, 423.
8. Peck A, Avanza P, Galli L, Brancato R. Laser photocoagulation of choroidal neovascularization in angioid streaks. Retina 1997;17:12–16.
9. Pece A, Russo G, Ricci F, et al. Verteporfin photodynamic therapy combined with intravitreal triamcinolone for choroidal neovascularization due to angioid streaks. Clin Ophthalmol 2010;4:525–530.
10. Menchini U, Virgili G, Introini U, et al. Outcome of choroidal neovascularization in angioid streaks after photodynamic therapy. Retina 2004;24:763–771.
11. Browning AC, Amoaku WM, Chung AK, et al. Photodynamic therapy for angioid streaks. Ophthalmology 2007;114:1592–1592.e1.

12. Heimann H, Gelisken F, Wachtlin J, et al. Photodynamic therapy with verteporfin for choroidal neovascularisation associated with angioid streaks. Graefe's Archive Clin Exp Ophthalmol 2005;243:1115–1123.
13. Tilleul J, Mimoun G, Querques G, et al. Intravitreal ranibizumab for choroidal neovascularization in angioid streaks: four-Year Follow-up. Retina 2016;36:483–491.
14. Mimoun G, Ebran JM, Grenet T, et al. Ranibizumab for choroidal neovascularization secondary to pseudoxanthoma elasticum: 4-year results from the PIXEL study in France. Graefes Arch Clin Exp Ophthalmol 2017;255:1651–1660.
15. Sawa M, Gomi F, Tsujikawa M, et al. Long-term results of intravitreal bevacizumab injection for choroidal neovascularization secondary to angioid streaks. Am J Ophthalmol 2009; 148:584–590.e2.
16. Myung JS, Bhatnagar P, Spaide RF, et al. Long-term outcomes of intravitreal antivascular endothelial growth factor therapy for the management of choroidal neovascularization in pseudoxanthoma elasticum. Retina 2010;30:748–755.
17. Finger RP, Issa PC, Schmitz-Valckenberg S, et al. Long-term effectiveness of intravitreal bevacizumab for choroidal neovascularization secondary to angioid streaks in pseudoxanthoma elasticum. Retina 2011;31:1268–1278.
18. Giacomelli G, Finocchio L, Biagini I, et al. Long-term follow-up of choroidal neovascularization due to angioid streaks with pro re nata intravitreal anti-VEGF treatment. Ophthalmologica 2017;238:44–51.
19. Ramakrishnan T, Chandra S, Sivaprasad S. Long-term follow-up of management of choroidal neovascularisation secondary to angioid streaks with intravitreal anti-vascular endothelial growth factor. Eye (Lond). 2021;35:853–857.
20. Mori H, Yamada H, Takahashi K. Long-term results of choroidal neovascularization secondary to angioid streaks. Graefes Arch Clin Exp Ophthalmol 2020;258:1863–1869.
21. Schoenberger SD, Agarwal A. Geographic chorioretinal atrophy in pseudoxanthoma elasticum. Am J Ophthalmol 2013; 156:715–723.
22. Orssaud C, Roche O, Dufier JL, Germain DP. Visual impairment in pseudoxanthoma elasticum: a survey of 40 patients. Ophthalmic Genet 2015;36:327–332.
23. Lim JI, Bressler NM, Marsh MJ, Bressler SB. Laser treatment of choroidal neovascularization in patients with angioid streaks. Am J Ophthalmol 1993;116:414–423.
24. Lee JM, Nam WH, Kim HK. Photodynamic therapy with verteporfin for choroidal neovascularization in patients with angioid streaks. Korean J Ophthalmol 2007;21:142–145.
25. Ozdek S, Bozan E, Gürelik G, Hasanreisoglu B. Transpupillary thermotherapy for the treatment of choroidal neovascularization secondary to angioid streaks. Can J Ophthalmol 2007;42: 95–100.
26. Eckstein M, Wells JA, Aylward B, Gregor Z. Surgical removal of non-age-related subfoveal choroidal neovascular membranes. Eye (Lond). 1998;12:775–780.
27. Lekha T, Prasad HN, Sarwate RN, et al. Intravitreal bevacizumab for choroidal neovascularization associated with angioid streaks: long-term results. Middle East Afr J Ophthalmol 2017; 24:136–142.
28. Ebran JM, Mimoun G, Cohen SY, et al. Treatment with ranibizumab for choroidal neovascularization secondary to a pseudoxanthoma elasticum: results of the French observational study PiXEL [in French]. J Français d'Ophtalmologie 2016;39:370–375.
29. Michels S, Schmidt-Erfurth U. Sequence of early vascular events after photodynamic therapy. Invest Ophthalmol Vis Sci 2003;44:2147–2154.
30. Martinez-Serrano MG, Rodriguez-Reyes A, Guerrero-Naranjo JL, et al. Long-term follow-up of patients with choroidal neovascularization due to angioid streaks. Clin Ophthalmol 2016; 11:23–30.

INVESTIGATION OF INCIDENCE AND CAUSES OF ACUTE VISION LOSS DURING ANTI–VASCULAR ENDOTHELIAL GROWTH FACTOR THERAPY FOR NEOVASCULAR AGE-RELATED MACULAR DEGENERATION DURING A FOUR-YEAR FOLLOW-UP

AKIRA MACHIDA, MD, AKIO OISHI, MD, PHD, EIKO TSUIKI, MD, PHD, YUKI MAEKAWA, MD, PHD, JUNKO KURIHARA, MD, YUKI HIRATA, MD, ERIKO MACHIDA, BA, TAKASHI KITAOKA, MD, PHD

Purpose: To investigate the incidence, risk factors, and outcomes of patients with age-related macular degeneration who experienced acute vision loss despite periodic injections of anti–vascular endothelial growth factor treatment for 4 years.

Methods: This retrospective cohort study included patients who were diagnosed with treatment-naive neovascular age-related macular degeneration and completed a 4-year follow-up. The incidence and risk factors for the occurrence of three or more lines of visual loss at every checkup were investigated.

Results: The analysis included 76 eyes of 76 patients. Acute vision loss occurred in 30 eyes (39.5%) over 4 years. Lower baseline best-corrected visual acuity and disrupted ellipsoid zone were independent predictors of vision loss occurrence. Although the causes and timing of visual acuity loss varied, retinal pigment epithelium tears were observed only in the first year. Most patients (86.7%) who experienced vision loss recovered their vision to pre-loss levels at least once; however, the final best-corrected visual acuity was worse than that in the group that did not experience acute vision loss.

Conclusion: Approximately half of the patients with age-related macular degeneration experienced acute vision loss during a 4-year follow-up, despite continuous anti–vascular endothelial growth factor treatment. Most patients recovered from vision losses temporarily; however, they experienced worse visual outcomes subsequently.

RETINA 43:888–896, 2023

Age-related macular degeneration (AMD) is a leading cause of visual impairment, particularly in developed countries.[1–3] The visual prognosis of patients with macular neovascularization (MNV) secondary to AMD has changed considerably since the introduction of anti–vascular endothelial growth factor (VEGF) treatment. Anti-VEGF agents include ranibizumab and aflibercept, which several large clinical studies have demonstrated to be efficacious.[4–7]

However, some patients still lose vision despite continuous anti-VEGF treatment.[8–11] Sub-analysis of pivotal clinical trials identified the incidence and risk of vision loss that occurs rapidly in the early phase of treatment.[12–14] This acute loss of vision, even if it improves quickly, is a predictor of poor visual outcomes in patients.[13] The causes of vision loss include the exacerbations of macular degeneration and also other ophthalmologic or systemic diseases. However, the cause is sometimes unknown.[12,13]

Although these studies provided important practical information, the observation period of the analyses was limited to 1 year or 2 years. Considering that longer checkups and treatment are required in real-world clinical practice, investigating the acute vision

loss over an extended follow-up period will help improve disease management by identifying preventable causes. It will help predict which patients would experience poor visual outcomes and enable appropriate management to optimize adherence and outcomes.

In this study, we investigated patients who lost more than three lines of vision at any visit compared with the previous visit during a 4-year follow-up despite periodic injections of anti-VEGF agents and explored the incidence rates and risk factors for developing vision loss.

Methods

Study Participants

This retrospective cohort study used data from all patients who were diagnosed with neovascular AMD (nAMD) and started anti-VEGF drug treatment at the Department of Ophthalmology, Nagasaki University Hospital from January 2013 to December 2016.

The inclusion criteria were as follows: 1) age >50 years, 2) presence of MNV, and 3) start of anti-VEGF therapy during the above period. Only one eye from each patient was included; if both eyes received treatment during the study period, the first eye was included in the analysis. In contrast, the exclusion criteria were as follows: 1) axial length >26.5 mm, 2) occurrence of inflammatory or hereditary diseases that may cause MNV, 3) previous treatments for MNV, 4) any other retinal or optic nerve diseases, 5) a history of intraocular surgery except for cataract surgery, and 6) observation period <4 years after the start of treatment.

All procedures conformed to the tenets of the Declaration of Helsinki, and the study design was approved by the institutional review board of Nagasaki University Hospital. The ethics committee waived the requirement for written informed consent, given the study's retrospective nature; instead, patients were allowed "opt-out" consent.

Intervention and Observation Procedure

We used the treat-and-extend regimen principle. We used aflibercept in most cases of Type 1 MNV and ranibizumab for Type 2 and Type 3 MNV. In addition, we chose ranibizumab for patients with a high risk of stroke and cardiovascular events. The initial drug may have been switched to another when the lesion is refractory. After an initial loading phase of 3 doses of anti-VEGF administered 4 weeks apart, the interval for the next injection was extended by 1 week to 2 weeks to a maximum of 16 weeks if there was no sign of exudation. The treatment interval was shortened by ≥2 weeks upon signs of disease recurrence, as shown by changes in anatomical parameters such as the presence of intraretinal or subretinal fluid. However, when no recurrence was observed at intervals of ≥12 weeks, treatment cessation was discussed with the patients. Treatment was also stopped in refractory cases, in which visual recovery was considered unlikely even with continued injections, when the patient was referred to another hospital for treatment, or when the patient refused further treatment. The interval between extension and shortening, timing of treatment discontinuation, and drug selection were at the discretion of the attending physician.

Patients underwent comprehensive examinations, including measurement of best-corrected visual acuity (BCVA), axial length (IOLMaster 500; Carl Zeiss Meditec, Dublin, CA), fundus photography, spectral-domain optical coherence tomography (SD-OCT, Spectralis; Heidelberg Engineering, Heidelberg, Germany), fluorescein angiography, indocyanine green angiography, fundus autofluorescence imaging (HRA2; Heidelberg Engineering), and OCT-angiography (Avanti; Optovue, Fremont, CA) at baseline. Anticoagulant and/or antiplatelet therapy was systematically administered during the initial checkup. The BCVA and SD-OCT measurements were performed at each checkup. Spectral-domain optical coherence tomography images

From the Department of Ophthalmology and Visual Sciences, Graduate School of Biomedical Sciences, Nagasaki University, Nagasaki, Japan.

Supported by a grant-in-aid for scientific research (no. 22K09793) from the Japan Society for the Promotion of Science, Tokyo, Japan.

A. Oishi received personal fees from Bayer Yakuhin, Ltd (Osaka, Japan), Santen Pharmaceutical Co, Ltd (Tokyo, Japan), and Novartis Pharma K.K. (Tokyo, Japan). T. Kitaoka received personal fees from Bayer Yakuhin, Ltd. (Osaka, Japan), Novartis Pharma K.K. (Tokyo, Japan), and Santen Pharmaceutical Co, Ltd (Tokyo, Japan) and grants from Santen Pharmaceutical Co, Ltd (Tokyo, Japan).

Access to data and data analysis: A. Machida had full access to all the data in the study and takes responsibility for the integrity of the data and the accuracy of data analysis.

Reprint requests: Akio Oishi, MD, PhD, Department of Ophthalmology and Visual Sciences, Nagasaki University, Sakamoto 1-7-1, Nagasaki 852-8102, Japan; e-mail: akio.oishi@nagasaki-u.ac.jp

included 30° horizontal regular and enhanced depth scans through the fovea and 15 raster scans covering a 20° × 15° oblong rectangle.

Subretinal hemorrhage in the fovea centralis was detected based on fundus photography and SD-OCT. Spectral-domain OCT images were reviewed to differentiate between hemorrhagic pigment epithelial detachment (PED). Choroidal thickness was measured using enhanced depth imaging scans as the length between the outer border of the Bruch membrane and the choriosclera interface. Pigment epithelial detachment height was defined as the distance between the outer border of the retinal pigment epithelium and the inner border of Bruch membrane, and the maximum PED height on the raster scans was recorded. The presence of foveal external limiting membrane (ELM), ellipsoid zone, and vitreoretinal adhesion was evaluated on vertical and raster scans.

Disease type was determined based on angiography, SD-OCT, OCT-angiography, and fundus photography. Fundus angiography was performed before or immediately after the start of treatment unless the patient experienced an allergy to the contrast agent or other systemic risk. We assessed the presence of polypoidal lesions on indocyanine green angiography at baseline in each case. A diagnosis of aneurysmal Type 1 neovascularization (also known as polypoidal choroidal vasculopathy) was made based on the finding of characteristic polypoidal lesions at the border of the branching vascular networks. Patients with retinochoroidal anastomosis were diagnosed with Type 3 neovascularization (also known as retinal angiomatous proliferation), whereas the other patients were diagnosed with Type 1 and Type 2 MNV.

Additionally, two graders (Y.H. and E.M), blinded to the visual outcome, performed these measurements and grading. The average of the measurements was used for the analysis, and the discrepancy in grading was arbitrated with discussion.

Main Outcome Measure

The main outcome measure was the incidence of more than three lines of vision loss compared with the previous examination. Best-corrected visual acuity was measured using Landolt C and converted to the logarithm of the minimum angle of resolution (logMAR) to perform statistical analysis. A decrease of >0.3 units was defined as >3 lines of vision loss.

Statistical Analysis

Values are presented as median and quartile ranges. All statistical analyses were performed using Easy R,[15] which is a modified version of R commander for statistical functions frequently used in biostatistics. Stepwise logistic regression analysis was performed using age, sex, baseline BCVA, presence of a polypoidal lesion, presence of Type 3 lesion, presence of a subretinal hemorrhage, central retinal thickness (CRT), maximum PED height, choroidal thickness, ELM status, ellipsoid zone status, vitreoretinal adhesion, anticoagulant therapy as independent factors, and loss of vision as dependent factors. A Kaplan–Meier curve was created to understand time-to-event scenarios. Statistical significance was set at $P < 0.05$.

Results

Overall, 155 eyes from 155 patients were diagnosed with nAMD, and anti-VEGF induction was started between 2013 and 2016. According to the criteria, 1, 9, 11, and 58 eyes were excluded because of age, previous treatment, other diseases or surgery, and terminated observation within 4 years, respectively. Of the 58 eyes that terminated observation, 28 stopped treatment without recurrence, 4 stopped treatment because of lack of or insufficient effect, 7 were transferred to another hospital for therapy, and 19 dropped out for unknown reasons. Finally, 76 eyes were included in the analysis. Fifty-nine of the 76 eyes continued anti-VEGF treatments for 4 years, and 17 eyes stopped treatment and continued coming for checkups (Figure 1). Among the 17 eyes, 12 eyes stopped treatment without recurrence, 4 eyes stopped treatment because of insufficient effect, and 1 eye refused to continue treatment.

Table 1 shows the demographic characteristics of the study population. This study included 52 men and 24 women. Fifty-five eyes had Type 1 MNV (42 of 55 had aneurysmal Type 1 MNV), 16 eyes had Type 2 MNV, and 5 eyes had Type 3 MNV. The median age was 71.0 years (quartile range: 65.0–79.3 years), and the median number of injections was 20.0 (13.0–28.3).

Acute vision loss occurred in 30 eyes (39.5%) at a median follow-up period of 11.5 months (4.0–22.6 months) after the initial treatment. The median period from the last injection to the occurrence of vision loss was 52 days (31–66 days), with no difference between aflibercept and ranibizumab ($P = 0.838$). The eyes with vision loss included 20 eyes with Type 1 MNV (36.4% of eyes with Type 1 MNV), 6 eyes with Type 2 MNV (37.5% of eyes with Type 2 MNV), and 4 eyes with Type 3 MNV (80.0% of eyes with Type 3 MNV). Although there were 22 eyes with multiple vision loss events during the 4-year observation period, only the

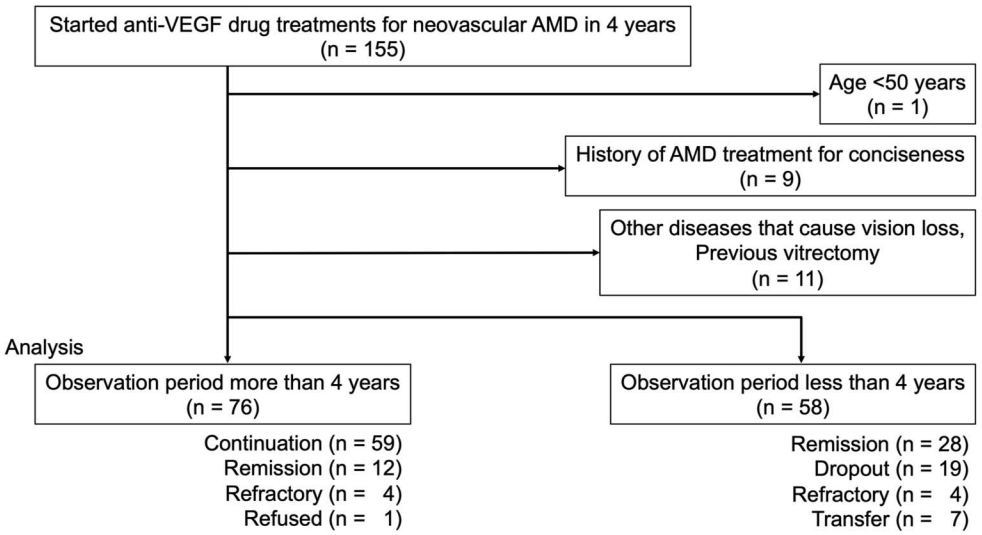

Fig. 1. Flowchart of screening process in the present study. We screened 155 patients with neovascular age-related macular degeneration, and 79 eyes were excluded according to the criteria. Finally, 76 eyes were used for analysis.

first event was analyzed in this study. The presumed cause for visual decline was an increase/development of subretinal fluid (4 eyes, 13.3%), increase/development of subretinal hemorrhage (4 eyes, 13.3%), an increase in macular edema (3 eyes, 10.0%), development of macular atrophy (3 eyes, 10.0%), formation of a fibrotic scar (3 eyes, 10.0%), formation of retinal pigment epithelium tears (3 eyes, 10.0%), and an increase/development of subretinal hyperreflective materials (SHRM; 2 eyes, 6.7%). Furthermore, 4 eyes (13.3%) developed cataracts, underwent cataract surgery, and experienced an improved vision. The progression of cataracts was determined to be the cause of vision loss in four eyes, and vision was improved by cataract surgery. One eye (3.3%) developed severe retinal schisis because of progressive traction, and no

Table 1. Baseline Characteristics and Changes in BCVA of Patients With AMD Treated With anti-VEGF Drugs

		Type 1			
	Total	Without Polyp	With Polyp (PCV)	Type 2	Type 3 (RAP)
No. of eyes	76	13	42	16	5
Age, years	71.0 (65.0–79.3)	72.0 (68.0–81.0)	68.0 (64.0–77.0)	74.5 (67.8–80.3)	77.0 (70.0–79.0)
Sex (male/female)	52/24	7/6	32/10	10/6	3/2
BCVA first, logMAR	0.52 (0.22–0.73)	0.52 (0.30–0.70)	0.46 (0.22–0.82)	0.52 (0.40–0.77)	0.52 (0.52–0.70)
BCVA max, logMAR	0.05 (−0.02–0.24)	0.15 (0.05–0.22)	0.00 (−0.08–0.25)	0.12 (0.00–0.15)	0.40 (0.10–0.40)
BCVA 4Y, logMAR	0.22 (0.05–0.40)	0.30 (0.30–0.40)	0.12 (0.00–0.40)	0.30 (0.20–0.30)	0.52 (0.40–0.52)
CRT, μm	378.5 (261.8–471.3)	354.0 (258.0–443.0)	312.5 (231.0–435.0)	427.0 (315.8–496.5)	512.0 (455.0–640.0)
Maximum PED, μm	230.5 (159.0–420.3)	236.0 (165.0–321.0)	362.0 (191.8–494.3)	150.5 (118.8–187.8)	221.0 (156.0–424.0)
Choroidal thickness, μm	231.0 (191.0–285.3)	223.0 (201.0–277.0)	238.0 (208.0–308.8)	238.5 (178.0–287.3)	208.0 (121.0–220.0)
Number of injections	20.0 (13.0–28.3)	20.0 (19.0–30.0)	20.5 (12.0–29.8)	20.0 (16.8–26.3)	13.0 (13.0–27.0)
Initial drug (aflibercept/ranibizumab)	54/22	10/3	36/6	8/8	0/5
Switch to another drug	6/11	2/3	4/3	0/4	0/1

Continuous values are shown as median and quartile ranges.

PCV, polypoidal choroidal vasculopathy; RAP, retinal angiomatous proliferation; BCVA first, best-corrected visual acuity at baseline; BCVA 4Y, best-corrected visual acuity at 4 years; BCVA max, maximum best-corrected visual acuity over 4 years.

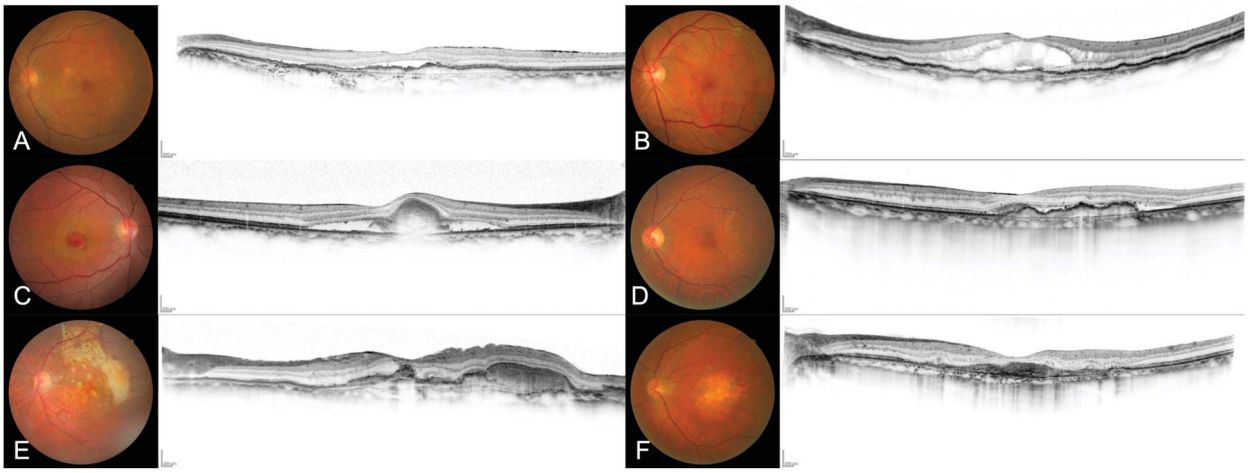

Fig. 2. Color fundus photography and optical coherence tomography images of representative cases with vision loss during the treatment of age-related macular degeneration. **A.** A case with BCVA loss from 20/50 to 20/100 because of subretinal fluid. **B.** A case with BCVA loss from 20/15 to 20/40 because of macular edema. **C.** A case with BCVA loss from 20/20 to 20/40 because of subretinal hemorrhage. **D.** A case with BCVA loss from 20/20 to 20/40 because of subretinal hyperreflective materials. **E.** A case with BCVA loss from 20/50 to 20/100 because of macular atrophy. **F.** A case with BCVA loss from 20/100 to 20/200 because of fibrotic scar.

treatment was administered. No apparent cause was identified in 3 eyes (10.0%). Of the 30 eyes with vision loss, only 1 eye developed vision loss after cessation of treatment, which was unrelated to AMD exacerbation. Figure 2 shows the representative cases.

No baseline characteristics were associated with a specific cause of vision loss, and anticoagulant use was not associated with the risk of subretinal hemorrhage-related vision loss. Vision loss because of any reason may occur at any time; however, retinal pigment epithelium tear tends to occur in the early phase; in this study, all retinal pigment epithelium tear-associated vision loss occurred in the first year.

Table 2 shows the comparisons of eyes with and without vision loss. Patients with vision loss had lower baseline BCVA, larger CRT, more frequent disruption of the ELM, and an ellipsoid zone. Logistic regression analysis identified lower baseline BCVA and disrupted ellipsoid zone as factors contributing to the incidence of vision loss. Odds ratios were 1.24 (95% confidence interval 1.06 to 1.46, $P = 0.007$) for a 0.1 logarithm of the minimum angle of resolution unit increase in BCVA and 6.28 (95% confidence interval 1.25–31.5, $P = 0.025$) for a disrupted ellipsoid zone.

Figure 3A shows the Kaplan–Meier survival curve. The survival rate (not losing 3 lines of vision) at 4

Table 2. Baseline Characteristics and Changes in BCVA of Patients With AMD Who Experienced Acute Vision Loss and Who Did Not

	No Vision Loss (n = 46)	With Vision Loss (n = 30)	*P*
Age, years	68.0 (64.3–77.8)	76.0 (66.5–81.8)	0.063
Sex (male/female)	31/15	21/9	1.000
Subtype (Type 1/2/3)	35/10/1	20/6/4	0.216
BCVA first, logMAR	0.40 (0.15–0.70)	0.70 (0.52–1.05)	<0.001
BCVA max, logMAR	0.00 (−0.08–0.05)	0.30 (0.15–0.40)	<0.001
BCVA 4Y, logMAR	0.10 (0.00–0.30)	0.46 (0.30–0.82)	<0.001
Central retinal thickness, μm	341.0 (256.5–411.5)	441.0 (276.8–513.5)	0.031
Maximum PED, μm	223.0 (136.0–377.0)	241.5 (184.8–462.8)	0.088
Choroidal thickness, μm	241.0 (211.5–286.0)	215.5 (138.5–282.3)	0.101
Subretinal hemorrhage	22 (47.8%)	16 (53.3%)	0.815
Disrupted foveal ELM	17 (37.0%)	20 (66.7%)	0.018
Disrupted foveal ellipsoid zone	26 (56.5%)	28 (93.3%)	0.001
Vitreoretinal detachment	40 (87.0%)	26 (86.7%)	1.000
Use of anticoagulant	6 (13.0%)	6 (20.0%)	0.524
Number of injections	21.0 (15.5–29.8)	18.5 (10.3–26.8)	0.159

Continuous values are shown as median and quartile ranges.

BCVA first, best-corrected visual acuity at baseline; BCVA 4Y, best-corrected visual acuity at 4 years; BCVA max, maximum best-corrected visual acuity during 4 years.

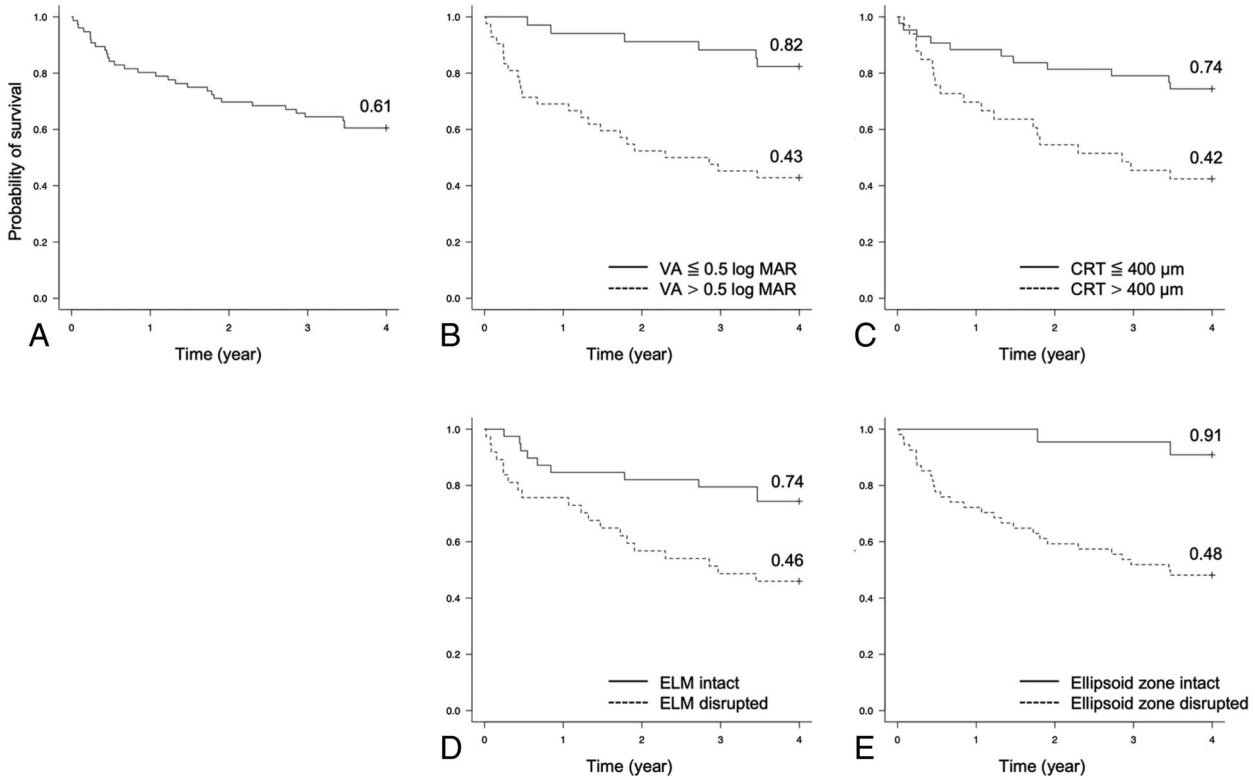

Fig. 3. Kaplan–Meyer survival curves (i.e., free of vision loss) for patients with age-related macular degeneration treated with anti-VEGF drugs. Vision loss was defined as more than three lines of vision loss compared with the previous examination. Panel (**A**) shows that the overall survival rate of 76 patients in 4 years was 60.5%. Patients with poor visual acuity (worse than 0.5 logMAR) showed a lower rate of survival ($P < 0.001$), Panel (**B**). Greater CRT was also associated with a higher incidence of vision loss ($P = 0.004$), Panel (**C**). Panels (**D** and **E**) show that eyes without an intact external limiting membrane ($P = 0.008$) and ellipsoid zone ($P < 0.001$) are associated with a higher incidence of vision loss.

years was 60.5%. Fifteen of the 30 patients with vision loss experienced an event during the first year. For additional analysis, the Kaplan–Meier survival curves for eyes with and without BCVA >0.5 logarithm of the minimum angle of resolution (the value was arbitrarily determined from the median BCVA of 0.52) are shown in Figure 3B, with and without CRT >400 μm (the value was arbitrarily determined from the median CRT of 368 μm) are shown in Figure 3C, and with and without disruption in the ELM and ellipsoid zone are shown in Figure 3, D and E. Eyes with lower baseline BCVA ($P < 0.001$, log-rank test), eyes with higher CRT ($P = 0.004$), eyes with disrupted ELM ($P = 0.008$), and eyes with disrupted ellipsoid zones ($P < 0.001$) had lower survival.

Subsequently, we investigated the clinical course of vision loss. Permanent vision loss (i.e., no return to the level before the vision loss event) was noted in 4 eyes among the 30 eyes that experienced vision loss. Table 3 presents a comparison of eyes with temporary and permanent vision loss. The eyes with permanent vision loss were in older patients ($P = 0.030$). The time to permanent vision loss was evenly distributed over the observation period, and no characteristic cause could be found. All vision loss events unrelated to MNV or of unknown cause were temporary and recovered to a pre-vision loss event.

Discussion

Incidence of Vision Loss in One and Four Years

This study focused on the incidence of three or more lines of acute vision loss during long-term anti-VEGF drug treatment. During the 4-year follow-up, 39.5% of patients with AMD experienced one or more episodes of acute vision loss. Particularly, 60.5% of the patients did not experience acute vision loss. Notably, half of the vision loss (19.7% of all patients) occurred in the first year, indicating the importance of the initial treatment. The 19.7% incidence of vision loss in the first year was slightly higher than the 13.9% reported in the MARINA and ANCHOR studies[12] and 8.2% in a previous report using aflibercept.[14] This may be because of inclusion bias; patients who were good responders may have stopped coming for checkups within those 4 years and were excluded from the analysis. Patients who experienced acute vision loss had

Table 3. Baseline Characteristics and Changes in BCVA of Patients With AMD Who Experienced Temporary or Permanent Acute Vision Loss

	Temporary Vision Loss (n = 26)	Permanent Vision Loss (n = 4)	*P*
Age, years	74.5 (65.3–79.8)	86.0 (80.5–89.0)	0.030
Sex (male/female)	19/7	2/2	0.563
BCVA first, logMAR	0.61 (0.52–1.04)	1.02 (0.88–1.14)	0.241
BCVA max, logMAR	0.26 (0.11–0.40)	0.46 (0.38–0.52)	0.090
BCVA 4Y, logMAR	0.40 (0.24–0.65)	1.50 (0.92–2.00)	0.010
Central retinal thickness, μm	441.0 (276.8–511.8)	497.5 (372.0–591.5)	0.855
Maximum PED, μm	241.5 (186.5–480.8)	274.0 (180.5–384.8)	0.583
Choroidal thickness, μm	207.5 (123.5–282.3)	229.5 (207.5–251.5)	0.692
Subretinal hemorrhage	14 (53.8%)	2 (50.0%)	0.563
Disrupted foveal ELM	18 (69.2%)	2 (50.0%)	0.584
Disrupted foveal ellipsoid zone	25 (96.2%)	3 (75%)	0.253
Vitreoretinal detachment	22 (84.6%)	4 (100%)	1.000
Use of anticoagulant	4 (15.4%)	2 (50.0%)	0.169
Number of injections	18.5 (11.3–27.8)	13.0 (7.0–20.3)	0.210

Continuous values are shown as median and quartile ranges.
BCVA first, best-corrected visual acuity at baseline; BCVA 4Y, best-corrected visual acuity at 4 years; BCVA max, maximum best-corrected visual acuity during 4 years.

lower BCVA at baseline, maximum BCVA during 4 years, and visual acuity at four years than the group that did not experience vision loss, which is generally consistent with previous reports.[13]

Causes of Acute Vision Loss

This study showed various causes of vision loss at different time intervals. However, a correlation between specific causes, early or late events, and patient background was not found. The exception was a retinal pigment epithelium tear, which developed only in the first year after the initial treatment, as previously reported.[16–18] Similar to previous reports, anticoagulant use was not associated with subretinal hemorrhage-related vision loss.[19,20]

We considered that we could find preventable vision loss, such as exacerbation of CME, subretinal fluid, and hemorrhage because of insufficient injections. However, in this study, not many vision loss events were associated with active exacerbation of MNV (13 cases, 43.3% of all vision loss), and all occurred during the treat-and-extend regimen rather than after treatment discontinuation. The number of injections was not associated with loss of vision. It is debatable whether more intensive drug administration would have effectively prevented the event; however, it would be difficult to apply more intensive treatment for these cases selectively in advance, given the absence of any predictive factors.

This study also identified a certain number of cases of unexplained vision loss and AMD-unrelated vision loss. Considering that studies of MNV essentially include elderly cohorts, cataract progression should be considered when interpreting long-term results. Unexplained vision loss may also be caused by fluctuations in examination results because of the patient's age. Additionally, all unexplained vision loss was temporary.

Risk of Acute Vision Loss

Patients with poor baseline BCVA may be expected to have fewer vision loss events because of floor effects; however, this study associated poor baseline BCVA with a risk of acute vision loss. Poor baseline BCVA indicates higher disease activity, which may lead to a higher incidence of vision loss.

Morphological analysis revealed an association between baseline disease activity and a higher incidence of vision loss. Patients with increased CRT, disrupted ELM, and ellipsoid zone were at a high risk of vision loss. A recent study showed that variability in CRT is a predictor of visual outcomes.[21] Eyes with higher CRT at baseline may have a higher magnitude of CRT variability, which may be the cause of the association between increased CRT and a higher incidence of vision loss.

The status of the ELM[22,23] and ellipsoid zone[24,25] has been suggested as a valid indicator of photoreceptor integrity in AMD. In this study, the integrity of the ellipsoid zone was found to be a more important predictor, probably because the baseline visual acuity was relatively good. External limiting membrane may be a better indicator in a cohort with poor baseline vision. Evaluating both the ELM and ellipsoid zones is generally recommended in clinical practice.

Temporary Vision Loss and Final Visual Outcome

Four of the 30 patients with acute vision loss experienced permanent vision loss. Specifically, 90% of vision loss improved to the pre-vision-loss level with continuous injection and other treatments such as cataract surgery at least during one checkup. Particularly, all the vision loss unrelated to MNV and of unknown cause improved.

Previous studies reported that acute vision loss increases the frequency of patient dropouts and cessation.[26,27] However, our data suggest that visual acuity is likely to improve with continued long-term treatment in most cases. Therefore, encouraging patients to continue treatment would help their recovery.

Meanwhile, it should be noted that the occurrence of vision loss is a risk factor for a worse long-term visual outcome. Even when vision loss is temporary, these patients are at a high risk of gradual loss of vision in the long term. The question of whether we should apply more intensive treatment for these patients needs to be investigated in the future.

Strength and Limitation

The strengths of this study were that the patients were treated with an identical protocol, examined systematically, and observed over a long period. The most significant limitation is the retrospective design and associated selection bias. Larger prospective studies would provide more detailed information about the causes and risks of acute vision loss. Most patients who stopped treatment for whatever reason did not continue follow-up for 4 years and were excluded from the study. In addition, the final treatment decision was at the physician's discretion. Nevertheless, we believe that the results represent a typical outcome in a clinical setting and can be generalized to various populations.

In conclusion, this study showed that about half of patients with AMD experience three lines of acute vision loss within years, despite treatment with continuous anti-VEGF medications. Poor baseline visual acuity and disrupted ellipsoid zones are risk factors for vision loss. Most patients' vision loss was recovered temporarily; however, they experienced a poor visual outcome after 4 years. These results suggest the importance of appropriate treat-and-extend regimen to avoid acute vision loss and the importance of continuing treatment and observation, even in the presence of acute vision loss.

Key Words: acute vision loss, age-related macular degeneration, anti–vascular endothelial growth factor treatment, intravitreal aflibercept, intravitreal ranibizumab, long-term follow-up, macular neovascularization, real-world date, treatment-naive neovascular AMD, treat-and-extend regimen.

Acknowledgments

Medical writing and editorial support for the preparation of this article, under the guidance of the authors, were provided by Editage.

References

1. Bressler NM. Age-related macular degeneration is the leading cause of blindness. Jama 2004;291:1900–1901.
2. de Jong PT. Age-related macular degeneration. N Engl J Med 2006;355:1474–1485.
3. Lim LS, Mitchell P, Seddon JM, et al. Age-related macular degeneration. The Lancet 2012;379:1728–1738.
4. Brown DM, Kaiser PK, Michels M, et al. Ranibizumab versus verteporfin for neovascular age-related macular degeneration. N Engl J Med 2006;355:1432–1444.
5. Rosenfeld PJ, Brown DM, Heier JS, et al. Ranibizumab for neovascular age-related macular degeneration. N Engl J Med 2006;355:1419–1431.
6. Fine SL, Martin DF, Maguire MG, et al. Ranibizumab and bevacizumab for treatment of neovascular age-related macular degeneration: two-year results. Ophthalmology 2012;119:1388–1398.
7. Rogers CA, Chakravarthy U, Harding SP, et al. Ranibizumab versus bevacizumab to treat neovascular age-related macular degeneration: one-year findings from the IVAN randomized trial. Ophthalmology 2012;119:1399–1411.
8. Rosenfeld PJ, Shapiro H, Tuomi L, et al. Characteristics of patients losing vision after 2 years of monthly dosing in the phase III ranibizumab clinical trials. Ophthalmology 2011;118:523–530.
9. Heier JS, Brown DM, Chong V, et al. Intravitreal aflibercept (VEGF trap-eye) in wet age-related macular degeneration. Ophthalmology 2012;119:2537–2548.
10. Schmidt-Erfurth U, Kaiser PK, Korobelnik JF, et al. Intravitreal aflibercept injection for neovascular age-related macular degeneration: ninety-six-week results of the VIEW studies. Ophthalmology 2014;121:193–201.
11. Ying GS, Kim BJ, Maguire MG, et al. Sustained visual acuity loss in the comparison of age-related macular degeneration treatments trials. JAMA Ophthalmol 2014;132:915–921.
12. Wolf S, Holz FG, Korobelnik JF, et al. Outcomes following three-line vision loss during treatment of neovascular age-related macular degeneration: subgroup analyses from MARINA and ANCHOR. Br J Ophthalmol 2011;95:1713–1718.
13. Kim BJ, Ying GS, Huang J, et al. Sporadic visual acuity loss in the comparison of age-related macular degeneration treatments trials (CATT). Am J Ophthalmol 2014;158:128–135.e10.
14. Hata M, Oishi A, Yamashiro K, et al. Incidence and causes of vision loss during aflibercept treatment for neovascular agre-related macular degeneration: one-Year Follow-up. Retina 2017;37:1320–1328.

15. Kanda Y. Investigation of the freely available easy-to-use software "EZR" for medical statistics. Bone Marrow Transpl 2013; 48:452–458.
16. Empeslidis T, Vardarinos A, Konidaris V, et al. Incidence of retinal pigment epithelial tears and associated risk factors after treatment of age-related macular degeneration with intravitreal anti-VEGF injections. Open Ophthalmol J 2014;8:101–104.
17. Nagiel A, Freund KB, Spaide RF, et al. Mechanism of retinal pigment epithelium tear formation following intravitreal antivascular endothelial growth factor therapy revealed by spectral-domain optical coherence tomography. Am J Ophthalmol 2013;156:981–988.e2.
18. Sastre-Ibáñez M, Martínez-Rubio C, Molina-Pallete R, et al. Retinal pigment epithelial tears. J Français d'Ophtalmologie 2019;42:63–72.
19. Ying GS, Maguire MG, Daniel E, et al. Association between antiplatelet or anticoagulant drugs and retinal or subretinal hemorrhage in the comparison of age-related macular degeneration treatments trials. Ophthalmology 2016;123:352–360.
20. Buitendijk GHS, Schauwvlieghe ASME, Vingerling JR, et al. Antiplatelet and anticoagulant drugs do not affect visual outcome in neovascular age-related macular degeneration in the BRAMD trial. Am J Ophthalmol 2018;187:130–137.
21. Ciucci F, Ioele G, Bardocci A, et al. Central retinal thickness fluctuations in patients treated with anti-VEGF for neovascular age related macular degeneration. Eur J Ophthalmol 2021;32: 2388–2394.
22. Oishi A, Hata M, Shimozono M, et al. The significance of external limiting membrane status for visual acuity in age-related macular degeneration. Am J Ophthalmol 2010;150: 27–32.e1.
23. Oishi A, Shimozono M, Mandai M, et al. Recovery of photoreceptor outer segments after anti-VEGF therapy for age-related macular degeneration. Graefes Arch Clin Exp Ophthalmol 2013;251:435–440.
24. Witkin AJ, Vuong LN, Srinivasan VJ, et al. High-speed ultrahigh resolution optical coherence tomography before and after ranibizumab for age-related macular degeneration. Ophthalmology 2009;116:956–963.
25. Hayashi H, Yamashiro K, Tsujikawa A, et al. Association between foveal photoreceptor integrity and visual outcome in neovascular age-related macular degeneration. Am J Ophthalmol 2009;148:83–89.e1.
26. Oishi A, Mandai M, Nishida A, et al. Remission and dropout rate of anti-VEGF therapy for age-related macular degeneration. Eur J Ophthalmol 2011;21:777–782.
27. Boulanger-Scemama E, Querques G, About F, et al. Ranibizumab for exudative age-related macular degeneration: a five year study of adherence to follow-up in a real-life setting. J Français d'Ophtalmologie 2015;38:620–627.

MEDIUM-TERM PERFLUORO-N-OCTANE AS RESCUE POSTOPERATIVE TAMPONADE FOR VERY COMPLEX RETINAL DETACHMENTS

ANATOMICAL AND FUNCTIONAL OUTCOMES

DHANANJAY SHUKLA, MS, MAMS,* ANURADHA DHAWAN, MS,† JAY KALLIATH, MS‡

Purpose: To report the anatomical and functional outcomes of medium-term perfluoro-n-octane (PFO) tamponade as a rescue procedure in very complex retinal detachments (RDs).

Methods: We reviewed the case records of 35 consecutive patients who underwent vitrectomy for very complex RDs due to diverse etiologies. The surgical complexity was so graded because of the intraoperative failure to ascertain complete retinal reattachment; perfluoro-n-octane was used as rescue tamponade for 2 to 4 weeks. The second intervention included additional membrane peeling, retinectomy, endophotocoagulation, and gas/silicone oil tamponade. The minimum follow-up was 3 months after the final intervention: the primary outcome was retinal reattachment and the secondary outcome was change in best-corrected visual acuity (BCVA).

Results: The most common presentations were severe trauma with retinal incarceration, preretinal and subretinal hemorrhage, or chronic/recurrent RDs with anterior proliferative vitreoretinopathy. Preoperative BCVA was ≤counting fingers in 31 (88.6%) patients. Complete retinal attachment without any tamponade was achieved in 33 (94.3%) eyes. best-corrected visual acuity improved in 30 (85.7%) eyes: 16 (45.7%) had BCVA ≥20/200 and 21 (60%) regained ambulatory vision (≥5/200). Two eyes developed keratopathy, and four needed antiglaucoma medications.

Conclusion: We achieved excellent anatomical outcomes and acceptable functional outcomes in nearly inoperable RDs with few side effects. Medium-term perfluoro-n-octane tamponade can be used as a salvage procedure in very complex RDs where intraoperative reattachment cannot be ensured.

RETINA 43:905–912, 2023

Complex or complicated retinal detachments (RDs) have been variously defined in the literature as those associated with proliferative vitreoretinopathy (PVR), trauma, inflammation, giant retinal tears, and postsurgical recurrences.[1–4] The unifying pathology in this heterogeneous compilation is PVR. The 5% to 10% cases of RDs that develop PVR remain a formidable challenge for vitreoretinal surgeons, notwithstanding the decades of innovations and improvements in surgical techniques, equipment, and adjuvants.[1] With progressive resurgeries and recurrent PVR, the chances of retinal reattachment and recovery of meaningful vision become bleaker.[3,5] At some point, the surgeon either declines further intervention[5] or takes the chance, sometimes only to abandon the procedure on the

From the *Ratan Jyoti Netralaya, India; †Calderdale Huddersfield Foundation NHS Trust Hospital, UK; and ‡NMC Specialty Hospital, UAE.

The study has been presented in part at Ocular TraumaCon Meeting, July 12 to 15, 2018, Chennai, India, jointly organized by Sankara Nethralaya, the Asia–Pacific Ophthalmic Trauma Society and the Ocular Trauma Society of India.

None of the authors has any financial/conflicting interests to disclose.

The study was performed at Ratan Jyoti Netralaya, Gwalior, India.

Reprint requests: Dhananjay Shukla, MS, MAMS, Ratan Jyoti Netralaya, 18 Vikas Nagar, Gwalior 474002, Madhya Pradesh INDIA; e-mail: daksh66@gmail.com

operating table in the face of irreparable PVR. Taking chances in similarly desperate situations may be worthwhile when the patient is young or one-eyed, in the hope for ambulatory vision, or at least a globe salvage. The use of perfluoro-n-octane (PFO, C_8F_{18}) as a short-term or medium-term tamponade in complex RDs has been reported in the literature for close to two decades.[6–12] These reports included detachments complicated by giant retinal tears,[8–10] trauma,[10] and inferior PVR,[7,11] where PFO was preferred over the conventional tamponade agents to reduce the recurrence of PVR and RD. Although both the functional and anatomical outcomes were good, the complexity of the reported cases was variable and mostly not severe enough to preclude tamponade with silicone oil or gas. This interventional case series records a senior surgeon's experience with very complex detachments where complete retinal reattachment could not be ensured intraoperatively, forcing the decision to leave PFO in the eyes as a rescue tamponade.

Materials and Methods

We reviewed the surgical case records of consecutive patients with complex RDs who underwent vitreoretinal surgery at a tertiary eye care center between 2016 and 2022. All the patients were operated by a single surgeon (D.S.) with 22 years of postfellowship surgical experience. The patients who underwent postvitrectomy medium-term PFO tamponade (2–4 weeks) and were followed up for at least three months after the last procedure (silicone oil removal or PFO–gas exchange) were included in this study. Preoperatively, patients were informed about the surgery, potential risks, benefits, and possible treatment outcomes and had signed informed consent for the procedure. To consider for inclusion in this study, a complex RD was defined as the RD with PVR Grade C posterior (diffuse/subretinal) or anterior (circumferential/anterior displacement) in ≥2 quadrants inferiorly ± superiorly, retinal incarceration or extensive subretinal hemorrhage in a penetrating/perforating eyeball trauma, RD with endophthalmitis, or a very longstanding total RD (>1 year duration) with subretinal strands or sheets. The subset of very complex RDs where PFO needed to be retained after intraoperative use had the following characteristics that prevented a reliable and complete retinal reattachment and barricade endophotocoagulation:

1. PVR or subretinal hemorrhage extensive enough to preclude retinal reattachment on table despite maximal membrane peeling/retinectomy (Figure 1).
2. Compromised visibility due to anterior segment trauma (repaired corneoscleral laceration/hazy cornea) hampering membrane peeling/endolaser photocoagulation (Figure 2).
3. Inflamed, necrotic midperipheral retina making endolaser unsafe (RD postendophthalmitis).

Data regarding complete ophthalmologic examination, including measurement of the best-corrected visual acuity (BCVA), slit-lamp biomicroscopy, intraocular pressure (IOP) indirect ophthalmoscopy, and fundus photography/B-scan ultrasonography at the baseline and at follow-up visits (one, three, six months after surgery, and every six months thereafter) were collected. Patients with preexisting glaucoma/macular degeneration were excluded from this study. This study complied with the Declaration of Helsinki and was approved by the institutional ethics committee.

Surgical Procedure

The surgical procedure involved 25G pars plana vitrectomy, base dissection with scleral depression, epiretinal and subretinal membrane removal to relieve traction, and relaxing retinectomies (if needed) to mobilize the stiff retina. Phacoemulsification or lensectomy was performed in phakic eyes to facilitate anterior membrane peeling and base dissection. Primary or secondary central posterior capsulotomy was performed in eyes with an intact posterior capsule after initial eight cases (vide infra). Perfluoro-n-octane (C_8F_{18}, Auro-Octane, Aurolab, Madurai, India) was used after initial membrane peeling to stabilize the posterior retina. Anterior membrane peeling was performed to a possible extent, and relaxing retinotomies were performed as needed. Intraocular foreign bodies were removed using intraocular forceps through enlarged sclerotomy. Perfluoro-n-octane was topped up until a complete vitreous cavity fill was achieved. Endophotocoagulation was then performed around the retinal breaks and into the periphery as far as feasible. Photocoagulation was deferred over unstable, inflamed, or necrotic retinal edge (especially in the eyes with trauma or endophthalmitis) or when visibility was compromised because of large corneal opacity/sutured corneal lacerations or peripheral vitreous exudates.

All surgeries were performed using the Alcon Constellation vitrectomy machine and a wide-angle noncontact viewing system. Scleral belt-buckle was not used in any patient, although one previously failed vitrectomy had concurrent encirclage. Postoperatively, patients were instructed to maintain a upright (face forward) or supine head position and to avoid face-down position.

After a period of 2 to 4 weeks, PFO was replaced with 1,500 centistokes silicone oil or a short-acting

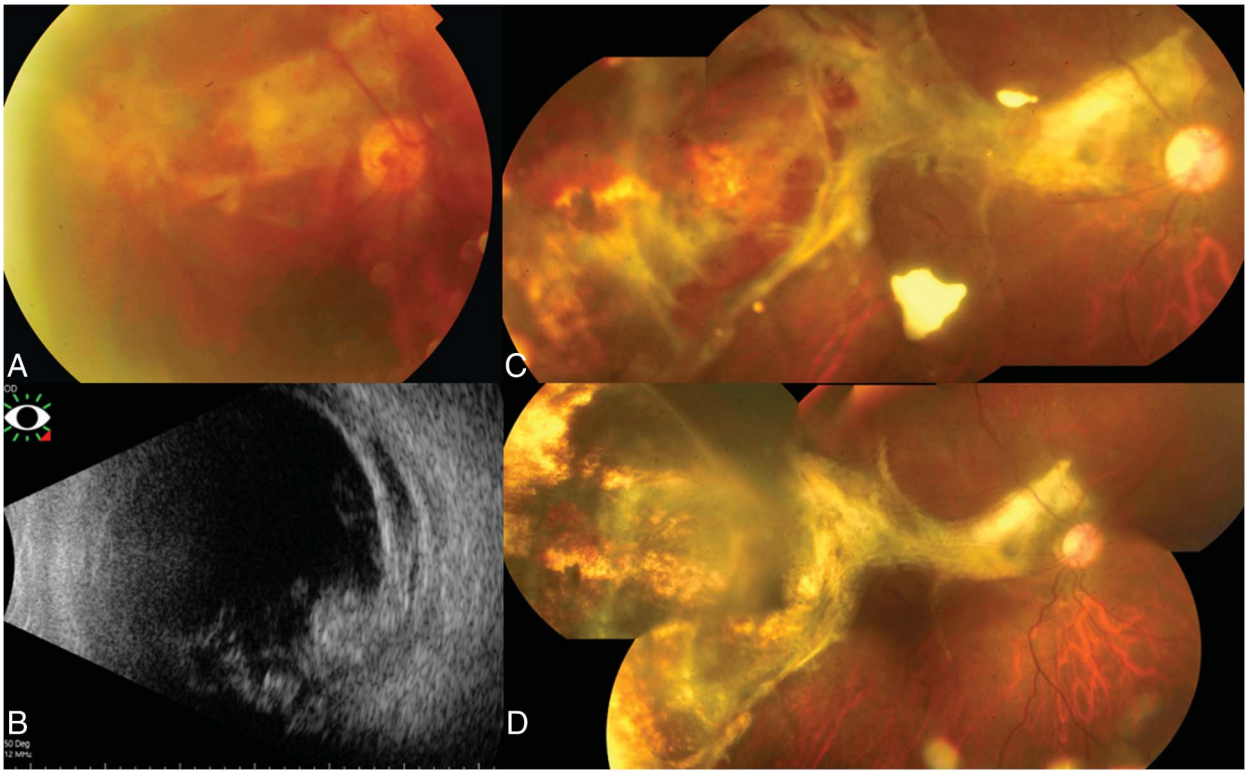

Fig. 1. This policeman suffered a blast injury in the right eye with a giant chorioretinal laceration and rupture temporally (**A**), the adjoining retina was detached and stiff, with subretinal fibrosis, as shown in B-scan ultrasonography (**B**). During vitrectomy, the reattached retina was stabilized under perfluoro-n-octane since the stiff, elevated edges could not be barricaded. Perfluoro-n-octane was exchanged with sulfur hexafluoride gas (SF_6, 25%) after 17 days, and the triamcinolone residues are visible a month after PFO–gas exchange (**C**). The retina remained attached with a recovery of best-corrected visual acuity of 20/400, 11 months after the last intervention (**D**).

(sulfur hexafluoride, SF_6) or long-acting (perfluoropropane, C_3F_8) gas. Additional membrane peeling, retinotomy, and endophotocoagulation were performed as required during PFO removal. The nature of post-PFO tamponade was based on the complexity of RDs and the extent of additional procedures during PFO removal. Silicone oil was retained beyond 3 to 6 months in the eyes with a high risk for redetachment (e.g., persistently stiff, elevated edge of the retinectomy under oil) or which had poor prognosis for visual gain with further surgeries.

The primary outcome was retinal reattachment without any tamponade at the end of the follow-up period. The secondary outcomes included change in BCVA, the number of operations required for complete retinal reattachment, nature of tamponade (silicone oil/gas), secondary glaucoma, keratopathy, or other postoperative complications. Besides the presence of RDs, retention of silicone oil in the eye at the conclusion of this study was also considered as anatomical failure.

Snellen BCVA was converted to a logarithm of minimum angle of resolution (logMAR) for statistical analysis. We used the decimal equivalent of 0.013 for a visual acuity of finger counting and 0.005 for hand motions. The logarithm of minimum angle of resolution values of 2.8 and 2.9 were assigned to light perception and no light perception (NLP), respectively. The comparison of preoperative and postoperative best-corrected logMAR Snellen visual acuity was performed using the Wilcoxon signed-rank test. Statistical analysis was performed using IBM SPSS Statistics 28.0.0 software.

Results

Two hundred and twenty-seven complex retinal detachments with a wide range of etiologies were operated by a single experienced surgeon at a tertiary eye care center over a 6-year period (January 2016–February 2022). A complete intraoperative retinal reattachment could not be ascertained in 35 eyes (35 patients), forcing the choice of leaving PFO in the eye as continued postoperative tamponade. Of the 35 patients included in this study, 22 were male, age ranged from 6 to 65 years (mean 30.9 years, median 27 years). The baseline characteristics of the patients are presented in Table 1. Baseline visual acuity was

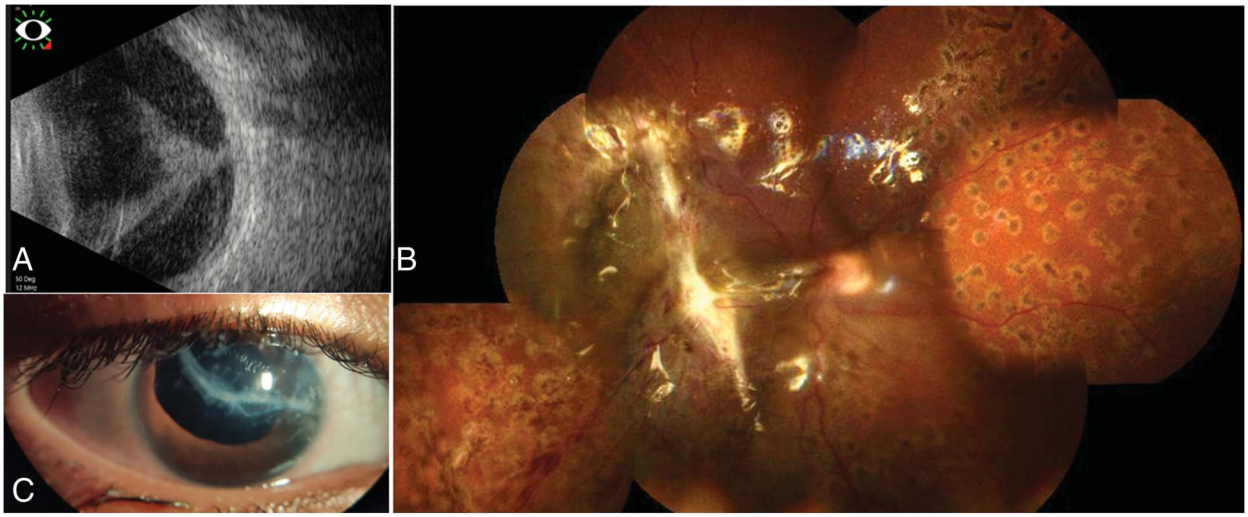

Fig. 2. A six-year-old child suffered an extensive globe laceration with a screwdriver. After primary corneal tear repair and cataract extraction, B-scan ultrasonography revealed a detached retina incarcerated at the macula (**A**). After media cleared sufficiently under topical and systemic corticosteroids, vitrectomy was performed, and the incarcerated macular retina was released as much as possible. Perfluoro-n-octane was left in situ to avoid central relaxing retinectomy. A month later, PFO was replaced with silicone oil after further membrane peeling and barricade endophotocoagulation (**B**). Silicone oil was removed after 4 months, and the retina remained attached 37 months after oil removal. The unaffected cornea remained clear despite the large scar; BCVA remained perception of light (**C**).

counting fingers or worse in 31 (88.6%) patients. Six patients were one-eyed with BCVA of hand motions–NLP in their other eye.

Morphologic characteristics of very complex RDs in the study eyes included inferior/inferolateral giant retinal tear (four eyes), retinal incarceration (three eyes), subretinal hemorrhage (five eyes), macular laceration (one eye), chorioretinal rupture (two eyes), impacted intraocular foreign body (two eyes), post-inflammation/necrosis retinal breaks (six eyes), tractional or combined mechanism RD (four eyes), and choroidal detachment (eight eyes). Three of the five cases of RDs with endophthalmitis were postcore vitrectomy, and one was postantibiotic injection. The overlapping etiologies of these presentations are summarized in Table 1. The duration of PFO tamponade ranged from 11 to 41 days (mean: 26.1; median: 26 days). In the postoperative period after PFO tamponade, hypopyon with inflammatory membrane was noted in one eye, high intraocular pressure was noted in four eyes, and PFO was seen in the anterior chamber in three eyes. All these adverse events were transient and were medically controlled. Dirty flake-like inflammatory deposits on posterior capsule and retina were observed predominantly in the initial 8 cases with intact posterior capsule. We subsequently started creating a primary posterior capsulotomy in all cases requiring cataract extraction or those with intact PC and did not observe the deposits on the retina or posterior capsule subsequently. There were no other signs of disproportionate inflammation in any eye.

After PFO removal, silicone oil injection was performed in 16 eyes and gas injection in 19 eyes (SF_6 in 11 eyes and C_3F_8 in 8 eyes). Of the 16 eyes with silicone oil tamponade, three developed recurrent RDs: one with oil in situ and two after silicone oil removal. In two eyes, retina was reattached with additional surgery and repeat silicone oil tamponade. Of the 19 eyes with gas tamponade, 2 eyes had recurrent retinal detachment during the follow-up period. Both had received SF_6 tamponade. They underwent additional surgery with silicone oil in one case and C_3F_8 in another. Both had attached retina at the final follow-up.

Complete retinal attachment without any tamponade at the final follow-up was achieved in 33 (94.3%) eyes. In one eye, retina was attached under oil, which was considered as anatomical failure; in another eye, the severely traumatized retina redetached after silicone oil removal. Both the surgical failures occurred in younger patients (below the median age of 27 years). There was no statistically significant difference in the rate of retinal attachment with silicone oil or gas tamponade after PFO removal ($P = 0.9$).

In the last follow-up, two patients (two eyes) had developed keratopathy and neither had PFO in the anterior chamber. One eye with visual potential underwent Descemet's stripping endothelial keratoplasty (DSEK) and improved to BCVA of 20/200, and the other eye remained at BCVA of hand motions. IOP was stabilized by antiglaucoma medication in four patients. Hypotony (IOP ≤6 mmHg) was noted in four eyes (12%). Small subretinal PFO bubbles were

Table 1. Baseline Characteristics of Patients and Etiologies of RDs

Parameter	No. (%)
Age (years)	
Mean ± SD	30.9 ± 16.06
Median	27
Range	6–65
Sex	
Male	22 (62.9)
Female	13 (37.1)
Operated eye	
Right	22
Left	13
Follow-up after last intervention (months)	
Mean ± SD	12.9 ± 12.6
Median	7
Range	3–57
Preoperative VA	
LP	23 (65.7)
HM–CF	8 (22.9)
20/1,250–20/200	4 (11.4)
Lens status (preoperative)	
Phakic	25
Pseudophakic	4
Aphakic	6
Etiology (overlapping groups)	
Trauma	10
Endophthalmitis-related	5
Chronic RD/complex treatment-naïve RD	7
Re-RD postvitrectomy	11
PDR with chronic extensive TRD	2

CF, counting fingers; HM, hand motions; LP, light perception; PDR, proliferative diabetic retinopathy; TRD, tractional retinal detachment.

trapped under paramacular retina in one eye. The final BCVA ranged from NLP to 20/30; 30 (85.7%) eyes had improved vision, four retained preoperative vision, and one eye got worsened. Sixteen (45.7%) eyes regained BCVA ≥20/200, and 21(60%) had ambulatory vision (≥5/200) (Table 2). Postoperative median logMAR Snellen BCVA (1.2; ≈20/320) was significantly better than preoperative median logMAR Snellen BCVA (2.8; ≈light perception) ($P < 0.0001$).

Discussion

This retrospective single-surgeon case series focused on 35 very complex RD surgeries, which required interim PFO tamponade as a salvage procedure. Most patients were legally blind in the eye to be operated and were likely to remain so in view of the residual detachment or long-term silicone oil tamponade with attendant complications.[5] Medium-term PFO tamponade (extended in six patients because of late review visits) allowed retinal reattachment in 94% eyes without any tamponade at the final visit; 17 (48.6%) did not require any intervention after PFO–gas exchange. Thirty eyes (85.7%) experienced visual improvement, and 21 eyes (60%) gained ambulatory vision. To the best of our knowledge, the role of PFO as a salvage tamponade for nearly inoperable complex detachments has not been reported in the literature so far.

Complex vitreoretinal surgeries, especially RDs with severe trauma or anterior/inferior PVR, with their high recurrence and failure rates, have long been a subject of myriad surgical manipulations, including tamponade with high-viscosity and heavy silicone oils,[13,14] double tamponade (perfluorodecalin + silicone oil),[15] and adjuncts such as systemic or intraocular corticosteroids, anti-VEGF agents, and immunosuppressants.[16] None of these procedures have shown any superiority to conventional management, notwithstanding the additional complications and expenses involved.[13,14,16] Universally, surgeons have most experience with silicone oil or perfluoropropane gas in such cases, which provide comparable although unsatisfactory outcomes in complex RDs.[13] Furthermore, these modest outcomes have been reported in

Table 2. Final Anatomical and Visual Outcomes

Parameter	No. (%)
Attached retina without any tamponade at the final FU	
Total number of eyes	33 (94.3)
Eyes with silicone oil tamponade post-PFO removal	15 (93.8)*
Eyes with gas tamponade post-PFO removal	18 (94.7)†
Anatomical failure at final FU	
Retina attached under silicone oil	1
Retina detached and inoperable	1
Phthisis	0
Surgeries required post-PFO tamponade for reattachment at the final FU	
Range	1–4
Mean	1.7
Median	2
Final BCVA	
20/30–20/200	16 (45.7)
<20/200–20/1,250	8 (22.8)
CF-LP	10 (28.6)
NLP	1 (2.9)
Change in BCVA (from preoperative to postoperative status)	
Improved	30 (85.7)
Stable	4 (11.4)
Worsened	1 (2.9)

*Success rate in eyes with silicone oil tamponade.
†Success rate in eyes with gas tamponade.
CF, counting fingers; FU, follow-up; LP, light perception; NPL, no light perception.

detachments with a range of complexity, as the definition of "complex RD" has been a variable in the literature, including not only advanced inferior and anterior PVR[2,4,7,11,14] but also much simpler cases than reported in this study, e.g., RD with PVR B-C and choroidal detachments.[17] Unlike this all-inclusive case series, studies reporting on RDs with inferior PVR frequently excluded trauma, diabetic detachments, endophthalmitis, and subretinal hemorrhage.[3,11,14] In very complex cases as included in this study, most surgeons choose silicone oil as long-term tamponade (sometimes for years), a Hobson's choice in absence of alternatives.[5,18] The double whammy of inferior predilection of PVR and insufficient inferior retinal tamponade by lighter-than-water silicone oil predisposes these complex RDs to anatomical failure after oil removal. Indeed, many of the studies which claimed good anatomical outcomes with silicone oil labeled oil-filled eyes as anatomical success,[2,3,5,19] although long-term silicone oil tamponade served only as a globe salvage procedure. If we apply the same surgical failure criteria as used in this study to the aforementioned studies, their success rates would reduce substantially (e.g., from 70–93% to ≈20–50%[2,3,19]). A recent study reported a surgical success rate of ≈75% not including eyes with residual oil. The better anatomical success was offset by multiple complications of long-term oil tamponade in some cases, leaving 75% of the cases legally blind (BCVA <20/200).[4] Another popular solution to the inefficiency of silicone oil for inferior PVR is the placement of an encircling band buckle, which has been claimed to obtain better single surgery outcomes in simple (but not complex) RDs,[20] although others dispute this claim.[21] In complex detachments, belt buckle has been reported by some to increase the surgical failure rates.[17] Two recent meta-analyses of approximately 16,000 eyes (including 8 randomized clinical trials) reported comparable outcomes with and without encirclage, sometimes with added complications of encircling band-like epiretinal membrane, band migration, strabismus, infection, etc., besides delayed postoperative recovery.[22,23]

Perfluoro-n-octane has been listed as a Class IIa short-acting medical device, meant for only intraoperative application.[24] Even with the conventional use, severe acute toxicity from PFO manufactured in Turkey, Germany, and India left 130 patients blind by necrotizing inflammation, vascular occlusion, and optic atrophy, attributable to the contaminants in the toxic batches.[25] Even without contaminants, PFO is known to cause mechanical damage by contact with retina, cornea, and trabecular meshwork and elicits ocular inflammatory response, which increases with the duration of PFO tamponade. The earlier use of PFO was therefore usually short term, e.g., in giant retinal tears to reduce the slippage of the tear edge and subsequent recurrence.[9,10] Besides retina, PFO-induced inflammation has been reported to affect cornea, lens, and trabecular meshwork.[26–28] However, it is noteworthy that all these studies date 1 to 2 decades back. A later analysis of 14 studies reported few serious adverse outcomes after short-term to medium-term tamponade (1–3 weeks) besides a reversible macrophage-mediated inflammatory response on the retina and lens in close to a third of the cases.[29] These flake-like dirty white deposits (macrophages engulfing PFO droplets) did not lead to PVR, cleared with corticosteroids after PFO removal,[6,26,29] and can be readily removed if required. We could circumvent this inflammatory response by creating a primary posterior capsulotomy in most cases, probably through drainage of the inflammatory mediators through the trabecular meshwork.

The largest published surgical experience on short-term and medium-term PFO tamponade has come from Charles et al.[6–8] In approximately 400 cases of PFO tamponade, they reported no irreversible retinal or corneal injury besides cataract formation (27% cases) and secondary ocular hypertension (34%); the inflammatory deposits were the most common complication, but they were reversible and did not affect the functional outcomes or reattachment rates; the latter were close to 90%.[6–8] Charles[30] summed up his 2 decade experience of over a 1,000 cases of medium-term PFO tamponade at the annual meeting of American Academy of Ophthalmology 2019, where he confirmed the previously reported excellent surgical outcomes and rubbished the claims of retinal or corneal toxicity. Like others,[31,32] we concur with these conclusions on the basis of our experience that PVR membranes did not progress under PFO in these very complex detachments, which could be reattached subsequently in >90% of the cases, similar to the reported success rates by Charles et al, as well as others. None of the three eyes with PFO droplets in the anterior chamber developed any keratopathy. Medically controlled secondary ocular hypertension persisted in four cases. Hypotony was noted in four eyes probably due to anterior PVR and need for multiple surgeries. Hypotony is a reported risk factor for surgical failure.[12] Although visual outcomes were modest in this case series, in view of the complexity of the cases, the anatomical outcomes compared with others' experience with less complex RDs were excellent.[2–8,12,14,15,17,19,28–30]

This series had the shortcomings inherent in a single-surgeon retrospective noncomparative small case series. The case selection was heterogenous, although it

reflected the real-time diversity of complex RDs in clinical practice. Inability to ensure intraoperative retinal reattachment was also a subjective criterion; another surgeon could arguably settle these detachments without PFO tamponade. The experience of a senior surgeon and review of the literature suggested the apparent inoperability of the recruited cases; the detachments of similar complexity have not been frequently documented, and the outcomes have been reported as uniformly disappointing (vide supra). The criteria of case selection for PFO tamponade were as objective as possible within these limitations. Finally, we retained PFO in the eyes for a longer time than that reported by several authors. The rationale for this extended tamponade was that our cases were far more complex than reported by the short-term users.[28,31,32] Furthermore, the optimum duration for super normal (300%) chorioretinal adhesion is reported to be about 2 weeks.[33] Finally, toxicity has not been clinically observed by others with similar duration of PFO tamponade.[6–8,29]

We report encouraging anatomical and functional outcomes with PFO tamponade in a unique group of very complex RDs which had a high probability of ending up with inoperable redetachments or with prolonged silicone oil tamponade and its attendant complications. We suggest that medium-term PFO tamponade is a viable option in detachments with extensive PVR that cannot be satisfactorily reattached intraoperatively, especially in young subjects with severely traumatized or infected eyes.

Key words: perfluoro-n-octane tamponade, complex retinal detachment, proliferative vitreoretinopathy, ambulatory vision.

Acknowledgments

The authors thank Mr. Rohit Ravindra Dusane for the proficient help with statistical analysis.

References

1. Charteris DG. Proliferative vitreoretinopathy: revised concepts of pathogenesis and adjunctive treatment. Eye 2020;34:241–245.
2. Banaee T, Hosseini SM, Eslampoor A, et al. Peripheral 360° retinectomy in complex retinal detachment. Retina 2009;29: 811–818.
3. Quiram PA, Gonzales CR, Hu W, et al. Outcomes of vitrectomy with inferior retinectomy in patients with recurrent rhegmatogenous retinal detachments and proliferative vitreoretinopathy. Ophthalmology 2006;113:2041–2047.
4. Hocaoglu M, Karacorlu M, Muslubas IS, et al. Peripheral 360 degree retinotomy, anterior flap retinectomy, and radial retinotomy in the management of complex retinal detachment. Am J Ophthalmol 2016;163:115–121.e1.
5. Vidne-Hay O, Platner E, Alhalel A, Moisseiev J. Long-term silicone oil tamponade in eyes with complicated retinal detachment. Eur J Ophthalmol 2022;32:1728–1734.
6. Sigler EJ, Randolph JC, Charles S. Foreign body response within postoperative perfluoro-N-octane for retinal detachment repair: clinical features, grading system, and histopathology. Retina 2014;34:237–246.
7. Sigler EJ, Randolph JC, Calzada JI, Charles S. Pars plana vitrectomy with medium-term postoperative perfluoro-N-octane for recurrent inferior retinal detachment complicated by advanced proliferative vitreoretinopathy. Retina 2013;33: 791–797.
8. Randolph JC, Diaz RI, Sigler EJ, et al. 25-gauge pars plana vitrectomy with medium-term postoperative perfluoro-n-octane for the repair of giant retinal tears. Graefes Arch Clin Exp Ophthalmol 2016;254:253–257.
9. Rofail M, Lee LR. Perfluoro-n-octane as a postoperative vitreoretinal tamponade in the management of giant retinal tears. Retina 2005;25:897–901.
10. Sirimaharaj M, Balachandran C, Chan WC, et al. Vitrectomy with short term postoperative tamponade using perfluorocarbon liquid for giant retinal tears. Br J Ophthalmol 2005;89:1176–1179.
11. Naz S, Naz U, Fahad HM, Rizvi SF. Outcomes of using perfluorocarbon liquid as postoperative tamponade in complex inferior retinal detachments. J Coll Physicians Surg Pak 2022;32:1454–1458.
12. Bhurayanontachai P, Seepongphun U. Outcomes of a postoperative perfluorocarbon liquid tamponade for complex retinal detachments: 12 years of experience in southern Thailand. BMC Ophthalmol 2020;20:358.
13. Schwartz SG, Flynn HW Jr, Wang X, et al. Tamponade in surgery for retinal detachment associated with proliferative vitreoretinopathy. Cochrane Database Syst Rev 2020;5: CD006126.
14. Dimopoulos S, William A, Voykov B, et al. Results of different strategies to manage complicated retinal re-detachment. Graefes Arch Clin Exp Ophthalmol 2021;259:335–341.
15. Zanzottera EC, Marchese A, Bandello F, Coppola M. Intraocular perfluorodecalin and silicone oil tamponade (double filling) in the management of complicated retinal detachment: functional and anatomical outcomes using small-gauge surgery. Graefes Arch Clin Exp Ophthalmol 2022;260:1105–1112.
16. Wu F, Eliott D. Molecular targets for proliferative vitreoretinopathy. Semin Ophthalmol 2021;36:218–223.
17. Adelman RA, Parnes AJ, Sipperley JO, Ducournau D. European Vitreo-Retinal Society (EVRS) Retinal Detachment Study Group. Strategy for the management of complex retinal detachments: the European vitreo-retinal society retinal detachment study report 2. Ophthalmology 2013;120:1809–1813.
18. Constable IJ, Nagpal M. Proliferative vitreoretinopathy. In: Schachat AP, ed. Ryan's Retina. 3. St. Louis: Elsevier; 2018:2031–2051.
19. Dave VP, Pathengay A, Relhan N, et al. Endophthalmitis and concurrent or delayed-onset rhegmatogenous retinal detachment managed with pars plana vitrectomy, intravitreal antibiotics, and silicone oil. Ophthalmic Surg Lasers Imaging Retina 2017;48:546–551.
20. Starr MR, Obeid A, Ryan EH, et al. Primary retinal detachment outcomes (PRO) Study Group. Retinal detachment with inferior retinal breaks: primary vitrectomy versus vitrectomy with scleral buckle (PRO Study Report No. 9). Retina 2021;41:525–530.
21. Hébert M, You E, Garneau J, et al. Outcomes in primary uncomplicated rhegmatogenous retinal detachment repair using pars plana vitrectomy with or without scleral buckle. Retina 2022;42:1161–1169.

22. Eshtiaghi A, Dhoot AS, Mihalache A, et al. Pars plana vitrectomy with and without supplemental scleral buckle for the repair of rhegmatogenous retinal detachment: a Meta-analysis. Ophthalmol Retina 2022;6:871–885.
23. Dhoot AS, Popovic MM, Nichani PAH, et al. Pars plana vitrectomy versus scleral buckle: a comprehensive meta-analysis of 15,947 eyes. Surv Ophthalmol 2022;67:932–949.
24. Romano MR, Ferrara M, Nepita I, et al. Biocompatibility of intraocular liquid tamponade agents: an update. Eye 2021;35:2699–2713.
25. Januschowski K, Irigoyen C, Pastor JC, et al. Retinal toxicity of medical devices used during vitreoretinal Surgery: a critical overview. Ophthalmologica 2018;240:236–243.
26. Elsing SH, Fekrat S, Green WR, et al. Clinicopathologic findings in eyes with retained perfluoro-n-octane liquid. Ophthalmology 2001;108:45–48.
27. Georgalas I, Ladas I, Tservakis I, et al. Perfluorocarbon liquids in vitreoretinal surgery: a review of applications and toxicity. Cutan Ocul Toxicol 2011;30:251–262.
28. Drury B, Bourke RD. Short-term intraocular tamponade with perfluorocarbon heavy liquid. Br J Ophthalmol 2011;95:694–698.
29. Figueroa MS, Casas DR. Inflammation induced by perfluorocarbon liquid: intra- and postoperative use. Biomed Res Int 2014;2014:1–8.
30. Charles ST. Giant Retinal Tears: Tips, Tricks, and a Novel Tamponade. Retina Subspecialty Day. San Francisco, United States: American Academy Ophthalmology; 2019. 2019 Oct 11-12. aaosub-2019-ret-syllabus-pdf. https://www.aao.org/Assets/7364867f-bde6-421f-8269-253cd29a6b86/637054418220570000/aaosub-2019-ret-syllabus-pdf?inline=1.
31. Imaizumi A, Kusaka S, Noguchi H, et al. Efficacy of short-term postoperative perfluoro-n-octane tamponade for pediatric complex retinal detachment. Am J Ophthalmol 2014;157:384–389.e2.
32. Babu N, Kohli P, Kumar K, et al. Two-staged surgery as an alternative to buckle-vitrectomy for rhegmatogenous retinal detachment complicated by choroidal detachment. Int Ophthalmol 2021;41:135–141.
33. Yoon YH, Marmor MF. Rapid enhancement of retinal adhesion by laser photocoagulation. Ophthalmology 1988;95:1385–1388.

SUBRETINAL LIPID GLOBULES AN EARLY BIOMARKER OF MACULAR NEOVASCULARIZATION IN EYES WITH INTERMEDIATE AGE-RELATED MACULAR DEGENERATION

SERENA FRAGIOTTA, PHD,* MARIACRISTINA PARRAVANO, MD,† ELIANA COSTANZO, MD,† DANIELE DE GERONIMO, MD,† MONICA VARANO, MD,† PEDRO FERNÁNDEZ-AVELLANEDA, MD,‡ K. BAILEY FREUND, MD§¶

Purpose: To explore the association between subretinal lipid globules (SLGs) detected in eyes with intermediate age-related macular degeneration with the presence of nonexudative macular neovascularization.

Methods: This was a retrospective analysis of 113 consecutive patients with bilateral intermediate age-related macular degeneration (226 eyes) followed for a least 6 months. All eyes underwent multimodal imaging with fundus autofluorescence, spectral-domain optical coherence tomography, and optical coherence tomography angiography. Subretinal lipid globules were identified on spectral-domain optical coherence tomography as round hyporeflective lesions measuring 31 to 157 μm located between the ellipsoid zone and the retinal pigment epithelium/Bruch membrane complex. Nonexudative macular neovascularization was detected with optical coherence tomography angiography. The features of NE-MNV lesions detected in eyes with SLGs were compared with those in eyes without SLGs.

Results: Subretinal lipid globules were identified in 15 eyes of which 14 eyes (93.3%) demonstrated NE-MNV on optical coherence tomography angiography. In the remaining 98 eyes without SLGs, 18 (18.4%) displayed NE-AMD on optical coherence tomography angiography. The macular neovascularization area was larger in the SLG subgroup (+0.38 vs. +0.21 mm^2, P = 0.008) and showed faster horizontal growth (+727 μm, CI 95% 250.4, 1,205.4) than MNV in eyes without SLGs (+64.9 μm, CI 95%, 24.3, 154) on optical coherence tomography B-scans. After a mean of 11.6 months, the conversion rate to exudative MNV was similar between eyes with SLGs and those without SLGs [8/26 (38.5%) versus 3/13 (27.3%), P = 0.56)].

Conclusion: The detection of SLGs in eyes with intermediate age-related macular degeneration was strongly correlated with the presence of NE-MNV. Although these MNV lesions were larger and grew faster than NE-MNV detected in eyes lacking SLGs, the rates of conversion to exudative MNV appeared similar.

RETINA 43:913–922, 2023

Subretinal lipid globules (SLGs) were recently described as an optical coherence tomography (OCT) biomarker of subretinal exudation. Subretinal lipid globules are believed to represent small spherical hyporeflective lipid droplets located between the photoreceptor outer segments and the apical processes of the retinal pigment epithelium (RPE).[1] The OCT features of SLGs resemble choroidal lipid globules described by Friedman and Smith on histopathology[1,2] as sudanophilic and osmophilic structures located in the extravascular and extracellular compartments. However, this feature lacks a direct clinicopathologic comparison within the same eye. Choroidal lipid globules represented a common histopathologic finding visible on both healthy and diseased eyes, often localized in the anterior choroid close to Bruch membrane.[2] Querques et al[3–5] coined the term "choroidal caverns" to describe the OCT findings of hyporeflective cavities occupying

areas devoid of vessels or blood flow, as confirmed on both indocyanine green angiography and OCT angiography (OCTA).[3] While these authors speculated that these structures corresponded to nonperfused ghost vessels and stromal pillars, Dolz-Marco et al showed that the multimodal imaging features of choroidal caverns, including a characteristic OCT hypertransmission tail, were more consistent with the choroidal lipid globules described by Friedman and Smith. These authors also demonstrated sub-RPE lipid globules to be a common feature of macular neovascularization (MNV) in eyes with age-related macular degeneration (AMD).[5]

The multimodal imaging features and optical proprieties of SLGs were detailed in the context of neovascular AMD as round hyporeflective lesions accompanied by a characteristic hypertransmission tail on OCT B-scans.[1] The hypertransmission tail relates to reduced signal attenuation through oil and a lensing effect created by a higher refractive index compared with the surrounding tissue. Subretinal lipid globules are frequently seen in eyes with type 1 MNV receiving intravitreal anti–vascular endothelial growth factor therapy, suggesting a likely connection with exudation from neovascular tissues.[1] In this study, we explored the presence of SLGs as a potential biomarker for identifying subclinical or nonexudative macular neovascularization (NE-MNV) in eyes with intermediate AMD. The associations of SLGs with NE-MNV lesion morphology, growth, and conversion to exudative MNV were investigated.

Material and Methods

A total of 113 patients with intermediate AMD according to the Beckman classification[6] and a minimum follow-up of 6 months were retrospectively evaluated. Patients were consecutively enrolled at IRCCS-Bietti Foundation after the approval of the Institutional Review Board committee. This study adhered to the tenets of the Declaration of Helsinki.

Patients were considered eligible if they presented complete medical and demographic records and multimodal imaging, including fundus autofluorescence (FAF), spectral-domain optical coherence tomography, and OCTA with either Heidelberg Spectralis OCT (HRA + optical coherence tomography, Heidelberg Engineering, Heidelberg, Germany) or PLEX Elite 9000 (Carl Zeiss Meditec, Inc, Dublin, CA). Exclusion criteria were severe ocular media opacities interfering with the imaging acquisition at any follow-up point, axial length $>$ 26 mm, or refractive error $>$6 diopters, complete RPE and outer retinal atrophy according to the CAM criteria,[7] the presence of other ophthalmic pathologies, and poor-quality images (signal strength index, SSI $<$8 for PLEX Elite, and a signal-to-noise ratio $<$25 dB for Spectralis OCTA), or motion artifacts. The eye with the highest image quality on cross-sectional and longitudinal evaluations was selected when both eyes were potentially eligible.

Multimodal Imaging

All patients underwent spectral-domain optical coherence tomography examination (Heidelberg Spectralis software, version 1.10.2.0) using a minimum scanning protocol of 20 × 20-degree rectangle centered on the fovea and 25 B-scans (~235 μm of spacing). However, a 49 B-scan (~125 μm of spacing) pattern was preferred in most cases when available. The baseline scan was set as a reference for repeated OCT examinations, acquiring all the subsequent scans using a "follow-up" mode to ensure reproducibility. For Spectralis OCTA, acquisition protocols included 3 × 3-mm or 6 × 6-mm volume cubes using the fully automated segmentation algorithms avascular complex and choriocapillaris. The boundaries were manually adjusted to maximize the visualization of the neovascular lesion if needed. Fundus autofluorescence was acquired during the same session through either Spectralis HRA + OCT (488 nm excitation, barrier filter transmitted light from 500 to 680 nm, 30° × 30°) or Topcon TRC-50DX (535–585 nm excitation, 615–715 barrier filter). Fluorescein and/or indocyanine green angiography were performed to confirm MNV activation or subtype if needed.

Swept-source OCTA using the PLEX Elite 9000 (software version 1.7.027959) was acquired with

From the *Ophthalmology Unit, Department NESMOS, S. Andrea Hospital, University of Rome "La Sapienza", Rome, Italy; †UOS Retina, IRCCS-Fondazione Bietti, Rome, Italy; ‡Department of Ophthalmology, Basurto University Hospital, Bilbao, Spain; §Vitreous Retina Macula Consultants of New York, New York, New York; and ¶Department of Ophthalmology, NYU Grossman School of Medicine, New York, New York.

The present work is supported by The Macula Foundation, Inc., New York, New York.

The remaining authors have no proprietary/financial interest regarding the publication of this study.

Parravano reports personal fees from Allergan, Novartis, Bayer, Zeiss, Omikron, Alfaintes, and Sifi outside the submitted work. Monica Varano reports personal fees from Allergan, Novartis, Bayer, and Sifi outside the submitted work. K. B. Freund is a consultant for Heidelberg Engineering, Zeiss, Allergan, Bayer, Genentech, and Novartis and receives research support from Genentech/Roche.

Reprint requests: Mariacristina Parravano, MD, IRCCS-Fondazione Bietti, Via Livenza 3, 00198 Roma RM, Italy; e-mail: mcparravano@gmail.com

3-mm and 6-mm volume cubes using active eye tracking, and projection artifact removal was enabled during image analysis. Automated segmentation of the RPE and RPE-fit approximating Bruch membrane were used as the upper and lower boundaries, respectively, to create the en face OCTA projections used to visualize Type 1 MNV.[8] All the patients analyzed were imaged with OCT and OCTA using the Spectralis, and then subsequently with PLEX Elite, for confirmation, when a MNV flow signal was detected with the Spectralis. Two experienced examiners (S.F. and E.C.) manually corrected segmentation errors when present.

Subretinal Lipid Globule Characterization and Image Analysis

Diagnostic criteria for SLGs included round hyporeflective structures with diameters ranging from 31 to 157 μm and a characteristic hypertransmission tail on OCT B-scans. These structures were located between the ellipsoid zone and the RPE/Bruch membrane complex. The integrity of RPE was verified through a multimodal imaging approach using color fundus photograph, near-infrared reflectance, FAF, and serial OCT B-scans. With structural en face OCT, SLGs appeared hyporeflective with the segmentation of the subretinal compartment. Segmentation of the choroid

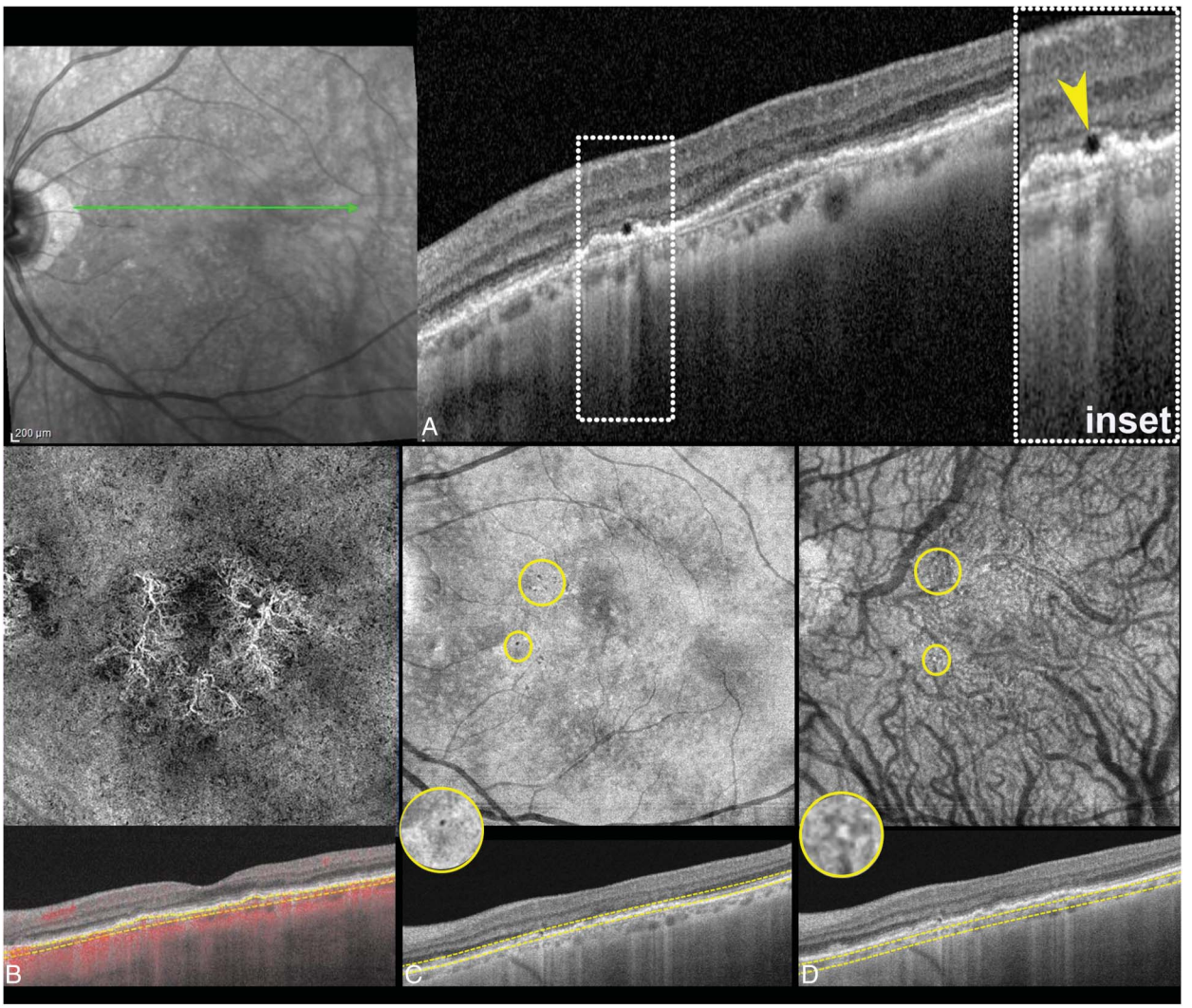

Fig. 1. Imaging features of subretinal lipid globules. **A.** Spectral-domain optical coherence tomography B-scans showing SLGs as round hyporeflective structures (yellow arrowhead, inset) with a characteristic hypertransmission tail. **B.** Swept-source OCT angiography (OCTA, PLEX elite 9000) slab segmented using RPE–RPE fit automatic segmentation demonstrated a Type 1 MNV lesion (better seen on magnification, inset). **C.** Structural OCT slab obtained with a customized segmentation (RPE fit, top: −57, bottom: 6) passing through the SLGs shows round hyporeflective lesions (yellow circles). **D.** Structural customized OCT slab (RPE fit, top: 30, bottom: 100) captures the projection tails of SLGs as round areas of hyperreflectivity within the choroid (yellow circles). On magnification, the corresponding B-scan lesions are isolated in C.

Table 1. Demographic of the Overall Population and the Association of Subretinal Lipid Globules and Double-Layer Sign With the Diagnosis of Nonexudative Macular Neovascularization

	Overall iAMD Population (n = 113)	
Age	71.2 ± 8.9	
Sex, F	76/113 (67.3)	
	SLGs	**DLS**
Sensitivity	43.7%	84.4%
Specificity	98.8%	88.9%
PPV	87.5%	55.4%
NPV	91.6%	97.2%
Youden's index	0.42	0.73

below the SLGs helped identify their characteristic hyperreflective projection tails (Figure 1).[1]

After SLGs were identified, two expert graders (S.F. and E.C.) reviewed the OCTA volumes of the entire intermediate age-related macular degeneration (iAMD) cohort for the presence of NE-MNV at any time point. In the case of disparate gradings, a third senior retinal specialist (M.P.) was consulted. The characteristics of NE-MNV lesions were analyzed at baseline and longitudinally to identify potential findings correlating with the presence or absence of SLGs. The greatest linear diameters (vertical and horizontal) on the fibrovascular pigment epithelium detachment of interest were measured using the digital calipers provided by the Spectralis review software. The graders also assessed the OCT B-scans for the presence of a double-layer sign (DLS) defined as two hyperreflective bands separated by a narrow hyporeflective space. The two reflective layers comprised the RPE-basal lamina complex and the Bruch membrane.[9] The MNV area on en face OCTA was manually traced using caliper tools provided by both SD and swept-source OCTA review software. Patients with NE-MNV and SLGs were matched 1:1 for age, sex, follow-up time, and image quality with controls consisting of NE-MNV patients without SLGs to account for the differences and homogenize the comparisons between groups for the main characteristics.

Exudative changes due to MNV were defined by the presence of subretinal fluid, intraretinal fluid, hemorrhage, hyperreflective exudation, or active leakage on dye angiography when these features were judged to be secondary to the MNV lesion.[10]

Statistical Analysis

Quantitative data were reported as mean ± SD or median (interquartile range, IQR) after verifying the distribution of normality through Shapiro–Wilk test. Categorical variables were analyzed using the Pearson chi-square test or Fisher exact test. The paired *t*-test was used to calculate differences within the same population at two different time points while the unpaired *t*-test was performed to assess the differences between groups at a given time point (Shapiro–Wilk, $P > 0.05$). The Wilcoxon signed-rank test (also known as the Mann–Whitney *U* test) was used as a nonparametric test (Shapiro–Wilk, $P < 0.05$). The prevalence of NE-MNV was adjusted using the data from the existing literature, considering only the largest observational studies (>50 cases) available. The estimated average prevalence was 13.9% (CI 95%: 9.56, 18.3).[11–15] The McNemar test was used to compare the discordance between the dichotomous response in detecting NE-MNV when observing SLGs and DLS. Statistical significance was set at $P < 0.05$. All calculations were carried out using SPSS statistical software (version 25; SPSS, Inc., Chicago, IL). To further understand the diagnostic performance for the biomarkers considered, the package cutpointr, version 1.1.2, was used in RStudio 2022.07.1. Youden's index was calculated to evaluate the overall discriminative power of either SLG or DLS biomarkers. The index ranges between 0 and 1, representing perfect diagnostic accuracy by 1 [Youden[16]'s index= (sensitivity + specificity)-1]. Moreover, a Cox regression model was used to predict the probability of exudative MNV based on the presence of SLGs and the follow-up time.

Results

A total of 15 of 113 iAMD eyes exhibited SLGs with a prevalence of 13.3%. Among the 15 eyes with SLGs, OCTA detected NE-MNV in 14 of 15 (93.3%) eyes, while in the remaining eyes without SLGs, OCTA detected NE-MNV in only 18 of 98 (18.4%) eyes.

Sensitivity, specificity, positive predictive value (PPV), negative predictive value, and Youden's index for SLGs and DLS are summarized in Table 1. PPV and negative predictive value included in the table were calculated using the adjusted prevalence of 13.9%. The accuracy of the SLG signature was 91.3%. The NE-MNV prevalence calculated in our sample was higher (28.3%, CI 95%: 0.19, 0.36), modifying the PPV and negative predictive value to 94.4% and 81.9%, respectively, and the accuracy to 83.5%.

Overall, 36 of 113 eyes presented a DLS (31.8%), of which 27 eyes (75%) exhibited NE-MNV on OCTA. The sensitivity and specificity for DLS were 84.4% and 88.9%, respectively, with a PPV of 55.4% and negative predictive value of 97.2%, considering the

Table 2. Demographic and Clinical Characteristics in Eyes With Nonexudative Macular Neovascularization With Subretinal Lipid Globules (SLGs) or Without SLGs (Controls)

	SLGs	Controls	*P*
Age	73.9 ± 7.4	72.1 ± 6.8	0.61
Sex, F	9/13 (69.2%)	6/13 (46.2%)	0.23
Follow-up time (months)	14 (13)	9 (15)	0.77*
Drusen phenotypes			0.01
Drusen	6/13 (46.2%)	1/13 (92.3%)	
Drusen + SDD	7/13 (53.8%)	12/13 (7.7%)	

F: female. The control group consisted of eyes with nonexudative macular neovascularization in the absence of SLGs.*For the Shapiro–Wilk test, *P*-value<0.05, and the Wilcoxon signed-rank test was used as a nonparametric test. Values are reported as median (IQR) if not normally distributed.

adjusted prevalence. The accuracy for DLS was 88.3%. The PPV and negative predictive value changed to 74.7% and 93.6%, respectively, when using the study prevalence, while the accuracy was 87.6%. The proportion of patients classified as having MNV was significantly different when observing SLGs and DLS ($P < 0.001$) despite the association between these two signatures (McNemar test, $P < 0.001$).

Clinical Characteristics of NE-MNV Associated With Subretinal Lipid Globules

In the SLG subgroup, one eye (1/15, 6.66%) was excluded from further analysis because the MNV lesion extended beyond the borders of the OCTA slabs, limiting the ability to measure and trace the lesion boundaries. The control group consisted of 13 age-matched and sex-matched NE-MNV eyes without SLGs fulfilling the inclusion criteria. The main demographic and clinical characteristics of the two cohorts are summarized in Table 2. Eyes with SLGs exhibited a higher prevalence of drusen combined with subretinal drusenoid deposits compared with the control group (53.8% vs. 7.7%, $P = 0.01$). Morphologic features of the NE-MNV lesions associated with SLGs are reported in Table 3. The fibrovascular pigment epithelium detachments associated with SLGs were larger (+563 μm, CI 95%: 29.6, 1,097.7) compared with the control group while the pigment epithelium detachment height, although numerically greater in eyes with SLGs, did not reach statistical significance. The MNV area measured on OCTA slabs was similar between groups at baseline.

Interestingly, as shown in Table 3, choroidal thickness was thinner in the SLG group both beneath the MNV lesion (−74.7 μm) and at the fovea (−84.1 μm).

Longitudinal Evaluation of the NE-MNV

The median follow-up time for each subgroup is reported in Table 2. On OCT B-scans, lateral growth of NE-MNV lesions associated with SLGs was greater (+727 μm, CI 95%, 250.4, 1,205.4, $P = 0.001$) than that seen in the control group (+64.9 μm, CI 95%, 24.3, 154). Similarly, the OCTA area measurements of NE-MNV in SLG eyes (+0.38 mm^2, CI 95%, 0.006, 0.73) were nearly twice that of controls (+0.20 mm^2, CI 95%, 0.28, 0.69, $P = 0.008$) (Figure 2). The NE-MNV lesions in the control group remained stable in horizontal ($P = 0.14$) and vertical ($P = 0.15$) growth and neovascular area expansion on OCTA ($P = 0.72$) (Figure 3). Table 3 summarizes morphologic characteristics at the last follow-up before exudative conversion.

After a mean of 11.6 months, 8 of 26 eyes converted exudative MNV, of which 5 of 13 eyes (38.5%, three eyes developed Type 1 MNV and two eyes developed

Table 3. Morphometric Characteristics of the Nonexudative Macular Neovascularization in Eyes With Subretinal Lipid Globules (SLGs) and Controls

	Baseline			Last Follow-Up		
	SLGs	Control	P	SLGs	Control	P
PEDw	1,454 ± 795	775.1 ± 505.3	0.01*	2,131.4 ± 1,133.8	858.4 ± 674.3	0.007*
PEDh	86 ± 27.9	56 ± 29.8	0.21	105 ± 77.9	54.7 ± 39.5	0.07*
CTles	140 ± 47.8	231 ± 101	0.03	130 ± 41	226.6 ± 98.1	0.06
SfCT	163.4 ± 62.1	260 ± 95.3	0.01	136.4 ± 57.3	230.4 ± 90.9	0.05
CMT	273 ± 26.8	282.6 ± 17.4	0.72	274 ± 40.6	287.4 ± 36.9	0.44
MNVa	0.48 ± 0.34	0.53 ± 0.96	0.17*	0.89 ± 0.71	0.89 ± 1.87	0.05*

CMT, central macular thickness; CTles, choroidal thickness calculated below the MNV; MNVa, area of macular neovascularization (mm^2); PED, pigment epithelium detachment; PEDw, PED width; PEDh, PED height; SfCT, subfoveal CT. The control group consisted of eyes with nonexudative MNV in the absence of SLGs.*For the Shapiro–Wilk test, *P*-value<0.05, and the Wilcoxon signed-rank test was used as a nonparametric test.

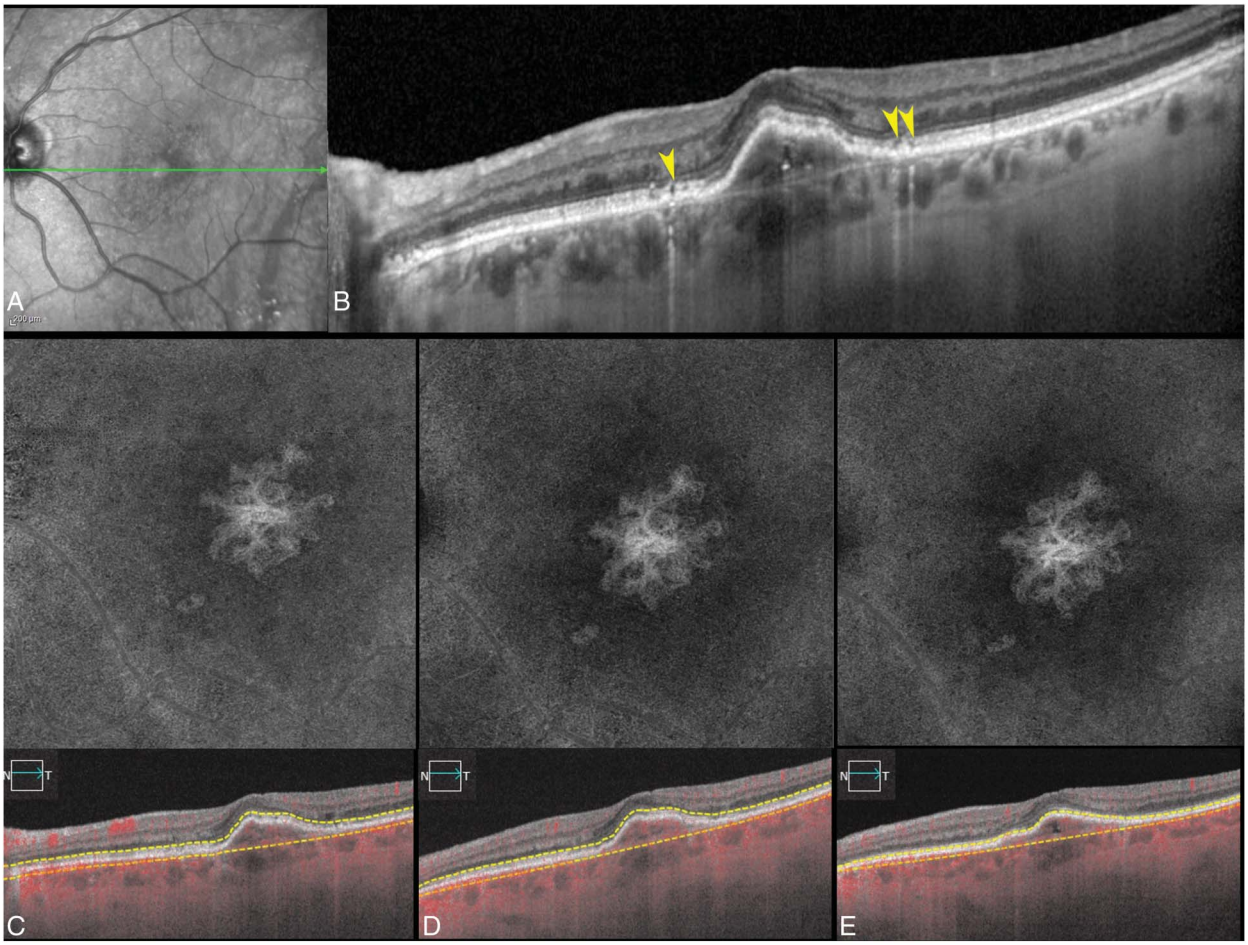

Fig. 2. Progression of Type 1 nonexudative macular neovascularization associated with subretinal lipid globules. **A.** Near-infrared reflectance. **B.** Spectral-domain optical coherence tomography B-scan passing through the NE-MNV lesion and showing multiple SLGs at the border of the lesion (yellow arrowheads). Serial swept-source OCT angiography (OCTA, PLEX elite 9000) slabs were obtained at baseline (**C**), 4 months (**D**), and 15 months of follow-up (**E**). The neovascular lesion is segmented using an RPE–RPE fit automatic segmentation.

Type 3 MNV) (Figure 4) in the SLG group and 3 of 13 (27.3%, Type 1 MNV) eyes in the control group, with no significant differences in the rate of conversion between groups ($P = 0.40$). The Cox regression model confirmed a nonsignificant rate of conversion into exudative MNV in the presence of SLGs (HR: 1.45, 95% CI, 0.35, 6.1, $P = 0.61$).

Duration of SLGs Over Time, Integrity of Overlying RPE Before and After Their Disappearance

Multiple SLGs were found in 9 of 13 eyes (69.2%), demonstrating a transitory and intermittent nature in all the cases examined. The integrity of RPE on OCT B-scans and FAF was confirmed in 10 of 13 eyes (76.9%) at baseline and after SLG disappearance. In the remaining 3 cases, 1 of 3 eyes presented iRORA and 2 of 3 of the eyes demonstrated a poor discernible RPE band on OCT with hypoautofluorescence on FAF at the last follow-up.

Discussion

This study investigated the clinical significance and prognostic implications of SLGs in eyes with iAMD. Multimodal retinal imaging was important in identifying these small structures that can be misinterpreted as other hyporeflective subretinal features, including subretinal fluid, outer retinal tubulation, and calcific nodules.[1,17–19] The frequency of SLGs in eyes with iAMD is likely underestimated, given a rather high prevalence of 13.3% in our cohort. Other factors that may contribute to an underestimation of SLGs in retrospective study designs include their transient nature and small size requiring dense OCT raster patterns to detect their presence.

In our study, a characteristic hypertransmission tail was an important criterion for identifying SLGs.[1,5] This OCT finding relates to the optical properties of these clear spherical structures acting as small lenses rather than choroidal hypertransmission due to

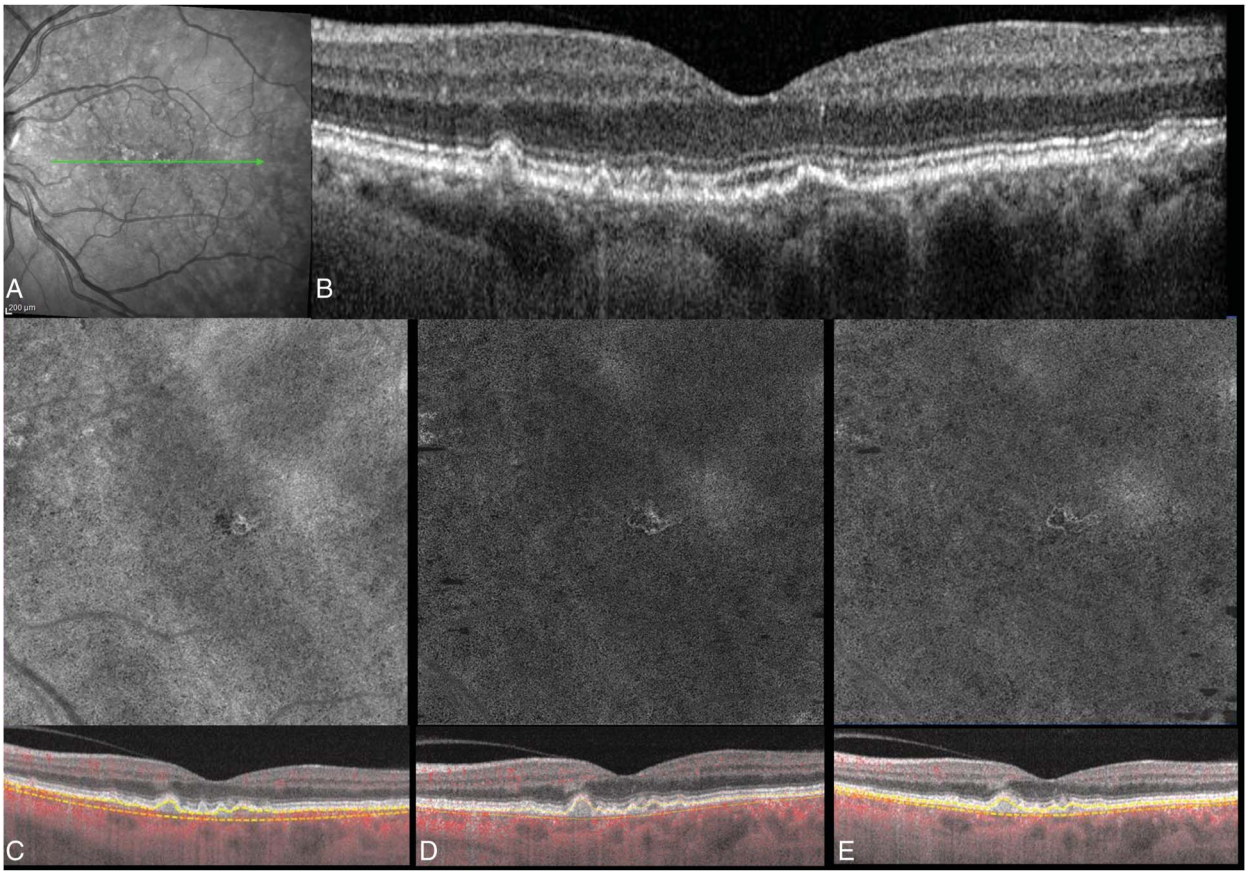

Fig. 3. Progression of a Type 1 nonexudative macular neovascularization without subretinal lipid globules. **A.** Near-infrared reflectance. **B.** Spectral-domain optical coherence tomography B-scan passing through the NE-MNV lesion and showing a shallow pigment epithelium detachment. Serial swept-source OCT angiography (OCTA, PLEX elite 9000) slabs were obtained at baseline (**C**), 6 months (**D**), and 12 months of follow-up (**E**). The neovascular lesion is segmented using an RPE–RPE fit automatic segmentation.

macular atrophy that is related to RPE and photoreceptor disruption.[7,20,21] Unlike persistent choroidal hypertransmission defects seen with macular atrophy, hypertransmission related to SLGs is transient and not associated with underlying RPE loss or permanent disruption of the photoreceptor ellipsoid zone on OCT (Figure 5). Similarly, unlike macular atrophy, SLGs are typically undetectable with FAF and near-infrared reflectance.

The presence of SLGs allowed the correct identification of 43.7% of the affected eyes with NE-MNV and 98.8% of nondiseased eyes. However, the SLG identification in iAMD eyes gives a probability of 87.5% (PPV) for the presence of a NE-MNV lesion, assuming the adjusted prevalence of 13.9%. The same probability was raised to 94.4%, considering the study prevalence of 28.3%. Most lesions were Type 1 MNV (85.7%) that were larger and more likely to show growth than NE-MNV lesions in eyes without SLGs. Despite SLGs possibly indicating a low level of subclinical exudation in growing lesions, we found the conversion rates to exudative MNV for these lesions to be similar to those of NE-MNV lesions for which SLGs were not detected. Therefore, our results did not seem to support a more aggressive approach about initiating treatment with intravitreal anti–vascular endothelial growth factor therapy for these eyes. The presence of SLGs as a potential biomarker of lesion growth was previously suggested by their frequent presence near the border of actively growing MNV lesions.[1] In AMD, some Type 1 MNV lesions may grow slowly while showing minimal exudation. This occurrence may support the idea of a potential protective function of some sub-RPE lesions that develop a "neochoriocapillaris" as a compensatory mechanism to replace a depleted native choriocapillaris and sustain overlying RPE and photoreceptors.[22,23] This process may be part of a physiological reorganization of the neovascular lesion where the use of anti–vascular endothelial growth factor may not necessarily have a beneficial role.

The greater prevalence of subretinal drusenoid deposits likely represents the reason for a thinner

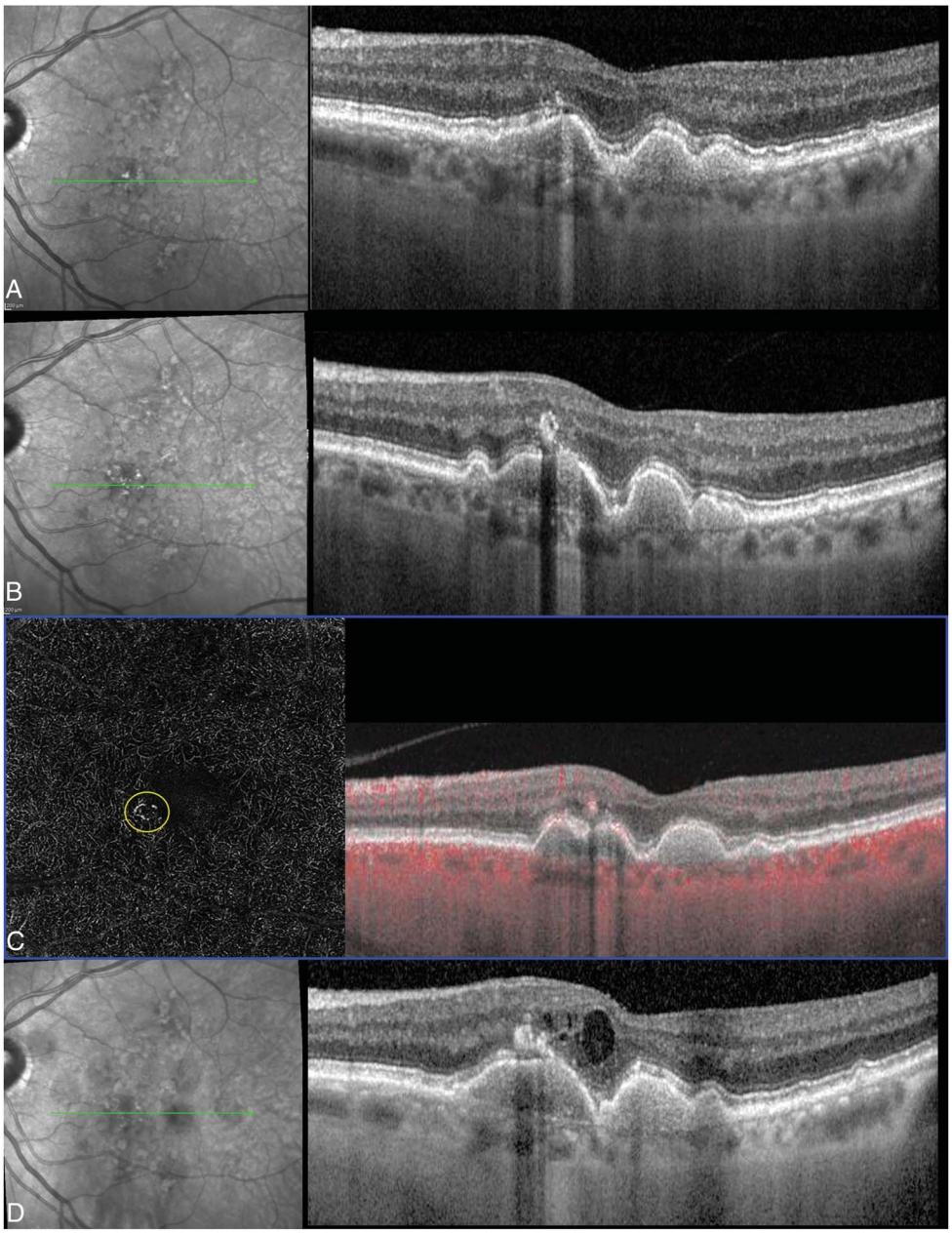

Fig. 4. Progression of a case with subretinal lipid globules in the absence of nonexudative lesion at baseline evolving into a Type 3 lesion. **A.** Spectral-domain optical coherence tomography (OCT) B-scan passes through the SLGs in the subretinal space above a drusenoid pigment epithelium detachment. **B.** OCT B-scan obtained 12 months later showed the disappearance of the SLGs accompanied by the presence of a hyperreflective lesion centered on the plexiform layer overlying the PED. **C.** Swept-source OCT angiography (OCTA, PLEX elite 9000) slabs obtained at the same follow-up interval (12 months) shows flow signal (yellow circle) within the hyperreflective lesion. **D.** At 15 months from baseline, an OCT B-scan demonstrates the presence of active exudation with intraretinal fluid.

choroid (Table 3) in the SLGs compared with controls.[24] However, other confounders may affect the choroidal thickness, including age, axial length, neovascular AMD in the fellow eye, and pigmentary changes. Therefore, the importance of subretinal drusenoid deposits as an independent factor associated with choroidal thinning has been questioned.[25]

The identification of DLS on structural OCT B-scans has been shown to be a useful biomarker of nonexudative Type 1 MNV, exhibiting diagnostic performance similar to our findings related to SLGs.[26] The detection of DLS presented higher sensitivity but lower specificity compared with SLGs in recognizing NE-MNV. As recently demonstrated, this finding may result from a non-neovascular splitting of the RPE/Bruch membrane complex representing thick basal laminar deposits on OCT B-scans.[27,28] Despite a higher specificity compared with the DLS, the diagnostic performance of SLGs as a biomarker for NE-MNV appears inferior to the DLS, as confirmed by Youden's index. Moreover, SLGs and DLS cannot be considered interchangeably, as they are more likely complementary predictors in NE-MNV.

Limitations of this study include its retrospective nature. In particular, an iAMD population selected

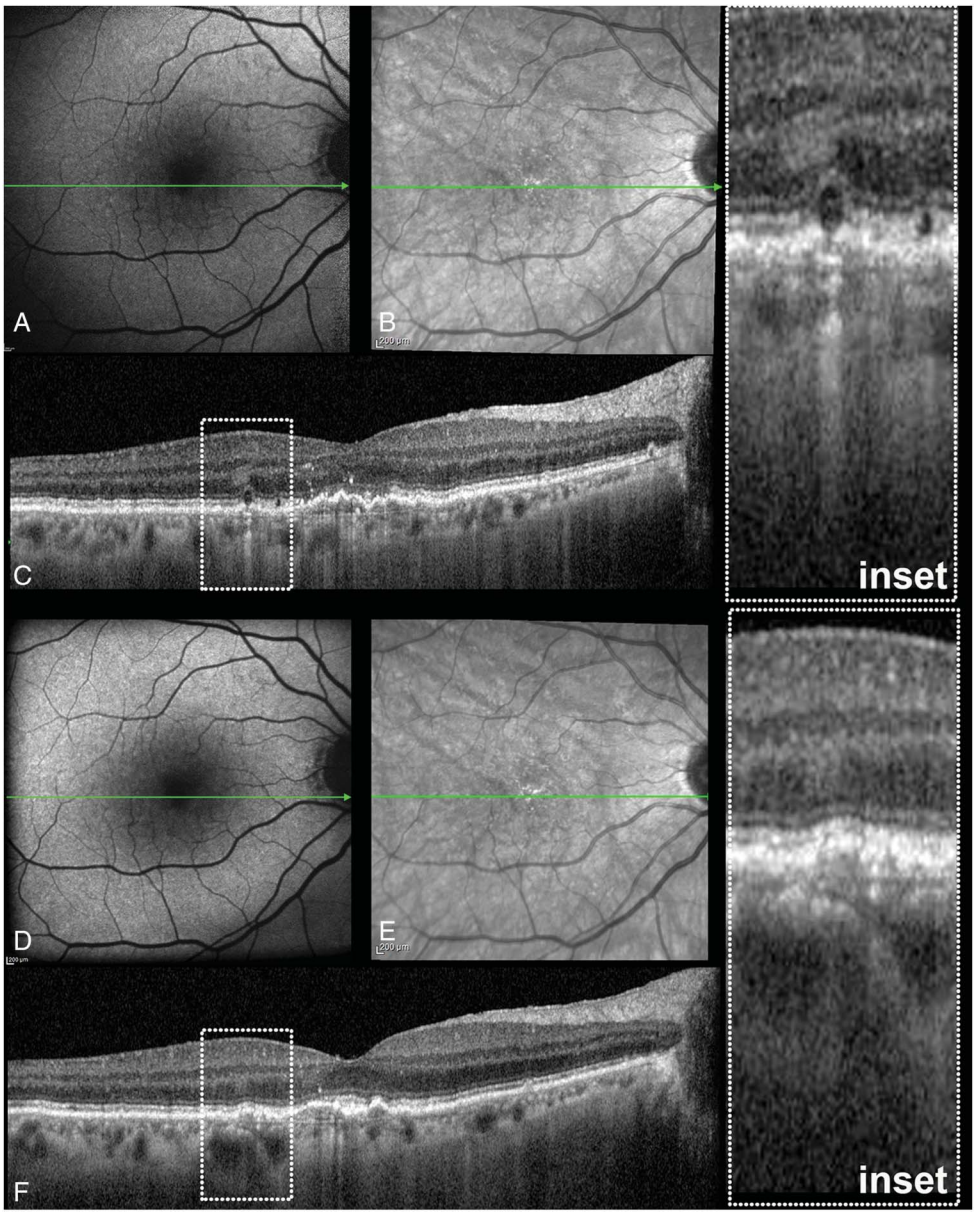

Fig. 5. Multimodal imaging shows that the retinal pigment epithelium remains intact beneath subretinal lipid globules. A. Fundus autofluorescence at baseline. **B.** Near-infrared reflectance (NIR) at baseline. **C.** Optical coherence tomography B-scan shows the presence of SLGs as round hyporeflective structures with hypertransmission tails (better seen on the magnified inset). One month later, after the SLGs disappear, the integrity of RPE is confirmed by preserved autofluorescence on FAF (**D**) and minimal changes in reflectivity on NIR (**E**). The OCT B-scan (**F**) shows the complete resolution of SLGs with intact external limiting membrane, ellipsoid zone, and RPE bands (inset).

retrospectively could increase the frequency of SLGs in our patient cohort. Patients undergoing OCTA may include those with more advanced AMD phenotypes, as confluent drusen or certain morphologies of pigment epithelium detachment felt to indicate a higher risk for MNV occurrence.

Our results support SLGs as a biomarker of subclinical activity in NE-MNV lesions. The SLGs colocalized with NE-MNV lesions almost invariably with high specificity, predictive values, and accuracy, demonstrating a good performance as a biomarker for subclinical lesions. Nonexudative macular neovascularization lesions associated with SLGs were larger and more likely to show growth than those without SLGs, but the conversion rates to exudative MNV were similar between the two groups. Our findings also demonstrated that on OCT, the hyperreflective tail beneath SLGs is not associated with macular atrophy, but rather, it represents a distinctive feature because of the optical properties of the globules. Further studies with a prospective design and a longer longitudinal evaluation would be necessary to better characterize the prognostic implications of SLGs in NE-MNV.

Key words: subretinal lipid globules, age-related macular degeneration, multimodal imaging, optical coherence tomography, optical coherence tomography angiography.

References

1. Fernandez-Avellaneda P, Freund KB, Wang RK, et al. Multimodal imaging features and clinical relevance of subretinal lipid globules. Am J Ophthalmol 2021;222:112–125.
2. Friedman E, Smith TR. Clinical and pathological study of choroidal lipid globules. Arch Ophthalmol 1966;75:334–336.
3. Querques G, Costanzo E, Miere A, et al. Choroidal caverns: a novel optical coherence tomography finding in geographic atrophy. Invest Ophthalmol Vis Sci 2016;57:2578–2582.
4. Sakurada Y, Leong BCS, Parikh R, et al. Association between choroidal caverns and choroidal vascular hyperpermeability in eyes with pachychoroid diseases. Retina 2018;38:1977–1983.
5. Dolz-Marco R, Glover JP, Gal-Or O, et al. Choroidal and subretinal pigment epithelium caverns: multimodal imaging and correspondence with friedman lipid globules. Ophthalmology 2018;125:1287–1301.
6. Ferris FL 3rd, Wilkinson CP, Bird A, et al. Clinical classification of age-related macular degeneration. Ophthalmology 2013;120:844–851.
7. Sadda SR, Guymer R, Holz FG, et al. Consensus definition for atrophy associated with age-related macular degeneration on OCT: classification of atrophy report 3. Ophthalmology 2018;125:537–548.
8. Parravano M, Borrelli E, Sacconi R, et al. A comparison among different automatically segmented slabs to assess neovascular AMD using swept source OCT angiography. Translational Vis Sci Technol 2019;8:8.
9. Sato T, Kishi S, Watanabe G, et al. Tomographic features of branching vascular networks in polypoidal choroidal vasculopathy. Retina 2007;27:589–594.
10. Spaide RF, Jaffe GJ, Sarraf D, et al. Consensus nomenclature for reporting neovascular age-related macular degeneration data: consensus on neovascular age-related macular degeneration nomenclature study group. Ophthalmology 2020;127:616–636.
11. Yanagi Y, Mohla A, Lee SY, et al. Incidence of fellow eye involvement in patients with unilateral exudative age-related macular degeneration. JAMA Ophthalmol 2018;136:905–911.
12. Yanagi Y, Mohla A, Lee WK, et al. Prevalence and risk factors for nonexudative neovascularization in fellow eyes of patients with unilateral age-related macular degeneration and polypoidal choroidal vasculopathy. Invest Ophthalmol Vis Sci 2017;58:3488–3495.
13. de Oliveira Dias JR, Zhang Q, Garcia JMB, et al. Natural history of subclinical neovascularization in nonexudative age-related macular degeneration using swept-source OCT angiography. Ophthalmology 2018;125:255–266.
14. Bailey ST, Thaware O, Wang J, et al. Detection of nonexudative choroidal neovascularization and progression to exudative choroidal neovascularization using OCT angiography. Ophthalmol Retina 2019;3:629–636.
15. Yang J, Zhang Q, Motulsky EH, et al. Two-year risk of exudation in eyes with nonexudative age-related macular degeneration and subclinical neovascularization detected with swept source optical coherence tomography angiography. Am J Ophthalmol 2019;208:1–11.
16. Youden WJ. Index for rating diagnostic tests. Cancer 1950;3:32–35.
17. Tan ACS, Pilgrim MG, Fearn S, et al. Calcified nodules in retinal drusen are associated with disease progression in age-related macular degeneration. Sci Transl Med 2018;10(466):eaat4544.
18. Litts KM, Wang X, Clark ME, et al. Exploring photoreceptor reflectivity through multimodal imaging of outer retinal tubulation in advanced age-related macular degeneration. Retina 2017;37:978–988.
19. Dolz-Marco R, Litts KM, Tan ACS, et al. The evolution of outer retinal tubulation, a neurodegeneration and gliosis prominent in macular diseases. Ophthalmology 2017;124:1353–1367.
20. Xu X, Liu X, Wang X, et al. Retinal pigment epithelium degeneration associated with subretinal drusenoid deposits in age-related macular degeneration. Am J Ophthalmol 2017;175:87–98.
21. Wolf-Schnurrbusch UEK, Enzmann V, Brinkmann CK, Wolf S. Morphologic changes in patients with geographic atrophy assessed with a novel spectral OCT–SLO combination. Invest Opthalmology Vis Sci 2008;49:3095–3099.
22. Chen L, Messinger JD, Sloan KR, et al. Nonexudative macular neovascularization supporting outer retina in age-related macular degeneration: a clinicopathologic correlation. Ophthalmology 2020;127:931–947.
23. Grossniklaus HE, Green WR. Choroidal neovascularization. Am J Ophthalmol 2004;137:496–503.
24. Cheung CMG, Gan A, Yanagi Y, et al. Association between choroidal thickness and drusen subtypes in age-related macular degeneration. Ophthalmol Retina 2018;2:1196–1205.
25. Wu Z, Fletcher EL, Kumar H, et al. Reticular pseudodrusen: a critical phenotype in age-related macular degeneration. Prog Retin Eye Res 2022;88:101017.
26. Shi Y, Motulsky EH, Goldhardt R, et al. Predictive value of the OCT double-layer sign for identifying subclinical neovascularization in age-related macular degeneration. Ophthalmol Retina 2019;3:211–219.
27. Fragiotta S, Parravano M, Sacconi R, et al. A common finding in foveal-sparing extensive macular atrophy with pseudodrusen implicates basal laminar deposits. Retina 2022;42:1319–1329.
28. Berlin A, Chen L, Messinger J, et al. Double-layer sign in neovascular age-related macular degeneration - do we treat?. Acta Ophthalmologica 2022;100:348–349.

LONG-TERM MICROVASCULAR REMODELING AND CYSTIC CHANGES AFTER RETINAL DETACHMENT TREATED WITH SILICON OIL TAMPONADE

NATHALIE PFISTER, MD, LÉA DORMEGNY, MD, LAURENT BALLONZOLI, MD, ARNAUD SAUER, MD, PHD, CLAUDE SPEEG-SCHATZ, MD, PHD, TRISTAN BOURCIER, MD, PHD, DAVID GAUCHER, MD, PHD

Purpose: To determine the long-term microvascular alterations associated with macular cystic changes after retinal detachment surgery with silicone oil tamponade.

Methods: The results of two optical coherence tomography angiographies performed at 11 months and 38 months after silicone removal were retrospectively analyzed for 30 eyes. The data were compared between both measurements and between eyes with macular cysts (MC+) and without macular cysts (MC−). Two patterns of cysts were identified and compared: cysts exclusively involving the inner nuclear layer (INLc) and cysts present in all retinal layers.

Results: At both end points, 20 eyes (67%) presented with macular cysts, 12 of them (40%) had INLc. At the first end point, vascular density of superficial capillary plexus was higher and superficial foveal avascular zone was smaller in MC+ eyes than in MC− eyes ($P = 0.04$ and $P = 0.017$, respectively). At the second end point, vascular density of superficial capillary plexus significantly decreased in MC+ eyes as compared with the first end point ($P < 0.001$) and superficial foveal avascular zone enlarged ($P < 0.001$). Macular central thickness decreased between follow-ups only in eyes with INLc ($P < 0.01$). The final best-corrected visual acuity was better in eyes with INLc than in eyes with cysts present in all retinal layers ($P < 0.01$). There was no difference between the final best-corrected visual acuity in eyes with INLc and MC− eyes.

Conclusion: Macular cysts are a common finding long after silicon removal. Vascular remodeling seems characterized by an initial increase of the vascular density of superficial capillary plexus in eyes with cysts, which is followed by its progressive decrease. The INLc is the most common pattern of cysts. They are associated with a progressive decrease of the central macular thickness without visual impairment.

RETINA 43:923–931, 2023

Silicone oil (SO) was introduced in Europe in 1974 as an adjunct in the management of complex retinal detachment surgery,[1] long before its approval by the U.S. Federal Drug Administration in 1994. It is still widely used when extended intraocular tamponade is required, especially in cases of severe proliferative vitreoretinopathy or giant retinal tear. The visual outcomes of these surgeries are poor because of various factors.

Recent developments in optical coherence tomography angiography (OCT-A) have shed new light on the retinal microcirculation after SO removal in cases of complex retinal detachments. Optical coherence tomography angiography parameters demonstrated modifications of the capillary density in those cases.[2,3] Hypothesis have been made that these modifications may be because of hypoxia or local conditions during the SO tamponade period.[4] Dormegny et al[7] recently

From the Department of Ophthalmology, New Civil Hospital, Strasbourg University Hospital, Strasbourg, France.

None of the authors has any financial/conflicting interests to disclose.

Reprint requests: David Gaucher, MD, PhD, Strasbourg University Hospital, Strasbourg 67000, France; e-mail: david.gaucher@chru-strasbourg.fr

reported a microvascular remodeling after vitreoretinal surgery with SO tamponade, which was associated with the presence of macular cysts. They reported an increase in the vascular density of the superficial capillary plexus (SCPvd) in eyes with macular cysts (MC+ eyes), as compared with eyes without macular cysts (MC− eyes), three months after silicon oil removal. The incidence rate of macular cysts was high in this cohort (nearly 60%). Furthermore, nearly two-third of these cysts were localized in the inner nuclear layer (INL) of the retina and showed similarities with degenerative microcystic edema as described in severe optic neuropathies[5] or chronic retinal pathologies[6] (Figure 1). Therefore, microcystic changes and vascular remodeling after silicon oil removal after retinal detachment (RD) surgery may represent a degenerative process in complicated RD cases. Evolution of microcystic change and vascular remodeling after RD surgery using SO has been poorly investigated.

The purpose of this study was to determine whether microvascular and cystic changes are durably associated in eyes operated for complex RD with SO tamponade. A secondary objective was to assess the eventual impact of this evolution on the visual outcomes.

Methods

Study Population

We conducted a retrospective monocentric study including 40 consecutive patients (40 eyes) who successfully underwent retinal detachment surgery with pars plana vitrectomy and SO tamponade (FCI S.A.S, France Chirurgie Instrumentation; viscosity

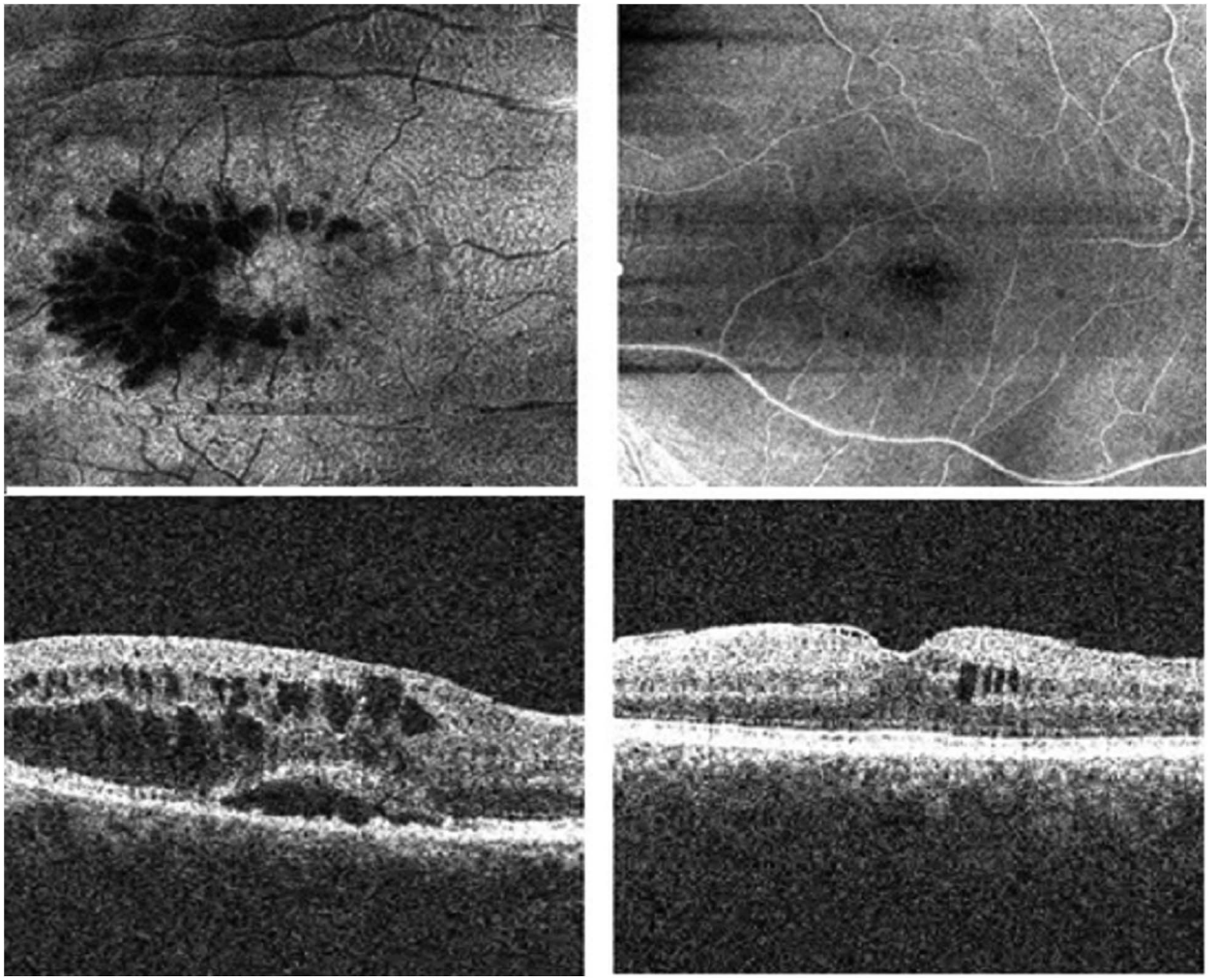

Fig. 1. Left: En Face and B-scan images of a macular cystoid edema located in both internal and external retina, with a small serous retinal detachment. Right: En face and B-scan images of a macular microcystic edema selectively located in the inner nuclear layer. Cysts are disposed in concentric rings around the fovea without distortion of the foveal profile.

1,000 cstokes), performed by two surgeons (L.B. and D.G.) from September 2015 to August 2018 in the University Hospital of Strasbourg (France).

Patients with insufficient image quality from any of the examinations and with ophthalmologic comorbidity were excluded.

The authors adhered to the tenets of the Declaration of Helsinki.

Data Collection

Patients underwent a preliminary OCT-A (Cirrus HD-OCT 5000; Carl Zeiss Meditec, Dublin, CA) examination at least 3 months after SO removal (first end point). Patients were followed and reexamined with the same machine after 2 years (second end point). A comprehensive clinical examination was also performed, including the best-corrected visual acuity (BCVA) with the Early Treatment Diabetic Retinopathy Study chart.

Optical coherence tomography angiography examination at both end points included the 3 × 3-mm macular cube (512 × 128) and 3 × 3-mm angiography measurements. The central macular thickness (CMT) and the thickness of the ganglion cell complex (GCC) and SCPvd and vessel density of deep capillary plexus (DCPvd) were calculated. Vascular density of superficial capillary plexus was generated by *AngioPlex Metric* software for the SCP. For the DCPvd, we used a binarization technique using the *ImageJ* software[7,8] (Figure 2A). Delineation of the area of the superficial foveal avascular zone (FAZ) was automatically generated, whereas the area of deep FAZ was measured manually using *ImageJ* and verified by two independent readers (Figure 2B).

The area occupied by retinal cysts was measured on OCT-A en face images of the midretina (Figure 2C). The retinal layer in which the cysts were located was noted using the B-scan images of the OCT. Macular cysts were noted either as present in the inner nuclear layer only (INLc) or in both outer and inner retinal layers (all layers cysts [ALc]).

Statistical Analysis

Data obtained during the first and second end points were compared for the study population for quantitative variables (BCVA, SCPvd and DCPvd, superficial and deep FAZ, macular thickness, and GCC). At each end point, data were compared between operated and contralateral eyes.

The presence of macular cysts was used as an indicator of retinal cystic remodeling; we compared the data of MC+ eyes versus MC− eyes at both end points. Data were also compared between INLc and ALc.

Student *t*-tests were performed to compare the mean values of Gaussian parameters obtained among the groups. Mann–Whitney *U* tests and Kruskall–Wallis tests were used to compare non-Gaussian parameters. A Wilcoxon signed rank exact test was used to compare operated and contralateral eyes.

Analyses were performed with *pvalue.io* software (Medistica, Paris, France).

Results

After exclusion, data from 30 patients (30 eyes) could be analyzed. The mean follow-up was 3.5 years after silicone removal, ranging from 2 years to 5.2 years. The mean delay between the first and the last OCT-A was 26 months, ranging from 21 months to 36 months. The mean duration of the SO tamponade was 122 days (min = 35 days, max = 469 days, median = 102 days). RD was macula-off in 21 of 30 eyes (70%). Preoperative and intraoperative clinic data are summarized in Table 1.

Vessel Density of Superficial Vascular Plexus and Superficial Foveal Avascular Zone

The mean SCPvd was 29.6% for all operated eyes at the first end point and 23% at the second end point. The difference between the two measurements was not statistically significant. At each end point, there was no significant difference between operated and nonoperated eyes.

The mean superficial FAZ was at 0.11 mm^2 at the first end point and 0.13 mm^2 at the second end point. There was no difference between both end points or between operated and nonoperated eyes.

Comparison Between Eyes With Macular Cysts and Eyes Without Macular Cysts

At the first end point, SCPvd was significantly higher in MC+ eyes than in MC− eyes (33% vs. 24%, $P = 0.03$, Mann–Whitney *U* test). The mean superficial FAZ was significantly smaller in MC+ eyes than in MC− eyes (0.16 mm^2 vs. 0.2 mm^2, $P = 0.041$, Mann–Whitney *U* test).

Between end points, SCPvd decreased in MC+ eyes ($P < 0.001$) and remained stable in MC− eyes (Figure 3). The superficial FAZ area increased significantly in MC+ eyes ($P = 0.02$), which is consistent with the SCPvd decrease observed (Figure 4 and Table 2).

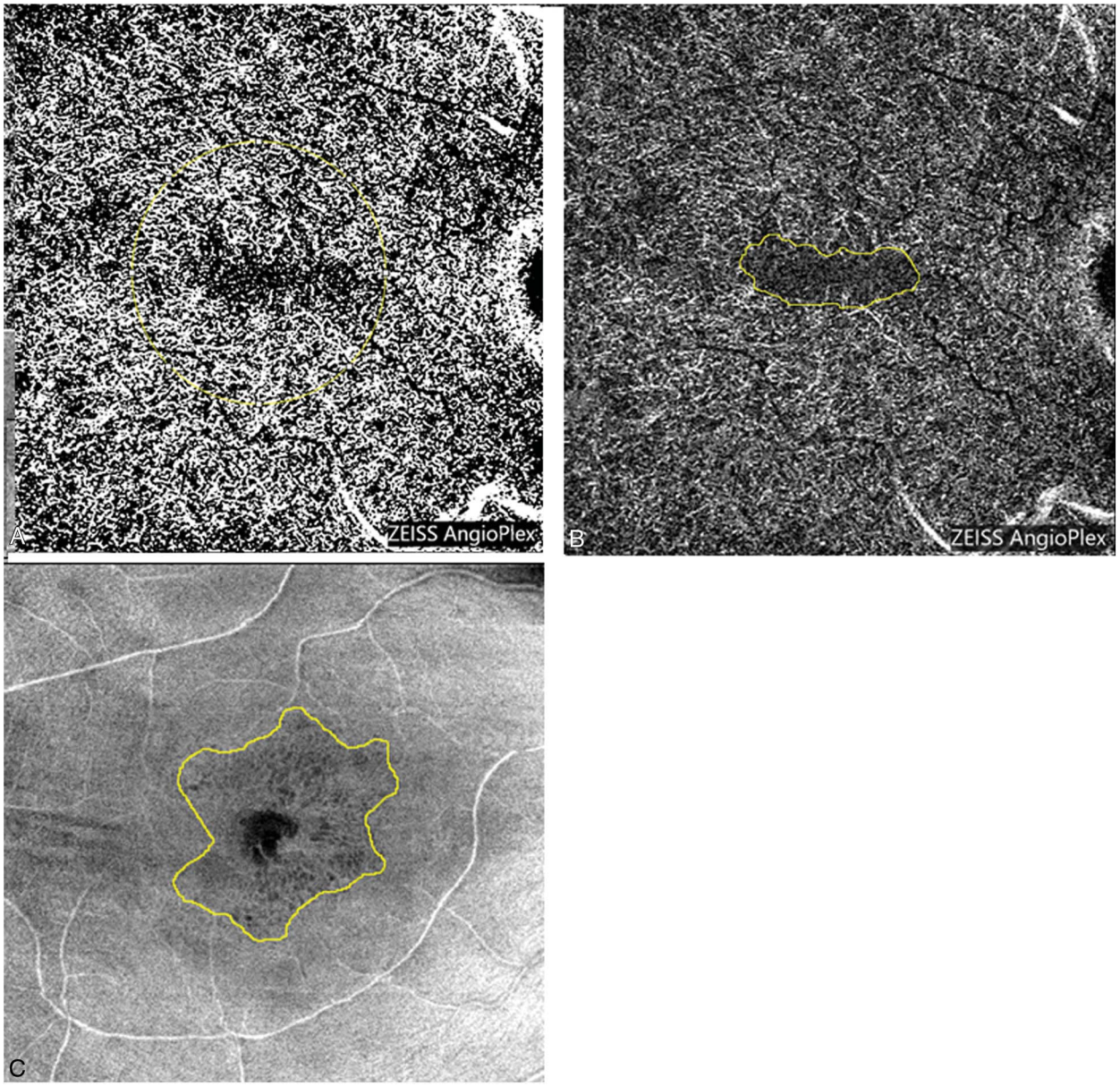

Fig. 2. A. Optical coherence tomography angiography image of the DCPvd after binarization using the ImageJ software: OCT-A en face images of the DCP were first digitalized in 8 bits. Gray levels were then converted into two values, white for the vessels and black for the background, the threshold level being calculated by the Otsu algorithm. The proportion of white pixels (corresponding to capillaries) was calculated in a circle of 3 mm diameter (yellow) centered by the fovea. **B**. Optical coherence tomography angiography image of the DCPvd: measure of the deep FAZ (yellow) with the freehand selection tool of ImageJ software. **C.** En face image at the midretina level: measure of the confluent cysts area (yellow) with the freehand selection tool of ImageJ software.

At the second end point, SCPvd was 23.9% in MC+ eyes and 21.1% in MC− eyes. No significant difference was noted between both groups ($P = 0.74$). The mean superficial FAZ was 0.16 mm^2 in MC+ eyes and 0.2 mm^2 in MC− eyes, which was not statistically different ($P = 0.31$).

In both the types of cysts (INLc and ALc), SCPvd decreased and FAZ area increased significantly between end points.

Vessel Density of Deep Vascular Plexus and Deep Foveal Avascular Zone

The mean DCPvd in our cohort was 30.7% at the first end point and remained stable at the second end point, with a mean value of 29%. At both end points, DCPvd was not different from the unaffected eye. The mean deep FAZ showed no difference between both end points (1.06 mm^2 vs. 1.11 mm^2, $P = 0.09$) nor about the contralateral eye.

Table 1. Clinical Parameters of the Study Population

Follow-up, months (mean ± SD)	42.7 ± 15.5
Age, years (mean ± SD)	57.6 ± 5.4
Tamponade duration, days (mean ± SD)	122 ± 85
BCVA, logMAR (mean ± SD)	
Initial end point visit	0.58 ± 0.54
During silicone tamponade	1.02 ± 0.71
One month after silicone removal	0.58 ± 0.54
Final end point visit	0.58 ± 0.49
Delay between silicone removal and initial endpoint visit, months (mean ± SD)	11 ± 8.2
Preoperative macular status	
Macula-on RD	9 eyes (30%)
Macula-off RD	21 eyes (70%)
Type of RD	
Giant retinal tear	6 eyes (20%)
Proliferative vitreoretinopathy	20 eyes (67%)
Open-globe injury	4 eye (13%)
Lens status at the final end point visit	
Pseudophakic	27 eyes (90%)
Phakic	3 eyes (10%)
Surgery features	
Relaxing peripheral retinectomy	11 eyes (37%)
Use of liquid perfluorocarbon	19 eyes (63%)
Combined cataract surgery	17 eyes (57%)
Epiretinal membrane removal	10 eyes (30%)
Treatment of postoperative macular edema	
In the first 3 months after silicone removal	12 (40%)
At the initial end point visit	4 (13%)
At the final endpoint visit	4 (13%)

logMAR, logarithm of the minimum angle of resolution.

There was no significant difference in mean DCPvd ($P = 0.6$ at the first end point and $P = 0.37$ at the second end point) or in mean deep FAZ ($P = 0.22$ at the first end point and $P = 0.21$ at the second end point) between MC+ eyes and MC− eyes.

Concerning the subgroup analysis, there was no significant difference in mean DCPvd ($P = 0.34$ at the first end point and $P = 0.25$ at the second end point, Mann–Whitney U test) or in mean deep FAZ ($P = 0.73$ at the first end point and $P = 0.7$ at the second end point, Mann–Whitney U test) between INLc eyes and ALc eyes.

Macular Cysts

We found macular cysts in 20 eyes (67%) at the first end point, 12 of them (40%) had macular INLc and 8 eyes (27%) had ALc. There was no eye with cysts in the outer retina only. The time of cysts onset after SO removal was 4.9 months on average. At the second end point, the prevalence of INL and ALcs remained unchanged. The preoperative macula-off status was significantly associated with the presence of macular cysts (85% MC+ eyes vs. 50% MC− eyes, $P = 0.03$, Fisher exact test). Among the 21 macula-off RD, 16 presented with MC during the follow-up (8 ALc and 8 INLc type). The mean preoperative BCVA was 20/125 in MC+ eyes versus 20/100 in MC− eyes ($P = 0.48$). Preoperative BCVA did not significantly differ between each group (mean = 20/100 in INLc eyes vs. 20/200 in ALc eyes, $P = 0.21$).

Among all clinical data, eyes with INLc were more often associated with an unoperated epiretinal membrane on the B-scan at both end points, as compared with eyes with ALc (6 eyes from 12 vs. 0 eye from 8, $P < 0.01$, Fisher exact test). In eyes with ALc, there was a higher prevalence of intraoperative relaxing peripheral retinectomy (7 eyes from 8, $P < 0.01$, Fisher exact test) and multiple interventions before silicone removal (7 eyes from 8, $P < 0.01$, Fisher exact test), as compared with eyes with INLc (Table 3).

The macular status did not significantly differ between ALc and INLc eyes (67% INL + eyes presented with macula-off RD vs. 100% ALc eyes, $P = 0.13$, Fisher exact test). Preoperative BCVA did not significantly differ between each group (mean = 20/100 in INLc eyes vs. 20/200 in ALc eyes, $P = 0.21$).

Evolution of the Cysts Area

The mean area of the cysts was 3.35 mm^2 at the first end point and 2.29 mm^2 at the second end point.

Considering separately INLc and ALc, different evolutionary profiles were observed. Most of INLc (n = 7) remained stable (Table 3).

Best-Corrected Visual Acuity

The mean BCVA remained stable in MC+ eyes, with 20/80 at both end points. The mean BCVA in MC− eyes was 20/50 at both end points. This difference between the two groups was not statistically significant.

At both end points, BCVA in MC+ eyes was negatively correlated with the cysts area ($P < 0.01$, Spearman test).

Eyes with ALc showed the worst visual outcome, with the mean BCVA of 20/160 at both end points. The mean BCVA in eyes with INLc was 20/100 at the first end point and improved up to 20/50 at the second end point. At the second end point, the mean BCVA was significantly different between INLc and ALc ($P < 0.01$) (Table 3).

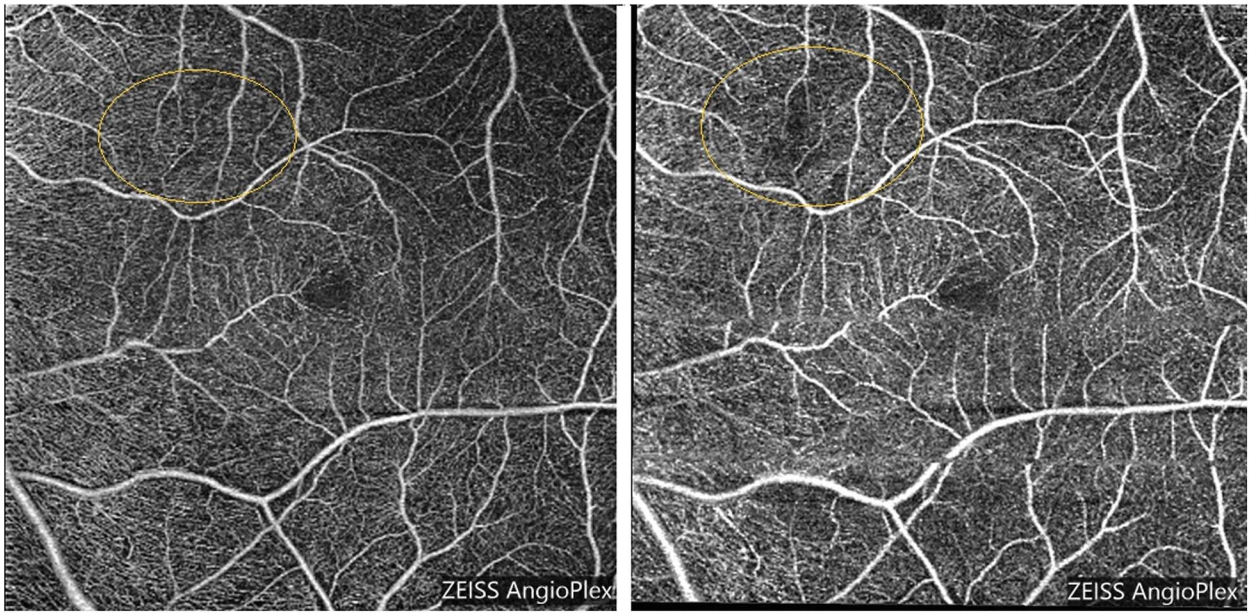

Fig. 3. Optical coherence tomography angiography images of the SCP in the same eye at the first (left) and the second (right) examinations: microvascular defects in the yellow circle increased.

Central Macular Thickness

Central macular thickness significantly decreased between the first and the second end points for eyes with INLc (364 μm vs. 302 μm, $P < 0.01$). Central macular thickness remained stable in eyes showing ALc (354 μm vs. 336 μm, $P = 0.95$) and in MC− eyes (290 μm vs. 281 μm, $P = 0.93$).

Ganglion Cell Complex

The ganglion cell complex thickness was not statistically different in MC+ eyes compared with MC− eyes at both end points.

In eyes presenting only with INLc, we observed a decrease in GCC that was not statistically significant (mean = 79 μm at the first end point and 72.5 μm at the

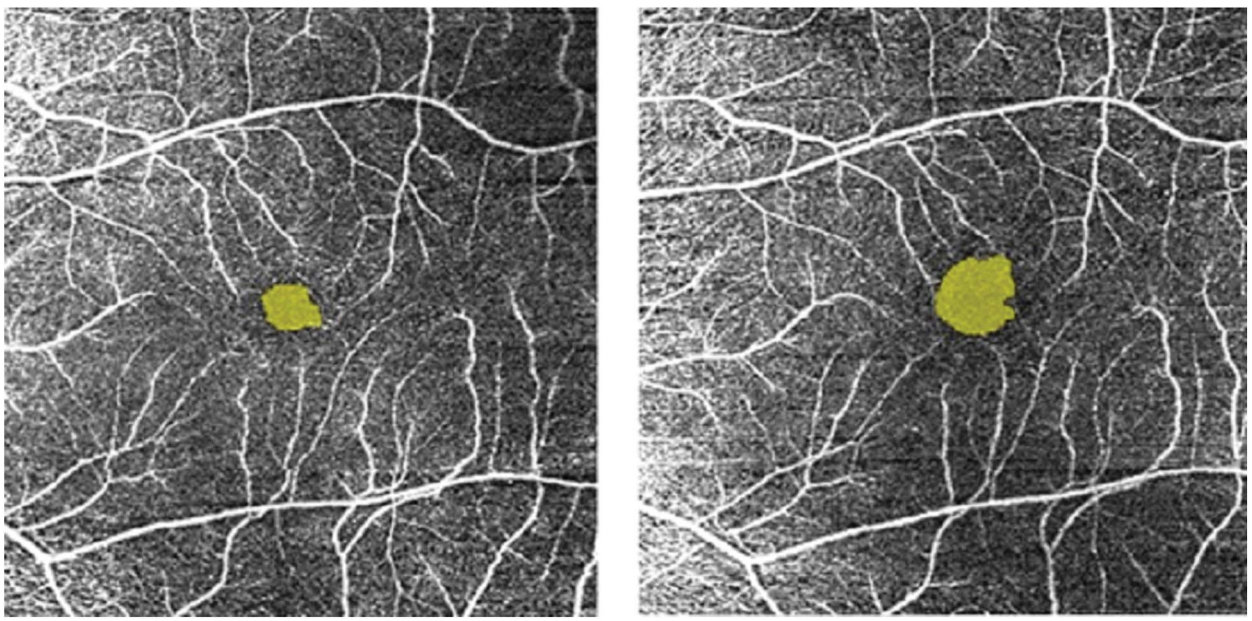

Fig. 4. Optical coherence tomography angiography images of the SCP in the same eye at the first (left) and the second (right) examinations: FAZ area enlarged.

Table 2. Comparison of Data Collected During the Two Examinations for the MC+ Eyes

	Initial End Point Visit	Final End Point Visit	*P*
BCVA (logMAR)	0.64 ± 0.5	0.65 ± 0.52	0.72
Cysts area (mm^2)	3.35 ± 6.78	2.29 ± 4.77	0.19
Macular central thickness (μm)	376 ± 52	337 ± 22	0.23
VD of SCP (%)	33 ± 1.1	23.9 ± 1.4	**<0.001**
Superficial FAZ area (mm^2)	0.118 ± 0.057	0.165 ± 0.101	**0.032**
VD of DCP (%)	31 ± 7.5	30 ± 7.1	0.28
Deep FAZ area (mm^2)	1.03 ± 0.53	1.07 ± 0.47	0.55
GCL thickness (μm)	79.1 ± 22.6	72.2 ± 17.5	0.74
OCT-A signal strength	8.15 ± 1.57	7.62 ± 1.63	0.21

All values are indicated as mean ± SD.
Bold entries are statistically significant values.
logMAR, logarithm of the minimum angle of resolution; VD, vascular density.

second end point, $P = 0.74$). Both values were interpreted as normal as compared with the normative database of the OCT and did not differ from the contralateral eye.

Discussion

The results of the present work demonstrate that in two-third of the cohort operated for RD with SO tamponade, microvascular changes were present and were exclusively associated with the presence of macular retinal cysts. Indeed, SCPvd increased during the first year after the SO removal period, and superficial FAZ area was reduced. Moreover, we also noticed a progressive and significant decrease of the SCPvd after the initial increase in eyes with retinal cysts.

Increased SCPvd and reduced FAZ were already reported by Dormegny et al[7] in eyes operated for RD after SO removal and also in eyes with macular cysts.

Dormegny et al hypothesized that either capillaries displacement by cystoid cavities or a compensatory mechanism of hypoxia during retinal detachment may lead to SCPvd increase. The slow restoration and then the decrease of SCPvd with time, despite the persistence of cysts in most of the eyes, suggest a vascular remodeling rather than a mechanical displacement by cysts. The pathophysiology could be an acute vascular reaction to hypoxia either during detachment or during SO tamponade, followed by a slow degenerative process. Indeed, in eyes with cysts, macular thickness decreased significantly during follow-up, together with superficial vascular density. The fact that alterations are limited to the SCP and do not affect DCP may be because of direct contact between SCP and SO tamponade, as suggested by Roohipoor et al.[2]

Another hypothesis for the transient increased vascular density could be a retinal contraction during macular detachment leading to microvascular densification in the superficial retina, gradually reversible over time.

Most of the published studies that analyzed the vascular density after RD surgery reported a decrease of either superficial or deep vascular plexus.[3,8] Bayraktar,[3] in a cohort of 24 eyes with macula-off detachments, observed a reduction in both SCPvd and

Table 3. Main Differences Between Eyes With Inner Nuclear Layer Cysts and Eyes With All Retinal Layers Cysts

	INLc	ALc	*P*
BCVA (logMAR, mean ± SD)			
Initial end point visit	0.7 ± 0.2	0.9 ± 0.7	0.24
Final end point visit	0.39 ± 0.1	0.9 ± 0.7	**<0.01**
Preoperative relaxing peripheral retinectomy, n (%)	1 (8%)	7 (87.5%)	**<0.01**
Multiple interventions before silicone removal, n (%)	5 (41.5%)	7 (87.5%)	**<0.01**
Necessity of medical treatment for macular edema, n (%)	0	4 (50%)	**0.014**
Stability of cysts area between the initial and final end point visits, n (%)	7 (58%)	0	**0.039**

Bold entries are statistically significant values.
ALc, eyes with all retinal layers cysts; INLc, eyes with inner nuclear layer cysts; logMAR, logarithm of the minimum angle of resolution.

DCPvd associated with FAZ enlargement and a thinner CMT, as compared with the fellow eye after 3 months.

Interestingly, none of these studies found an increased SCPvd after surgery as we did. This discrepancy may be because of the short follow-up limited to 3 months in these studies. Indeed, we noticed an increased density in the SCPvd during the first year after silicon oil removal. Moreover, in our study, increased SCPvd was noticed in eyes with retinal cysts. The presence of cysts was not mentioned in the other studies. Furthermore, the comparison with contralateral eye might expose an underestimation of vascular density in the operated eye because of worse signal strength quality compared with nonoperated eyes.[8]

In our cohort, we found a high prevalence (67%) of macular cysts more than 2 years after SO removal. Previously published studies found variable incidence rates of macular edema after surgery with silicone tamponade (18%–66%).[9,10] As reported by Dormegny et al[7] we found a negative correlation between BCVA and cysts area. However, we did not find any more difference in BCVA between MC− eyes and MC+ eyes, perhaps because of an insufficient statistical power resulting from the small size of our cohort. We have identified two different patterns of cysts: macular cysts involving both the outer and inner retinal layers are associated with clinical proinflammatory factors such as peripheral retinectomy and multiple interventions and can be identified as chronic postoperative edema in eyes with poor visual prognosis. All the eyes with ALc in our cohort underwent treatment using intravitreal dexamethasone; the edema regressed in all cases but also recurred in all cases. It may be interesting to try to prevent ALc edema intraoperatively in cases of peripheral retinectomy instead of waiting for edema to appear. Further studies should be addressed to validate this hypothesis. The macula-off status could also be a factor that promotes the presence of ALc and the worst visual prognosis associated; however, the results of this study do not support this hypothesis because the rate of macula-off RD was not statistically different between groups.

Most cysts in our cohort (64%) were exclusively localized in the INL. They remained stable over time, and the final BCVA was similar to eyes without cysts. They adopted a specific microcystic pattern, in the form of small lacunar areas of hyporeflectivity disposed concentrically around the fovea (Figure 1). This appearance is similar to the degenerative microcystic edema described by Gelfand et al[5] in optic neuropathies. It has also been described in chronic retinal pathologies[6] or after vitrectomy for epimacular membrane.[11–16.] Dormegny et al[7] also reported this pattern of cysts with a high prevalence (48%) after retinal surgery with SO tamponade. A few case reports[17,18] also reported INLc, in association with unexplained acute vision loss after the silicone removal. In our study, eyes with INLc did not present with visual loss; in contrast, they had a stable BCVA, which was similar to eyes without cysts at the end of the follow-up. Those results concerning fair BCVA in eyes with INLc were also reported by Dormegny et al.[7]

The pathophysiology of these INLc might be different from the pathophysiology of postoperative inflammatory edema as suggested in the literature by the absence of leakage on fluorescein angiography,[21] the absence of conventional treatments response,[19] and their long-term stability. The role of loss or dysfunction of Müller cells in the pathophysiology of INLc has been evocated since 2010[20] and is widely admitted[21] in various causes of degenerative microcysts. Müller cells are glial cells whose bodies are located in the INL, and they are a key factor in the regulation of intraretinal fluids through ionic and aquaporin channels. However, the origin of the Müller cell loss or dysfunction postvitrectomy is not yet well understood and may involve several factors. Possible candidates are a retrograde maculopathy primarily involving the ganglion cells such as in optic neuropathies, a tractional mechanism through an epiretinal membrane as also suggested by Lee et al,[22] a minimal inflammatory involvement, and an ischemic damage of the retinal microcirculation during retinal detachment or silicone tamponade. Govetto et al[11] noted a higher prevalence of INLc in glaucomatous eyes and suggested a synergy effect between tractional factors and ganglion cells fragility before surgery. However, we did not observe any correlation between the presence of INLc and any GCC alteration in our cohort. Our study indicates a higher prevalence of nonoperated epiretinal membranes in eyes with INLc, so that tractional mechanisms cannot be excluded. However, CMT significantly decreased with time in eyes with INLc; this could be an indicator of progressive atrophy of the internal retina associated with microcystic degeneration. Furthermore, we observed a microvascular remodeling associated with the presence of macular cysts. The cause of this remodeling is not known but hypoxic phenomena could be involved in the process and may lead to damage of Müller cells. Inner nuclear layer cysts do not seem to affect BCVA or require any specific treatment. It seems quite useful to be aware of this specific pattern of cysts to avoid useless medications.

This study has several limitations. First, it was a retrospective monocentric study with a limited number of included patients and a high amount of loss to follow-up. Second, the measurements of vascular density and FAZ area were automatic for the SCP

and semiautomatic for the DCP because the software of our OCT-A provides automatic measurement for SCPvd alone. This allowed to compare results during follow-up for the same plexus but compromised the comparison of our results with other studies. Finally, the median delay between SO removal and the first end point was 11 months. It may be interesting to detect early macular changes associated with SO before 6 months of the postoperative follow-up. This would also facilitate comparison with data of other studies with a short follow-up.

Conclusion

In conclusion, macular cysts have a high prevalence in patients who have successfully undergone retinal reattachment surgery with SO tamponade, even after a mean follow-up of 39 months. They are associated with a short-time increase of the SCPvd, which then decreases over time.

Most of them are exclusively located in the INL and do not affect BCVA; they are associated with progressive decreased CMT. They do not seem to require any specific treatment but may reflect a degenerative process of the retina.

Key words: capillary density, macular cysts, macular edema, inner nuclear layer, microvascular remodeling, OCT–angiography, retinal detachment, retrograde maculopathy, silicone oil.

References

1. Jean Haut, Coulombel G, Larricart P, Ullern etVan Effenterre MG. Traitement en première intention de certains décollements de rétine souple (trou maculaire, déchirure géante) par la technique de vitrectomie-silicone. Bull Soc Ophthalmol Fr 1982; 82:305–309. 24.
2. Roohipoor R, Tayebi F, Riazi-Esfahani H, et al. Optical coherence tomography angiography changes in macula-off rhegmatogenous retinal detachments repaired with silicone oil. Int Ophthalmol 2020;40:3295–3302.
3. Bayraktar Z, Pehlivanoglu S, Hagverdiyeva S, et al. Longitudinal evaluation of retinal thickness and OCTA parameters before and following silicone oil removal in eyes with macula-on and macula-off retinal detachments. Int Ophthalmol 2022;42:1963–1973.
4. Christou EE, Stavrakas P, Batsos G, et al. Association of OCT-A characteristics with postoperative visual acuity after rhegmatogenous retinal detachment surgery: a review of the literature. Int Ophthalmol 2021;41:2283–2292.
5. Dormegny L, Jeanjean LC, Liu X, Messerlin A, et al. Visual impairment and macular vascular remodeling secondary to retrograde maculopathy in retinal detachment treated with silicone oil tamponade. Retina 2021;41:309–316.
6. Burggraaff MC, Trieu J, de Vries-Knoppert WAEJ, et al. The clinical spectrum of microcystic macular edema. Invest Ophthalmol Vis Sci 2014;55:952–961.
7. Gelfand JM, Nolan R, Schwartz DM, et al. Microcystic macular oedema in multiple sclerosis is associated with disease severity. Brain 2012;135:1786–1793.
8. Lim HB, Kim YW, Kim JM, et al. The importance of signal strength in quantitative assessment of retinal vessel density using optical coherence tomography angiography. Sci Rep 2018;8:12897.
9. Kiss CG, Richter-Müksch S, Sacu S, et al. Anatomy and function of the macula after surgery for retinal detachment complicated by proliferative vitreoretinopathy. Am J Ophthalmol 2007;144:872–877.e1.
10. Benson SE, Grigoropoulos V, Schlottmann PG, et al. Analysis of the macula with optical coherence tomography after successful surgery for proliferative vitreoretinopathy. Arch Ophthalmol 2005;123:1651–1656.
11. Govetto A, Su D, Farajzadeh M, et al. Microcystoid macular changes in association with idiopathic epiretinal membranes in eyes with and without glaucoma: clinical insights. Am J Ophthalmol 2017;181:156–165.
12. Sigler EJ, Randolph JC, Charles S. Delayed onset inner nuclear layer cystic changes following internal limiting membrane removal for epimacular membrane. Graefes Arch Clin Exp Ophthalmol 2013;251:1679–1685.
13. Chen SJ, Tsai FY, Liu HC, et al. Postoperative Inner NuclearLayer Microcysts Affecting Long-Term Visual Outcomes after Epiretinal Membrane Surgery. Philadelphia, PA: Retina; 2016.
14. Hsieh MH, Chou YB, Huang YM, et al. Inner nuclear layer microcyst configuration, distribution, and visual prognosis in patients with epiretinal membrane after vitrectomy and membrane peeling. Sci Rep 2019;9:11570.
15. Lee JJ, Jo YJ, Kwon HJ, et al. Perioperative intraretinal fluid observed using optical coherence tomography in the epiretinal membrane. BMC Ophthalmol 2020;20:33.
16. Güler M, Urfalıoğlu S, Damar Güngör E, et al. Clinical and optical coherence tomography analysis of intraretinal microcysts in patients with epiretinal membrane. Semin Ophthalmol 2021;36:787–793.
17. Shalchi Z, Mahroo OA, Shunmugam M, et al. Spectral domain optical coherence tomography findings in long-term silicone oil–related visual loss. Retina 2015;35:555–563.
18. Scheerlinck LM, Schellekens PA, Liem AT, et al. Incidence, risk factors, and clinical characteristics of unexplained visual loss after intraocular silicone oil for macula-on retinal detachment. Retina 2016;36:342–350.
19. Spaide RF. Retinal vascular cystoid macular edema: review and new theory. Retina 2016;36:1823–1842.
20. Francone A, Govetto A, Yun L, et al. Evaluation of non-exudative microcystoid macular abnormalities secondary to retinal vein occlusion. Graefes Arch Clin Exp Ophthalmol 2021;259:3579–3588.
21. Cohen SY, Dubois L, Nghiem-Buffet S, et al. Retinal pseudocysts in age-related geographic atrophy. Am J Ophthalmol 2010;150:211–217.e1.
22. Lee DH, Park SE, Lee CS. Microcystic macular edema and cystoid macular edema before and after epiretinal membrane surgery. Retina 2021;41:1652–1659.

ULTRA-WIDEFIELD OPTICAL COHERENCE TOMOGRAPHY ANGIOGRAPHY IN MILD FAMILIAL EXUDATIVE VITREORETINOPATHY

YOU WANG, MD, YANTING LAI, MD, XIAODI ZHOU, MD, TING ZHANG, MD, PHD, LIMEI SUN, MD, PHD, ZHAOTIAN ZHANG, MD, PHD, LI HUANG, MD, PHD, SONGSHAN LI, MD, PHD, XIAOYAN DING, MD, PHD

Purpose: To investigate ultra-widefield optical coherence tomography angiography (UWF-OCTA) to detect and evaluate mild familial exudative vitreoretinopathy and compare the detective ratio of UWF-OCTA with ultra-widefield scanning laser ophthalmoscopy and ultra-widefield fluorescein angiography.

Methods: The patients with familial exudative vitreoretinopathy were included in this study. UWF-OCTA, using a 24- × 20-mm montage, was performed for all patients. All images were independently tested for the presence of familial exudative vitreoretinopathy-associated lesions. Statistical analysis was performed with SPSS V.24.0.

Results: Forty-six eyes of 26 participants were included in the study. Ultra-widefield optical coherence tomography angiography was found to be greatly superior to ultra-widefield scanning laser ophthalmoscopy in detecting peripheral retinal vascular abnormality ($P < 0.001$) and peripheral retinal avascular zone ($P < 0.001$). The detection rates of peripheral retinal vascular abnormality, peripheral retinal avascular zone, retinal neovascularization, macular ectopia, and temporal midperipheral vitreoretinal interface abnormality were comparable with ultra-widefield fluorescein angiography images ($P > 0.05$). Furthermore, vitreoretinal traction (17/46, 37%) and small foveal avascular zone (17/46, 37%) were detected effectively on UWF-OCTA.

Conclusion: Ultra-widefield optical coherence tomography angiography is a reliable noninvasive tool to detect familial exudative vitreoretinopathy lesions, especially in mild patients or asymptomatic family members. The unique manifestation of UWF-OCTA offers an alternative to ultra-widefield fluorescein angiography for the screening and diagnosis of FEVR.

RETINA 43:932–939, 2023

Familial exudative vitreoretinopathy (FEVR) is a hereditary disease that was first described by Criswick and Schepens in 1969.[1] It is manifested by different retinal pathologic features, including hardly detectable peripheral retinal vascular anomalies, temporal midperipheral vitreoretinal interface abnormality (TEMPVIA), neovascularization, small foveal avascular zone (FAZ), macular ectopia, and retinal detachment.[1–5] Advanced stages of FEVR can be detected by ocular routine examinations, whereas multimodal imaging, such as ultra-widefield scanning laser ophthalmoscopy (UWF-SLO) and ultra-widefield fluorescein angiography (UWF-FA), is required for asymptomatic patients.[6] Ultra-widefield scanning laser ophthalmoscopy can provide a 200° photographic view of a fundus and assist in the investigation of the changes, including the far peripheral vascular abnormality in FEVR.[3] However, despite the rapid evolution of retinal imaging in recent years, fluorescein angiography (FA) remains the gold standard for the diagnosis of FEVR. Conventional fundus cameras capture a field of 45 to 60° in one

From the State Key Laboratory of Ophthalmology, Zhongshan Ophthalmic Center, Sun Yat-sen University, Guangdong Provincial Key Laboratory of Ophthalmology and Visual Science, Guangzhou, China.

Supported by the Construction Project of High-Level Hospitals in Guangdong Province (303020107, 303010303058); the National Natural Science Foundation of China (82271092)

None of the authors has any financial/conflicting interests to disclose.

Y. Wang and Y. Lai contributed equally to this work as co-first authors.

Reprint requests: Xiaoyan Ding, MD, PhD, State Key Laboratory of Ophthalmology, Zhongshan Ophthalmic Center, Sun Yat-sen University, 54 Xianlie Road, Guangzhou 510060, China; e-mail: dingxiaoyan@gzzoc.com

exposure. Moreover, UWF-FA developed in recent years can provide data covering even 200° in one single image.[7] The use of UWF-FA has been documented in diabetic retinopathy, retinal vein occlusion, retinopathy of prematurity, and FEVR.[3,8–11] However, it is invasive and time-consuming.

Recently, the ability to detect detailed microstructure changes in FEVR with a noninvasive, safe, fast, and reliable instrument has become available with the development of optical coherence tomography angiography (OCTA).[12,13] Our previous study reported a significantly smaller FAZ and decreased vascular density in the parafoveal area by OCTA in FEVR.[4] However, the small retinal field covered by the early device limited its utility in the peripheral retina. To our knowledge, only a few reports in the literature have focused on OCTA in the peripheral retina of FEVR.

The recently developed ultra-widefield optical coherence tomography angiography (UWF-OCTA) system can acquire data from an area of 24 mm in width (120° of fundus view) in a single image while retaining the same resolution with an inbuilt lens, similar to smaller scan sizes.[14] This can allow us to observe the changes in the peripheral retina successfully. Herein, we aim to present a prospective, observational study to compare UWF-OCTA with UWF-SLO and UWF-FA to detect the FEVR lesions located in the peripheral, midperipheral, and posterior retina.

Methods

Subjects

This prospective, observational study was conducted at the Zhongshan Ophthalmic Center, Sun Yat-sen University, from February 2022 to April 2022. It was compiled with the tenets of the Declaration of Helsinki and approved by the institutional review board. Informed written consent was obtained from all the subjects or their legal guardians. To obtain a qualified OCTA image, the fixation is pivotal. Thus, 46 eyes of 26 clinically confirmed mild FEVR patients were included. The exclusion criteria included eyes with poor fixation or a low automated quality index of images (less than 6, ranging from 1 to 10). The severity of FEVR was staged using Trese's staging system.[15]

Data Collection

The data collected included detailed demographics (sex, age, and genotypic mutations) and current ophthalmologic examination findings (best-corrected visual acuity (BCVA), slit-lamp biomicroscopy, dilated fundus examination, and color fundus photography). Multimodal imaging included UWF-SLO (California FA, Optos, Dunfermline, United Kingdom), UWF-FA (California FA, Optos, Dunfermline, United Kingdom), swept-source optical coherence tomography (SS-OCT), and UWF-OCTA (TowardPi BMizar, TowardPi Medical Technology, Beijing, China). The UWF-SLO, UWF-OCTA, and UWF-FA images were evaluated by two masked ophthalmologists (W.Y. and L.Y.). If the results from two evaluators was different, the third masked evaluator, Pro. Ding would evaluate again. And the results from Pro. Ding were accepted. For each image, the presence of the FEVR lesions in the peripheral, midperipheral, and posterior retina were recorded, including the avascular zone, neovascularization, increased branching and/or the straightening of peripheral vessels, vascular leakage, abnormal arteriovenous (A-V) shunt, TEMPVIA, vitreoretinal traction (VRT), macular ectopia, small FAZ, and increases in posterior vessels. Small FAZ was defined as the area <0.18 mm2.[4] For the VRT and neovascularization, each B-scan was examined manually. The sensitivity and specificity for the detection of FEVR lesions were calculated using UWF-FA as the gold standard.

Image Acquisition Protocol

Ultra-widefield optical coherence tomography angiography was obtained using TowardPi BMizar. A swept-source vertical-cavity surface-emitting laser with an A-scan rate of 400 kHz and wavelength centered at 1,060 nm was used, which provided a homogeneous signal strength over a depth range of 6 mm for the vitreous, retina, choroid, and sclera. After pupil dilation, SS-OCT and UWF-OCTA were performed on all patients to obtain amplitude-decorrelation angiography images. To obtain a 200° ultra-wide fundus view, a montage was generated from five 24- × 20-mm OCTA data cubes positioned at five predefined locations (central, superotemporal, superonasal, inferotemporal, and inferonasal), with every single image consisting of 1,280 line positions, 1536 A-scans of each line, and 2,560 points on each A-scan, with the scanning repeated twice. For the UWF-OCTA imaging, automatic segmentation was first used to identify the retinal layers, and manual adjustment of the segmentation was conducted in all images to optimally visualize the morphology of the vasculature. UWF-SLO and UWF-FA were taken on the same day as SS-OCT and UWF-OCTA. A montage was generated from the center and four peripheral (superotemporal, superonasal, inferotemporal, and inferonasal) images of UWF-SLO/FA were obtained.

Statistical Analysis

Statistical analysis was performed using SPSS 24.0 (IBM Corp, Armonk, NY, USA). Normally distributed continuous variables were presented as mean ± SD. Familial exudative vitreoretinopathy lesion detection rate differences between the groups were compared using the chi-square test or Fisher's exact test, and multiplicity adjustments were conducted using the Bonferroni method. Interrater agreement was calculated using kappa statistics—a kappa value of more than 0.61 means good or almost perfect agreement, 0.41 to 0.60 moderate agreement, and less than 0.40 slight or fair agreement. A nominal two-sided *P* value of 0.05 was conside red to indicate statistical significance.

Results

Demographics

In this study, 26 patients were included. The average age was 19.9 ± 15.1 years, and 19 (73.1%) patients were male. Of the 46 eyes included, 41 (89.1%) were diagnosed clinically as stage 1 FEVR, 3 (6.5%) were in stage 2, and 2 (4.4%) were in stage 3. The BCVA ranged from 20/200 to 20/20.

Detection of Peripheral Retinal Vascular Abnormality

The FEVR lesions in the peripheral retina, including the avascular zone, neovascularization, increased branching and/or the straightening of peripheral vessels, and the A-V shunt, were recorded. In UWF-OCTA, the avascular zone appears as a zone with an absent flow signal, and neovascularization appears as a vascular branch with irregular new vessels, adjacent to the avascular zone, which corresponds to the avascular zone evidenced in UWF-FA. B-scans of the neovascularization show ILM breaching and flow signal. An abnormal A-V shunt tends to present at the end of peripheral vessels and seems to match directly without functional capillaries. The manifestation of UWF-SLO, UWF-FA, and UWF-OCTA of representative cases are shown in Figure 1 (UWF-SLO, A and B; UWF-FA, C and D; UWF-OCTA, E and F).

The interrater agreement was 1.0 for avascular zone detection on OCTA, 1.0 for increased branching in and straightening of peripheral vessels, 1.0 for neovascularization, and 0.90 for the abnormal A-V shunt on OCTA. The detective ratio of the avascular zone was 80.4% (37 eyes) on OCTA, about 2 times of that on UWF-SLO (41.3%, 19 eyes, $P < 0.001$), and was comparable with UWF-FA (82.6%, 38 eyes, $P = 0.79$). OCTA also performed better in detecting the increased branching and straightening of peripheral vessels than UWF-SLO ($P < 0.001$), which was similar to UWF-FA ($P = 1.00$). An abnormal A-V shunt was detected in 30 eyes using OCTA and in 29 eyes using UWF-FA ($P = 1.00$), which was difficult to detect by UWF-SLO because of low-resolution vessels. Neovascularization was detected in five eyes (10.9%) on OCTA, with a flow signal on the B-scan. The difference in detective ratio in neovascularization was insignificant using three methods. However, UWF-FA, not OCTA and UWF-SLO, was able to detect vascular leakage effectively (Table). The representative cases are shown in Figure 1.

Detection of Midperipheral and Posterior Retinal Abnormality

Abnormality in the midperipheral retina included TEMPVIA and VRT (Figure 2, UWF-SLO, A; UWF-FA, B; UWF-OCTA, C). The interrater agreement was 1.0 for both lesions on OCTA. Enface OCT of the TEMPVIA showed multiple hyperreflective and hyporeflective lesions in the V-shaped degeneration in the midperipheral retina (Figure 2D). The detective ratio of TEMPVIA was 37% (17 eyes) on OCTA, was comparable with UWF-SLO (39.1%, 18 eyes, $P = 0.83$), and UWF-FA (43.5%, 20 eyes, P=0.524). Vitreoretinal traction was detected in 17 eyes (37%) on OCTA, which cannot be observed on UWF-SLO and UWF-FA (Figure 2, E–G). The abnormality in the posterior retina included macular ectopia, small FAZ, and an increase in posterior vessel. The interrater agreement was 1.0 for macular ectopia, small FAZ detection on OCTA, and 0.66 for the increase in posterior vessels. Macular ectopia was detected in two eyes (6.5%) on OCTA, same as UWF-SLO and UWF-FA (Figure 3A and B). For the increase in posterior vessels, OCTA showed a comparable detection rate with UWF-SLO and UWF-FA ($P > 0.05$). Small FAZ was detected in 17 eyes (37%) on OCTA, which cannot be observed on UWF-SLO and UWF-FA (Figure 3C and D).

Discussion

In this study, we performed a prospective and observational study to evaluate the value of UWF-OCTA in FEVR. To our best knowledge, this study is the first to observe OCTA changes in the peripheral retina and a montage showing a wide-field view in FEVR. Compared with previous studies that focused on macular microvasculature using relatively limited OCTA techniques, our results provide greater insight into a broader range of retina.[4,16,17] We found that

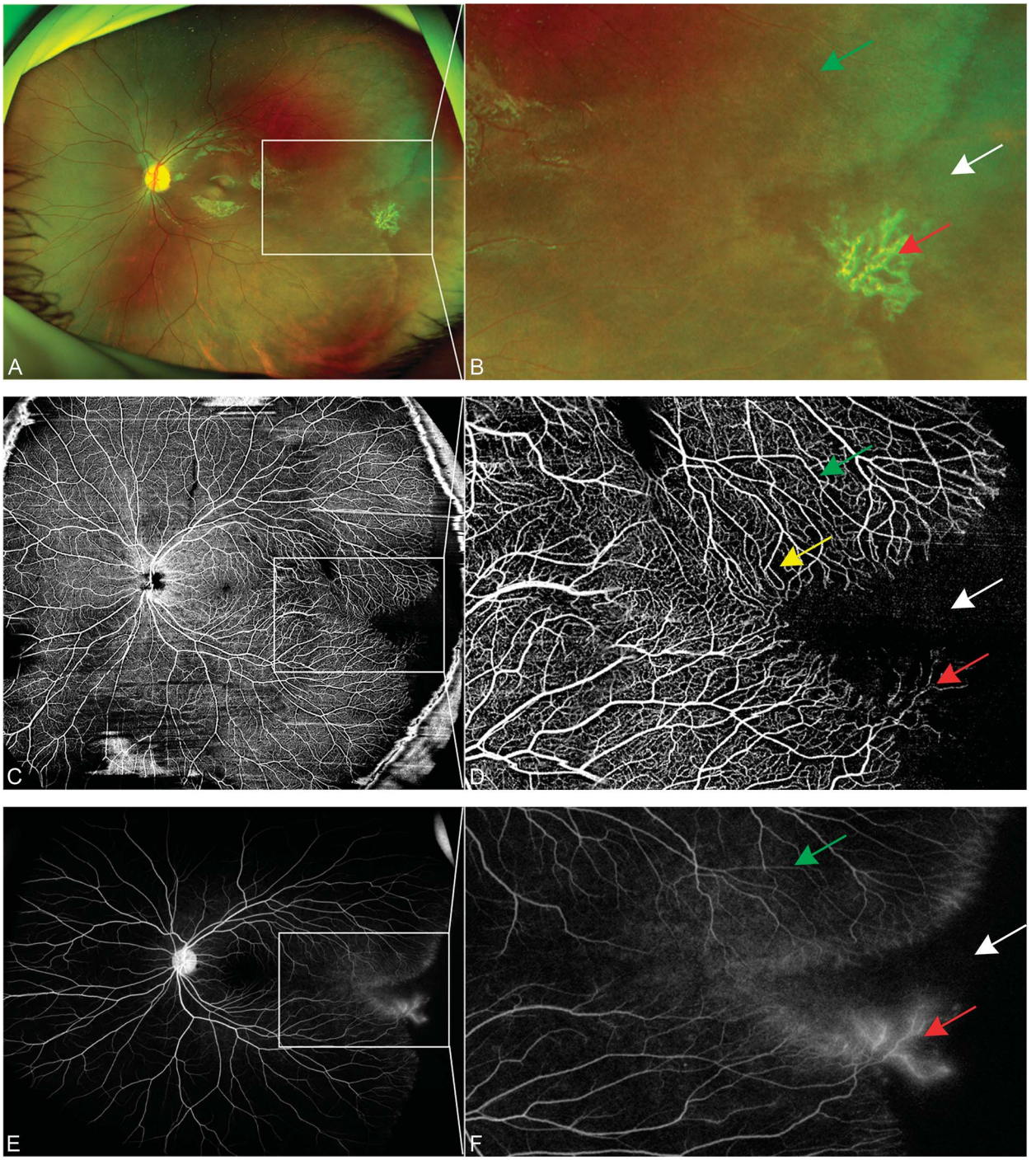

Fig. 1. Representative images of abnormality in temporal peripheral retina in familial exudative vitreoretinopathy on UWF-OCTA versus UWF-SLO and UWF-FA. The photograph was from a ten-year-old boy with 20/20 vision in his left eye. The avascular zone (white arrow), neovascularization (red arrow), and increased branching or straightening of vessels (green arrow) in the peripheral retina was shown on UWF-SLO (**A** and **B**), UWF-OCTA (**C**, **D**, montage image), and UWF-FA (**E** and **F**) images. The abnormal A-V shunt (yellow arrow) was demonstrated on UWF-OCTA.

UWF-OCTA was a highly sensitive noninvasive tool to detect FEVR lesions and was superior to UWF-SLO. Moreover, VRT and small FAZ, which are impossible to observe on UWF-SLO and UWF-FA, were detected effectively on UWF-OCTA.

Ultra-widefield optical coherence tomography angiography facilitates fundus screening for asymptomatic or early-stage FEVR with high diagnostic capability. The peripheral retinal lesions are common among asymptomatic FEVR and can be detected by

Table. The Detection Rate of FEVR Lesions on UWF-OCTA Versus UWF-SLO and UWF-OCTA Versus UWF-FA

FEVR Lesions	UWF-OCTA	UWF-SLO	UWF-FA	*P* UWF-OCTA versus UWF-SLO	*P* UWF-OCTA Versus UWF-FA
Peripheral retinal vascular abnormality					
Avascular zone	37/46 (80.4)	19/46 (41.3)	38/46 (82.6)	<0.001	0.79
Neovascularization	5/46 (10.9)	3/46 (6.5)	5/46 (10.9)	0.459	1
Increase or straightening of peripheral vessels	46/46 (100)	36/46 (78.3)	46/46 (100)	<0.001	1
Vascular leakage	NA	NA	24/46 (52.2)	NA	NA
Abnormal A-V shunt	30/46 (65.2)	0	29/46 (63.0)	NA	1
Midperipheral retinal abnormality					
TEMPVIA	17/46(37.0)	18/46 (39.1)	20/46 (43.5)	0.83	0.524
VRT	17 (37.0)	NA	NA	NA	NA
Posterior retinal abnormality					
Macular ectopia	3/46 (6.5)	2/46 (4.3)	2/46 (4.3)	1.00	1
Small FAZ	17/46 (37.0)	NA	NA	NA	NA
Increase of posterior vessels	45/46 (97.8)	44/46 (95.6)	46/46 (100)	1.00	NA

Small FAZ is defined as the area <0.18 mm^2.

UWF-SLO effectively.[18,19] Lyu et al[6] suggested that UWF-SLO was highly effective in diagnosing FEVR compared with FA as a standard, but the changes in the increased branching or straightening of peripheral vessels and abnormal A-V shunt were not evaluated. Published studies usually use OCTA to evaluate the microstructure of fovea in FEVR for the limited 3-mm × 3-mm or 6-mm × 6-mm view field. In this study, using the montage, the UWF-OCTA provided a 200° view, which is comparable to that of UWF-SLO. The detective ratio of the avascular zone was two times of that on UWF-SLO and was comparable with UWF-FA. Similar results were also shown in detecting the increased branching and straightening of peripheral vessels. These results demonstrated that UWF-OCTA was superior in detecting the avascular zone and the increased branching or straightening of the peripheral retina compared with UWF-SLO. Ultra-widefield optical coherence tomography angiography and UWF-FA had comparable detective ratios in the avascular zone, neovascularization, increased branching or straightening of the peripheral retina, abnormal A-V shunt, TEMPVIA, and macular ectopia. These results showed that UWF-OCTA could be an effective and noninvasive alternative to screen, diagnose, and monitor FEVR, especially for the family members of probands.

Furthermore, UWF-OCTA is effective in detecting TEMPVIA, which we reported in the previous study, and can be also detected by UWF-SLO and UWF-FA.[3] The remarkable vitreous proliferative traction and thinning retina located at the anterior margin of TEMPVIA were noted on UWF-OCT. The identification of TEMPVIA facilitates the diagnosis and management of mild FEVR. In this study on OCTA, TEMPVIA was characterized by a hyporeflective zone with a V-shape and an increase in the superficial loss of deep retinal vessels and capillaries at the vascular–avascular zone. The image of the enface showed a remarkable vascular–avascular junction line and a mottled reflective zone is detected at the peripheral anterior retina of the junction. The manifestation confirms the hypothesis that the vessels become arrested at the posterior margin of TEMPVIA during the development of the retinal vasculature, followed by an increased branching and straightening of pathologic superficial vessels. In this stage, the functional capillaries and deep vessels do not grow as superficial vessels, which is probably related to the thinning of the peripheral retina with TMEPVIA. Further research is warranted to explore the underlying mechanism of the differentiation.

Finally, UWF-OCTA showed the same detective ratio of neovascularization as FFA. Because of severe complications, such as vitreous hemorrhage and retinal detachment, the detection of neovascularization is essential for the management of FEVR. Unlike FFA, which showed hyperfluorescence and leakage in lesions, UWF-OCTA is advantageous in detecting neovascularization with a B-scan, which helps identify neovascularization and distinguishes whether it is located in the vitreous or retina. Moreover, OCTA greatly enhanced the detection of vitreoretinal traction. Consequently, these findings could provide sufficiently important information before further invasive fundus examinations.

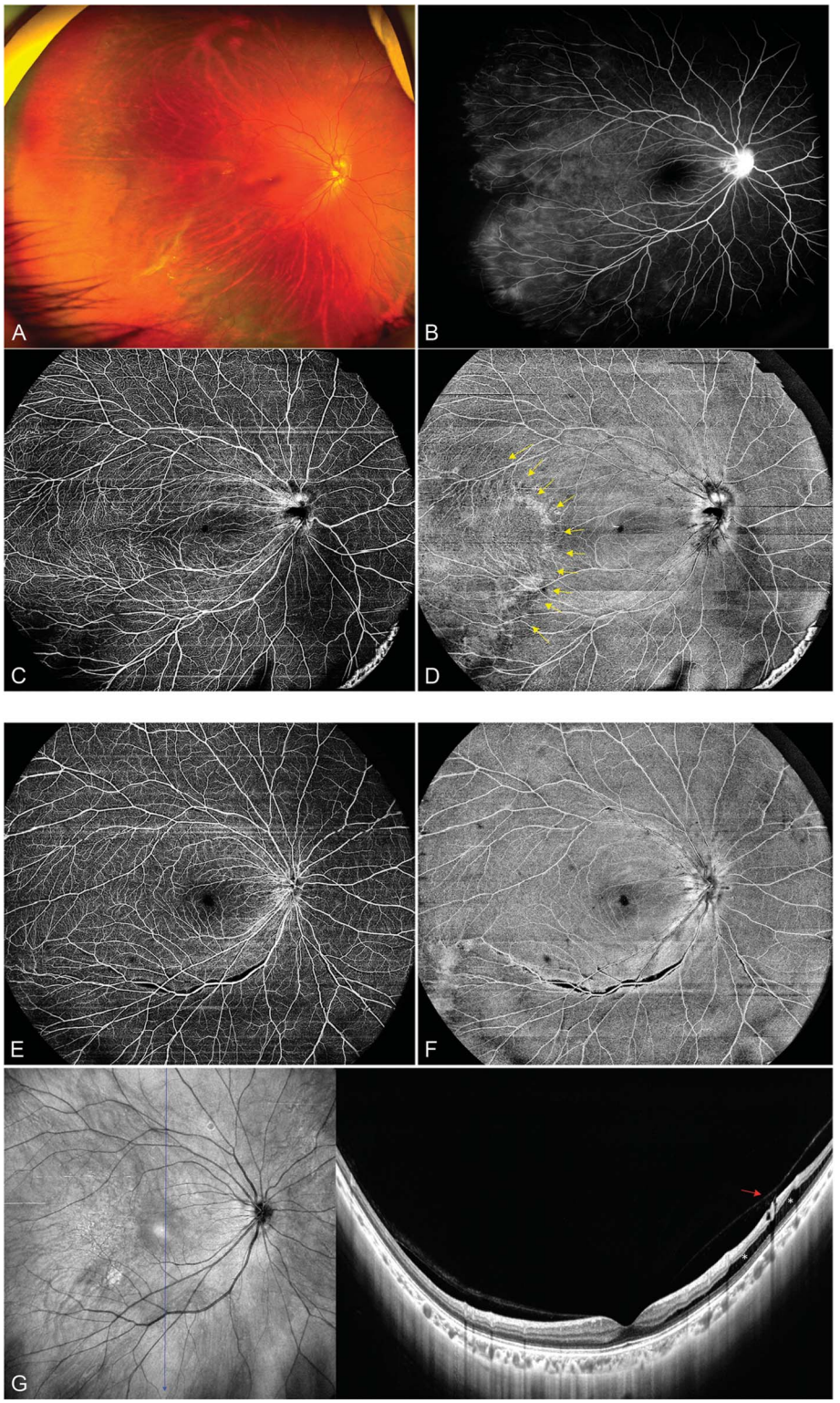

Fig. 2. The representative TEMPVIA was seen on a ten-year-old girl. UWF-SLO (**A**), UWF-FA (**B**), UWF-OCTA (**C**), and en face UWF-OCTA (**D**) of the same section were displayed. Optical coherence tomography angiography demonstrated that TEMPVIA was characterized by a hyporeflective zone with a V-shape (*yellow arrow*) and an increase of superficial and loss of deep retinal vessels and capillary at the vascular–avascular zone. The image of en face showed a remarkable vascular–avascular junction line, and a mottled zone is detected at the peripheral anterior retina of the junction. The representative VRT was observed on a 27-year-old woman. Ultra-widefield optical coherence tomography angiography (**E**), enface UWF-OCTA (**F**), and B-scan (**G**) were displayed. The B-scan showed an incomplete posterior vitreous detachment with the persistently adherent vitreous exerting tractional pull on the retina (*red arrow*) and consequent retinoschisis (asterisks).

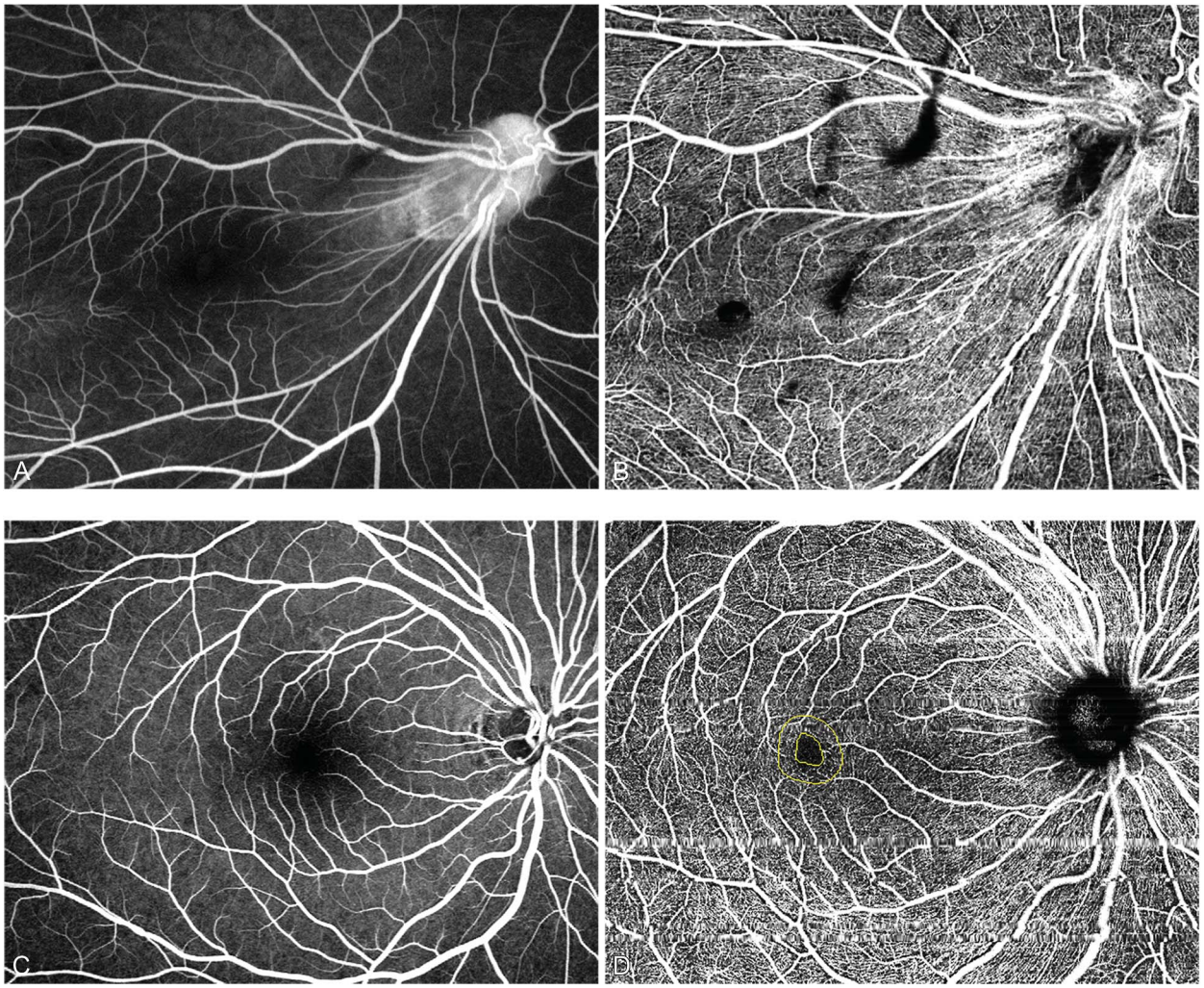

Fig. 3. The representative macular ectopia (**A** and **B**) from a ten-year-old boy and small foveal avascular zone and increase of posterior vessels (**C** and **D**) from a 32-year-old man were shown on FA and OCTA. Small FAZ was defined as the area < 0.18 mm^2.

Our results must be considered in light of several limitations. First, because of the requirement for good fixation, this examination is suitable for patients with good vision or asymptomatic family members. For patients with poor vision, it is difficult to obtain high-quality images. Second, the retinal vascular leakage cannot be detected with UWF-OCTA, which is also important for the evaluation of FEVR. Consequently, an invasive evaluation, such as UWF-FA, is still necessary.

Conclusion

In conclusion, we have shown that UWF-OCTA is a reliable noninvasive tool to detect FEVR, especially in mild symptomatic or asymptomatic family members. UWF-OCTA offered a safe, fast alternative for the screening and diagnosis of FEVR and may be a great help in the early treatment of this disease.

Key words: ultra-widefield optical coherence tomography angiography, familial exudative vitreoretinopathy, neovascularization, temporal midperipheral vitreoretinal interface abnormality.

Acknowledgments

The authors are grateful to Dr. Yu Shanshan for her help with the examination of patients in this study.

References

1. Gilmour DF. Familial exudative vitreoretinopathy and related retinopathies. Eye (Lond) 2015;29:1–14.
2. Miyakubo H, Hashimoto K, Miyakubo S. Retinal vascular pattern in familial exudative vitreoretinopathy. Ophthalmology 1984;91:1524–1530.
3. Zhang T, Wang Z, Sun L, et al. Ultra-wide-field scanning laser ophthalmoscopy and optical coherence tomography in FEVR:

findings and its diagnostic ability. Br J Ophthalmol 2021;105: 995–1001.
4. Chen C, Liu C, Wang Z, et al. Optical coherence tomography angiography in familial exudative vitreoretinopathy: clinical features and phenotype-genotype correlation. Invest Ophthalmol Vis Sci 2018;59:5726–5734.
5. Criswick VG, Schepens CL. Familial exudative vitreoretinopathy. Am J Ophthalmol 1969;68:578–594.
6. Lyu J, Zhang Q, Wang SY, et al. Ultra-wide-field scanning laser ophthalmoscopy assists in the clinical detection and evaluation of asymptomatic early-stage familial exudative vitreoretinopathy. Graefes Arch Clin Exp Ophthalmol 2017;255:39–47.
7. Wessel MM, Aaker GD, Parlitsis G, et al. Ultra-wide-field angiography improves the detection and classification of diabetic retinopathy. Retina 2012;32:785–791.
8. Cui Y, Zhu Y, Wang JC, et al. Comparison of widefield swept-source optical coherence tomography angiography with ultra-widefield colour fundus photography and fluorescein angiography for detection of lesions in diabetic retinopathy. Br J Ophthalmol 2021;105:577–581.
9. Ashraf M, Sampani K, AbdelAl O, et al. Disparity of microaneurysm count between ultrawide field colour imaging and ultrawide field fluorescein angiography in eyes with diabetic retinopathy. Br J Ophthalmol 2020;104:1762–1767.
10. Ryu G, Park D, Lim J, et al. Macular microvascular changes and their correlation with peripheral nonperfusion in branch retinal vein occlusion. Am J Ophthalmol 2021;225:57–68.
11. Gunay M, Tugcugil E, Somuncu AM, et al. The clinical use of ultra - wide field imaging and intravenous fluorescein angiography in infants with retinopathy of prematurity. Photodiagnosis Photodynamic Ther 2022;37:102658.
12. Yonekawa Y, Thomas BJ, Drenser KA, et al. Familial exudative vitreoretinopathy: spectral-domain optical coherence tomography of the vitreoretinal interface, retina, and choroid. Ophthalmology 2015;122:2270–2277.
13. Zhang J, Jiang C, Ruan L, et al. Macular capillary dropout in familial exudative vitreoretinopathy and its relationship with visual acuity and disease progression. Retina 2020;40:1140–1147.
14. Xuan Y, Chang Q, Zhang Y, et al. Clinical observation of choroidal osteoma using swept-source optical coherence tomography and optical coherence tomography angiography. Appl Sci 2022;12:4472.
15. Pendergast SD, Trese MT. Familial exudative vitreoretinopathy. Results of surgical management. Ophthalmology 1998; 105:1015–1023.
16. Koulisis N, Moysidis SN, Yonekawa Y, et al. Correlating changes in the macular microvasculature and capillary network to peripheral vascular pathologic features in familial exudative vitreoretinopathy. Ophthalmol Retina 2019;3:597–606.
17. Hsu ST, Finn AP, Chen X, et al. Macular microvascular findings in familial exudative vitreoretinopathy on optical coherence tomography angiography. Ophthalmic Surg Lasers Imaging Retina 2019;50:322–329.
18. Yuan M, Yang Y, Yu S, et al. Posterior pole retinal abnormalities in mild asymptomatic FEVR. Invest Ophthalmol Vis Sci 2014;56:458–463.
19. Kashani AH, Learned D, Nudleman E, et al. High prevalence of peripheral retinal vascular anomalies in family members of patients with familial exudative vitreoretinopathy. Ophthalmology 2014;121:262–268.

IMMEDIATE VITRECTOMY vs TAP AND INJECT IN EYES WITH ACUTE POSTCATARACT ENDOPHTHALMITIS AND VISUAL ACUITY ≥HM

A Randomized Clinical Trial

ALOK C. SEN, MS,* SONALI M. MEHTA, DNB,‡ ASHITA SULE, MBBS,§ AMRUTA V. MORE, MS,* SACHIN B. SHETTY, MS,* JAYANTI SINGH, MS,† SHUBHI TRIPATHI, DNB,* RUPESH AGRAWAL, MS,¶ DINESH TALWAR, MD**

Purpose: To compare the outcomes of immediate pars plana vitrectomy (PPV) and tap and inject in eyes with postcataract surgery endophthalmitis.

Methods: Patients presenting with acute postcataract surgery endophthalmitis and visual acuity between ≥ hand movement and <6/18 were randomized to receive either PPV (Group A) or tap and inject (Group B).

Results: There were 26 and 31 eyes in Group A and Group B, respectively. The final mean visual acuity at 6 weeks [0.14 (Snellen equivalent 6/7.5) versus 0.22 (Snellen equivalent 6/9.5) LogMAR in Groups A and B, respectively; $P = 0.2$] was similar. However, eyes in Group A had significantly greater mean letter gain in vision compared with Group B (66.36 vs. 43.36, $P = 0.02$), and more eyes in Group A (88%) than in Group B (65%) attained a visual acuity of ≥ 6/18 ($P = 0.06$). Eyes in Group B needed more reinterventions including delayed vitrectomy after tap and inject than those in Group A (39% vs. 8%; $P = 0.09$). On subgroup analysis, the mean visual acuity at the final follow-up was significantly better in the immediate PPV group compared with the delayed PPV group ($P = 0.04$).

Conclusion: PPV resulted in earlier recovery, lesser interventions, and greater change in visual acuity than tap and inject in eyes with postcataract surgery endophthalmitis presenting with visual acuity of ≥HM.

RETINA 43:940–946, 2023

The management of postcataract surgery endophthalmitis (PCE) is traditionally guided by the Endophthalmitis Vitrectomy Study, which recommends primary tap and injection (T&I) in eyes with vision better than the perception of light.[1] With the advent of microincision vitreoretinal surgery, surgeons now have a lower threshold for pars plana vitrectomy (PPV) irrespective of the presenting visual acuity.[2] Microincision vitreoretinal surgery results in lesser postoperative inflammation with faster recovery.[3] Recent studies have indicated better clinical outcomes and the need for fewer procedures in eyes undergoing primary PPV.[4,5] Conversely, a meta-analysis of 15 retrospective case series found intravitreal injections to be noninferior to PPV in the management of PCE.[6] Thus, whether immediate PPV gives better outcomes than primary T&I remains debatable. In this prospective randomized study, we investigated the efficacy of immediate PPV as compared with immediate T&I in patients with PCE presenting with hand movement (HM) or better vision.

From the *Department of Vitreo-retina; and †Department of Vitreo-retina; and ‡Sadguru Netra Chikitsalaya and Post Graduate Institute of Ophthalmology, Chitrakoot; §Yong Loo Lin School of Medicine, National University of Singapore, Singapore; ¶National Healthcare Group Eye Institute, Tan Tock Seng Hospital, Singapore; and **Department of Vitreo-retina, Indraprastha Apollo Hospital & Centre for Sight, New Delhi.

The authors reported that there is no funding associated with the work featured in this article.

No potential conflict of interest was reported by the authors.

Reprint requests: Alok Sen, MS, Department of Vitreo-retina, Sadguru Netra Chikitsalaya and Post Graduate Institute of Ophthalmology, Chitrakoot, Madhya Pradesh, 210204, India; e-mail: draloksen@gmail.com

Materials and Methods

This randomized control study was conducted at a tertiary eye care center in Central India (performing >100,000 cataract surgeries/year). The institute performed 122,104 small-incision cataract surgeries and 51,012 phacoemulsification surgeries from September 2019 to June 2021. The aim of this study was to compare functional and anatomical outcomes between eyes undergoing either immediate PPV or T&I for acute PCE presenting with a visual acuity of ≥HM. This study was approved by the institutional ethics committee and adhered to the tenets of the Declaration of Helsinki.

Patients older than 18 years presenting with clinical features of acute PCE within 6 weeks of the uneventful cataract surgery, either small-incision cataract surgery (73.68%) or phacoemulsification (26.32%), were included. Only those eyes with the best-corrected visual acuity (BCVA) of ≥HM and < 6/18 were recruited. Patients undergoing small-incision cataract surgery were predominantly from lower socioeconomic backgrounds.

Patients with a history of treatment for PCE; cluster endophthalmitis; intraoperative (cataract surgery) complications; bleb-related, endogenous, or traumatic etiologies; endophthalmitis after infectious keratitis; corneal infiltration or melt; and the presence of retinal or choroidal detachment at presentation were excluded.

Data were collected using a deidentified study proforma that included age, sex, onset and duration of symptoms, detailed history, date of surgery, type of cataract surgery, and any intraoperative complications. Postcataract surgery BCVA was documented in the clinical case sheet. Early treatment for diabetic retinopathy study (ETDRS) vision was recorded at presentation and at 1 week, 4 weeks, and 6 weeks postintervention. The visual acuity was converted to the LogMAR using the conversion table given by the ICO (International Congress of Ophthalmology) report, 2002. Intraocular pressure was recorded using a noncontact tonometer, and the findings of anterior and posterior segment examination including anterior chamber reaction and vitritis/media haze (Nussenblatt scale) were noted at each visit. An ultrasound B-scan was performed whenever the fundus details were not visible.

All the included patients were admitted after informed consent and randomized into treatment Group A or Group B as per a predecided randomization order using the random number tables on the GraphPad Prism application.

All patients underwent their respective interventions on the day of the presentation. Eyes in Group A (PPV) underwent a 25-gauge three-port PPV + intravitreal antibiotics (IVAB) as the primary intervention. PPV was performed by one of the two senior vitreoretinal surgeons (AS and SS). The infusion was switched on after obtaining an undiluted vitreous sample. A posterior vitreous detachment was performed if not present and as much of the peripheral vitreous was removed as possible without scleral indentation. Eyes in Group B (T&I) underwent a 25-gauge single-port vitreous biopsy + IVAB as the primary intervention. All the eyes received IVAB as 0.1 mL (1 mg/0.1 mL) of vancomycin + 0.1 mL (2.25 mg/0.1 mL) of ceftazidime. A 0.5-mL undiluted vitreous sample was collected for all the patients. This sample was sent in a sterile vial and nutrient broth for microbiological analysis.

All the patients were reevaluated on postintervention days 1, 3, 7, 14, 28, and 42. The decision to retreat was taken 48 to 72 after the primary intervention. Eyes showing worsening of anterior segment inflammation and/or media haze from baseline, as per the clinical judgment of two senior vitreoretinal surgeons (AS and SS), were advised retreatment. Eyes in Group B were advised PPV along with repeat IVAB while those in Group A underwent a repeat IVAB.

The primary end points were the mean change in BCVA at 7 days and 42 days and the proportion of patients achieving BCVA >6/18 at 42 days in each group. Secondary end points were reintervention rate and proportion of patients with persistent media haze at the end of 6 weeks.

To look for the effect of delay in PPV on outcomes, a subgroup analysis was performed comparing the outcomes of eyes that underwent immediate PPV (Group A eyes) with delayed PPV (Group B eyes with reintervention).

Statistical Analysis

The sample size was calculated based on the expected change in the final BCVA. In a similar protocol,[7] 23% of patients achieved a final BCVA of 20/40 after early PPV, which is lower than that reported in another series (40%–91%).[5,6] Applying these to the sample size formulae, the sample size was calculated as 40 with 80% power and a 5% significance level.

For the feasibility of analysis, we converted Snellen acuity to LogMAR acuity. We applied the Fisher exact test to compare the categorical outcome variables and the nonparametric Mann–Whitney *U* test to compare the continuous ones between the two groups of patients. Frequencies and percentages summarized categorical variables, and continuous variables were summarized by means and standard deviations. Statistical analysis was performed using R version 4.0.5.

Table 1. Demographic Data, Baseline Clinical Features, and Baseline Visual Acuity

Data	Group A (Immediate Pars Plana Vitrectomy)	Group B (Tap and Inject)	*P*, Statistical Tests
Mean age in years (range)	59.81 (32–72)	61.54 (45–74)	0.56, Mann–Whitney *U* test
Sex			0.79, Fisher exact test
Male	14 (53.85%)	15 (48.38%)	
Female	12 (46.15%)	16 (51.62%)	
Type of surgery			0.67, Fisher exact test
SICS	19 (73.08%)	23 (74.19%)	
Phacoemulsification	7 (26.92%)	8 (25.81%)	
Clinical Charateristics			
Mean duration of symptoms in days (range)	7.88 (1–23)	7.1 (1–25)	0.41, Mann–Whitney *U* test
Corneal edema	6 (23.08%)	5 (16.13%)	0.52, Fisher exact test
Hypopyon	16 (61.54%)	16 (51.61%)	0.5, Fisher exact test
Bag exudates	7 (7.25%)	7 (22.58%)	0.76, Fisher exact test
Fibrin in AC	21 (80.77%)	23 (74.19%)	0.75, Fisher exact test
Mean intraocular pressure (range)	13.65 mmHg (8–24)	13.35 mmHg (7–20)	0.99, Mann–Whitney *U* test
Media haze			0.75, Fisher exact test
Vitreous haze 0	1(3.85%)	0 (0%)	
Vitreous haze 1	5 (19.23%)	4 (12.90%)	
Vitreous haze 2	4 (15.38%)	5 (16.13%)	
Vitreous haze 3	3 (11.54%)	8 (25.81%)	
Vitreous haze 4	7 (26.92%)	7 (22.58%)	
Vitreous haze 5	6 (23.08%)	7 (22.58%)	
Baseline visual acuity			
Visual acuity at presentation with endophthalmitis	1.5 LogMAR (Snellen equivalent <6/60)	1.24 LogMAR (Snellen equivalent <6/60)	0.08, Mann–Whitney *U* test
ETDRS letter count at baseline	25.19	38.23	0.08, Mann–Whitney *U* test

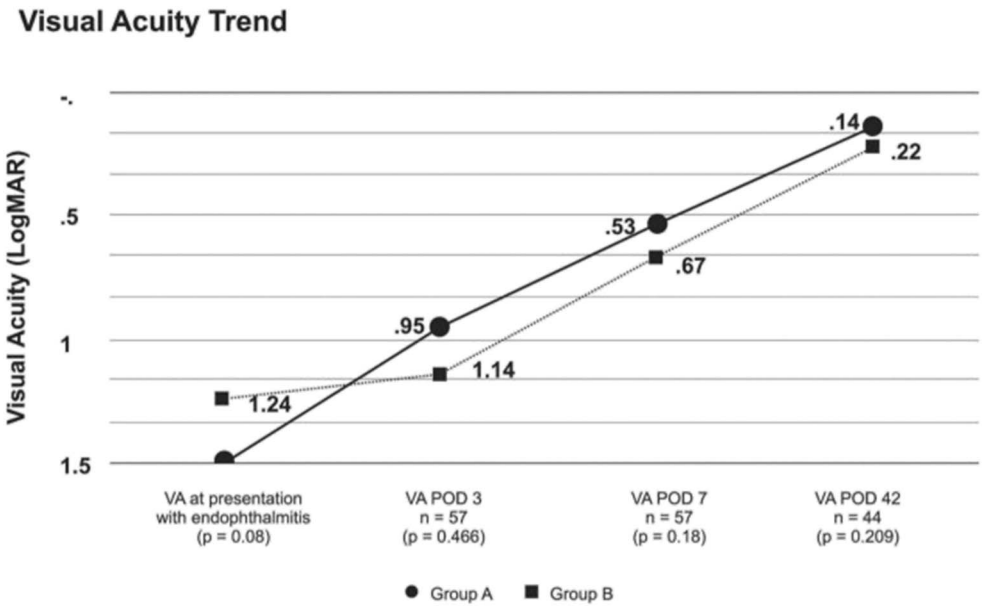

Fig. 1. A line diagram showing the visual acuity trend (in LogMAR) over the 6-week follow-up duration in the eyes that underwent PPV (Group A —solid line) and T&I (Group B —dotted line). Group A shows a faster visual recovery, and Group B shows an improving trend in visual acuity after re-interventions at POD 3.

Table 2. Mean Letters Gain Visual Acuity in Each Group (ETDRS Letters)

	Baseline Letter Count at Presentation	Letter Gain at POD 7 (Letter Count at POD 7—Baseline Letter Count)	Letter Gain at POD 42 (Letter Count at POD 42—Baseline Letter Count)
Group A (primary pars plana vitrectomy)	25.19	47.69 (72.88–25.19)	66.36 (93.19–25.19)
Group B (primary tap and inject)	38.23	28.23 (66.45–38.23)	43.36 (85.64–38.23)
P value	0.08	0.005	0.02

Results

During the 18-month study period, of 164,366 patients who underwent cataract surgery, 84 patients were diagnosed with acute PCE. The incidence of endophthalmitis was noted to be 0.051%. Of these, 60 eyes of 60 patients met the study's inclusion and exclusion criteria. Three patients did not give consent to receive treatment as per protocol and were excluded. The remaining 57 eyes were randomized to either immediate PPV (n = 26) or immediate IVAB (n = 31).

The mean age was 60.7 ± 8.3 years (range, 32–74 years). The baseline demographics were comparable between the two groups (Table 1). The distribution of presenting signs of inflammation in the form of aqueous cells and flare was similar in both the groups ($P = 0.11$ and $P = 0.31$, respectively, Fisher exact test). Similarly, the distribution of posterior segment inflammation and media haze at presentation was similar between the two groups ($P = 0.75$, Fisher exact test) (Table 1).

Visual Acuity Outcomes

Although the mean baseline BCVA was slightly better in Group B, the difference was not statistically significant ($P = 0.08$) (Table 1). There was no significant difference between the mean visual acuity in each group on postoperative days 7 or 42 (P values = 0.18 and 0.209, respectively, Mann–Whitney U test) (Figure 1). However, there was a significant difference in the mean change in BCVA (letter gain) from presentation to postintervention days 7 and 42 between the two groups in favor of Group A (Table 2). At the final follow-up, the proportion of patients who achieved a BCVA beyond 6/18 (0.5 LogMAR) in Group A was 88% and 65% in Group B ($P = 0.06$, Fisher exact test).

On subgroup analysis of eyes that underwent immediate (n = 26) versus delayed PPV (n = 12), at the baseline, there was no significant difference in the mean visual acuity and visual acuity distribution. However, at 1 week, the mean visual acuity was better in the immediate PPV group ($P = 0.086$) and a higher proportion of eyes in this group had >6/18 vision ($P = 0.003$). The mean visual acuity at the final follow-up was significantly better (0.14 vs. 0.45, $P = 0.04$, Mann–Whitney U test) in the immediate PPV compared with delayed PPV subgroups (Table 3). In addition, at the final follow-up, the proportion of patients with BCVA greater than 6/18 (0.5 LogMAR) was significantly higher in the immediate PPV subgroup (84.61%) compared with the delayed PPV subgroup (33.33%) ($P = 0.004$, Fisher exact test) (Table 4).

Reinterventions

The percentage of eyes needing reintervention was significantly higher in Group B [12/31 (39%)] compared with Group A [2/26 (8%)] ($P = 0.012$, Mann–Whitney U

Table 3. Comparison of the Visual Acuity Trend Between the Primary Vitrectomy and Delayed Vitrectomy (Group IVAB Patients Who Required Reintervention as a Delayed PPV Within 72 hours)

	Baseline	Day 7 Mean Visual Acuity (LogMAR)	Day 7 Gain in Mean Visual Acuity (LogMAR)	Day 7 Mean Visual Acuity (LogMAR)	Final Gain in Mean Visual Acuity (LogMAR)
Primary vitrectomy (26)	1.5	0.53	−0.96	0.14	−1.33
Delayed vitrectomy[8]	1.38	0.99	−0.38	0.45	−0.67
P value (Mann–Whitney *U* test)	0.7	0.004	0.009	0.069	0.01

Table 4. Subgroup Analysis of Primary PPV Versus Delayed PPV

	HM	CF-6/60	>6/60–6/18	>6/18	*P*
Baseline					
Group A (26)	15 (57.69%)	7 (26.92%)	4 (15.38%)	0 (0)	0.718
Delayed PPV[8]	7 (58.33%)	2 (16.67%)	3 (25%)	0 (0)	
1-week follow-up					
Group A (26)	1 (3.85%)	2 (7.70%)	10 (38.46%)	13 (50%)	0.086
Delayed PPV[8]	3 (25%)	1 (8.33%)	6 (50%)	2 (16.67%)	
6-week follow-up					
Group A (26)	0 (0)	1 (3.85%)	3 (11.54%)	22 (84.62%)	0.004
Delayed PPV[8]	2 (16.67%)	2 (16.67%)	4 (33.33%)	4 (33.33%)	

test). Similarly, the average number of reinterventions per eye was significantly higher in Group B (0.37) compared with Group A (0.08) (P = 0.006, Mann–Whitney U test) (Table 5). The mean time to reintervention was 2.5 days in Group A (range, 2–3 days) and 2.8 days in Group B (range, 2–4 days). The eyes presenting with HM vision needed a greater number of interventions in the IVAB group as compared with the immediate PPV group (Table 6). Table 7 summarizes the statistical significance of this difference.

The distribution of vitreous haze grading was similar between the groups at the baseline. At the last follow-up, two eyes in Group B had a vitreous haze of Grades 1 and 2. By contrast, none in Group A had persistent vitreous haze. The mean intraocular pressure at baseline and that at the final follow-up were comparable between both the groups (P = 0.99 and P = 0.27, Mann–Whitney U test). One patient in Group A had primary angle-closure glaucoma and needed antiglaucoma medication. One patient in Group B had a final intraocular pressure of 4 mmHg and needed permanent silicone oil fill. In addition, one patient in Group B developed retinal detachment.

The overall culture positivity rate was 26.32%. In Group A, six of 26 eyes compared with nine of 31 eyes in Group B were culture-positive. The rate was similar between the two groups (23.08% vs. 29.03%, respectively; P value = 0.76, Fisher exact test). Positive cultures were not obtained from any of the eyes that underwent reintervention. The most common organisms isolated were Gram-positive cocci (90% on stain and 46% on culture). *Staphylococcus epidermidis* was the most common isolate seen in four samples (2 eyes in each group) (Table 8).

Discussion

In this study, we aimed to compare the outcomes of immediate PPV and T&I in patients with acute PCE presenting with BCVA between HM and 6/18. Most of our patients underwent small-incision cataract surgery. We found that although patients in both groups had a comparable mean visual acuity at 7 days and 42 days postintervention, the mean change in the visual acuity (ETDRS letters) was significantly higher in the PPV group. Moreover, nearly 40% of patients required retreatment in the T&I group compared with just 10% of patients in the PPV group. We also noted that eyes undergoing immediate vitrectomy had significantly better visual acuity gains at 6 weeks as compared with those that underwent delayed PPV.

The Endophthalmitis Vitrectomy Study[1] observed that in the subgroup of patients presenting with BCVA better than or equal to HM, the chance of achieving a BCVA better than 20/40 at the 9-month follow-up was similar for patients in both the treatment groups (64% vs. 62%). They recommended T&I in eyes with visual acuity equal to or better than HM. However, the findings of Endophthalmitis Vitrectomy Study were influenced by the protocol of performing a limited vitrectomy and a lack of early postoperative outcome analysis. In this study, a more extensive PPV was performed including PVD induction and base dissection as far as possible. With the availability of microincision vitreoretinal surgery and faster recovery post-PPV, it is prudent to revisit the benefit of immediate PPV using microincision vitreoretinal surgery over immediate T&I, especially during the early postoperative period.

In this study, a greater improvement in vision was seen in the patients Group A during the early postintervention period compared with the patients in Group B (Figure 1). Although the final mean vision

Table 5. Retreated Patients

Retreatment	Group A (26)	Group B (31)	Total	*P*
Yes	2 (7.70%)	12 (38.70%)	14	0.012
No	24 (92.30%)	19 (61.29%)	43	
Total	26	31	57	

Table 6. Distribution of Retreated Patients as per the Baseline Visual Acuity

Presenting Visual Acuity	Retreated Group A (2/26)	Retreated Group B (12/31)	Total	*P*
HM	1 (1/15)–6%	7 (7/13)–53%	8	0.692
CF–6/60	1 (1/7)–14%	2 (2/9)–22%	3	
>6/60–6/18	0 (0)	3 (3/9)–33%	3	
Total	2	12	14	

was similar in both the groups, the visual gain (ETDRS letters) was significantly higher for the patients in Group A compared with the patients in Group B at each evaluation time point (Table 2). The eyes that underwent delayed vitrectomy did show improvement. However, the final visual acuity was significantly better in eyes that underwent immediate vitrectomy. It is well known that PPV not only helps in reducing the microbiological load but also reduces the inflammatory cytokines, and both aid in reducing the tissue damage and improve outcomes.[2]

Altan et al[7] reported better visual outcomes with immediate PPV compared with immediate intravitreal injection in eyes with HM or better vision. Their criteria for immediate PPV in these eyes included the presence of diabetes, absence of red reflex, presence of an afferent pupillary defect, and hypopyon of >1.5 mm. Similarly, a retrospective study by Crosby et al[4] reported a better mean visual improvement in the primary PPV group compared with the primary tap and inject group. They noted a significant difference in median gain in the visual acuities between the two groups in favor of early PPV (P = 0.02). More recently, Tabatabaei et al[5] in a prospective nonrandomized study demonstrated significantly better visual outcomes with early PPV compared with T&I at a 6-month follow-up. This study only included eyes presenting with HM vision, and the results corroborate well with our study.

The guidelines for the management of acute postoperative endophthalmitis published by the European Society of Cataract and Refractive Surgery recommended immediate complete vitrectomy including in eyes with visual acuity better than PL.[9] More recently, the European Vitreo-Retinal Society Endophthalmitis Study Report 2[10] showed that despite the increasing use of vitrectomy in the treatment of PCE, the visual outcomes between PPV and T&I alone may be similar. However, even in this report, more patients in the PPV (14.7%) group had a final vision of >20/25 compared with the T&I group (3.6%), suggesting the advantage of PPV over IVAB in selected patients.

A recent meta-analysis of 15 case series showed T&I noninferior to PPV in the management of postcataract, postintravitreal injection, and post-PPV endophthalmitis, and the inclusion criteria varied in these studies.[6] However, in our study that included only acute postcataract surgery endophthalmitis, the proportion of patients achieving visual acuity better than 6/18 was higher in Group A compared with Group B (P = 0.06). The difference just approached statistical significance. We speculate that the lack of statistical significance in our series could be because almost 40% of patients who underwent T&I received delayed PPV. Moreover, on comparing eyes that underwent immediate PPV with those that underwent delayed PPV after primary IVAB, we noted a significantly greater improvement in the final visual acuity in favor of the former at 6 weeks.

It is difficult to do a direct comparison of results across these studies because of the heterogeneity of the sample, differences in inclusion and exclusion criteria, and outcome measures. However, it does seem likely that early PPV may provide superior outcomes, particularly during the early postintervention period, while delaying PPV may result in suboptimal outcomes in some of the cases.

In this study, a greater proportion of eyes in Group B needed reintervention (39%) compared with Group A (10%, P = 0.09). Similarly, a much higher number of retreatments per eye were required in Group B patients (P = 0.006). Our data suggest that eyes undergoing immediate PPV were more likely to benefit from a single intervention than those undergoing initial IVAB. The greatest benefit of immediate PPV was seen in eyes presenting with visual acuity of HM.

In congruence with our results, other studies[10–12] have also reported a greater need for reinterventions in eyes undergoing primary intravitreal injections compared with primary vitrectomy. Even Endophthalmitis Vitrectomy Study showed that significantly more eyes needed retreatments in eyes undergoing T&I compared with vitrectomy.[8] Inadequate clearing of bacteria with

Table 7. Retreatment in Patients With HM Vision

Presenting Visual Acuity (HM)	Group A	Group B	Total	*P* (Fisher Exact Test)
Retreated	1 (1/15)–6%	7 (7/13)–53%	8	0.010
Not retreated	14 (14/15)–93.3%	6 (6/13)–46.1%	20	
Total	15	13	28	

Table 8. Distribution of Microorganisms

Organism	Group A	Group B
Gram-positive cocci	4 (15.38%)	4 (12.90%)
Gram-positive bacilli	2 (7.69%)	4 (12.90%)
Gram-negative bacilli	1 (3.85%)	1 (3.23%)

intravitreal injections alone may be the reason for the need for more reinterventions with T&I.[4,5,12]

We noted almost similar improvement in media clarity in both groups at the final follow-up. Again, this could be because almost 40% of the eyes in the initial tap and injection group underwent secondary PPV.

Poor anatomical outcomes were seen in three eyes in Group B. However, it is hard to conclude whether this was due to a delay in PPV in these eyes because of the smaller sample size. However, none of the eyes undergoing primary PPV had poor anatomical outcomes, suggesting that the procedure is safe.

Our study was limited by a small sample size. Owing to a low incidence of endophthalmitis, it was difficult to obtain a large sample size from a single center. Although we did stratify the patients based on baseline media haze, we could not do a meaningful statistical analysis because of the small number. Finally, the reintervention criteria were not completely objective and depended on the treating surgeon's clinical judgment.

Despite these limitations, our study showed early visual rehabilitation in the PPV group, a greater number of reinterventions in the early tap and inject group, and poorer outcomes in the delayed PPV group. With the ever-increasing expectations of patients undergoing cataract surgery, it would be prudent to subject these eyes to early vitrectomy rather than delayed vitrectomy to achieve a faster recovery.

Conclusion

PPV resulted in earlier recovery, lesser interventions, and greater change in visual acuity than T&I in eyes with PCE presenting with visual acuity of ≥HM. Although the overall final visual acuity was similar between the two primary groups, delaying PPV may adversely affect the outcomes.

Key words: endophthalmitis, cataract surgery, pars plana vitrectomy, intravitreal antibiotics.

References

1. Endophthalmitis Vitrectomy Study Group. Results of the Endophthalmitis Vitrectomy Study: a randomised trial of immediate vitrectomy and of intravenous antibiotics for the treatment of postoperative bacterial endophthalmitis. Arch Ophthalmol 1995;113:1479–1496.
2. Kuhn F, Gini G. Ten years after. Are findings of the Endophthalmitis Vitrectomy Study still relevant today?. Graefe's Archive Clin Exp Ophthalmol 2005;243:1197–1199.
3. Fujii GY, De Juan E Jr, Humayun MS, et al. Initial experience using the transconjunctival sutureless vitrectomy system for vitreoretinal surgery1 1The new Transconjunctival Sutureless Vitrectomy System is disclosed to Bausch & Lomb Surgical, St. Louis, MO. The Microsurgery Advanced Design Laboratory (MADLAB) may receive royalties related to the sale of this and other instruments mentioned in the article. Ophthalmology 2002;109:1814–1820.
4. Crosby NJ, Westcott M, Michael E, et al. Comparative outcomes of primary vitrectomy versus tap and inject for endophthalmitis following phacoemulsification cataract surgery. Ocul Immunol Inflamm 2020;15:1–7.
5. Tabatabaei SA, Aminzade S, Ahmadraji A, et al. Early and complete vitrectomy versus tap and inject in acute post-cataract surgery endophthalmitis presenting with hand motion vision; a quasi-experimental study. BMC Ophthalmol 2022;22:16.
6. Far PM, Yeung SC, Farimani PL, et al . Tap and inject versus pars plana vitrectomy for postprocedural endophthalmitis. Retina 2021;41:2009–2016.
7. Altan T, Acar N, Kapran Z, et al. Acute-onset endophthalmitis after cataract surgery: success of initial therapy, visual outcomes, and related factors. Retina 2009;29:606–612.
8. Doft BH, Kelsey SF, Wisniewski SR. Additional procedures after the initial vitrectomy or tap-biopsy in the endophthalmitis vitrectomy study. Ophthalmology 1998;105:707–716.
9. Barry P, Cordovés Luis, Gardner Susanne. ESCRS Guidelines for Prevention and Treatment of Endophthalmitis Following Cataract Surgery: Data, Dilemmas and Conclusions; 2013. [Internet]. Escrs.org. Co Dublin, Ireland: European Society of Cataract and Refractive Surgeons; 2013. Available from: https://www.escrs.org/downloads/Endophthalmitis-Guidelines.pdf
10. Soliman MK, Gini G, Kuhn F, et al. Visual outcome of early vitrectomy and intravitreal antibiotics in acute postsurgical and post intravitreal injection endophthalmitis. Retina 2021;41:423–430.
11. Ho IV, Fernandez-Sanz G, Levasseur S, et al. Early pars plana vitrectomy for treatment of acute infective endophthalmitis. Asia Pac J Ophthalmol 2019;8:3–7.
12. Dib B, Morris RE, Oltmanns MH, et al. Complete and early vitrectomy for endophthalmitis after cataract surgery: an alternative treatment paradigm. Clin Ophthalmol 2020;14:1945–1954.

CLINICAL OUTCOMES OF ACUTE ENDOPHTHALMITIS AFTER INTRAVITREAL DELIVERY OF VASCULAR ENDOTHELIAL GROWTH FACTOR INHIBITORS VERSUS STEROIDS

OLUFEMI E. ADAMS, MD,* GUNEET S. SODHI, MD,† TOMMASO VAGAGGINI, MD,† ZEESHAN HAQ, MD,† CHRISTIAN D. CURRAN, MD,* MICHAEL L. PRAIRIE, BA,‡ SANDRA R. MONTEZUMA, MD,* DARA D. KOOZEKANANI, MD, PHD,* EDWIN H. RYAN, MD,*† DAVID WILKIN PARKE III, MD,*† ROBERT A. MITTRA, MD,† PETER H. TANG, MD, PHD*†

Purpose: To compare patients with acute endophthalmitis after intravitreal injection of vascular endothelial growth factor (VEGF) inhibitors vs. steroids.

Methods: Retrospective single-center, nonrandomized interventional study from 2013 to 2021.Patients underwent vitreous biopsy before initiating treatment and were divided into the following cohorts: (1) anti-VEGF managed medically (T&I–anti-VEGF), (2) anti-VEGF managed by immediate pars plana vitrectomy (PPV–anti-VEGF), and (3) steroid therapy and managed medically or by pars plana vitrectomy (steroid).

Results: A total of 141 patients were analyzed. The steroid cohort demonstrated significantly worse presenting (median = 2.80 logarithm of the minimum angle of resolution [logMAR]; $P \leq 0.01$) and final (median = 2.30 logMAR) best-corrected visual acuity compared with T&I–anti-VEGF (presenting: median = 2.00 logMAR; final: median = 0.40 logMAR) and pars plana vitrectomy–anti-VEGF cohorts (presenting: median = 2.30 logMAR; final: median = 0.48 logMAR). There was no significant ($P = 0.33$) difference in the final best-corrected visual acuity between T&I–anti-VEGF and pars plana vitrectomy–anti-VEGF cohorts. There were no significant ($P \geq 0.63$) differences among cohorts in best-corrected visual acuity before acute endophthalmitis diagnosis (T&I–anti-VEGF: median = 0.40 logMAR; pars plana vitrectomy–anti-VEGF: median = 0.40 logMAR; steroid: median = 0.44 logMAR). Microbial cultures revealed similar profiles for all cohorts.

Conclusion: Acute endophthalmitis after intravitreal injection steroid therapy had worse outcomes compared with anti-VEGF therapy.

RETINA 43:947–954, 2023

A feared complication of any intraocular procedure is acute infectious endophthalmitis (AE), commonly caused by introduction of bacteria into the eye, which can result in devastating loss of vision or loss of the eye itself.[1] This condition is an ophthalmic emergency and requires antibiotics and/or surgical intervention. As a result, landmark studies such as the Endophthalmitis Vitrectomy Study[2] and the European Society for Cataract and Refractive Surgery Study[3] have been undertaken to reduce the incidence of and develop effective treatment algorithms for AE, respectively, in commonly performed procedures such as cataract surgery.

Intravitreal injection (IVI) of therapeutics is used for a wide spectrum of posterior segment diseases such as exudative age-related macular degeneration, diabetic macular edema, and retinal vein occlusion.[4] Among medications delivered, vascular endothelial growth

From the *Department of Ophthalmology and Visual Neurosciences, University of Minnesota Medical School, Minneapolis, MN; †Retina Consultants of Minnesota, Edina, MN; and ‡University of Minnesota Medical School, Minneapolis, MN.

No financial support exists for authors.

EHR receives royalties for licensed patents from Alcon, Inc. DWP receives royalties for licensed patents from Vortex Surgical, Inc. No disclosures exist for the remaining authors.

Reprint requests: Peter H. Tang, MD, PhD, Retina Consultants of Minnesota, 3601 West 76th Street, Suite 300, Edina, MN 55435.

factor (VEGF) inhibitors are the most common and have been shown to have a low AE incidence (0.016%).[5] Other agents such as steroids are less commonly used; however, they play an important role in therapy.[6] Previous studies have reported the incidence of AE from steroids ranging from 0.10%[7] to 0.87%.[8] It is unclear whether these higher rates relative to anti-VEGF therapy are due to the use of larger-caliber needles, variations in techniques, or lower statistically powered studies because the sample size for steroid therapy is often smaller.

Early inhibition of local immune response to combat exogenous bacteria from IVI steroid therapy could contribute to higher AE incidence rates. Furthermore, this could potentially lead to more serious disease when compared with anti-VEGF therapy. Although numerous case reports describe clinical features of AE after IVI steroid therapy[9–13], there has been no direct comparison between IVI anti-VEGF therapy and IVI steroids when these common procedures are complicated by AE. Our aim was to evaluate and compare the clinical presentations and outcomes of IVI-related AE in patients receiving steroids versus anti-VEGF agents.

Methods

Design

This retrospective cohort study was conducted according to the Declaration of Helsinki and the US Health Insurance Portability and Accountability Act of 1996 with Institutional Review Board approval by Allina (Reference:1881491). This study was HIPAA-compliant and conducted at a multiprovider, multilocation, single-subspecialty (retina-only) institution (Retina Consultants of Minnesota) located within metropolitan Twin Cities of Minneapolis/St. Paul in Minnesota, USA.

Inclusion/Exclusion Criteria

Billing data from January 1, 2013, through December 31, 2021, were queried for International Classification of Disease revision 10 code H44.X (purulent endophthalmitis) of right (X = 0.001) and left (X = 0.002) eyes and International Classification of Disease revision 9 code 360.01 (AE). Charts were retrospectively reviewed, and cases with AE occurring within 3 weeks after IVI anti-VEGF or steroid treatments were included. Patients with AE related to IVI therapy performed by us and external referring physicians were included.

All patients underwent either vitreous biopsy ("vitreous tap") before antibiotic therapy in clinic or at the time of surgery by pars plana vitrectomy (PPV). The sample was sent for Gram stain and microbial culture. If vitreous tap was unsuccessful, anterior chamber paracentesis was performed. All patients received treatment either in clinic or were brought to surgery on the same day as presentation.

The treatment choice was dependent on the clinical judgment of the treating physician. Patients were categorized into cohorts: (1) those who received vitreous tap & IVI of antibiotics in clinic after anti-VEGF therapy (T&I–anti-VEGF cohort); (2) those who underwent PPV with intraocular antibiotics after anti-VEGF therapy (PPV–anti-VEGF cohort); and (3) those who underwent either surgical or clinic-based treatment after steroid therapy (steroid cohort).

Patients with any history of intraocular or extraocular surgery within 1 year of receiving their last IVI of anti-VEGF agent or steroids were excluded. Cases were excluded if AE developed after trauma. Patients who were treated for AE with follow-up durations less than 6 months were excluded.

Injection Technique

The IVI technique applied only to patients treated by our group. Anti-VEGF agents included bevacizumab (Genentech, South San Francisco, CA), ranibizumab (Genentech), aflibercept (Regeneron, Tarrytown, NY), and brolucizumab (Novartis, Cambridge, MA). Steroid agents included triamcinolone, dexamethasone implant (Allergan, Dublin, Ireland), 0.19 mg fluocinolone implant (Alimera, Alpharetta, GA), and 0.18 mg fluocinolone implant (EyePoint, Watertown, MA). Facemasks were not universally used until March 2020 after coronavirus disease 2019 pandemic precautions were implemented. Before universal facemask policy, talking during injection was minimized. Topical anesthetic (0.5% proparacaine), viscous anesthetic (0.5% tetracaine), and subconjunctival 2% lidocaine were used. Topical 5% povidone–iodine (Betadine) was used to prepare the eye. All anti-VEGF agents were injected through pars plana (PP) using 30-gauge short needle, while steroids were injected using 22-gauge (dexamethasone), 25-gauge (0.18 and 0.19 mg fluocinolone), or 27-gauge needle (triamcinolone). Variation in technique included differences in injection location (majority being superotemporal quadrant and minority in inferotemporal quadrant) and having eyelids held open with a speculum. Eyelashes were kept out of field, and no blink was allowed after the last Betadine drop was placed.

Tap and Injection

All eyes received immediate vitreous tap through PP followed by injection of vancomycin (1.0 mg/0.1 mL) and ceftazidime (2.25 mg/0.1 mL). Vitreous tap involved inserting a short 25-gauge or 27-gauge needle to aspirate the sample. If adequate sample could not be obtained, AC paracentesis was performed using a short 30-gauge needle at corneal limbus. Adjuvant intravitreal steroids were not administered. Topical steroid and antibiotic drops were prescribed, and patients were followed daily until clinical improvement.

Pars Plana Vitrectomy

Patients were anesthetized using retrobulbar block in the periorbital space. The eye was prepped and draped in the usual sterile fashion, and the eyelid speculum was inserted. PPV (23 or 25 gauge) was performed, and all opacified vitreous was removed. Undiluted vitreous sample with infusion line turned off was sent for Gram stain and culture at the initiation of surgery. Peripheral vitreous was shaved with the aid of scleral depression. Inspection was performed, and any retinal breaks were demarcated with laser retinopexy. Partial or complete air–fluid exchange was performed at the discretion of the surgeon. Leaking sclerotomy wounds were sutured with 6-0 plain gut. At conclusion, vancomycin (1.0 mg/0.1 mL) and ceftazidime (2.25 mg/0.1 mL) were injected through PP with a short 30-gauge needle.

Variables of interest

Characteristics included age, sex, diabetes mellitus status, and indication for IVI. Signs, symptoms, and clinical findings on presentation included hypopyon, intraocular pressure, duration of symptoms (i.e., pain, redness, vision loss, photophobia, or floaters), and time between IVI and diagnosis of presumed AE. Baseline Snellen best-corrected visual acuity (BCVA) was obtained from the visit where patients received the IVI that was presumed to have caused AE. Presenting Snellen BCVA was obtained from the visit where patients were diagnosed with AE by our clinic. The final Snellen BCVA was determined at the longest postprocedural visit. Information about the therapeutic agent that patients received before presumed AE, culture growth results, initial treatment (T&I vs. PPV), and follow-up duration were collected.

Statistical Analysis

Statistical analysis was performed on JMP software (SAS Institute, Cary, NC). Snellen BCVA was converted to logarithm of the minimum angle of resolution (logMAR) units with logMAR values for "light perception," "hand motion," and "counting fingers" assigned values of 2.7, 2.3, and 2.0, respectively.[14] Comparison of categorical variables between two cohorts was performed using the 2-tailed Fisher exact test. Continuous quantitative variables including age, duration of symptoms, and logMAR BCVA were nonnormal using the Shapiro–Wilk test. The median test using median rank scores was used for comparisons involving logMAR BCVA. Other nonnormal distributions were compared using the Mann–Whitney *U* test. Multivariate analysis by least squares fitting was used to study the influence of continuous variables on final BCVA: baseline and presenting BCVA, time from initial IVI therapy to treatment, and age. For all tests, P value < 0.05 was statistically significant.

Results

Baseline Characteristics

Querying billing data for International Classification of Disease-9 and ICD-10 codes for a 9-year period generated 492 patients. After excluding patients with AE unrelated to IVI and without at least 6 months of follow-up, a total of 141 patients were analyzed. Patients underwent vitreous biopsy before initiating treatment and were divided into the following cohorts: (1) anti-VEGF managed medically (T&I–anti-VEGF), (2) anti-VEGF managed by immediate pars plana vitrectomy (PPV–anti-VEGF), and (3) steroid therapy managed medically or by PPV (steroid).

The mean age of study sample was 81.81 years (SD, 11.51), and 66.90% of the patients were male. Approximately 17.61% of patients were referrals to our practice, and 26.76% had a diagnosis of type 1 or 2 diabetes mellitus. The mean duration that presumed AE was diagnosed after IVI was 4.94 days (SD, 4.07), and the mean duration of symptoms experienced by the patient was 2.10 days (SD, 1.82). Approximately 70.42% of the study population were pseudophakic, and 54.61% demonstrated positive culture growth.

Various characteristics are summarized in Table 1. There were no significant differences among the three cohorts regarding age ($P = 0.89$), duration from IVI therapy ($P = 0.90$), or duration of symptoms experienced by the patient ($P = 0.88$). A significantly ($P <$

Table 1. Baseline Characteristics of Cohorts

	T&I–anti-VEGF	PPV–anti-VEGF	Steroids
No. of patients	64	63	14
Male sex (%)	73.44	66.67	42.86
External patients (%)	14.06	15.87	42.86
Age (years) mean ± SD	82.48 ± 11.15	82.49 ± 11.15	75.64 ± 13.60
Diabetes mellitus (%)	25.00	26.98	35.71
Duration from IVI therapy (days), mean ± SD	5.56 ± 3.58	4.81 ± 4.57	3.79 ± 1.19
Duration of symptoms (days), mean ± SD	2.44 ± 2.36	1.76 ± 1.10	2.07 ± 1.38
Pseudophakia (%)	71.88	73.02	50.00
Positive cultures (%)	32.81	69.84	100
IOP > 25 mmHg (%)	15.62	34.92	71.43
Presence of hypopyon (%)	59.38	76.19	85.71

Patients were divided into three cohorts: (1) patients who previously underwent IVI of anti-VEGF therapy who were biopsied in the clinic (T&I–anti-VEGF cohort) or during surgery (PPV–anti-VEGF cohort) and those who underwent IVI of steroid therapy who were biopsied in clinic or during surgery (steroid cohort). There was no significant difference among the three cohorts regarding age ($P = 0.89$), duration from IVI therapy ($P = 0.90$), or duration of symptoms experienced by the patient ($P = 0.88$). Steroid cohort presented with significantly greater proportion of patients with elevated IOP ($P < 0.01$) and presence of hypopyon ($P < 0.01$) compared with the other cohorts on clinical examination.

0.01) greater proportion of the steroid cohort presented with intraocular pressure above 25 mmHg and with the presence of hypopyon compared with other cohorts at the time of diagnosis of presumed AE.

Incidence of Acute Endophthalmitis

Patients with presumed AE after IVI therapy by both our practice (internal) and by referring physicians (external) were included. Excluding external patients, our practice performed 117 IVI procedures that resulted in AE, divided into anti-VEGF and steroid treatments of 109 and 8, respectively. During this time, our practice performed 596,574 and 5,864 IVI anti-VEGF and steroid treatments, respectively. We found that our incidence of presumed AE after IVI therapy of steroids (0.136%) was significantly greater ($P < 0.01$) compared with anti-VEGF agents (0.018%).

Microbial Culture Results

Samples collected by vitreous tap, AC paracentesis, or PPV were sent for microbial analysis. Of the 141 samples obtained, we observed 79 positive cultures, divided into 21, 44, and 14 cultures for T&I–anti-VEGF, PPV–anti-VEGF, and steroid cohorts, respectively. Therefore, positive culture growth was observed in 32.81%, 69.84%, and 100% of collected samples from T&I–anti-VEGF, PPV–anti-VEGF, and steroid cohorts, respectively (Table 1).

Of the 21 patients with culture-positive results from the T&I–anti-VEGF cohort, nine were obtained by AC paracentesis and 12 were by vitreous tap. Within the steroid cohort, we obtained positive culture growth in samples collected from all 14 patients, of which 12 underwent PPV biopsy and two underwent vitreous tap. Thus, a total of 39 patients in the entire study (all belonging to the T&I–anti-VEGF cohort) underwent AC paracentesis to produce nine positive cultures, yielding a rate of 23.08%. Vitreous tap from a total of 27 patients (25 from T&I–anti-VEGF cohort and two from steroid cohort) produced 14 positive cultures, yielding a rate of 51.85% which was significantly ($P < 0.01$) greater than AC paracentesis. Finally, PPV biopsy from a total of 63 patients produced 44 positive cultures, yielding a rate of 69.84% which was significantly ($P < 0.01$) greater than vitreous tap.

Identification of the causative bacteria from biopsy samples showed the majority to be coagulase-negative *staphylococcus* across all three cohorts (T&I–anti-VEGF = 78.95%, PPV–anti-VEGF = 79.55%, steroids = 78.57%; Figure 1). The remainder of identified organisms were evenly divided (5.26%) among *Serratia marcescens*, methicillin-sensitive *Staphylococcus aureus*, methicillin-resistant *Staphylococcus aureus*, and *Streptococcus pneumoniae* in the T&I–anti-VEGF cohort (Figure 1A). As for the PPV–anti-VEGF cohort, the next most prevalently identified bacteria were methicillin-sensitive *Staphylococcus aureus* (4.54%), *Streptococcus mitis* (4.54%), and *Cutibacterium acnes* (4.54%; formerly *Propionibacterium acnes*), followed by *Streptococcus pneumoniae* (2.27%), *Streptococcus salivarius* (2.27%), and *Pseudomonas aeruginosa* (2.27%; Figure 1B). For the steroid cohort, the remainder of identified bacteria were evenly divided (7.14%) among methicillin-sensitive *Staphylococcus aureus*, *Streptococcus pneumoniae*, and *Hemophilus influenza* (Figure 1C).

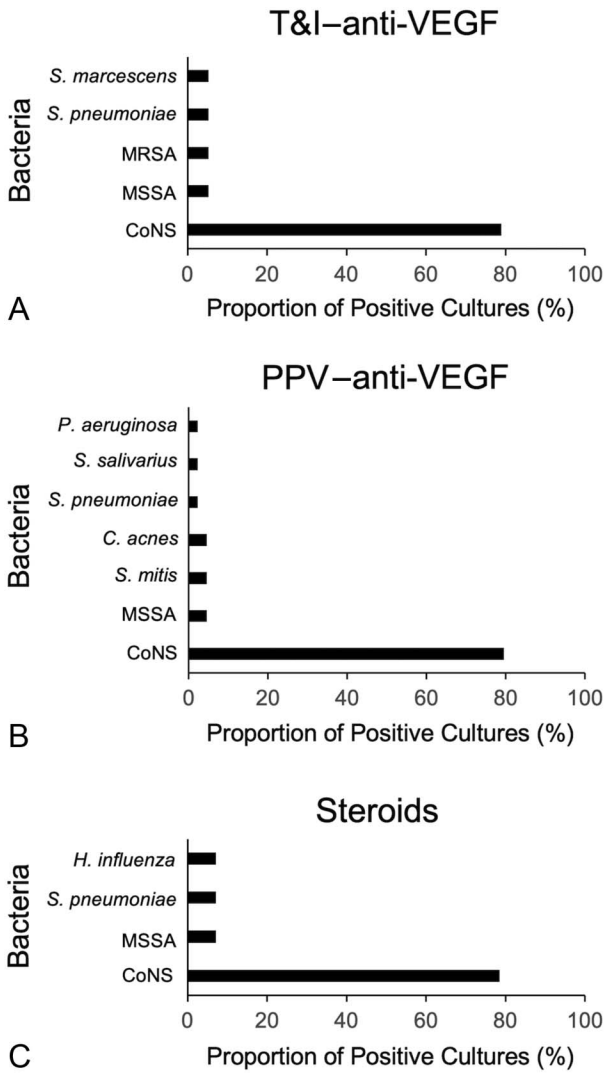

Fig. 1. Microbial culture growth results. Patients presenting with presumed AE underwent biopsy for microbial culture analysis, and positive growth results are displayed with microbial identification and proportional data. Cohorts included patients who previously underwent IVI anti-VEGF therapy who were biopsied in clinic (T&I–anti-VEGF cohort; **A**) or during pars plana vitrectomy surgery (PPV–anti-VEGF cohort; **B**) and patients who previously underwent steroid therapy (steroid cohort; **C**).

Visual Acuity

There were no significant differences ($P \geq 0.63$) in BCVA measured at the initial visit where IVI therapy was administered to have caused presumed AE (baseline BCVA) among T&I–anti-VEGF (median = 0.40 logMAR; [20/50 Snellen]), PPV–anti-VEGF (median = 0.40 logMAR; [20/50 Snellen]), and steroid cohorts (median = 0.44 logMAR; [20/55 Snellen]; Figure 2A). As for the BCVA at the initial diagnosis of presumed AE (presenting BCVA), the PPV–anti-VEGF cohort (median = 2.30 logMAR; [hand motion vision]) was significantly ($P < 0.01$) worse compared with the T&I–anti-VEGF cohort (median = 2.00 logMAR; [counting fingers vision]) and the steroid cohort (median = 2.8 logMAR; [light perception vision]) was significantly ($P = 0.01$) worse compared with the PPV-anti-VEGF cohort. Analysis of the final BCVA showed no significant ($P = 0.33$) difference between T&I–anti-VEGF (median = 0.40 logMAR; [20/50 Snellen]) and PPV–anti-VEGF cohorts (median = 0.48 logMAR; [20/60 Snellen]); however, there was a significant ($P < 0.01$) decline in the steroid cohort (median = 2.30 logMAR; [hand motion vision]). There was no significant difference in the final BCVA for all cohorts when analyzed by sex ($P = 0.54$) or by diabetes mellitus status ($P = 0.62$). There was a significantly ($P < 0.01$) increased time to treatment by the PPV–anti-VEGF cohort compared with the T&I–anti-VEGF cohort; however, there were no significant differences ($P = 0.54$) among these cohorts and the steroid cohort.

BCVA was then reanalyzed only in patients with culture-confirmed AE, and similar trends were identified (Figure 2B). Of note, there was no change in BCVA values for the steroid cohort as we obtained 100% culture growth. Baseline BCVA analysis showed no significant ($P \geq 0.50$) differences among T&I–anti-VEGF (median = 0.40 logMAR; [20/50 Snellen]), PPV–anti-VEGF (median = 0.40 logMAR; [20/50 Snellen]), and steroid cohorts (Figure 2B). Presenting BCVA analysis showed the PPV–anti-VEGF cohort (median = 2.30 logMAR; [hand motion vision]) to be significantly ($P = 0.03$) worse than the T&I–anti-VEGF cohort (median = 2.00 logMAR; [counting fingers vision]) and the steroid cohort to be significantly ($P = 0.02$) worse than the PPV–anti-VEGF cohort. The final BCVA analysis showed no significant ($P = 0.61$) differences between the T&I–anti-VEGF (median = 0.40 logMAR; [20/50 Snellen]) and the PPV–anti-VEGF cohorts (median = 0.48 logMAR; [20/60 Snellen]). However, the steroid cohort was significantly worse when compared with both ($P < 0.01$).

Discussion

Our study included patients who were diagnosed with AE after IVI anti-VEGF or steroid therapy performed by our group and patients who were emergently referred for management. We do not have access to referring physician metrics, so we excluded external patients when calculating our incidence rates. Our incidence for internal patients after IVI anti-VEGF therapy was 0.018%, similar to what has been previously reported.[5] For internal patients after IVI steroid therapy, our incidence was 0.136%, which is also similar to what has

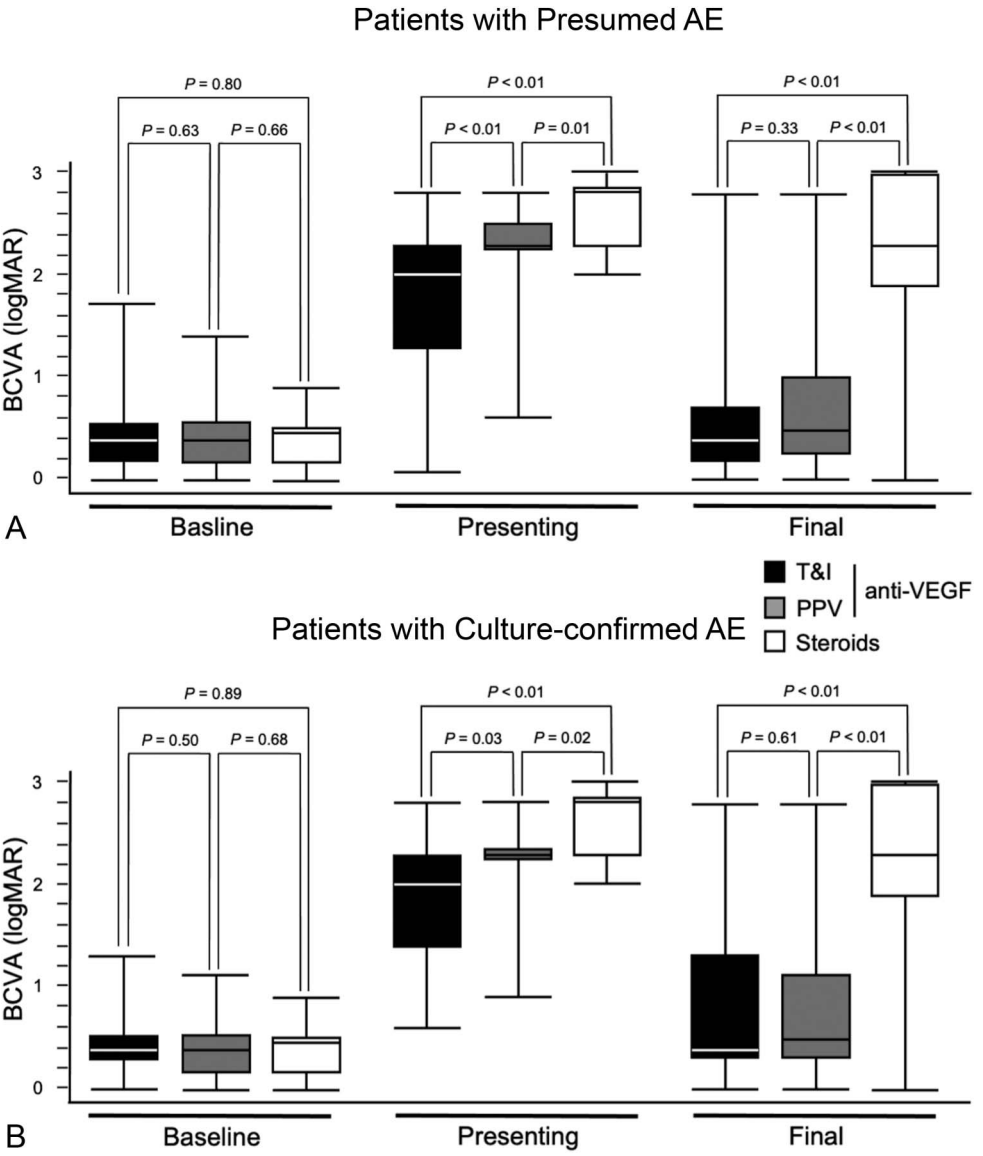

Fig. 2. Distribution of visual acuity by cohort. Box and whisker plot illustrating the distribution of logMAR BCVA among the T&I–anti-VEGF (black box), PPV–anti-VEGF (gray box), and steroid cohorts (white box) from the visit where they initially received IVI therapy that caused the presumed AE (baseline), from the visit where presumed AE was initially diagnosed (presenting), and from the most recent visit (final). When considering all patients presenting with presumed AE (**A**), there was no significant ($P \geq 0.63$) differences among all three cohorts for baseline BCVA (left); however, the PPV–anti-VEGF cohort demonstrated significantly ($P < 0.01$) worse presenting BCVA compared with the T&I–anti-VEGF cohort. The steroid cohort also demonstrated significantly ($P \leq 0.02$) worse presenting BCVA compared with the other cohorts (middle). The final BCVA analysis did not show significant ($P = 0.33$) differences between the T&I–anti-VEGF and PPV–anti-VEGF cohorts; however, the steroid cohort demonstrated significantly ($P < 0.01$) worse final BCVA compared with the other cohorts (right). When culture-negative patients were excluded from analysis (**B**), the previously described clinical trends remained valid. Of note, BCVA values for the steroid cohort remained the same between A and B because we obtained 100% culture growth from all biopsies performed for these patients. $P < 0.05$ was considered significant.

been previously reported by Moshfeghi et al.[8] We show that the incidence of AE after IVI steroid therapy was significantly greater than that after anti-VEGF therapy, likely due to a combination of factors. We hypothesize that some of these contributing factors include suppression of the local innate immune response by steroids, thereby decreasing the ability of the eye to combat bacteria, as well as the fact that larger-caliber needles required for steroid injections (22-gauge to 27-gauge) pose greater risk of bacterial introduction and transmigration when compared with smaller-caliber needles for anti-VEGF agents (30-gauge).

Microbial cultures from biopsies showed coagulase-negative *staphylococcus* to be the causative agent in most cases, irrespective of patient previously receiving anti-VEGF or steroid agents. This suggests that the significantly worse presenting and final BCVA observed after steroids could not be attributed to infections by more virulent pathogens. Instead, we believe this further supports our hypothesis that IVI steroid therapy suppresses ocular immune response, allowing pathogens to go unchallenged. Additional evidence comes from clinical examination at the time of diagnosis, where greater proportions of poststeroid patients presented with elevated intraocular pressure and hypopyon, both suggesting more advanced disease.[2,5,15,16] As such, 12 of 14 patients in the steroid cohort (85.71%) presented with enough worrisome findings that prompted immediate surgical intervention. It is important to note that there were no significant differences in baseline BCVA of patients before the diagnosis of AE, indicating that visual potential was

similar among all patients analyzed. Further multicenter studies are necessary to expand the numbers of patients with AE after IVI steroid therapy to further investigate.

We found that patients with presumed AE after anti-VEGF therapy demonstrated similar clinical outcomes irrespective of whether they were managed in clinic or with surgery. This is in agreement with previously reported findings from our group.[5] Interestingly, patients undergoing immediate surgery showed significantly worse presenting BCVA, likely due to selection bias, because clinical evidence of more advanced disease would prompt urgent surgery. Thankfully, there was no significant difference in visual outcomes between the two cohorts.

A possible confounder is sterile endophthalmitis, an ocular immune reaction to a noninfectious agent introduced during IVI that is difficult to differentiate from infectious endophthalmitis.[17,18] This is a rare occurrence that has been reported after IVI of all anti-VEGF agents and steroids and may involve contaminants during drug preparation and/or from the syringe.[17,19,20] Sterile endophthalmitis did not affect our data involving AE after IVI steroid therapy because all 14 patients in this cohort were culture-confirmed. Furthermore, when eliminating patients without culture-confirmed AE, trends for our main outcome results involving BCVA remained unchanged.

Our biopsy data showed that diagnostic yield for positive culture growth was significantly higher in patients receiving vitreous tap or PPV biopsy compared with AC paracentesis. This is in agreement with previously reported data.[21,22] A likely explanation is that both vitreous tap and PPV biopsy produce greater quantities of sample for diagnosis. Furthermore, both techniques obtain biopsies directly from the posterior segment where the initial insult originated (i.e., introduction of pathogens into the vitreous cavity from IVI). These factors would account for the greater yield of positive culture growths.

There were several important limitations to our study. Because this was a nonrandomized study, patients presenting with more advanced disease were selected for immediate surgical intervention, whereas those who were treated in clinic had less severe disease. Our sample size was relatively small due to the uncommon nature of the disease. Furthermore, we used visual performance at least 6 months after presumed AE treatment as the main outcome measure, which may cause unintended bias because many of our patients had exudative age-related macular degeneration that could progress over time. Although the role of steroids as adjuvant therapy for AE remains controversial, our current study does not attempt to address this.[23–25] Finally, as the low incidence of AE after IVI therapy meant that our small sample size depended heavily on external patient referrals, this could have been a significant source of bias. It is likely that these patients were referred to our practice for advanced management because they presented with more advanced/serious disease. With external patients composing a greater proportion of the steroid cohort (42.86%) compared with the anti-VEGF cohorts (14.96% combined), this could explain the large discrepancy in presenting and final BCVA outcomes. Because excluding these patients would severely underpower statistical calculations for our study, this further highlights the need for a multicenter prospective randomized trial to further investigate this important question.

Our study is the first to directly compare the clinical characteristics and outcomes of patients with presumed AE after IVI treatment with either anti-VEGF or steroid agents. We found that patients with AE after IVI steroid therapy presented with more advanced disease and had worse clinical outcomes despite immediate surgery. This highlights the need for extreme caution when attempting to apply guidelines from studies based on postcataract surgery AE such as endophthalmitis vitrectomy study. We recommend timely and aggressive therapy when these patients initially present to maximize every opportunity for salvaging vision in this devastating disease.

Key words: endophthalmitis, anti-VEGF, bevacizumab, ranibizumab, aflibercept, dexamethasone, triamcinolone, infection, vascular endothelial growth factor, avastin, lucentis, eylea, ozurdex.

Acknowledgments

The authors thank Cheryl Warner for assistance with data collection and interpretation.

References

1. Chiquet C, Bron AM, Lundström M, Maurin M. Acute postoperative endophthalmitis: microbiology from the laboratory to the bedside. In: Print. Surv Ophthalmol 2022;67:1698–1710.
2. Results of the Endophthalmitis Vitrectomy Study. A randomized trial of immediate vitrectomy and of intravenous antibiotics for the treatment of postoperative bacteral endophthalmitis. Endophthalmitis Vitrectomy Study Group. Arch Ophthalmol 1995;113:1479–1496.
3. Barry P, Seal DV, Gettinby G, et al. ESCRS study of prophylaxis of postoperative endophthalmitis after cataract surgery: preliminary report of principal results from a European multicenter study. J Cataract Refractive Surg 2006;32:407–410.
4. Patel D, Patel SN, Chaudhary V, Garg SJ. Complications of intravitreal injections: 2022. Curr Opin Ophthalmol 2022;33:137–146.

5. Xu K, Chin EK, Bennett SR, et al. Endophthalmitis after intravitreal injection of vascular endothelial growth factor inhibitors: management and visual outcomes. Ophthalmology 2018; 125:1279–1286.
6. Ghanchi F, Bourne R, Downes SM, et al. An update on long-acting therapies in chronic sight-threatening eye diseases of the posterior segment: AMD, DMO, RVO, uveitis and glaucoma. Eye 2022;36:1154–1167.
7. Westfall AC, Osborn A, Kuhl D, et al . Acute endophthalmitis incidence: intravitreal triamcinolone. Arch Ophthalmol 2005; 123:1075–1077.
8. Moshfeghi DM, Kaiser PK, Scott IU, et al. Acute endophthalmitis following intravitreal triamcinolone acetonide injection. Am J Ophthalmol 2003;136:791–796.
9. Bastakis GG, Stavrakakis A, Nikolaos A, et al . Acute onset of exogenous endophthalmitis after dexamethasone implant injection treated without implant removal. Case Rep Ophthalmological Med 2018;2018:1–3.
10. Mahalingam P, Topiwalla TT, Ganesan G. Drug-resistant coagulase-negative staphylococcal endophthalmitis following dexamethasone intravitreal implant. Indian J Ophthalmol 2017;65:634–636.
11. Esen E, Sizmaz S, Demircan N. Two cases of acute endophthalmitis after intravitreal dexamethasone implant injection. RETINAL Cases Brief Rep 2016;10:154–156.
12. Aggermann T, Stolba U, Brunner S, Binder S. Endophthalmitis with retinal necrosis following intravitreal triamcinolone acetonide injection. Ophthalmologica 2006;220:131–133.
13. Samuelson AG, Nahar A, Patel SN, et al. Clinical outcomes of patients with endophthalmitis after dexamethasone intravitreal implant. Retina 2022;42:1915–1920.
14. Schulze-Bonsel K, Feltgen N, Burau H, et al . Visual acuities "hand motion" and "counting fingers" can be quantified with the freiburg visual acuity test. Invest Ophthalmol Vis Sci 2006; 47:1236–1240.
15. Hoevenaars NED, Gans D, Missotten T, et al . Suspected bacterial endophthalmitis following intravitreal anti-VEGF injection: case series and literature review. Ophthalmologica 2012;228:143–147.
16. Lalwani GA, Flynn- HW Jr, Scott IU, et al. Acute-Onset endophthalmitis after clear corneal cataract surgery (1996–2005). Ophthalmology 2008;115:473–476.
17. Anderson WJ, da Cruz NFS, Lima LH, et al . Mechanisms of sterile inflammation after intravitreal injection of antiangiogenic drugs: a narrative review. Int J Retina Vitreous 2021;7:37.
18. Schwartz SG, Flynn- HW Jr, Emerson GG, et al . Distinguishing between infectious endophthalmitis and noninfectious inflammation following intravitreal anti-VEGF injection. J VitreoRetinal Dis 2019;3:42–44.
19. Kim M, Kim JT. Differences in the incidence of aflibercept-related sterile endophthalmitis according to types of disposable syringes used. Graefes Arch Clin Exp Ophthalmol 2022;260: 1139–1145.
20. Fong AHC, Chan CKM. Presumed sterile endophthalmitis after intravitreal triamcinolone (kenalog) - more common and less benign than we thought?. Asia-Pacific J Ophthalmol 2017;6:45–49.
21. Feng HL, Robbins CB, Fekrat S. A nine-year analysis of practice patterns, microbiologic yield, and clinical outcomes in cases of presumed infectious endophthalmitis. Ophthalmol Retina 2020;4:555–559.
22. Barza M, Pavan PR, Doft BH, et al. Evaluation of microbiological diagnostic techniques in postoperative endophthalmitis in the Endophthalmitis Vitrectomy Study. Arch Ophthalmol 1997;115:1142–1150.
23. Shah GK, Stein JD, Sharma S, et al. Visual outcomes following the use of intravitreal steroids in the treatment of postoperative endophthalmitis. Ophthalmology 2000;107:486–489.
24. Bui DK, Carvounis PE. Evidence for and against intravitreous corticosteroids in addition to intravitreous antibiotics for acute endophthalmitis. Int Ophthalmol Clin 2014;54:215–224.
25. Emami S, Kitayama K, Coleman AL. Adjunctive steroid therapy versus antibiotics alone for acute endophthalmitis after intraocular procedure. Cochrane Database Syst Rev 2022;6: CD012131.

OPEN

DO DAILY ACTIVITIES AFFECT GAS TAMPONADE–RETINA CONTACT AFTER PARS PLANA VITRECTOMY?

A Computational Fluid Dynamics Study

TOMMASO ROSSI, MD,* MARIA GRAZIA BADAS, PHD,† FEDERICO ANGIUS, DENG,† GIORGIO QUERZOLI, PHD†

Purpose: To calculate the retinal surface alternatively in contact with gas and aqueous because of fluid sloshing during daily activities such as ocular saccade, turning the head, standing up, and being a passenger of a braking car.

Methods: Fluid dynamics of aqueous and gas tamponade was reproduced using computational methods using the OpenFOAM open-source library. The double-fluid dynamics was simulated by the volume of fluid method and setting the contact angle at the aqueous–gas–retina interface.

Results: Sloshing increased the retinal surface in contact with aqueous by 13% to 16% regardless of fill rate and standing up determined the largest area of wet retina, followed by car braking, head rotation, and ocular saccade ($P < 0.001$). All activities except the ocular saccade determined a significant increase in the surface of retina in contact with the aqueous ($P < 0.005$). Car braking induced the highest shear stress (6.06 Pa); standing up determined the highest specific impulse and saccade the lowest.

Conclusion: Daily activities instantaneously reduce the amount of retina consistently in contact with gas tamponade and increase shear stress giving aqueous a potential access to the subretinal space regardless of patients' compliance.

RETINA 43:955–963, 2023

Pars plana vitrectomy is the preferred surgical technique for many types of retinal detachment, especially in pseudophakic eyes and in the presence of giant, multiple, or posterior retinal tears[1] and macular holes.[2]

Gas tamponade of varying duration is often injected after pars plana vitrectomy[3] to prevent aqueous from accessing retinal tears[4] until retinopexy establishes a solid retinal adhesion because fluid leakage into the subretinal space may lead to recurrent retinal detachment.

Patients are instructed to position after surgery so that the retinal tear(s) contact the shrinking gas bubble as long as possible.[5] In fact, gas tamponade reabsorption exposes increasing retinal portions to aqueous that may leak into the subretinal space through yet unsealed retinal tears.[6]

Although the gas–fluid interface and the fraction of retinal surface in contact with gas at rest have been thoroughly studied,[7,8] less is known about the extent of retinal surface affected by the sloshing of aqueous because of eye and patients' movements. During daily activities, retinal tears contacting gas under static conditions may temporarily fall under the air–fluid interface, giving aqueous a potential access to the subretinal space thus increasing the risk of recurrent retinal detachment or retinal shifting.

The purpose of this study was to calculate the extension of the retinal surface, temporarily wet by

From the *IRCCS Fondazione G.B. Bietti ONLUS, Roma, Italy; and †DICAAR, Università degli Studi di Cagliari, Cagliari, Italy.

None of the authors has any financial/conflicting interests to disclose.

Reprint requests: Tommaso Rossi, MD, IRCCS Fondazione Bietti ONLUS—Via Livenza 3, Roma 00198, Italy; e-mail: tommaso.rossi@usa.net

aqueous during daily activities, and as a function of gas fill.

Materials and Methods

Computational Fluid Dynamics Model

A numerical model was implemented within OpenFOAM[9] to simulate the flow of the gas and aqueous at rest and during the prescribed movements. It consists in resolving the mass conservation and Navier–Stokes equations together with an additional transport equation for the water volume fraction (volume of fluid technique[10]). The approach has already been successfully applied to the study of tamponades.[11,12]

The equations were solved over an unstructured mesh (consisting of 350,000 hexahedral and tetrahedral cells) generated by the "snappyHexMesh" tool, included in the OpenFOAM library. Five layers of hexahedral cells with progressively increasing height at the eye surface were extruded from the eye surface. The no-slip boundary condition was imposed at the walls for velocity, while a contact angle model was assumed to reproduce the gas–aqueous–retina interface behavior.

The pressure-implicit split-operator method[13] was adopted for solving the pressure–velocity coupling. Numerical integration was performed using second-order accurate schemes in space and first-order accurate, Euler scheme.

Physical properties of fluids used during the present simulations are summarized in Table 1.

Simulated Conditions

We investigated the statics of a patient standing in the upright position or supine and the dynamics of the following:

1. Sudden car braking;
2. Standing up from supine to sitting position;
3. Left–right head rotation; and
4. Saccadic motion.

Table 1. Physical Properties of Involved Fluids

	Air	Aqueous
Density	1 Kg/m^3	997 Kg/m^3
Dynamic viscosity	0.01813 mPa s	1 mPa s
Interfacial tension versus water	0.07 N/m	
Contact angle versus water and retina	16.2°	

In all the cases, 30%, 50%, and 80% volumetric tamponade filling fractions were considered.

The aim of the latter set of cases was to assess the impact of daily activities on the amount of retina remaining in contact with the tamponade and the shear stress caused by the fluid sloshing.

Car Braking

A 0.5 g (4.9 m/second^2) sudden car braking was simulated. The maneuver consists of three deceleration phases: a linear increase from zero to 0.5 g, a 1.0 seconds constant phase, and a linear decrease to zero in 0.1 seconds as the brake pedal is released. During the maneuver, the car speed drops from approximately 20 km/hour to zero. Deceleration and corresponding velocity–time laws are shown in Figure 1A. Although at the end of deceleration, the car is stationary, the computation is extended up to a total simulation time of 3 seconds to evaluate the tamponade behavior during its finale settling. At the end of the simulation, the tamponade interface reached the steady equilibrium again.

Standing up and head rotation. The time–laws of motion of standing up from supine to sitting position and the left–right head rotation were obtained recording the movement of a volunteer and tracking the eye's motion by means of image analysis techniques. The resulting time–laws (Figures 1, B–D) were implemented in the computational fluid dynamics model using the dynamic mesh technique. Figure 1B shows the eye trajectory during standing up from supine to sitting position (solid line) and lying down again (dashed line), while accelerations as functions of time are shown in Figure 1C. The whole movement lasts for 5 seconds. Figure 1D shows the eye rotation as a function of time in the case of head rotation (black line) and the corresponding angular acceleration (red line). The motion lasts for 2.2 seconds and achieves a maximum observed rotation angle as large as 66°.

Saccade. A horizontal saccade with 50° amplitude and 0.1375 seconds duration, attaining a 546.67°/s peak angular velocity, was simulated. It was obtained by the same polynomial law as in Rossi et al.[14] Figure 1E shows the eye rotation and the angular velocity as functions of time. The dynamic mesh technique was adopted to numerically simulate the prescribed motion.

Main outcome measures. The main study outcome measures include the retinal contact measured as the percentage value of retinal surface in contact with gas and aqueous, the shear stress at the retinal surface, and the specific impulse (SI). The vitreous chamber surface was divided into the following regions to better

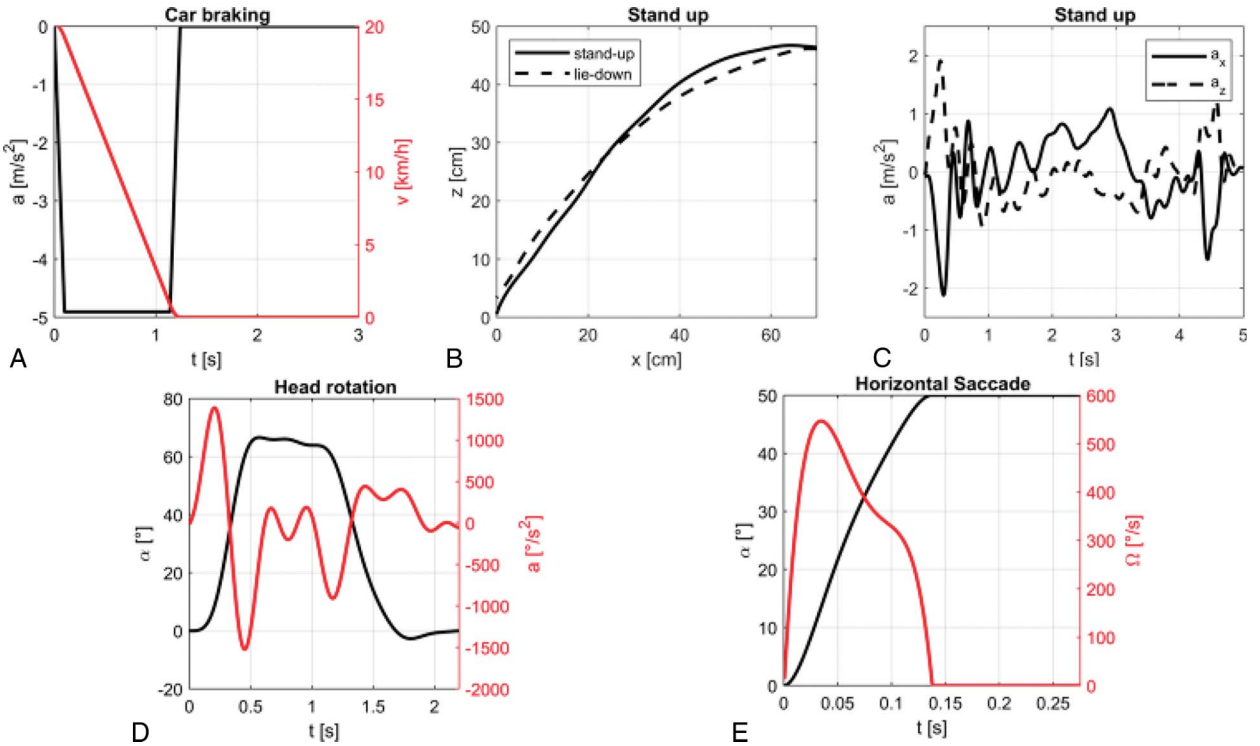

Fig. 1. Characterization of the simulated dynamical conditions: Car braking (**A**), standing up (**B** and **C**), head rotation (**D**), and saccade (**E**).

highlight the effect of the movement on the retina (Figure 2).

1. Macula (dark green): the retinal surface centered on the geometric posterior pole and extending 20° anteriorly;
2. Postequatorial retina (light green): the surface posterior to the geometric equator excluding the macula;
3. Preequatorial retina (blue): the surface anterior to the geometric equator comprised between the equator and the *pars plana*;
4. *Pars plana* ciliary body and posterior intraocular lens surface are represented in light blue and have been excluded from tamponade contact computation because they are retina. The presence of an artificial crystalline lens has been modeled because most eyes are rendered pseudophakic when gas tamponade is deemed necessary.

The SI describes the overall amount of solicitation on the retinal surface because of the considered activities. It is defined as the time integral of the instantaneous spatially averaged shear stress on the retinal surface:

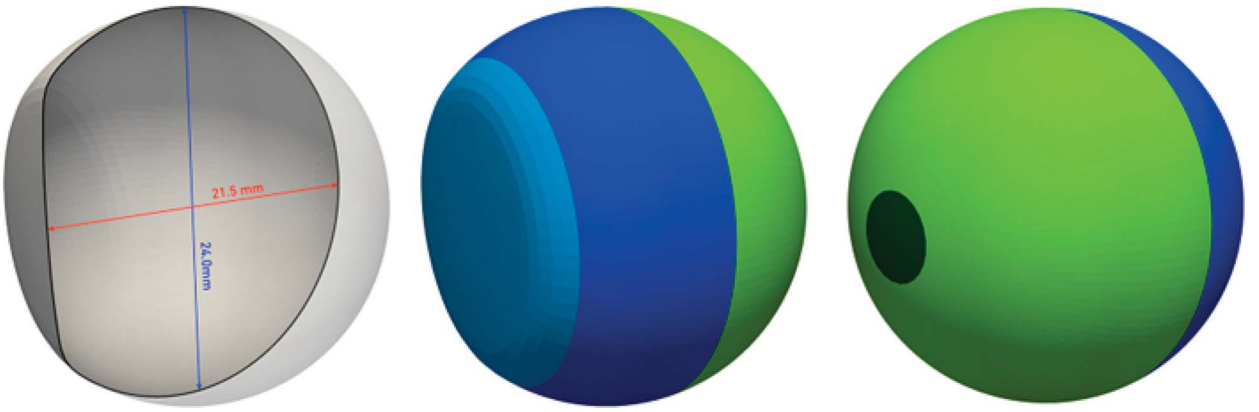

Fig. 2. Vitreous chamber morphology and segmentation. Light blue: pars plana; blue: preequatorial retina; green: postequatorial retina; and dark green: macula.

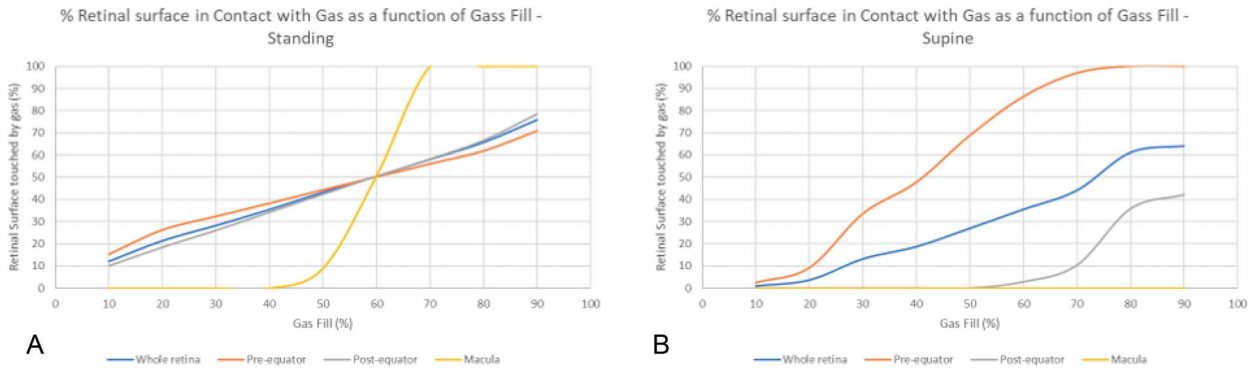

Fig. 3. Fraction of retinal surface in contact with gas under static conditions for a standing (**A**) and supine (**B**) patient as a function of the gas filling percentage.

$$\mathrm{SI} = \int_0^T \frac{1}{S} \int_S \mathrm{WSS}(t)\, dSdt$$

where WSS(t) is the instantaneous shear stress at each point of the retinal surface, T is the duration of the simulation, and S is the area of the retinal surface.

We introduced the SI because the considered motions differ significantly for both acceleration and duration. In addition, some of them include relatively long periods of time with low accelerations, e.g. during the two final seconds of the car braking or the second half of the simulation time in the saccade. These periods, although significant, would artificially decrease any time average.

Statistical analysis. The analysis of variance is applied to statistically evaluate the significance of shear stress values at different locations and to compare the outcomes obtained for different regions. The P values lower than 0.05 were considered statistically significant.

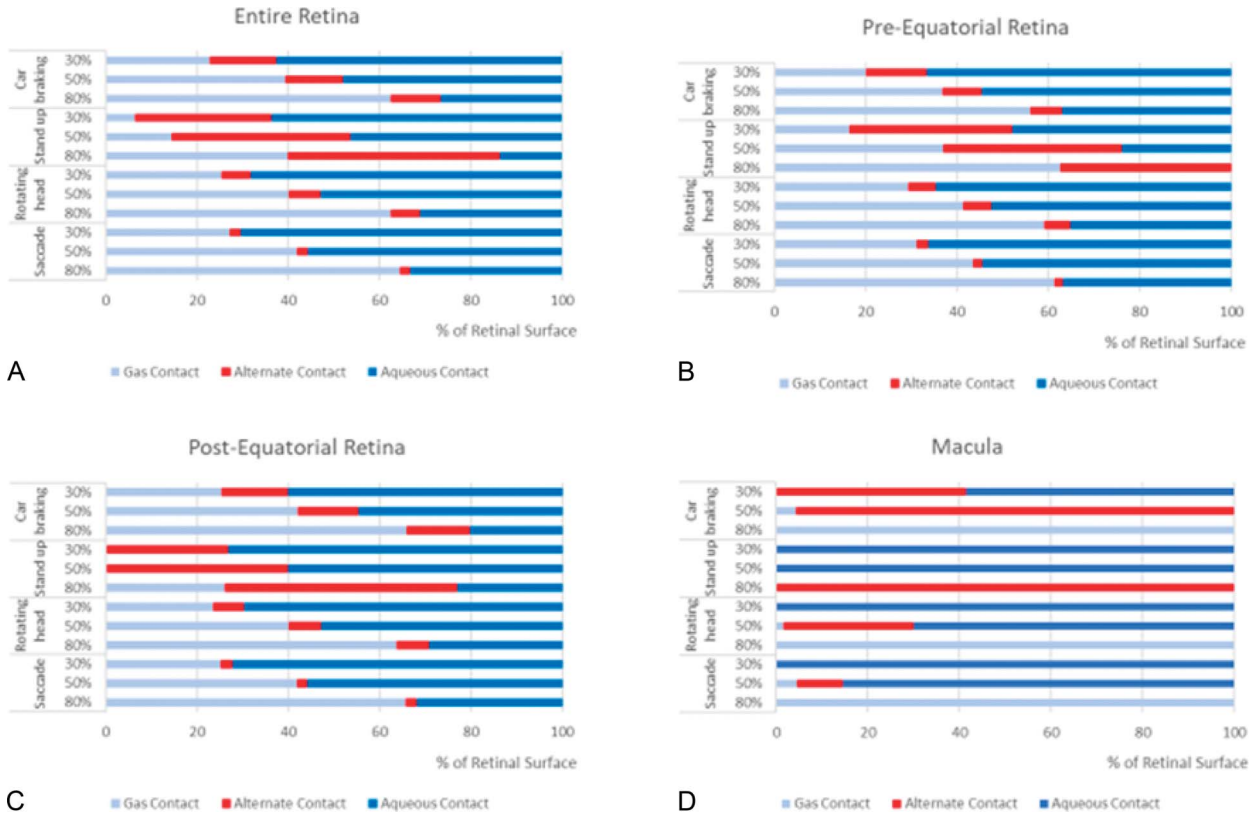

Fig. 4. Percentage of retinal surface in contact with gas (dry area, light blue bars), aqueous (wet area, dark blue bar) of wettable (red bar) for the considered daily activities and gas fill fractions.

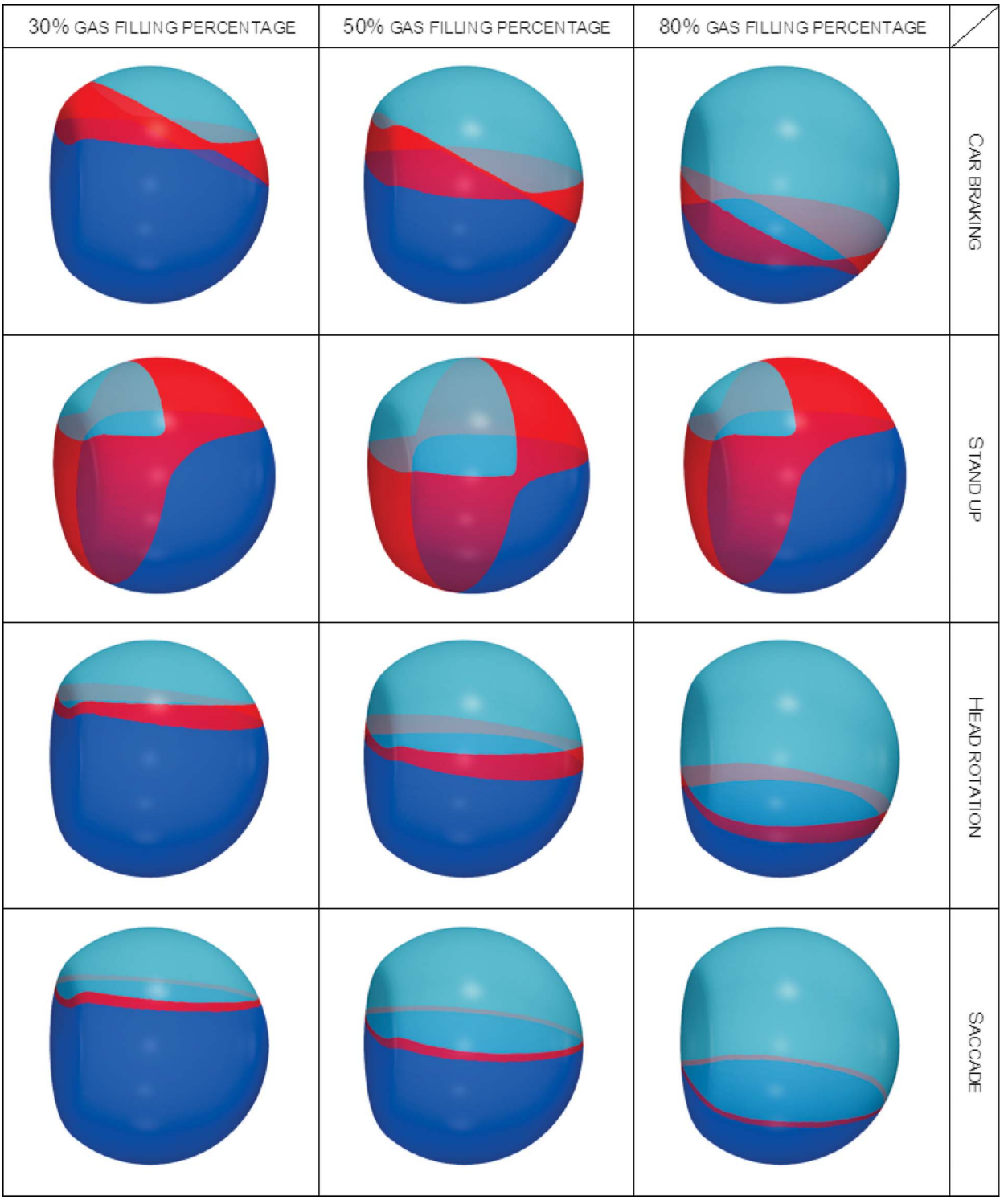

Fig. 5. Maps of wet, dry, and wettable areas for the four considered movements. Cyan areas are permanently in contact with the gas tamponade, blue areas are permanently wet by aqueous, and red areas come into contact both with tamponade and with aqueous during the motion.

Results

Gas–Retina Contact Under Static Conditions

The percentage of retinal surface touched by gas under static conditions for a supine and standing patient is shown in Figure 3.

Gas–Retina Contact Under Dynamic Conditions

Figure 4 shows the percentages of retinal surface wet by the aqueous during the whole motion time (blue bars), the surface percentages of retina always in contact with the tamponade (cyan bars), and the percentage wet by aqueous for a fraction of the motion and touching gas for the remaining time (red bars). Those will be hereafter referred to as "wet," "dry," and "wettable" areas, respectively (Figure 5).

Different activities significantly affected the retinal surface extension affected by fluid sloshing.

Standing up from the supine position determined the largest fraction of wettable retina, followed by car braking and ocular saccade (Figure 4; $P < 0.001$).

The extension of retina affected by aqueous sloshing was not significantly affected by gas fill irrespective of the considered activity (Figure 4 A–C) except for the macular region (Figure 4D), where the status of wet, dry, or wettable largely depended on gas fill ($P < 0.01$ for all activities except for the case of standing up).

When the wettable retinal surface is analyzed primarily as a function of gas fill (Figures 5 and 6), it becomes apparent that standing up exposes the largest retinal surface to aqueous contact (more than 60%) even at 80% gas fill and more than 90% at 30% filling percentage. At 50% gas fill, all other activities expose 50% to 60% of the postequatorial retina to aqueous (Figure 6C), while the preequatorial retina (where most retinal tears occur) is significantly less wettable only for the standing-up activity ($P < 0.05$). Regardless of gas fill percentage, all activities except the ocular saccade determined a significant increase in the surface of retina in contact with aqueous (wettable area; $P < 0.005$ except for the macula).

The mean percentage of "wettable" retina during all considered activities is summarized in Table 2 regardless of gas fill, between 13% and 16% of the entire retinal surface intermittently contacted aqueous. There was no significant difference across the different retinal sectors and/or gas fill.

Shear Stress

Car braking induced a significantly higher shear stress (6.06 Pa, $P = 0.018$) than any other activity regardless of the fill fraction (Figure 7; $P < 0.05$). The lower gas fill simulations returned significantly higher shear stress values for all considered activities

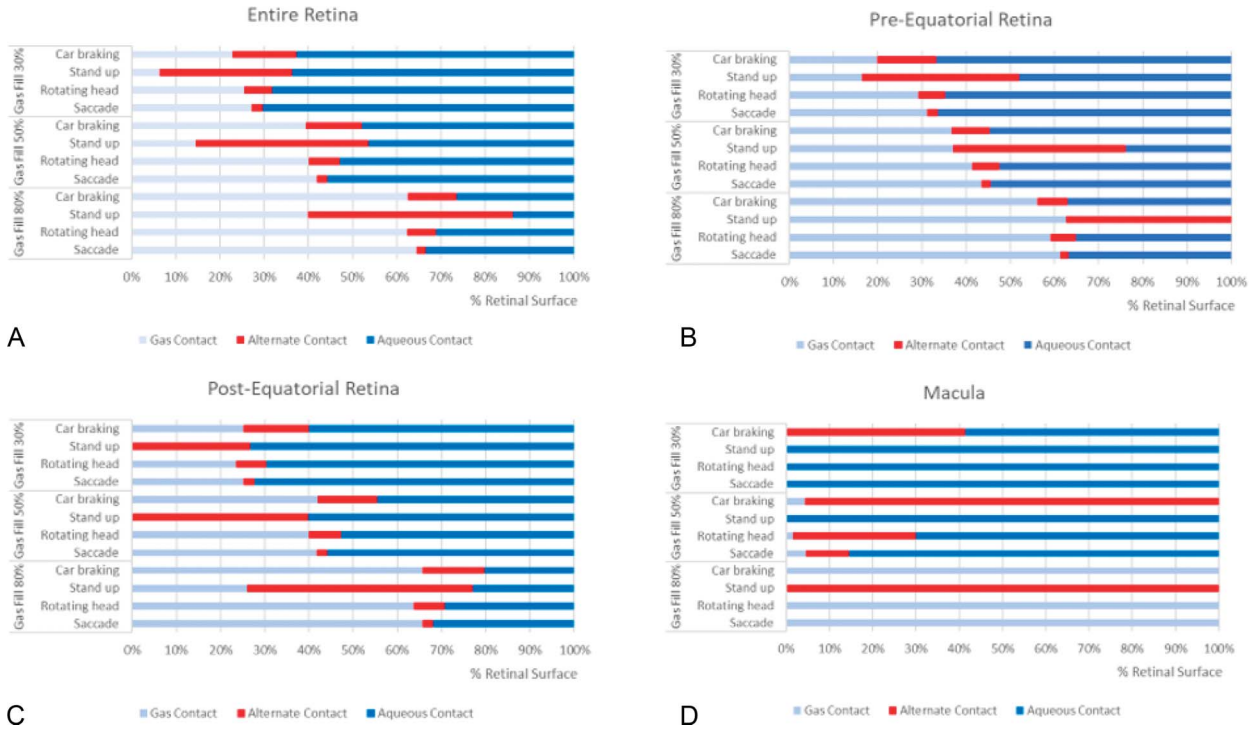

Fig. 6. Proportion of retinal surface in contact with gas (dry, light blue bar), aqueous (wet, dark blue bar) of wettable (red bar) for each considered activity and gas fill percentage.

Table 2. Average Percentage of Retinal Surface Becoming "Wet" During all Considered Activities

Gas Fill	Entire Retina	Preequator	Postequator	Macula	*P*
30%	13.3 ± 10.2	14.3 ± 12.2	12.7 ± 9.2	10.3 ± 17.9	n.s.
50%	15.2 ± 14.2	13.9 ± 14.7	15.7 ± 14.5	33.5 ± 37.3	n.s
80%	16.5 ± 17.5	13.0 ± 14.2	18.6 ± 19.2	25.0 ± 43.3	n.s
P	n.s.	n.s.	n.s.	n.s	

($P < 0.05$) except for standing up when the 50% gas fill reached the highest shear stress.

Specific Impulse

The specific impulse was significantly different among activities (Figure 8; $P < 0.001$); standing up determined a significantly higher SI and the saccade lower SI than any other activity. Gas fill did not significantly affect SI (Figure 8).

Discussion

Maintaining retinal tears in contact with gas as long as possible is important to promote long-term adhesion after retinal detachment surgery[15–17] and represents the rationale of patients positioning according to the tears location.[18] Patients' compliance has also been demonstrated to significantly influence anatomical outcome,[19] and devices intended to favor, alert, instruct, and keep record of adherence to those instructions have been proposed.[20,21] Vitrectomy without the use of any gas tamponade, conversely, has been advocated as an alternative by many authors and for different indications[22–24] because the need for positioning significantly disrupts the daily routine.

Irrespective of patients' willingness and ability to comply with prescribed positioning, the daily activities significantly affect the proportion of "dry" and "wet" retina as the dynamics of eye and head motion determines fluid sloshing and a third "gray" zone of "wettable" or alternatively "dry" and "wet" retina creates. Our data show that during such activities, an average 15% of the overall retinal surface (Table 2) temporarily loses its contact with gas regardless of gas fill and patients' compliance.

It is interesting to note that as gas fill reduces, the extension of "wettable" retina does not significantly change for any considered activity (Figures 4–6), thus acquiring more proportional importance. In other words, the "wettable" retinal surface to be added to "wet" retina remains fairly invariant, while gas bubble reduces its volume.

Not surprisingly, standing up causes the largest variation of wettable retinal surface as it implies the transition from supine to standing posture so that approximately half the retinal surface is affected by a change in gas/fluid contact, even with almost complete gas fill. Deceleration associated to car braking represented the second most important activity in retinal surface becoming "wet," followed by head rotation and eye saccade. This means that stenopeic goggles once advocated to keep the eye in primary position would very marginally help because head motion seems more important than eye motion, as also reported by Angunawela et al.[25]

The macula deserves a separate mention because it is the site for specific pathology (macular holes and myopic retinal detachment within the staphyloma only to name a few) and is extremely sensitive to both head positioning and gas fill. Figures 4–6 show how the macula becomes temporarily wet during virtually all activities unless when gas fill is very high. This notion suggests that a higher compliance with positioning is advisable after macular surgery especially in highly myopic eyes[19] as well as the use of longer-lasting gases.

Across considered activities and gas fill fraction, the preequatorial retina (Figure 6) maintained a much larger gas contact, on average, than the postequatorial, which became almost entirely "wet." Because many challenging retinal tears occur posterior to the equator,[26] the patient should be instructed to reduce head motion as much as possible and longer-acting gases are preferred under those circumstances also.

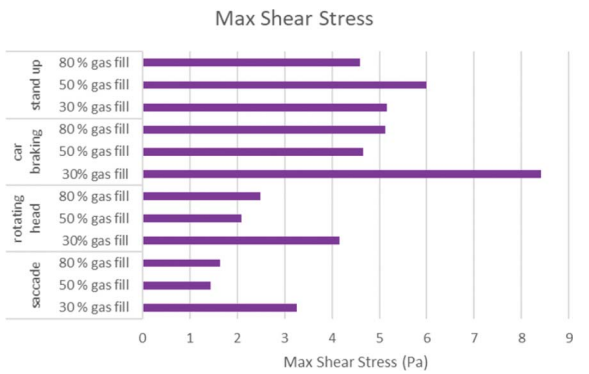

Fig. 7. Maximum shear stress for each inquired retinal section and patient activity standing up (**B** and **C**), head rotation (**D**), and saccade (**E**).

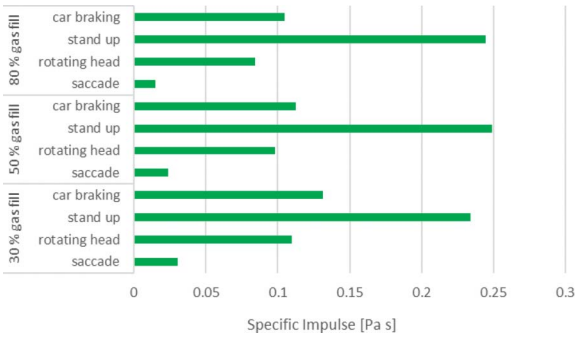

Fig. 8. Specific impulse for each activity and as a function of gas fill percentage. Note how activity determines the magnitude of SI, whereas gas fill does not significantly affect it.

Whether the shear stress generated by aqueous sloshing can elevate retinal tears and allow fluid into the subretinal space is a lengthy debated issue.[18] Retinal adhesion strength has been estimated across a broad range (4–266 Pa),[27–29] and it is known to temporarily decline after retinopexy[30] to less than 4 Pa or approximately 50% of the initial strength after 8 hours and then increase within 24 hours[31]; such values are lower than those calculated in our model and suggest this mechanism is conceivable. Although it is simplistic to believe that this is the only or main factor responsible for retinal redetachment, many activities resulted in shear stress exceeding this value (Figure 7).

Magnitude combined to the duration of applied shear stress may also concur in defining the activities to be restricted: Standing up determined the largest SI regardless of gas fill percentage (Figure 8), followed by car braking and turning head. The ocular saccade being almost instantaneous seemed safer than all other activities for this standpoint.

In summary, our study shows that along with portions of the retina known to be consistently in contact with gas or aqueous as a function of gas fill at rest, patients' activities cause a significant proportion of retinal surface to become momentarily wet by aqueous regardless of patients' compliance. This should be considered by surgeons because sloshing significantly reduces the amount of retina to be considered permanently "dry" and therefore "safe." Surgeons should also be aware that the shear stress and SI determined by the sloshing may exceed the retinal adhesion force, concurring to aqueous leaking into the subretinal space and possibly retinal shifting, therefore instructing patients to longer or different positioning and/or using longer-acting cases if deemed necessary.

Key words: pars plana vitrectomy, computational model, computational fluid dynamics, gas tamponade, shear stress.

Acknowledgments

The authors thank the "Fondazione Roma," the Italian Ministry of Health and CINECA (within study IsC99 "Fluos"), for financial support.

References

1. Amara A, Bernabei F, Chawki MB, et al. Comparison between air and gas as tamponade in 25-gauge pars plana vitrectomy for primary superior rhegmatogenous retinal detachment. Eye (Lond) 2021;36:2028–2033.
2. Romano MR, Rossi T, Borgia A, et al. Management of refractory and recurrent macular holes: a comprehensive review. Surv Ophthalmol 2022;67:90800007–90809318.
3. Neffendorf JE, Gupta B, Williamson TH. The role of intraocular gas tamponade in rhegmatogenous retinal detachment: a synthesis of the literature. Retina 2018;38:S65–S72.
4. Gozawa M, Kanamoto M, Ishida S, et al. Evaluation of intraocular gas using magnetic resonance imaging after pars plana vitrectomy with gas tamponade for rhegmatogenous retinal detachment.Sci Rep. 2020;10:1521.
5. Hostovsky A, Mandelcorn MS, Mandelcorn ED. Orbital magnetic resonance imaging demonstrates better contact between the gas and anterior inferior retina in side versus face-down position. Ophthalmol Retina 2020;4:911–918.
6. Govers BM, Lamers MPM, Klevering BJ, Keijser S. Air versus fluorinated gas tamponades in pars plana vitrectomy treatment for primary rhegmatogenous retinal detachment. Acta Ophthalmologica 2022;100:e1600–e1605.
7. Eames I, Angunawela RI, Aylward GW, Azarbadegan A. A theoretical model for predicting interfacial relationships of retinal tamponades. Invest Ophthalmol Vis Sci 2010;51:2243–2247
8. Hartmann GC. Physical model for absorption of intraocular gas. Digit J Ophthalmol 2013;19:18–20
9. Greenshields C, Weller H. Notes on Computational Fluid Dynamics: General Principles. 2022. ISBN 978-1-3999-2078-0. Reading, UK: CFD Direct Ltd.
10. Hirt CW, Nichols BD. Volume of fluid (VOF) method for the dynamics of free boundaries. J Comput Phys 1981;39:201–225.
11. Rossi T, Querzoli G, Badas MG, et al. Computational fluid dynamics of intraocular silicone oil tamponade. Translational Vis Sci Technol 2021;10:22.
12. Rossi T, Querzoli G, Badas MG, et al. Silicone oil tamponade–retina contact in highly myopic eyes with and without encircling bands: a computational fluid dynamics study. Translational Vis Sci Technol 2022;11:1.
13. Ferziger JH, Perić M. Solution of the Navier-Stokes equations. In: Ferziger JH, Perić M, eds. Computational Methods for Fluid Dynamics. New York, NY, USA: Springer; 2002:157–216. doi. 10.1007/978-3-642-56026-2_7
14. Rossi T, Badas MG, Querzoli G, et al. Does the Bursa Pre-Macularis protect the fovea from shear stress? A possible mechanical role. Exp Eye Res 2018;175:159–165.
15. Parver LM, Lincoff H. Geometry of intraocular gas used in retinal surgery. Mod Probl Ophthalmol 1977;18:338–343.
16. Casswell EJ, Yorston D, Lee E, et al. Effect of face-down positioning vs support-the-break positioning after macula-involving retinal detachment repair: the PostRD randomized clinical trial. JAMA Ophthalmol. 2020;138:634–642.

17. Otsuka K, Imai H, Miki A, Nakamura M. Impact of postoperative positioning on the outcome of pars plana vitrectomy with gas tamponade for primary rhegmatogenous retinal detachment: comparison between supine and prone positioning. Acta Ophthalmol 2018;96:e189–e194.
18. Chen X, Yan Y, Hong L, Zhu L. A comparison of strict facedown positioning with adjustable positioning after pars plana vitrectomy and gas tamponade for rhegmatogenous retinal detachment. Retina 2015;35:892–898
19. Pasu S, Bell L, Zenasni Z, et al. Positioning in macular hole surgery (pims) study group. Facedown positioning following surgery for large full-thickness macular hole: a multicenter randomized clinical trial. JAMA Ophthalmol. 2020;138:725–730.
20. Brodie FL, Ramirez DA, Pandian S, et al. Novel positioning sensor with real-time feedback for improved postoperative positioning: pilot study in control subjects. Clin Ophthalmol 2017;11:939–944.
21. Brodie FL, Woo KY, Balakrishna A, et al. Validation of sensor for postoperative positioning with intraocular gas. Clin Ophthalmol 2016;10:955–960
22. Martínez-Castillo V, Zapata MA, Boixadera A, et al. Pars plana vitrectomy, laser retinopexy, and aqueous tamponade for pseudophakic rhegmatogenous retinal detachment. Ophthalmology 2007;114:297–302.e1.
23. Sato T, Emi K, Bando H, Ikeda T. Retrospective comparisons of vitrectomy with and without air tamponade to repair lamellar macular hole. Ophthalmic Surg Lasers Imaging Retina 2015;46:38–43.
24. Lee KH, Chung YR, Yeo S, et al. Is gas/air tamponade essential for eyes with small peripheral retinal breaks without detachment during vitrectomy? BMC Ophthalmol. 2022;22:186.
25. Angunawela RI, Azarbadegan A, Aylward GW, Eames I. Intraocular fluid dynamics and retinal shear stress after vitrectomy and gas tamponade. Invest Ophthalmol Vis Sci 2011;52:7046–7051.
26. Abdolrahimzadeh S, Piraino DC, Scavella V, et al. Spectral domain optical coherence tomography and B-scan ultrasonography in the evaluation of retinal tears in acute, incomplete posterior vitreous detachment. BMC Ophthalmol 2016;16:60.
27. DeGuillebon H, Zauberman H. Experimental retinal detachment. Biophysical aspects of retinal peeling and stretching. Arch Ophthalmol 1972;87:545–548.
28. Kita M, Marmor MF. Retinal adhesive force in living rabbit, cat, and monkey eyes. Normative data and enhancement by mannitol and acetazolamide. Invest Ophthalmol Vis Sci 1992;33:1879–1882.
29. Kain HL. A new model for examining chorioretinal adhesion experimentally. Arch Ophthalmol 1984;102:608–611.
30. Kain HL. Chorioretinal adhesion after argon laser photocoagulation. Arch Ophthalmol 1984;102:612–615.
31. Yoon YH, Marmor MF. Rapid enhancement of retinal adhesion by laser photocoagulation. Ophthalmology 1988;95:1385–1388.

RISK FACTORS FOR PUPILLARY OPTIC CAPTURE FOLLOWING SUTURELESS FLANGED INTRAOCULAR LENS FIXATION FOR INTRAOCULAR LENS DISLOCATION

JAE ROCK DO, MD,* SU JIN PARK, MD,† JIN YOUNG KIM, MD,* JAE PIL SHIN, MD, PHD,* DONG HO PARK, MD, PHD*‡

Purpose: To identify risk factors for pupillary optic capture after sutureless flanged intraocular lens (IOL) fixation for IOL dislocation.

Methods: This retrospective comparative study enrolled consecutive patients who underwent flanged IOL fixation using 25-gauge pars plana vitrectomy. One hundred twenty-six eyes (126 patients) were divided into two groups according to the presence or absence of pupillary optic capture. A swept-source anterior segment optical coherence tomography and a rotating Scheimpflug camera were used to analyze and compare surgical parameters, including axial length, anterior chamber depth, differences in scleral tunnel angle and length, and IOL tilt and decentration, between the two groups.

Results: Compared with the nonpupillary optic capture group (106 eyes, 84.1%), the pupillary optic capture group (20 eyes, 15.9%) had larger differences in the nasal and temporal scleral tunnel angles and larger horizontal tilt ($P < 0.05$). Multivariate regression analysis demonstrated that these factors correlated with the occurrence of pupillary optic capture ($P < 0.05$).

Conclusion: To prevent pupillary optic capture after flanged IOL fixation, surgeons should avoid asymmetry in the angles of the nasal and temporal scleral tunnels, which causes horizontal IOL tilt and subsequent pupillary capture.

RETINA 43:964–971, 2023

Intraocular lens (IOL) dislocation is one of the most common major complications of cataract surgery.[1] Cumulative risk for IOL dislocation after cataract surgery is 0.55% for 10 years and 1.00% for 15 years.[2]

To manage IOL dislocation, various surgical techniques for secondary IOL implantation have been used, including sutured scleral IOL fixation.[3] Recently, Yamane et al[4] developed a novel surgical technique for sutureless IOL fixation in which the IOL haptics are fixed to the sclera by cauterization of haptic ends, termed flanged IOL fixation. This technique showed shorter operation time and similar clinical outcomes compared with the sutured scleral fixation technique.[5]

Pupillary optic capture of the fixated IOL is one of the most common complications of transscleral sutured IOL fixation with vitrectomy, ranging from 7.9% to 23%.[6,7] Pupillary optic capture causes blurred vision and photophobia, and it can cause serious abnormalities such as chronic uveitis, macular edema, and secondary glaucoma.[8]

Recent studies have reported that pupillary optic capture is also a complication of flanged IOL fixation, with complication rates ranging from 8% to 38.9%.[4,9,10] However, the risk factors for this complication have not been fully elucidated for flanged IOL fixation, a relatively new technique. The aim of this study is to determine the risk factors for pupillary optic capture following flanged IOL fixation in patients with

From the *Department of Ophthalmology, School of Medicine, Kyungpook National University, Kyungpook National University Hospital, Republic of Korea; †Metro Eye Clinic, Republic of Korea; and ‡Kyungpook National University, Cell and Matrix Research Institute, Republic of Korea.

None of the authors has any financial/conflicting interests to disclose.

Supplemental digital content is available for this article. Direct URL citations appear in the printed text and are provided in the HTML and PDF versions of this article on the journal's Web site (www.retinajournal.com).

Reprint requests: Dong Ho Park, MD, PhD, Department of Ophthalmology, School of Medicine, Kyungpook National University, Kyungpook National University Hospital, 130 Dongdeok-ro, Jung-gu, Daegu 41944, Republic of Korea; e-mail: DongHo_Park@knu.ac.kr

IOL dislocation. Furthermore, because construction of scleral tunnels is an imperative process for successful flanged IOL fixation, the study quantitatively measured the dimensions of the nasal and temporal scleral tunnels, which have not previously been fully evaluated.

Methods

The study protocol was approved by the Institutional Review Board of the Kyungpook National University Hospital and was conducted in accordance with the tenets of the Declaration of Helsinki. Written informed consent was obtained from all study participants.

Participant selection

The records of all patients who underwent combined 25-gauge vitrectomy and flanged IOL fixation for management of dislocated IOL in the Department of Ophthalmology at the Kyungpook National University from June 2018 to December 2021 were retrospectively reviewed. All surgeries were performed by a single operator (Dong Ho Park) and had a follow-up of at least six months. Patients with choroidal, retinal, or corneal disease that could affect clinical outcomes were excluded.

Surgical technique

After 25-gauge pars plana vitrectomy and IOL removal using a Constellation Vision System (Alcon Laboratories, Inc, Duluth, GA), flanged IOL fixation was performed as described previously.[4] All IOL removals were performed through a superior corneal limbal incision. If the dislocated IOL optics material was hydrophobic or hydrophilic foldable acrylic, it was cut with a lens cutter and removed through a 3-mm corneal incision. If the IOL optics material was polymethyl methacrylate, it was extracted through a 6-mm extension of the corneal incision. Briefly, a 3-piece IOL (Sensar AR40e from June 2018 to October 2020 and Tecnis ZA9003 from November 2020 to December 2021; Abbott Medical Optics Inc, Santa Ana, CA) was inserted into the anterior chamber. A 30-gauge thin-walled needle (TSK ultra-thin wall needle; Tochigi Seiko, Tochigi, Japan) was used to make angled scleral tunnels 2 mm from the limbus at the 3-o'-clock to 4-o'-clock and 9-o'-clock to 10-o'-clock positions. The leading and trailing haptics were docked into the 30-gauge needle lumen using 25-gauge forceps. After both haptics were removed and extracted from the needles, the haptic ends were cauterized with an ophthalmic cautery device to form a flange. A peripheral iridotomy was made using a vitrectomy cutter to prevent IOL pupillary optic capture. The cornea incision was sutured with 10-0 nylon.

Ophthalmic examinations

Preoperatively and at every visit for 6 months postoperatively, all patients underwent ophthalmologic examinations, including Snellen best-corrected visual acuity, slit-lamp biomicroscopy, intraocular pressure (IOP), and fundus examination. If IOL optics were captured during the follow-up period (Figure 1), the eyes were assigned to the pupillary optic capture group. Axial length and white-to-white (WTW) distance were measured using a swept-source optical coherence tomography–based biometric device (IOL master 700, Carl Zeiss Meditec, Jena, Germany). Postoperative anterior chamber depth (ACD), defined as the distance from the corneal endothelium to the anterior surface of the IOL, was measured with a rotating Scheimpflug camera (Pentacam, Oculus Optikgeräte GmbH, Wetzlar, Germany), as described previously.[11]

Measurement of Scleral Tunnel Dimensions and Intraocular Lens Position by Anterior Segment Optical Coherence Tomography

To evaluate the dimensions of nasal and temporal scleral tunnels, angle and length were measured by two independent graders (S.P. and J.K.) masked to

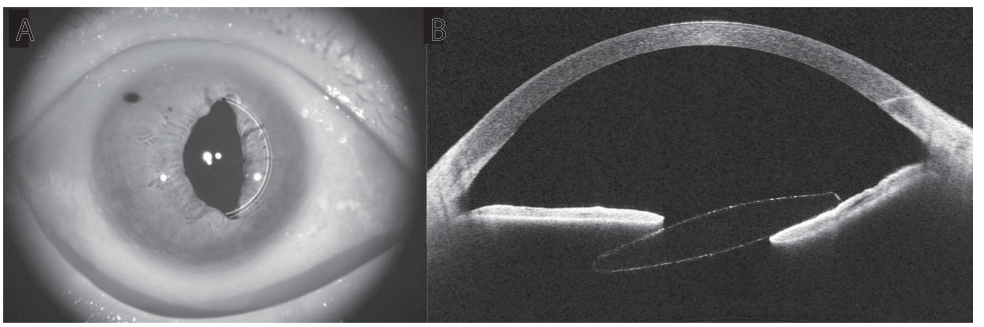

Fig. 1. Anterior segment (**A**) and sagittal (**B**) swept-source anterior segment optical coherence tomography images of an eye with pupillary optic capture after flanged IOL fixation.

patient information and study groups, with a swept-source anterior segment optical coherence tomography system (CASIA2; Tomey Corporation, Nagoya, Japan) and the associated software (CASIA bleb assessment software, Tomey) at one postoperative month. Scleral tunnel angle (Figure 2A) and length (Figure 2B) were measured using the caliper function of the anterior segment optical coherence tomography software. Scleral tunnel angle was defined as the angle between the haptic and the line tangential to the sclera, and scleral tunnel length was defined as the length between the flanged haptic end and the other haptic point piercing the sclera. The mean angles and lengths of all sclera tunnels in each group were measured and assigned as mean scleral tunnel angles and lengths, respectively. Differences in angle and length between the nasal and temporal scleral tunnels in each individual eye were measured and assigned as differences in scleral tunnel angle and length, respectively.

Intraocular lens positions, including IOL tilt and decentration at horizontal and vertical planes, were analyzed automatically with anterior segment optical coherence tomography, which was performed by one operator (S.P.) masked to patient information and study groups, as described previously.[5]

Management of pupillary optic capture

After verifying that the peripheral iridotomy site was opened, IOL repositioning was performed with a 30-gauge needle through the peripheral cornea. In the anterior chamber, the captured optic was pushed back into its position posterior to the iris with the needle tip, and pilocarpine 2.0% twice daily was prescribed postoperatively.

Statistical Analyses

Data were analyzed using SPSS V.21.0 for Windows (SPSS Inc, Chicago, IL). Quantitative data are expressed as means ± SD, and qualitative data are expressed as percentages. Independent *t*-tests and chi-square tests were used to compare numeric and categorical data, respectively, between the two groups at baseline. Correlations between parameters were analyzed using Pearson's correlation coefficient test. Univariate regression and multivariate regression analyses were used to evaluate factors associated with the incidence of pupillary optic capture. To evaluate the repeatability of angle and length of scleral tunnel measurements by two different investigators, interclass correlation coefficient analysis was performed. *P* values of <0.05 were considered statistically significant.

Results

During the study period, 25 of 131 eyes (19.1%) were excluded from the nonpupillary capture group because of the history of retinal detachment (16 eyes) or corneal opacity (9 eyes). Five of 25 eyes (20.0%) were excluded from the pupillary optic capture group because of the history of retinal detachment (three eyes) or corneal opacity (two eyes). Thus, the final study was composed of 126 eyes in 126 patients, with 106 eyes (84.1%) in the nonpupillary optic capture group and 20 eyes (15.9%) in the pupillary optic capture group. Mean duration to onset of pupillary optic capture from flanged IOL fixation was 5.2 ± 3.3 weeks. Table 1 shows patient clinical characteristics. The groups did not differ in age, gender, baseline best-corrected visual acuity, IOP, axial length, or WTW distance ($P > 0.05$, respectively). Furthermore, the proportion of IOL type for fixation and postoperative ACD were not different between the two groups ($P > 0.05$, respectively). In the nonpupillary optic capture group, 85 eyes (80.2%) had dislocated foldable acrylic IOLs, and 21 eyes (19.8%) had dislocated polymethyl methacrylate IOLs (see **Table, Supplemental Digital Content 1**, http://links.lww.com/IAE/B918, which shows types and numbers of dislocated IOLs). In the pupillary optic capture group, 16 eyes (80.0%) had dislocated foldable acrylic

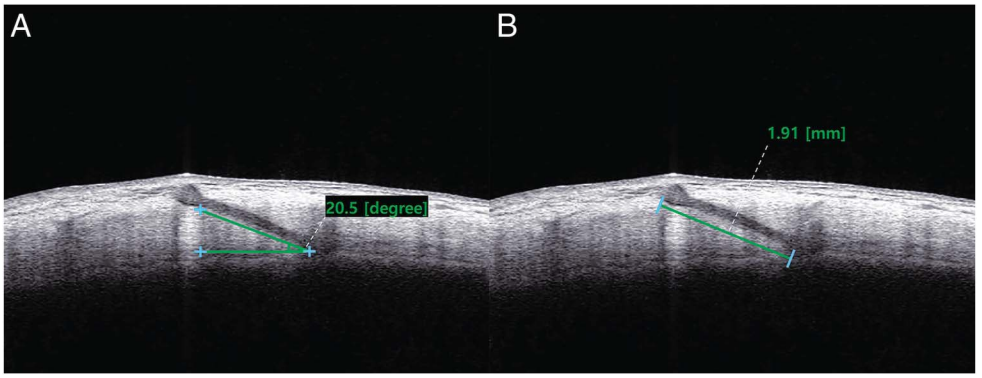

Fig. 2. Measurement of angle (**A**) and length (**B**) of scleral tunnels using swept-source anterior segment optical coherence tomography.

Table 1. Patient Clinical Characteristics

	Nonpupillary Optic Capture Group (n = 106)	Pupillary Optic Capture group (n = 20)	*P*
Age, years	63.3 ± 8.2	61.1 ± 11.5	0.322*
Male gender, n (%)	83 (86.6)	18 (90.0)	0.679†
Onset from previous cataract surgery, months	121.5 ± 88.5	119.8 ± 90.5	0.944*
Mean IOP, mmHg	16.7 ± 5.5	16.8 ± 6.1	0.969*
Preoperative axial length, mm	23.3 ± 4.2	24.6 ± 1.4	0.182*
Preoperative WTW, mm	11.8 ± 1.1	12.0 ± 0.4	0.677*
Mean corneal incision length, mm	3.59 ± 1.20	3.60 ± 1.23	0.937*
Preoperative BCVA, logMAR (Snellen)	0.43 ± 0.56 (20/54)	0.39 ± 0.57 (20/49)	0.857*
Preoperative astigmatism, diopters	1.52 ± 1.60	1.36 ± 1.49	0.997*
Types of dislocated IOLs, foldable acrylic/PMMA	85/21	16/4	0.968†
Types of IOLs for fixation, AR40e/ZA9003	55/51	14/6	0.136†
Postoperative ACD, mm	4.52 ± 0.53	4.57 ± 0.32	0.792*

BCVA, best-corrected visual acuity; logMAR, logarithm of the minimum angle of resolution; PMMA, polymethyl methacrylate.
*Two-tailed, unpaired two-sample *t*-test.
†Chi-square test.

IOLs and 4 eyes (20.0%) had dislocated polymethyl methacrylate IOLs. The proportions of dislocated IOL types did not differ between the two groups ($P > 0.05$). Mean corneal incision length was 3.59 ± 1.20 mm (range: 3.00–6.00 mm) for the nonpupillary optic capture group and 3.60 ± 1.23 mm (range: 3.00–6.00 mm) for the pupillary optic capture group, which did not differ between the two groups ($P > 0.05$).

Comparison of Scleral Tunnel Dimensions and Intraocular Lens Position

The interclass correlation coefficients of scleral tunnel angle and length measurements between the two graders were 0.966 and 0.937, respectively ($P < 0.01$, respectively). Mean scleral tunnel angle and mean scleral tunnel length did not differ between the groups ($P > 0.05$, respectively). The pupillary optic capture group had larger differences in scleral tunnel angle than the nonpupillary optic capture group ($P = 0.010$) (Table 2). However, differences in scleral tunnel lengths did not differ between the groups ($P > 0.05$). The pupillary optic capture group had larger horizontal IOL tilt than the nonpupillary optic capture group ($P = 0.003$). There were no differences in vertical tilt or horizontal or vertical decentration between the groups ($P > 0.05$, respectively).

Table 2. Comparison of Scleral Tunnel Dimensions and Intraocular Lens Position Between the Pupillary Optic Capture and Nonpupillary Optic Capture Groups

	Nonpupillary Optic Capture group (n = 106)	Pupillary Optic Capture Group (n = 20)	*P*
Dimensions of scleral tunnels			
Mean scleral tunnel angle, degree	26.1 ± 5.62	26.5 ± 6.07	0.706
Mean scleral tunnel length, mm	1.88 ± 0.45	1.93 ± 0.39	0.519
Difference in scleral tunnel angles, degree	4.85 ± 3.93	7.34 ± 3.13	0.010
Difference in scleral tunnel lengths, mm	0.45 ± 0.36	0.47 ± 0.38	0.828
IOL tilt			
Horizontal tilt, degree	3.37 ± 1.85	5.36 ± 1.72	0.003
Vertical tilt, degree	3.98 ± 3.27	4.06 ± 3.82	0.936
IOL decentration			
Horizontal decentration, mm	0.33 ± 0.30	0.29 ± 0.16	0.229
Vertical decentration, mm	0.36 ± 0.26	0.27 ± 0.13	0.662

Correlation Between Differences in Scleral Tunnel Angle and Length and Intraocular Lens Position

Difference in scleral tunnel angle correlated with horizontal tilt (r = 0.221, P = 0.037) (Figure 3A). However, difference in scleral tunnel length did not correlate with horizontal tilt ($P > 0.05$) (Figure 3B). Neither difference in scleral tunnel angle nor difference in scleral tunnel length correlated with vertical tilt ($P > 0.05$) (Figure 3, C and D).

Regression analyses were performed to identify factors associated with horizontal and vertical tilts (see **Table, Supplemental Digital Content 2**, http://links.lww.com/IAE/B919, which shows factors associated with horizontal and vertical IOL tilt). In univariate regression analysis, difference in scleral tunnel angles was associated with horizontal tilt (β = 0.680, P = 0.001), although this variable was not associated with vertical tilt (β = 0.036, $P > 0.05$). In multivariate regression analysis, difference in scleral tunnel angles was associated with horizontal tilt (β = 0.460, P = 0.002).

Regression Analyses for Risk Factors Associated With Pupillary Optic Capture

Univariate regression analysis was performed to identify risk factors for pupillary optic capture (Table 3). Difference in scleral tunnel angles (P = 0.013) was associated with the incidence of pupillary optic capture. Furthermore, horizontal IOL tilt was associated with the incidence of pupillary optic capture (β = 0.314, P = 0.003), whereas vertical IOL tilt was

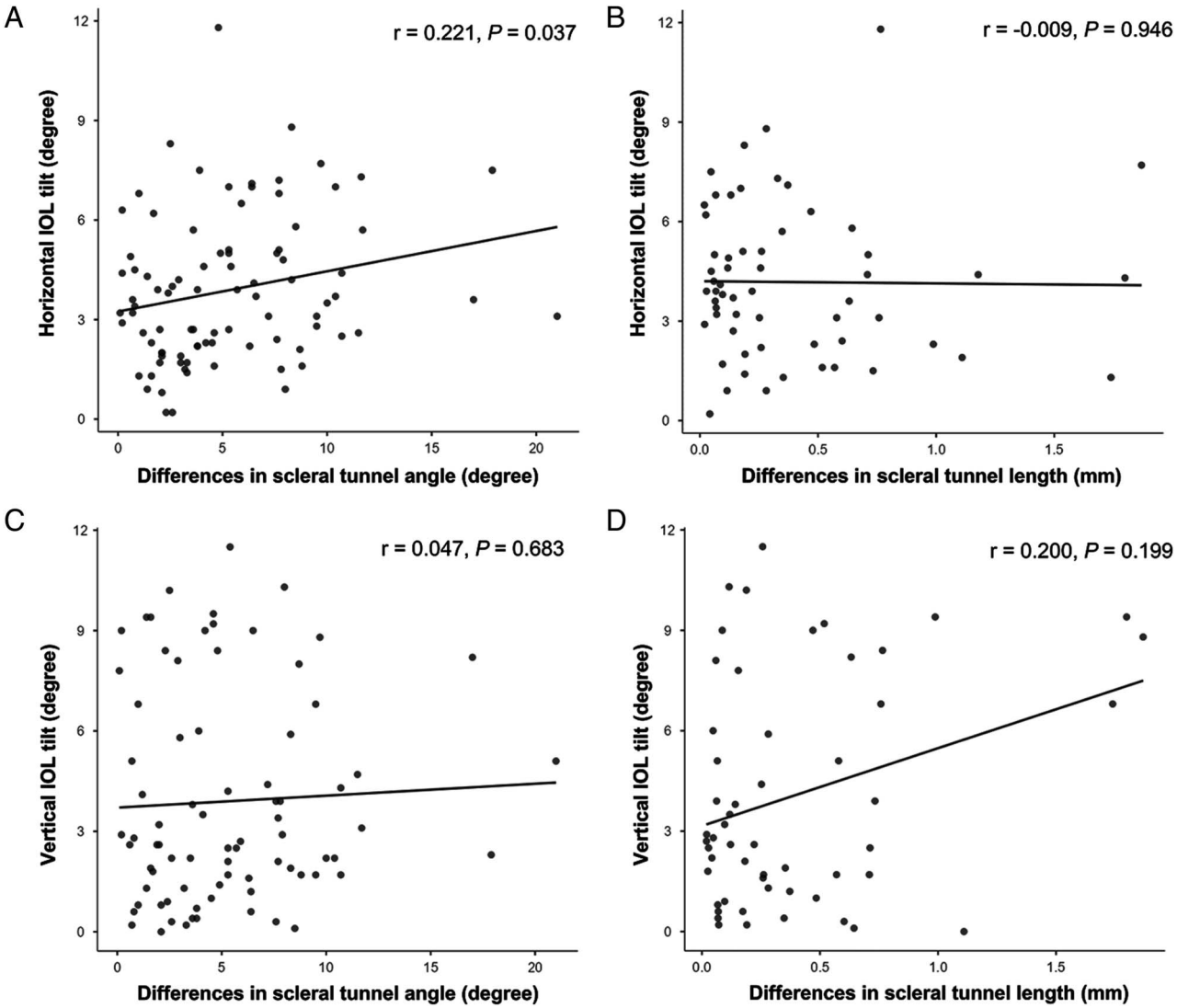

Fig. 3. Correlation between differences in scleral tunnel angle/length and intraocular lens position. Difference in scleral tunnel angles correlated with horizontal tilt (r = 0.221, P = 0.037) **(A)**, although difference in scleral tunnel lengths did not correlate with horizontal tilt ($P > 0.05$) **(B)**. Difference in scleral tunnel angles **(C)** and lengths **(D)** did not correlate with vertical tilt ($P > 0.05$, respectively).

not associated with the incidence of pupillary optic capture ($\beta = -0.019$, $P > 0.05$). In multivariate regression analysis, difference in scleral tunnel angles ($P = 0.037$) and horizontal IOL tilt ($P < 0.001$) were associated with the development of pupillary optic capture.

Management of Pupillary Optic Capture and Comparison of Postoperative Complications and Best-Corrected Visual Acuity at 6 Months

All 20 eyes with pupillary optic capture had a patent peripheral iridotomy site. Intraocular lens repositioning followed by pilocarpine 2.0% twice daily was performed in all cases as soon as optic capture was detected, which successfully maintained stable IOL position without recurrent or persistent pupillary optic capture, at least for the 6-month follow-up period. No postoperative complications, including iatrogenic retinal tears, retinal detachment, or IOL dislocation, occurred in either group. Final best-corrected visual acuity at 6 months postoperatively did not differ between the groups (0.19 ± 0.29 logarithm of the minimum angle of resolution, 20/30 vs. 0.13 ± 0.14 logarithm of the minimum angle of resolution, 20/27, $P > 0.05$).

Discussion

Recently, flanged IOL fixation first reported by Yamane et al has been widely used for secondary IOL implantation because of the short operation time and similar clinical outcomes compared with conventional sutured scleral fixation.[5] However, several postoperative complications after flanged IOL fixation can occur, including vitreous hemorrhage, transient hypotony, IOP elevation, cystoid macular edema, and pupillary optic capture. Pupillary optic capture after flanged IOL scleral fixation is a relatively common postoperative complication, and its incidence in this study was similar to that of previous studies.[4,9,10] Although the mechanism of pupillary optic capture is not fully understood, axial length, ACD, and IOL tilt have been suggested as possible causes of the complication after sutured scleral IOL fixation.[12–14] For flanged IOL fixation, construction of the nasal and temporal scleral tunnels is a critical step because both haptics are directly fixed to the sclera instead of the suture thread. Therefore, the risk factors for pupillary optic capture following flanged IOL fixation could be different from those of sutured scleral fixation.

Several studies reported that IOL tilt is related to pupillary optic capture,[15–17] and various factors contribute to IOL tilt after scleral fixation. Gao et al[18] reported that asymmetric IOL fixation causes IOL tilt or decentration after sutured scleral fixation. Yamane et al[19] reported that the IOL tilt was decreased when using a needle stabilizer, which aided in the formation of consistent scleral tunnel angles, although the angles were not quantitatively measured. Combined with the findings of this study, this result suggests that the construction of scleral tunnels affects the IOL tilt after flanged IOL fixation. This study quantitatively measured scleral tunnel dimensions for the first time, revealing differences in scleral tunnel angle and horizontal IOL tilt as the main risk factors for pupillary optic capture. Teichmann et al[20] reported that asymmetrical suture placement creates torque on the haptics, resulting in IOL tilt. Similarly, asymmetric scleral tunnel angles could also impose torque on the haptics with subsequent IOL tilt. This study demonstrated that differences in scleral tunnel angles positively correlated with horizontal tilt, consistent with this hypothesis. Thus, construction of symmetric scleral tunnel angles to avoid horizontal IOL tilt could be an important factor for the prevention of postoperative pupillary optic capture.

Table 3. Regression Analyses for Risk Factors Associated With Pupillary Optic Capture

Variable	Univariate Analysis		Multivariate Analysis	
	β	P	β	P
Onset from previous cataract surgery	0.016	0.876		
Preoperative axial length	0.012	0.228		
Preoperative WTW	0.008	0.694		
IOL type	−0.080	0.269		
Corneal incision length	0.029	0.773		
Postoperative ACD	0.039	0.792		
Difference in scleral tunnel angles	0.027	0.013	0.023	0.037
Difference in scleral tunnel lengths	0.041	0.738		
Horizontal IOL tilt	0.314	0.003	0.389	< 0.001
Vertical IOL tilt	−0.019	0.138		
Horizontal IOL decentration	−0.177	0.298		
Vertical IOL decentration	−0.029	0.838		

There are several potential reasons for asymmetry of scleral tunnel angles. First, when making scleral tunnels, a hypotonic eyeball could hinder construction of the intended scleral tunnel angles by surgeons. Thus, it would be important to maintain constant IOP for consistent scleral rigidity. Second, when subconjunctival hemorrhage or chemosis is present in the marking points, the sclera might not be visible through the conjunctiva, which could hinder the surgeons' ability to construct symmetric scleral tunnel angles. In this case, it would be helpful to open the conjunctiva and make the sclera visible or to change the direction of scleral tunnels.

Although we have provided precise data for quantitative measurement of the dimensions of the nasal and temporal scleral tunnels, we are at present unable to provide a practical means to consistently avoid the construction of asymmetric intrascleral haptic tunnels. This challenge is complex and varies significantly between the cases. For example, the dimensions of the globe and curvature of the nasal versus temporal scleral surface could differ between the patients. In addition, insertion of the 30-gauge needle to construct the intrascleral tunnels for the 2 haptics is in a diametrically opposite direction rather than in the same direction, makes creation of identical angles more challenging. Moreover, during insertion of each haptic into the sclera, the haptic could be bent unevenly or asymmetrically between the two sides. Together, these factors complicate the development of a consistent surgical technique for making identical insertion angles for both sides.

It is interesting to note that difference in scleral tunnel angles associated with horizontal tilt but not vertical tilt. This could be related to the surgical method, in which scleral tunnels were created at 3 to 4-o'-clock and 9 to 10-o'-clock positions, which could affect tilt of the horizontal plane rather than tilt of the vertical plane. If haptic insertion had been performed along the vertical meridian instead of the horizontal meridian, vertical tilt could be a more important parameter than horizontal tilt. Because all scleral tunnels were created with the horizontal meridian in this study, future studies using haptic insertions with the vertical meridian would be informative in determining the differential effects of horizontal versus vertical tilt.

Correlation of the ACD, defined as the distance from the corneal endothelium to the anterior surface of the IOL, with pupillary optic capture has historically been controversial in studies of sutured IOL fixation. Kang et al reported that deeper ACD correlated with the incidence of pupillary optic capture, whereas Choi et al reported that shallow ACD correlated with pupillary optic capture.[12,14] In this study, postoperative ACD was similar to that of flanged IOL fixation reported by Torii et al[21] and did not differ between the two groups with and without pupillary optic capture.

It is interesting that the mean duration to the onset of pupillary optic capture from flanged IOL fixation was 5.2 weeks, which demonstrates that follow-up is necessary to observe postoperative pupillary optic capture, especially at 1 month postoperatively.

In this study, no recurrence of pupillary optic capture occurred after IOL repositioning with postoperative pilocarpine 2.0%. Kim et al[22] reported that peripheral iridotomy helped to prevent pupillary capture after conventional sutured scleral fixation. However, in this study, peripheral iridotomy sites were constructed in all cases, and they did not completely prevent pupillary optic capture. However, this could help to prevent recurrence of pupillary optic capture after IOL repositioning and pilocarpine treatment by decreasing the pressure difference between the anterior and posterior chambers.

There are several limitations in this study that should be considered in its interpretation. First, since November 2020, the type of 3-piece IOL was changed from AR40e to ZA9003 because of the ease of docking caused by the thinner haptic thickness (0.17 mm for AR40e vs. 0.15 mm for ZA9003). However, the proportion of IOL type did not differ between the groups with and without pupillary optic capture. Second, this study used only two types of IOLs with a 6-mm optic diameter. It is interesting to note that in the earlier study by Yamane et al, use of 6-mm IOLs, including ZA9003, PN6A (Kowa, Tokyo, Japan), and MA60MA (Alcon laboratories, Fort worth, TX), resulted in a 7-times higher incidence of pupillary optic capture compared with X-70 (Santen, Osaka, Japan) IOLs, which have a 7-mm optic diameter (14% vs. 2% incidence, respectively).[4] Miura et al[10] also reported similar outcomes. Although the 7-mm optics could be more advantageous to avoid pupillary optic capture compared with 6-mm optics, the X-70 is available only in Japan. Thus, surgeons who are not able to use these IOLs should be especially cautious of risk factors such as asymmetric scleral tunnel angle. Third, the needle stabilizer used in the study of Yamane et al, which was developed to create a 10° angle, was not used in this study. The reason is that the fixed inner ring diameter made it difficult to maintain the same limbal distance in all patients who have their own different WTW diameters. In future studies, we will compare the symmetry of scleral tunnel angle with or without the use of the needle stabilizer.

Fourth, because we could not precisely quantify scleral tunnel angles during tunnel construction, we

were unable to suggest a practical solution to avoid asymmetric scleral tunnel angles. If intraoperative anterior segment swept-source optical coherence tomography becomes available, intraoperative measurement can then be tested with future comparison studies. Fifth, because of the imbalance in sample size between the two groups, the statistical power of the study is limited by the pupillary optic capture group with the smaller sample size, a limitation commonly encountered in clinical studies of postoperative complications.

In conclusion, in flanged IOL fixation, surgeons should avoid asymmetry in the angles of the nasal and temporal scleral tunnels, which causes horizontal IOL tilt and subsequent pupillary capture. Furthermore, meticulous follow-up is necessary to evaluate postoperative pupillary optic capture even when the IOL position is stable intraoperatively.

Key words: flanged intraocular lens fixation, intraocular lens dislocation, pupillary optic capture.

Acknowledgments

D.H. Park is financially supported by the Basic Science Research Program of the National Research Foundation of Korea, funded by the Korean government (Ministry of Science and ICT) (2019R1A2C1084371). D.H. Park is also supported by the Ministry of Science and ICT, Korea, under the Information Technology Research Center support program (IITP-2023–2020-0-01808) supervised by the Institute of Information and Communications Technology Planning and Evaluation (IITP). This research was supported by the Korea Drug Development Fund, funded by the Ministry of Science and ICT, Ministry of Trade, Industry, and Energy, and Ministry of Health and Welfare (HN21C0923000021, Republic of Korea). This research was supported by a grant of the Korea Health Technology R&D Project through the Korea Health Industry Development Institute, funded by the Ministry of Health and Welfare, Republic of Korea (HR22C1832).

References

1. Clark A, Morlet N, Ng JQ, et al. Whole population trends in complications of cataract surgery over 22 years in Western Australia. Ophthalmology 2011;118:1055–1061.
2. Dabrowska-Kloda K, Kloda T, Boudiaf S, et al. Incidence and risk factors of late in-the-bag intraocular lens dislocation: evaluation of 140 eyes between 1992 and 2012. J Cataract Refractive Surg 2015;41:1376–1382.
3. Bastawrous A, Parkes C, Prasad S. Choices in correction of aphakia during vitrectomy. Ophthalmologica 2011;226:46–52.
4. Yamane S, Sato S, Maruyama-Inoue M, Kadonosono K. Flanged intrascleral intraocular lens fixation with double-needle technique. Ophthalmology 2017;124:1136–1142.
5. Do JR, Park SJ, Mukai R, et al. A 1-year prospective comparative study of sutureless flanged intraocular lens fixation and conventional sutured scleral fixation in intraocular lens dislocation. Ophthalmologica 2021;244:68–75.
6. Cho B-J, Yu HG. Surgical outcomes according to vitreous management after scleral fixation of posterior chamber intraocular lenses. Retina 2014;34:1977–1984.
7. Bading G, Hillenkamp J, Sachs HG, et al. Long-term safety and functional outcome of combined pars plana vitrectomy and scleral-fixated sutured posterior chamber lens implantation. Am J Ophthalmol 2007;144:371–377.e1.
8. Nagamoto S, Kohzuka T, Nagamoto T. Pupillary block after pupillary capture of an AcrySof intraocular lens. J Cataract Refractive Surg 1998;24:1271–1274.
9. Tao Y, Ren X, Zhang Y, et al. Outcomes of the flanged intrascleral haptic fixation with double-needle technique in patients with Marfan syndrome. Eur J Ophthalmol 2021;32:2166–2172.
10. Miura Y, Harada Y, Kiuchi Y. Comparison of different IOL types in the flanged IOL fixation technique. J Ophthalmol 2020;2020:1–6.
11. Ryu S, Yoon SH, Jun I, et al. Anterior ocular biometrics using placido-scanning-slit system, rotating Scheimpflug tomography, and swept-source optical coherence tomography. Korean J Ophthalmol 2022;36:264–273.
12. Kang DJ, Kim HK. Clinical analysis of the factors contributing to pupillary optic capture after transscleral fixation of posterior chamber intraocular lens for dislocated intraocular lens. J Cataract Refractive Surg 2016;42:1146–1150.
13. Bartholomew RS. Incidence, causes, and neodymium: YAG laser treatment of pupillary capture. J Cataract Refractive Surg 1997;23:1404–1408.
14. Choi SR, Jeon JH, Kang JW, Heo JW. Risk factors for and management of pupillary intraocular lens capture after intraocular lens transscleral fixation. J Cataract Refractive Surg 2017;43:1557–1562.
15. Higashide T, Shimizu F, Nishimura A, Sugiyama K. Anterior segment optical coherence tomography findings of reverse pupillary block after scleral-fixated sutured posterior chamber intraocular lens implantation. J Cataract Refractive Surg 2009;35:1540–1547.
16. Lin K, Hu Z, Lin Z, et al. Rectangular loop suture to correct iris capture of the posterior chamber intraocular lens. BMC Ophthalmol 2020;20:383–385.
17. Bowman BC, Hansen SO, Olson RJ. Noninvasive repositioning of a posterior chamber intraocular lens following pupillary capture. J Cataract Refractive Surg 1991;17:843–847.
18. Gao S, Qin T, Wang S, Lu Y. Sulcus fixation of foldable intraocular lenses guided by ultrasound biomicroscopy. J Ophthalmol 2015;2015:1–4.
19. Yamane S, Maruyama-Inoue M, Kadonosono K. Needle stabilizer for flanged intraocular lens fixation. Retina 2019;39:801.
20. Teichmann KD, Teichmann IA. The torque and tilt gamble. J Cataract Refractive Surg 1997;23:413–418.
21. Torii T, Tamaoki A, Kojima T, et al. Comparison of clinical outcomes between intracapsular implantation and intrascleral fixation using the same model of intraocular lens. Clin Ophthalmol 2020;14:3965–3974.
22. Kim DY, Lim HB, Kang TS, Kim JY. Preventing pupillary capture after vitrectomy and transscleral fixation of an intraocular lens: iridotomy using a vitrectomy probe. Retina 2017;37:2112–2117.

LONG-TERM EVOLUTION OF MYOPIC RETINOSCHISIS WITH A DOME-SHAPED MACULA AND PREDICTORS OF PROGRESSION AND VISUAL PROGNOSIS

SHIWEI LI MD, TINGTING LI, MD, DA LONG, MD, BIN LU, MD, YAN CHEN, MD, XUEYAN ZHANG, MD, JIANYAN HU, MD, QIANG WU, MD, PHD

Purpose: To study the long-term natural course of myopic retinoschisis (MRS) with a dome-shaped macula (DSM) and to identify the factors affecting its development and visual prognosis.

Methods: In this retrospective case series study, we followed 25 MRS eyes with a DSM and 68 MRS eyes without a DSM for at least two years and observed changes in optical coherence tomography morphologic features and best-corrected visual acuity.

Results: During the mean follow-up of 48.3 ± 13.24 months, the difference in the rate of MRS progression between the DSM and non-DSM groups was not significant ($P = 0.7462$). In the DSM group, the patients whose MRS progressed were older and had a higher refractive error than those whose MRS was stable or improved ($P = 0.0301$ and 0.0166, respectively). The patients whose DSM was located in the central fovea had a significantly higher progression rate than those whose DSM was located in the parafovea ($P = 0.0421$). For all DSM eyes, BCVA did not decrease significantly in eyes with extrafoveal retinoschisis ($P = 0.2500$), patients whose best-corrected visual acuity decreased more than two lines had a greater central foveal thickness initially than those whose best-corrected visual acuity decreased less than two lines during the follow-up period ($P = 0.0478$).

Conclusion: A DSM did not delay the progression of MRS. The development of MRS in DSM eyes was associated with age, myopic degree, and DSM location. A higher schisis cavity predicted visual deterioration, and a DSM protected visual function in extrafoveal MRS eyes during the follow-up period.

RETINA 43:972–983, 2023

A dome-shaped macula (DSM) is characterized by inward convexity of the macula in highly myopic patients with posterior staphyloma and was first observed by Gaucher et al[1] using optical coherence tomography (OCT). It has been reported that the prevalence of DSM in high myopia is between 10.7% and 20.1%, depending on ethnicity.[1–3] Three DSM subtypes, including a round dome and a horizontal and vertical oval-shaped dome, were identified by Caillaux et al[4] with OCT. The pathogenesis of DSM is not yet fully understood, and the mechanism of its occurrence is believed to be because of genetic and environmental factors, the thickness of the sclera in the macula increasing and protruding inward to resist the uneven growth of the eyeball and the progression of posterior staphyloma, and it alleviates the high degrees of myopia in the macula.[1,5]

The presence of DSM is related to highly myopic macular changes, including choroidal neovascularization, serous retinal detachment, and myopic retinoschisis (MRS).[2,6] The forces exerted by the vitreous body and the uneven elongation of the eyeball act on the

From the Department of Ophthalmology, Shanghai Jiaotong University Affiliated Sixth People's Hospital, Shanghai, China.

None of the authors has any financial/conflicting interests to disclose.

Reprint requests: Qiang Wu, MD, PhD, Department of Ophthalmology, Shanghai Jiaotong University Affiliated Sixth People's Hospital, No. 600 Yishan Road, Xuhui District, Shanghai 200233, People's Republic of China; e-mail: qiang.wu@shsmu.edu.cn

retina and macula, leading to the occurrence and progression of MRS.[7–10] It has been reported that in at least 3 years of follow-up of large samples, the progression rate of MRS is 11.6% to 43.4%.[11–14] Mechanical traction and/or insufficient choroidal blood perfusion may cause damage to the ellipsoid zone, which is a predictor of vision deterioration.[12] Cross-sectional studies have found that in DSM eyes, MRS is more inclined to affect the extrafoveal region and less likely to affect the foveal region, and in eyes with MRS,[2,15] the shape of a DSM is steeper than that in eyes without MRS,[15] which may be because of the distribution and strength of the mechanical stress produced by DSM of different shapes. Furthermore, several reports found that even though DSM eyes with various kinds of macular complications had a much longer axial length and a higher degree of myopia, their visual function was not worse than that of eyes without a DSM,[2,15,16] suggesting that the macular convexity of a DSM protects the foveal anatomical structure and visual function. However, few studies have investigated the effect of a DSM on the progression of MRS and its impact on the change in visual acuity in MRS eyes.

For this reason, our study aimed to observe the natural course of MRS in eyes with a DSM and to assess the effect of a DSM on the OCT morphologic changes and visual changes of MRS in the follow-up period.

Methods

Patients

This retrospective, consecutive case series study followed MRS eyes with and without a DSM in highly myopic patients at the Department of Ophthalmology of the Sixth People's Hospital Affiliated to Shanghai Jiao Tong University, whose medical records were reviewed from October 2014 to February 2021. The inclusion criteria were as follows: 1) MRS with and without a DSM diagnosed by OCT and 2) highly myopic eyes, defined as an axial length $\geq$26 mm and a spherical equivalent refractive error of ≥ -6.00 diopter. The exclusion criteria were as follows: 1) eyes with tilted-disk syndrome or inferior staphyloma; 2) the quality scores of spectral domain OCT (SD-OCT) images less than 20 dB because of the opacity of the refractive medium; 3) a lamellar or full-thickness macular hole or foveal detachment at baseline; 4) macular complications secondary to high myopia, such as choroidal neovascularization; and 5) a history of vitreoretinal surgery. The study conformed to the tenets of the Helsinki Declaration, was approved by the Ethics Committee of Sixth People's Hospital Affiliated to Shanghai Jiao Tong University, Shanghai, China, and was registered in the Chinese clinical trial registry (http://www.chictr.org.cn/, registration number: ChiCTR2000038824). Informed consent forms were signed by all participants.

Clinical Examinations

All patients underwent a complete ocular examination, including slit-lamp examination, fundus photography, BCVA analysis with Snellen charts, refractive error assessment using a refractor, axial length measurement using an Intraocular Lens(IOL)-Master, determination of the presence of posterior staphyloma using B-scan ultrasonography, and OCT examinations. We used the Lens Opacity Classification System (III) to determine the severity of the lens opacities in phakic eyes by slit-lamp examination, and classified the cortical opacities into C0, C1, C2, C3, C4, and C5 grades, classified the nuclear opacities into N0, N1, N2, N3, N4, N5, and N6 grades, and classified the posterior subcapsular opacities into P0, P1, P2, P3, P4, and P5 grades respectively.[17] Snellen BCVA was converted to logarithmic minimal angle of resolution units for statistical analysis. OCT images were obtained with an SD-OCT (Heidelberg Engineering, Heidelberg, Germany). The SD-OCT scanning protocol consisted of an A-scan through the center of the macula, with a length between 7.7 mm and 11.5 mm in the horizontal and vertical directions and 31 B-scans covering an area of $30° \times 25.0°$ centered on the fovea at an interval of 256 μm. Outer schisis (in or out of the outer plexiform layer) and inner schisis (in the inner plexiform layer and/or internal limiting membrane detachment) were recorded according to the location of intraretinal layers in which the schisis was involved. The eyes were classified into five subgroups (S0, S1, S2, S3, and S4) according to the classification method of Shimada et al.[14] S1 MRS was recorded as extrafoveal schisis, and S2, S3, and S4 schisis were recorded as foveal schisis. The central foveal thickness (CFT) was measured and characterized as the distance between the hyperreflective band of the internal limiting membrane and the hyperreflective band of the retinal pigment epithelium through the central fovea. The values measured in the horizontal and vertical A-scans were averaged. The presence of partial posterior vitreous detachment PVD), an epimacular membrane, was evaluated by OCT. ADSM is defined as an inward protrusion of the retinal pigment epithelium of the macula with 50 μm or more in the horizontal or vertical section or both by OCT examination.[18] The location of the DSM (below the

foveola or below the parafoveola) (below the center fovea or below the paracentral fovea) was observed. The width of the macular bulge was defined as the distance between the two tangent points in the outer surface of the retinal pigment epithelium, and the height of the dome was defined as the distance between the peak at the plane of the retinal pigment epithelium and the base of the dome. Then, the ratio of the height and width (H/W ratio) of the dome was calculated.[14] The choroidal thickness (CT) was measured at the center of the fovea and at the top of the dome. All patients were divided into two groups: the MRS with DSM group and the MRS without DSM group. The definition of progression for MRS in all patients was an increase in height of outer schisis by 100 μm, the extent of outer schisis expanded, the development of a lamellar or full-thickness macular hole or foveal or macular detachment. A reduction in the height or extent of outer schisis without the development of a lamellar or full-thickness macular hole or foveal or macular detachment was considered improvement. Eyes that did not show progression or improvement were categorized as stable.[11] All patients underwent at least two examinations, including assessment of BCVA and an OCT examination. The shortest follow-up period was 24 months.

Statistical Analysis

All statistical computations were performed using SAS software version 9.13 (SAS Institute Inc, Chicago, IL). Data are described as the mean ± SD. *t*-tests were used to compare the paired and unpaired measurement data, and if the data did not have a normal distribution, the Kruskal–Wallis test was used. The chi-square test was applied for statistical analysis of the count data, and

Table 1. Comparison of Baseline Clinical Characteristics of Myopic Retinoschisis Eyes With and Without Dome-Shaped Macula

	Eyes with DSM	Eyes without DSM	*P*
No. of eyes	25	68	
Age (years), mean ± SD	67.7 ± 7.39 (48–78)	62.3 ± 8.80 (41–82)	0.0080
Sex (Female/Male), n	20/5	48/20	0.4195
Pseudophakic eyes, n	7	25	—
Refractive error(diopter)*, mean ± SD	−15.1 ± 5.19 (−8.0 to −26.75)	−13.0 ± 5.05 (−6.0 to −30.0)	0.0344
Axial length (mm), mean ± SD	30.6 ± 1.15 (28.48 −32.06)	29.2 ± 1.43 (26.44 −33.02)	<.0001
Lens status*, n			
Cortical opacity			0.8835
C0	8	20	
C1	10	23	
Nuclear opacity			0.1871
N0	1	1	
N1	3	19	
N2	12	20	
N3	2	3	
Posterior subcapsular opacity			0.8393
P0	17	40	
P1	1	3	
BCVA (Snellen equivalent)	20/40 ± 20/100 (20/400–20/20)	20/32 ± 20/100 (20/1,000–20/16	—
BCVA (logMAR), mean ± SD	0.41 ± 0.34 (0–1.3)	0.29 ± 0.25 (–0.1 to 1.7)	0.1274
Schisis group, n			0.8512
S0	3	5	
S1	8	26	
S2	1	4	
S3	8	23	
S4	5	10	
Schisis subtype, n			0.7617
Outer schisis	10	31	
Outer and inner schisis	12	32	
Partial PVD, n	7	21	0.7882
Epimacular membrane, n	12	27	0.4724
CFT (μm), mean ± SD	237.6 ± 103.18	236.6 ± 62.12	0.9520
Subfoveal CT (μm), mean ± SD	26.7 ± 16.26	37.0 ± 24.78	0.0570

*Phakic eyes only, n = 18 in DSM group and n = 43 in non-DSM group.
logMAR, logarithmic minimal angle of resolution.

if the sample size in the group was <5, Fisher's exact test was performed. A P value <0.05 was considered to indicate statistical significance.

Results

Baseline Characteristics

A total of 93 eyes from 93 highly myopic patients were included in this retrospective study, consisting of 25 MRS eyes with a DSM from 25 patients and 68 MRS eyes without a DSM. Table 1 lists the demographics and baseline OCT characteristics of MRS eyes with and without a DSM. Myopic retinoschisis patients with a DSM were significantly older and had a higher myopic refractive error and a longer axial length than those without a DSM ($P < 0.05$, respectively). There were no significant differences in sex, lens status, logarithmic minimal angle of resolution BCVA, schisis subgroup, schisis subtype, or the presence of partial PVD or an epimacular membrane between the two groups ($P > 0.05$, respectively).

Lens Status at the Last Follow-Up and Progression of the Lens Opacities

The mean follow-up period was 48.3 ± 13.24 months (ranging from 24 to 86 months).

Among the 18 phakic eyes with a DSM, at the last follow-up, 3 eyes were graded as C0, 12 eyes as C1, and 3 eyes as C2. One eye was graded as N0, 3 eyes as N1, 9 eyes as N2, 3 eyes as N3, and 2 eyes as N4. Fifteen eyes were graded as P0, and 3 eyes as P1. During the follow-up period, 3 eyes developed from N2 to N3, and 2 eyes developed from N3 to N4. Among the 43 phakic eyes without a DSM, at the last follow-up, 11 eyes were graded as C0, 27 eyes as C1, and 5 eyes as C2. One eye was graded as N0, 18 eyes as N1, 17 eyes as N2, 4 eyes as N3, and 3 eyes as N4. Thirty-eight eyes were graded as P0 and 5 eyes as P1. During the follow-up period, 1 eye developed from N1 to N2, 4 eyes developed from N2 to N3, and 3 eyes developed from N3 to N4.

MRS Progression

During the follow-up period, the difference in the rate of MRS progression between the DSM and non-DSM groups was not significant (40.0% vs. 47.1%) ($P = 0.7462$) (Figures 1–4), and for the foveoschisis and extrafoveal retinoschisis eyes, there were no significant differences in the rate of progression between the DSM and non-DSM groups ($P = 0.8019$ and 0.6954, respectively) (Table 2).

Factors Influencing the Natural Course and Best-Corrected Visual Acuity

In the DSM group, patients whose MRS progressed were older and had a higher myopic refractive error than patients whose MRS was stable or improved ($P = 0.0301$ and 0.0166, respectively), and the patients whose DSM was located in the central fovea had a significantly higher progression rate (61.5%) than those whose DSM was located in the parafovea (16.7%) ($P = 0.0421$). The axial length, schisis group, schisis subgroup, subfoveal CT, vitreoretinal traction, CT at DSM, width of the DSM, height of the DSM, and H/W ratio of the DSM were not significantly different between the eyes that progressed and those that were stable or improved ($P > 0.05$, respectively). In the non-DSM group, eyes that progressed had a significantly higher proportion (75.0%) of partial PVD than those that were stable or improved (58.3% and 41.7%, respectively) ($P = 0.0341$), and the differences in age, refractive error, axial length, schisis group, schisis subgroup, and subfoveal CT were not significant between the eyes that progressed and those that were stable or improved ($P > 0.05$, respectively) (Table 3). In the DSM group, foveoschisis eyes had a significantly worse BCVA at the last visit than at the first visit ($P = 0.0020$), whereas there was no significant difference in BCVA between the first and the last visit in extrafoveal retinoschisis eyes ($P = 0.2500$). In the non-DSM group, foveoschisis and extrafoveal retinoschisis eyes had a significantly worse BCVA at the last visit than at the first visit ($P = 0.0494$ and $P = 0.0091$) (Table 4). In the DSM group, patients whose BCVA decreased more than 2 lines had a significantly greater CFT (292.8 ± 143.73 μm) initially than those whose BCVA decreased less than 2 lines (206.6 ± 63.22 μm) during the follow-up period ($P = 0.0478$). In the non-DSM group, MRS eyes with vitreomacular traction had a significantly higher proportion of visual loss greater than two lines during the follow-up period than those without vitreomacular traction (23.3% vs. 4.0%) ($P = 0.0232$) (Table 5).

Discussion

The main findings of our study were that MRS eyes with a DSM were older, more myopic, and had a longer axial length than those without a DSM at baseline. There was no significant difference in the progression rate between MRS eyes with and without a DSM during an average follow-up period of 48.3 months. MRS in eyes with a DSM, which tended to be older and have a higher degree of myopia and a

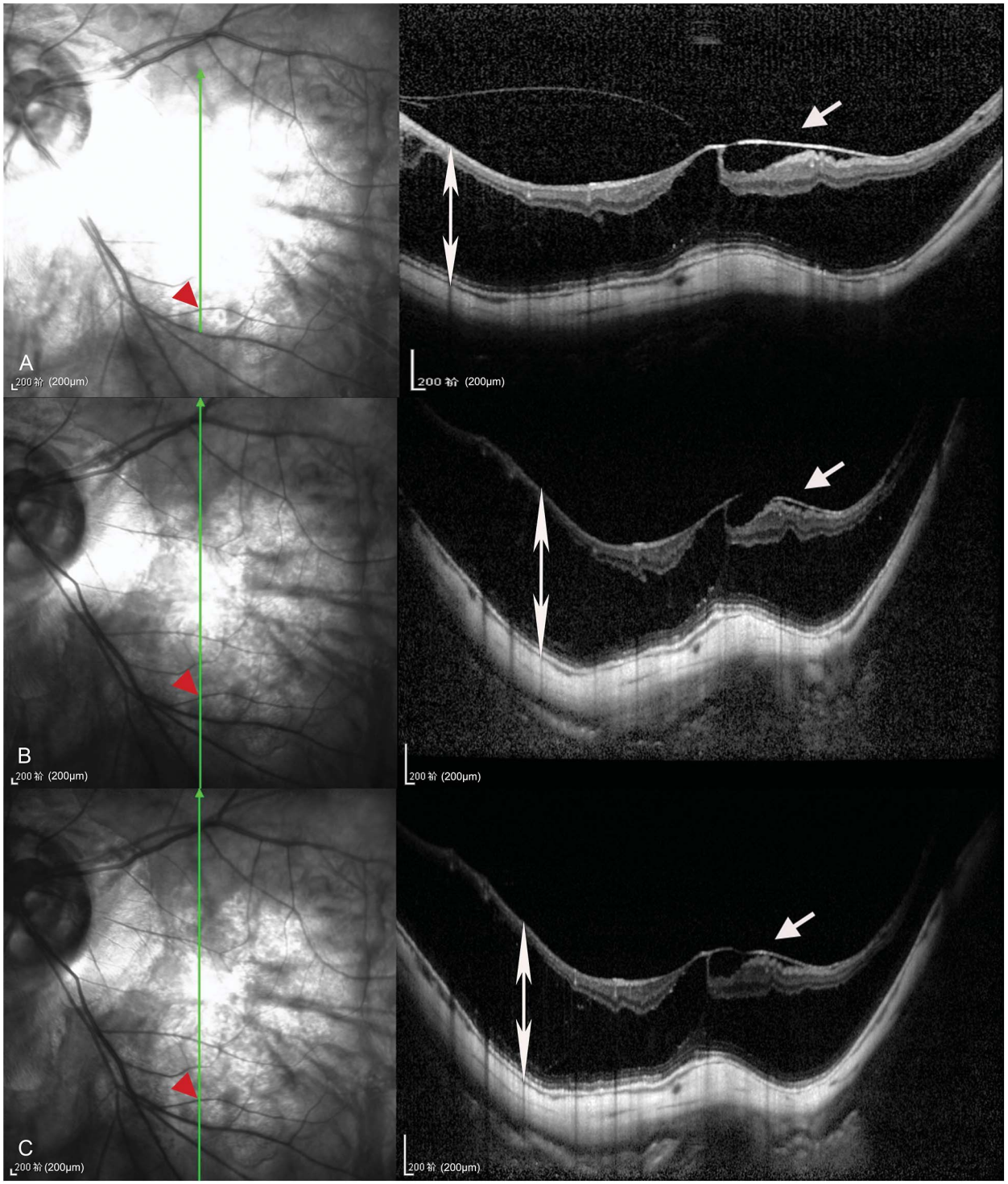

Fig. 1. A–C. Showed infrared fundus and OCT images of the left eye of a 73-year-old man with MRS progression and a DSM located in the fovea during the follow-up period in the vertical scan. **A.** At baseline, the case had S4 outer schisis with epimacular membrane (white arrow), the spherical equivalent refractive error was −20.50 D, the axial length was 31.91 mm, the CFT was 524 μm, the retinal thickness (white double arrow) at the branch vessel of the lower vascular arcade (red arrow head) was 654 μm, and BCVA was 20/63. **B.** After 35 months, the CFT was 537 μm, the retinal thickness (white double arrow) at the branch vessel of the lower vascular arcade (red arrow head) was 795 μm, and BCVA decreased to 20/100. **C.** Forty-one months after the first visit, the CFT was 535 μm, the retinal thickness (white double arrow) at the branch vessel of the lower vascular arcade (red arrow head) was 761 μm, and BCVA was 20/100.

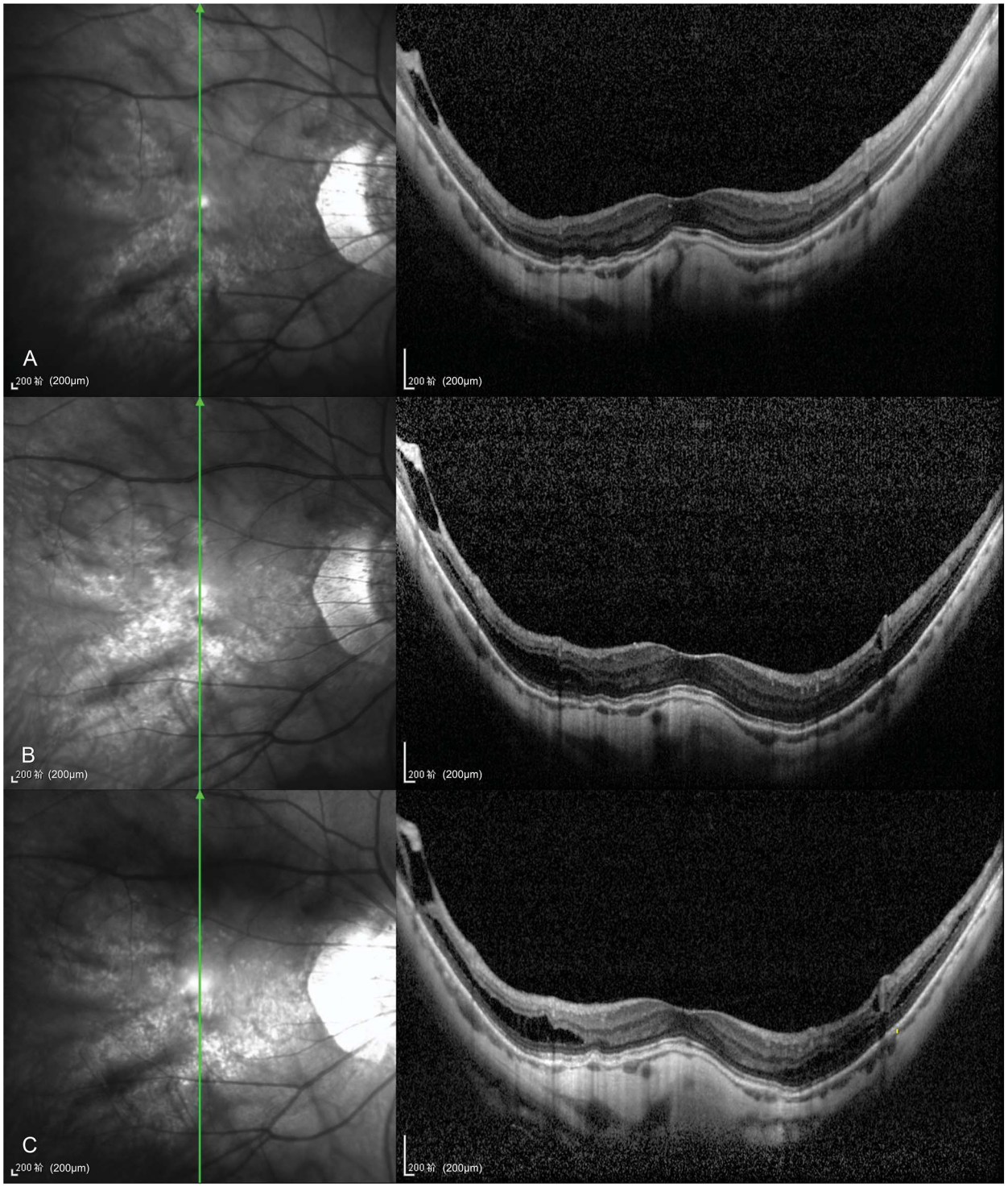

Fig. 2. A–C. showed infrared fundus and OCT images of the right eye of a 68-year-old woman with MRS progression and a DSM located in the fovea during the follow-up period in the vertical scan. **A.** At baseline, the case had S0 outer schisis and paravascular inner schisis, a DSM was located in the fovea, the spherical equivalent refractive error was −12.00 D, the axial length was 31.15 mm, the CFT was 198 μm, and BCVA was 20/40. **B.** After 50 months, MRS occurred in the parafoveal region, the CFT was 214 μm, and BCVA was 20/40. **C.** Seventy-nine months after the first visit, the extent of MRS expanded, the CFT was 217 μm, and BCVA was 20/50.

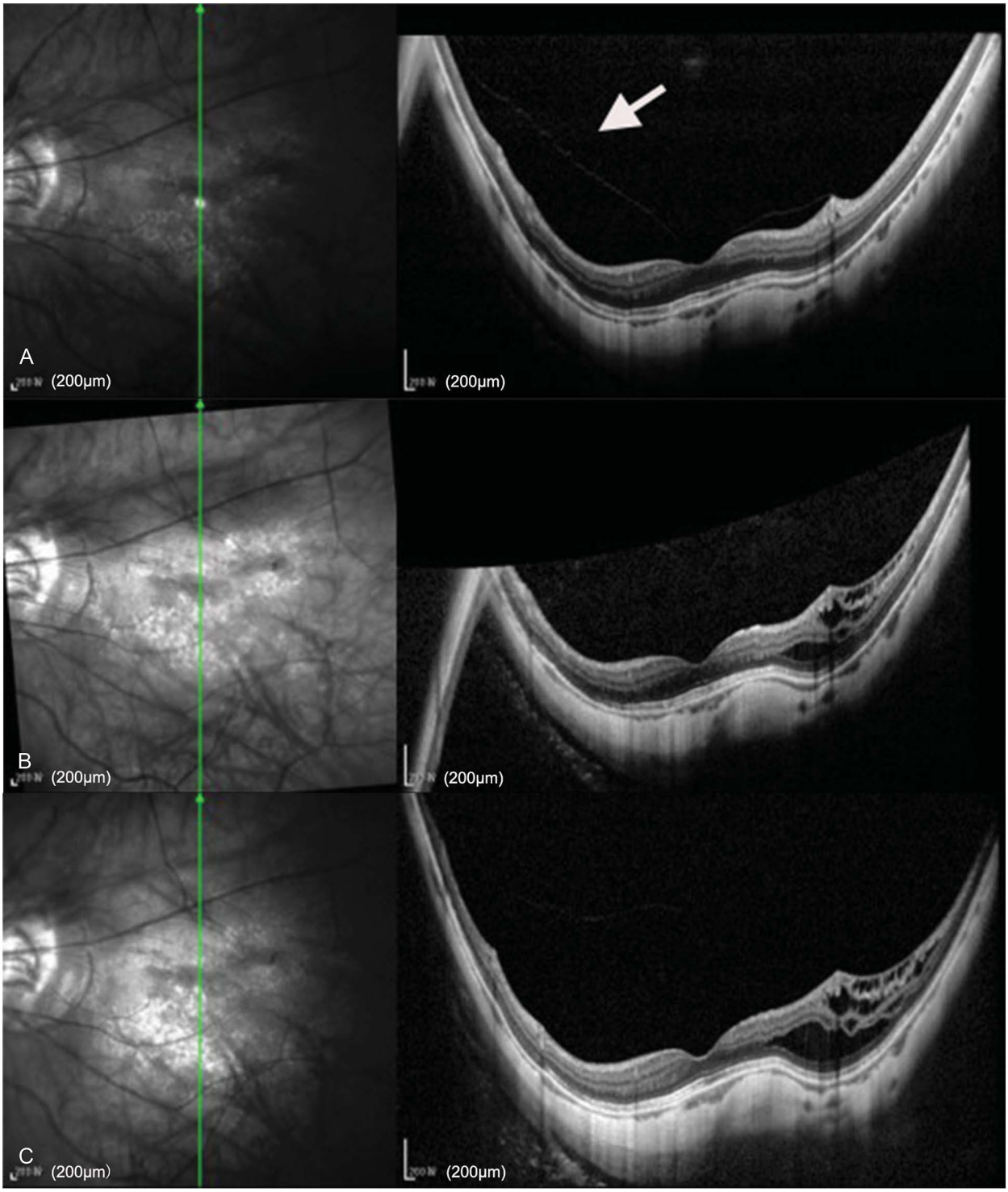

Fig. 3. A–C. showed infrared fundus and OCT images of the left eye of a 64-year-old woman with MRS progression and a DSM located in the parafovea during the follow-up period in the vertical scan. **A.** At baseline, the case had S0 outer schisis and paravascular retinal cyst with PVD (white arrow), a DSM was located in the parafovea, the spherical equivalent refractive error was −15.25 D, the axial length was 31.16 mm, the CFT was 191 μm, and BCVA was 20/25. **B.** After 57 months, outer schisis, inner schisis and ILM detachment occurred in the parafoveal region, the CFT was 179 μm, and BCVA was 20/25. **C.** Eighty-six months after the first visit, the extent of outer and inner schisis expanded, the height increased, the CFT was 175 μm, and BCVA was 20/25. ILM, internal limiting membrane.

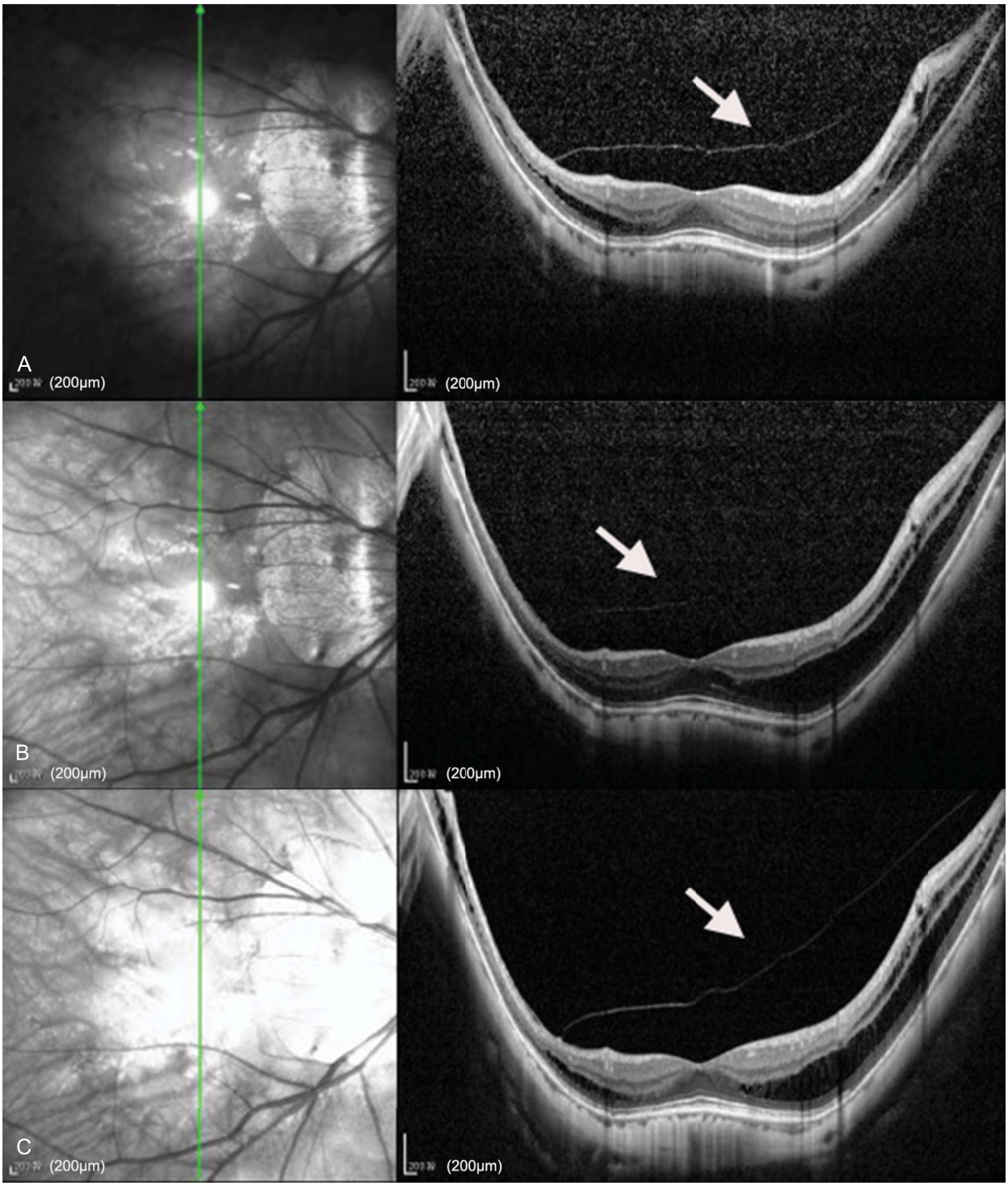

Fig. 4. A–C. Showed infrared fundus and OCT images of the right eye of a 64-year-old woman with MRS progression without a DSM during the follow-up period in the vertical scan. **A.** At baseline, the case had S3 outer schisis and paravascular inner schisis with partial PVD (white arrow), the spherical equivalent refractive error was −11.00 D, the axial length was 30.77 mm, the CFT was 253 μm, and BCVA was 20/20. **B.** After 28 months, the extent of outer and inner schisis expanded, the height of outer schisis increased, the CFT was 257 μm and the BCVA was 20/20. **C.** 50 months after the first visit, the height of the schisis cavity in the superior region around the foveola decreased, the CFT was 252 μm, and BCVA was 20/20.

DSM located in the central fovea, progressed rapidly. Best-corrected visual acuity remained stable in extrafoveal retinoschisis eyes, whereas visual acuity decreased in foveoschisis eyes during the follow-up period, and CFT was associated with visual deterioration.

Table 2. Comparison of the Progression Rate of Myopic Retinoschisis Eyes With and Without Dome-Shaped Macula Based on Retinoschisis Classification

	Progressed	Stable	Improved	*P*
DSM (n)				0.7462
Present	10	9	6	
Absent	32	24	12	
Foveoschisis (n)				0.8019
DSM	5	7	4	
Non-DSM	17	19	8	
Extrafoveal retinoschisis (n)				0.6954
DSM	2	2	2	
Non-DSM	10	5	4	

Based on the current study**,** MRS eyes with a DSM exhibited a higher degree of myopia and a longer axial length than MRS eyes without a DSM, which was consistent with previous reports.[2,15,16] The occurrence of a DSM is believed to be compensatory for uneven expansion of the eyeball at the posterior pole. A cross-sectional study with a large sample by Fang et al applied a simulation model of the ocular wall at the posterior pole and found that the extrafoveal region is much weaker than the central fovea in the presence of a DSM and inward traction, which may lead to MRS occurring more often in the extrafoveal region. As the applied stress increases, the DSM becomes more pronounced, which leads to a higher incidence of MRS.[15] In our study, the location of MRS was not significantly related to the presence of a DSM. The reason for the inconsistency with previous reports may be because of the small sample size, selection bias of the specific population, and the different states of inward forces acting on the retina in our study.

The axial elongation of the eyeball and posterior staphyloma are considered to be the main factors in the pathogenesis of MRS, and vitreoretinal traction also plays an important role in MRS progression.[8,10,19] In eyes with DSM, macular elevation alleviates the outward traction produced by uneven globe elongation to some extent; as a result, the likelihood of the occurrence of foveoschisis is reduced.[18] Our results showed that there was no significant difference in progression rates between MRS patients with and without a DSM during an average follow-up period of 48.3 months; that is, the presence of a DSM did not seem to delay the progression of MRS, for foveoschisis or extrafoveal retinoschisis, which suggested that many factors may be involved in the pathogenesis of MRS. These causative factors were also dynamic throughout the natural course of MRS, such as progressive posterior staphyloma and increased vitreoretinal traction. In the progression of MRS, the protective effect of a DSM on the macula may be weak and may not completely counteract the multidirectional tractions, even for the eyes with extrafoveal MRS.

In our study, in non-DSM eyes, the MRS progression rate was significantly higher in MRS eyes with vitreoretinal traction than in MRS eyes without vitreoretinal traction (55.8% vs. 32%), and the result was similar to our previous report.[12] Meanwhile, we found that MRS eyes with a DSM located in the central fovea showed a significantly higher MRS progression rate than those with a DSM located in the parafovea (61.5% vs. 16.7%) in the follow-up period, whereas there were no significant differences in the width, height, or H/W ratio of the DSM between the progressive, stable, and improved groups. In eyes with DSM, the progression of MRS was related to the location of the dome, but not to the shape of the dome. The inward and outward traction causing the occurrence of MRS may be predominantly oblique in some MRS cases, and DSM located in an eccentric position of the fovea pressed the macula inward and may produce an oblique force that is axially close to the force produced by the posterior staphyloma simultaneously, which resists outward traction from irregular axial growth more effectively than DSM located in the central fovea and may delay the development of MRS to some extent.

Earlier studies found that although DSM eyes are in a more myopic state, their visual function was not significantly affected, probably because they have a low incidence of macular lesions (i.e., choroidal neovascularization and foveoschisis), which threaten visual function.[2,15,16] According to our observation, the difference in BCVA between the DSM group and non-DSM group was not significant at baseline, and during the follow-up period, BCVA decreased significantly in foveoschisis eyes with a DSM and in foveoschisis and extrafoveal MRS eyes without a DSM, whereas BCVA did not change significantly between the first and last visits in extrafoveal MRS eyes with a DSM. In the study of Cheng et al,[20] poor visual acuity was associated with ellipsoid zone disruption, and MRS eyes involving the entire macula and with a CFT greater than 300 μm had a higher risk of damage to the ellipsoid zone. In the current study, we found by SD-OCT that the ellipsoid zone in most DSM eyes was intact; moreover, for extrafoveal MRS eyes, the structure of the entire macular neuroepithelial layer was relatively intact in the fovea, which led to a better BCVA. In our study, DSM eyes with visual loss greater than two lines during follow-up had a significantly higher CFT than those with visual loss less than two lines, indicating that higher schisis cavity MRS may indicate severe dysfunction of the visual

Table 3. Clinical and OCT Morphologic Characteristics Associated With Natural Course of Myopic Retinoschisis Eyes With and Without Dome-Shaped Macula

Characteristics	DSM Group				Non-DSM Group			
	Progressed	Stable	Improved	*P*	Progressed	Stable	Improved	*P*
Age (years), mean ± SD	71.4 ± 4.16	68.0 ± 8.58	61.5 ± 5.54	0.0301	61.1 ± 7.61	64.7 ± 10.28	60.8 ± 8.23	0.2571
Refractive error (D), mean ± SD	−19.6 ± 6.5	−15.4 ± 4.1	−12.0 ± 3.00	0.0166	−12.4 ± 4.86	−13.0 ± 4.58	−14.7 ± 6.37	0.5066
Axial length (mm), mean ± SD (range)	30.4 ± 0.16	30.7 ± 1.27	30.7 ± 1.10	0.8122	29.4 ± 1.39	28.9 ± 1.57	29.0 ± 1.28	0.5166
Schisis group (n)				0.2009				0.3166
Foveal	3	6	2		17	19	9	
Extrafoveal	4	3	4		10	5	3	
Schisis subtype (n)				0.1652				0.5354
Outer schisis	4	5	1		15	9	6	
Outer and inner schisis	3	4	5		12	15	6	
Vitreoretinal traction				0.5081				0.0341
Present	7	5	5		24	14	5	
Absent	3	4	1		8	10	7	
Subfoveal CT (μm)	26.0 ± 10.7	27.3 ± 21.4	26.4 ± 18.2	0.8822	34.7 ± 21.1	42.6 ± 32.1	31.0 ± 14.4	0.7823
CT at DSM (μm)	26.9 ± 13.86	31.4 ± 23.00	18.0 ± 8 0.20	0.3368	—	—	—	—
Width of DSM (μm)	1979.7 ± 269.80	1868.0 ± 308.67	1986.5 ± 331.60	0.6613	—	—	—	—
Height of DSM(μm)	92.5 ± 38.70	83.0 ± 29.35	86.0 ± 54.6	0.6621	—	—	—	—
H/W ratio of DSM	0.05 ± 0.02	0.04 ± 0.01	0.04 ± 0.03	0.8849	—	—	—	—
Location of DSM				0.0421	—	—	—	—
Central fovea	8	3	2		—	—	—	—
Parafovea	2	6	4		—	—	—	

H, height; W, width.

Table 4. BCVA at the Initial and Last Visit in Myopic Retinoschisis Eyes With and Without Dome-Shaped Macula Based on Retinoschisis Classification

	BCVA at First Visit	BCVA at Last Visit	*P*
DSM group (n = 25)	0.41 ± 0.34	0.56 ± 0.51	0.0002
Foveochisis (n = 14)	0.33 ± 0.33	0.36 ± 0.34	0.0020
Extrafoveal retinoschisis (n = 11)	0.48 ± 0.35	0.72 ± 0.58	0.2500
Non – DSM group (n = 68)	0.29 ± 0.25	0.34 ± 0.28	0.0019
Foveochisis (n = 37)	0.27 ± 0.28	0.31 ± 0.30	0.0494
Extrafoveal retinoschisis (n = 31)	0.31 ± 0.19	0.37 ± 0.26	0.0091

conduction pathway at the retinal level, which has a notable impact on vision prognosis. Meanwhile, we found that MRS eyes with vitreoretinal traction had a higher rate of visual loss in the non-DSM group. Given its impact on macular configuration in the natural course of MRS, we speculated that vitreoretinal traction promoted the progression of MRS and predicted the visual prognosis.

There were several limitations in the current study. First, the impact of the different subtypes of DSM on the natural history and visual prognosis of MRS could not be analyzed because of the small sample size. Second, we were unable to investigate the effect of the interaction between the type of posterior staphyloma, the location of vitreoretinal traction, and DSM on the development of MRS because of the limitations of the range and mode of the OCT scan.

To summarize, the current study demonstrated that MRS eyes with a DSM were older and had a more myopic status, including a longer axial length. The presence of a DSM did not slow the progression of retinoschisis, even for eyes with extrafoveal retinoschisis. In DSM eyes, the progression rate of MRS was higher in eyes with an older age, a higher myopic degree, and a DSM located in the central fovea. The height of the schisis cavity was a risk factor for visual deterioration, and a DSM acted as a protective factor for visual function in extrafoveal MRS eyes.

Table 5. Comparison of Factors at the First Visit Between the Two Groups With BCVA Deterioration Greater and Less Than Two Lines in MRS With and Without DSM

Factors	DSM			Non-DSM		
	BCVA deterioration ≥ 2 lines (n = 9)	BCVA deterioration < 2 lines (n = 16)	*P*	BCVA deterioration ≥ 2 lines (n = 11)	BCVA deterioration < 2 lines (n = 57)	*P*
Age (years), mean ± SD	68.3 ± 8.02	67.3 ± 7.26	0.7480	62.6 ± 6.96	62.3 ± 9.16	0.8986
Refractive error(D), mean ± SD	−15.9 ± 5.32	−13.6 ± 5.06	0.2943	−11.0 ± 3.35	−13.4 ± 5.25	0.1576
Axial length (mm), mean ± SD (range)	30.5 ± 1.14	30.6 ± 1.19	0.7333	28.9 ± 1.69	29.2 ± 1.39	0.6421
Schisis group (n)			0.9056			0.0764
Foveal	7	8		7	20	
Extrafoveal	2	8		4	37	
Schisis subtype (n)			0.4281			0.1435
Outer schisis	5	5		8	28	
Outer and inner schisis	4	8		3	29	
Vitreoretinal traction			0.9148			0.0232
Present	6	12		10	33	
Absent	3	4		1	24	
CFT (μm)	292.8 ± 143.73	206.6 ± 63.22	0.0478	233.3 ± 70.29	237.2 ± 61.09	0.8518
Subfoveal CT (μm)	30.4 ± 21.50	24.4 ± 12.76	0.0776	37.3 ± 23.8	36.8 ± 25.2	0.9499
CT at DSM (μm)	26.7 ± 19.70	26.3 ± 16.01	0.9546	—	—	—
Width of DSM (μm)	1886.3 ± 329.96	1972.0 ± 274.38	0.4930	—	—	—
Height of DSM(μm)	98.9 ± 38.17	81.1 ± 38.52	0.2784	—	—	—
H/W ratio of DSM	0.05 ± 0.02	0.04 ± 0.02	0.1376	—	—	—
Location of DSM			0.4941	—	—	—
Central fovea	6	7		—	—	—
Parafovea	3	9		—	—	—

Key words: high myopia, myopic retinoschisis, dome-shaped macula, natural course, visual acuity, optical coherence tomography.

References

1. Gaucher D, Erginay A, Lecleire-Collet A, et al. Dome-shaped macula in eyes with myopic posterior staphyloma. Am J Ophthalmol 2008;145:909–914.e1.
2. Liang IC, Shimada N, Tanaka Y, et al. Comparison of clinical features in highly myopic eyes with and without a dome-shaped macula. Ophthalmology 2015;122:1591–1600.
3. Ceklic L, Wolf-Schnurrbusch U, Gekkieva M, Wolf S. Visual acuity outcome in RADIANCE study patients with domes-haped macular features. Ophthalmology 2014;121:2288–2289.
4. Caillaux V, Gaucher D, Gualino V, et al. Morphologic characterization of domeshaped macula in myopic eyes with serous macular detachment. Am J Ophthalmol 2013;156:958–967.e1.
5. Ohsugi H, Ikuno Y, Oshima K, et al. Morphologic characteristics of macular complications of a dome-shaped macula determined by swept-source optical coherence tomography. Am J Ophthalmol 2014;158:162–170.e1.
6. Zhao X, Ding X, Lyu C, et al. Observational study of clinical characteristics of dome-shaped macula in Chinese Han with high myopia at Zhongshan Ophthalmic Centre. BMJ Open 2018;8:e021887.
7. Song M, Shen M, Zhou Y, et al. Observation of vitreous features using enhanced vitreous imaging optical coherence tomography in highly myopic retinoschisis. Retina 2019;39:1732–1741.
8. Takahashi H, Tanaka N, Shinohara K, et al. Ultra-widefield optical coherence tomographic imaging of posterior vitreous in eyes with high myopia. Am J Ophthalmol 2019;206:102–112.
9. Philippakis E, Gualino V, Gaucher D, et al. Posterior vitreous detachment in highly myopic eyes undergoing vitrectomy. Acta Ophthalmologica 2013;91:1070–1075.
10. Yu X, Ma W, Liu B, et al. Morphological analysis and quantitative evaluation of myopic maculopathy by three-dimensional magnetic resonance imaging. Eye (Lond) 2018;32:782–787.
11. Shimada N, Tanaka Y, Tokoro T, Ohno-Matsui K. Natural course of myopic traction maculopathy and factors associated with progression or resolution. Am J Ophthalmol 2013;156:948–957.e1.
12. Li S, Li T, Wang X, et al. Natural course of myopic traction maculopathy and factors influencing progression and visual acuity. BMC Ophthalmol 2021;21:347.
13. Xia HJ, Wang WJ, Chen F, et al. Long-term follow-up of the fellow eye in patients undergoing surgery on one eye for treating myopic traction maculopathy. J Ophthalmol 2016;2016:1–10.
14. Rey A, Jürgens I, Maseras X, Carbajal M. Natural course and surgical management of high myopic foveoschisis. Ophthalmologica 2014;231:45–50.
15. Fang D, Zhang Z, Wei Y, et al. The morphological relationship between dome-shaped macula and myopic retinoschisis: a cross-sectional study of 409 highly myopic eyes. Invest Ophthalmol Vis Sci 2020;61:19.
16. Zhu X, He W, Zhang S, et al. Dome-shaped macula: a potential protective factor for visual acuity after cataract surgery in patients with high myopia. Br J Ophthalmol 2019;103:1566–1570.
17. Chylack LT Jr, Wolfe JK, Singer DM, et al. The lens opacities classification System III. Arch Ophthalmol 1993;111:831–836.
18. Ellabban AA, Tsujikawa A, Matsumoto A, et al. Three-dimensional tomographic features of dome-shaped macula by swept-source optical coherence tomography. Am J Ophthalmol 2013;155:320–328.e2.
19. Shinohara K, Tanaka N, Jonas JB, et al. Ultrawide-field OCT to investigate relationships between myopic macular retinoschisis and posterior staphyloma. Ophthalmology 2018;125:1575–1586.
20. Cheng C, Teo K, Tan CS, et al. Myopic retinoschisis in Asians: structural features and determinants of visual acuity and prognostic factors for progression. Retina 2016;36:717–726.

SDC

OMEGA-3 FATTY ACIDS ARE ASSOCIATED WITH DECREASED PRESENCE AND SEVERITY OF DIABETIC RETINOPATHY

A Combined Analysis of MESA and GOLDR Cohorts

NATALIE L. WEIR, MS,* WEIHUA GUAN, PHD,† AMY B. KARGER, MD, PHD,* BARBARA E. K. KLEIN, MD, MPH,‡ STACY M. MEUER, BS,‡ MARY FRANCES COTCH, PHD,§ XIUQING GUO, PHD,¶ XIAOHUI LI, PHD,¶ JINGYI TAN, PHD,¶ PAULINE GENTER, PHD,** YII-DER IDA CHEN, PHD,¶ JEROME I. ROTTER, MD,¶ ELI IPP, MD,** MICHAEL Y. TSAI, PHD*

Purpose: Inflammation is associated with diabetic retinopathy development and progression, and previous studies have demonstrated that omega-3 polyunsaturated fatty acids have anti-inflammatory properties. Therefore, the goal of this study was to determine if omega-3 polyunsaturated fatty acids, docosahexaenoic acid (DHA) and eicosapentaenoic acid (EPA), are associated with decreased risk and severity of retinopathy in individuals with type 2 diabetes.

Methods: In a combined population of 1,356 individuals with type 2 diabetes from the Multi-Ethnic Study of Atherosclerosis and Genetics of Latino Diabetic Retinopathy cohorts, odds ratios using logistic regression were determined to assess the association between polyunsaturated fatty acids and retinopathy.

Results: In 1,356 participants with type 2 diabetes, individuals in the fourth quartile of DHA were 17% less likely to have retinopathy compared with the first quartile ($P = 0.009$, CI: 0.72–0.95). Secondary analysis revealed 38% lower severity of retinopathy in individuals in the fourth quartile compared with the first quartile of DHA ($P = 0.006$; CI: 0.44–0.87) and EPA + DHA ($P = 0.004$; CI: 0.44–0.85). No significant associations were observed between EPA and retinopathy.

Conclusion: DHA is inversely associated with the presence and severity of diabetic retinopathy. Increased intake of dietary sources of DHA may provide some protection against retinopathy in individuals with type 2 diabetes and warrants more research as a preventative option.

RETINA 43:984–991, 2023

Diabetic retinopathy (DR), a vision-threatening microvascular complication of type 2 diabetes (T2D), is a leading cause of blindness in adults, affecting up to 33% of those with T2D in the United States.[1] Evidence suggests that inflammation plays a role in the development and progression of DR.[2–5] In fact, characteristics of inflammation such as retinal leukostasis, vascular permeability, capillary degeneration, and proinflammatory cytokines have been documented previously in both animal and human studies.[2–5] Thus, DR could, in part, be related to an irregular inflammatory environment, allowing damage to the retina.

Polyunsaturated fatty acids (PUFAs) have a wide range of functions including regulating the inflammatory response.[6] More specifically, omega-3 PUFAs, eicosapentaenoic acid (EPA) and docosahexaenoic acid (DHA), have the ability to mitigate inflammation through reducing pathologic angiogenesis, suppressing reactive oxygen species, and inhibiting inflammatory cytokine production.[7–10] Several studies have reported beneficial roles of DHA and/or EPA in various diseases. DHA is associated with decreased risk of Alzheimer disease, whereas supplementation with EPA is more therapeutic for depression, and a combined EPA + DHA supplement

seems to improve cardiovascular outcomes.[11–13] However, few studies have examined the association of individual circulating levels of omega-3 PUFAs with DR.

Thus, the aim of the present study was to determine the association between omega-3 PUFAs, EPA and DHA, and the prevalence and severity of DR in a combined cohort of individuals with diabetes from the Multi-Ethnic Study of Atherosclerosis (MESA) and Genetics of Latino Diabetic Retinopathy (GOLDR).

Methods

Population

The primary aim of MESA (http://www.mesa-nhlbi.org) is to investigate the clinical and subclinical coronary heart disease development and progression, and the study design has been previously described.[14] The study adhered to the tenets of the Declaration of Helsinki, and approval was obtained by each participating site's Institutional Review Board; all participants provided written informed consent. Briefly, MESA is a prospective cohort of 6,814 adults, aged 45 to 84 years at baseline (between 2000 and 2002), sampled from six communities in the United States (Baltimore, MD; Chicago, IL; Forsyth County, NC; Los Angeles County, CA; New York, NY; and St. Paul, MN), without evidence of clinical coronary heart disease at entry. We included 785 participants with T2D at the second examination for the current analysis. Diabetes was defined as fasting glucose ≥7.0 mmol/L (≥126 mg/dL) or use of insulin or oral hypoglycemic medication. Plasma measurement of PUFAs was performed on samples collected at Examination 1, whereas retinal photography was performed at Examination 2 of the study (approximately 2 years after the initial sample collection). Of the 6,814 participants, 911 were diabetic at Exam 2. We excluded those missing phospholipid fatty acids (n = 42), those without retinal photography data (n = 29), and those missing demographic and other covariates (n = 55), leaving a total of 785 individuals in this MESA subcohort (Figure 1).

The GOLDR study is family-based study assessing diabetes and diabetic complications in families (siblings and/or parents) of a proband, defined as having T2D and either known DR or a diabetes duration of ≥10 years, and the study design has been previously described.[15] Participants are all Latinos of Mexican or Central American origin, recruited, and studied between 2007 and 2012 at the Lundquist Institute (formerly the Los Angeles BioMedical Research Institute) at Harbor-UCLA Medical Center. In total, data from 612 participants with T2D from 216 families, with sizes ranging from one to eight members per family, were used in the analyses. The study adhered to the tenets of the Declaration of Helsinki, and approval was obtained by each site's Institutional Review Board; all participants provided written informed consent. Exclusions for this analysis were those missing data for DR (n = 13), urine albumin (n = 9), and phospholipid fatty acids (n = 19), with 571 GOLDR participants remaining for analysis (Figure 1).

Retinal Photography and DR Grading

A standardized study protocol was followed for digital fundus photography and retinal grading for MESA at Exam 2 (between August 2020 and January 2004) and during the study period (2007 and 2012) for GOLDR subcohorts. In MESA, both eyes of each participant were photographed without pharmacologic dilatation using a 45° 6.3-megapixel digital nonmydriatic camera (Canon, Lake Success, NY). GOLDR

From the *Laboratory Medicine & Pathology, University of Minnesota, Minneapolis, Minnesota; †School of Public Health, University of Minnesota, Minnesota; ‡Department of Ophthalmology & Visual Sciences, University of Wisconsin-Madison, Madison, Wisconsin; §Division of Epidemiology and Clinical Applications, National Eye Institute (NEI), Bethesda, Maryland; ¶The Institute for Translational Genomics and Population Sciences, Department of Pediatrics, The Lundquist Institute for Biomedical Innovation at Harbor-UCLA Medical Center, Torrance, California; and **Division of Endocrinology and Metabolism, Department of Medicine, The Lundquist Institute for Biomedical Innovation at Harbor-UCLA Medical Center, Torrance, California.

Supported by the Multi-Ethnic Study of Atherosclerosis (MESA) contracts 75N92020D00001, HHSN268201500003I, N01-HC-95159, 75N92020D00005, N01-HC-95160, 75N92020D00002, N01-HC-95161, 75N92020D00003, N01-HC-95162, 75N92020D00006, N01-HC-95163, 75N92020D00004, N01-HC-95164, 75N92020D00007, N01-HC-95165, N01-HC-95166, N01-HC-95167, N01-HC-95168, and N01-HC-95169 from the National Heart, Lung, and Blood Institute, and by grants UL1-TR-000040, UL1-TR-001079, and UL1-TR-001420 from the National Center for Advancing Translational Sciences (NCATS). This article was also supported in part by the Genetics of Latinos Diabetic Retinopathy (GOLDR) Study grant EY14684. The authors thank the other investigators, the staff, and the participants of the MESA study for their valuable contributions. A full list of participating MESA investigators and institutions can be found at http://www.mesa-nhlbi.org. This manuscript is dedicated to the late Dr. Ronald Klein, who passed away on August 31, 2019. Dr. Klein served as co-principal investigator for the MESA study and was strongly involved in the GOLDR study, providing instrumental expertise on the epidemiology of eye diseases.

No conflicting relationship or proprietary interests exists for any author.

Supplemental digital content is available for this article. Direct URL citations appear in the printed text and are provided in the HTML and PDF versions of this article on the journal's Web site (www.retinajournal.com).

Reprint requests: Michael Y. Tsai, PhD, Department of Laboratory Medicine and Pathology, University of Minnesota, 312 Church St. SE, NHH 3-110 Minneapolis, MN; e-mail: tsaix001@umn.edu

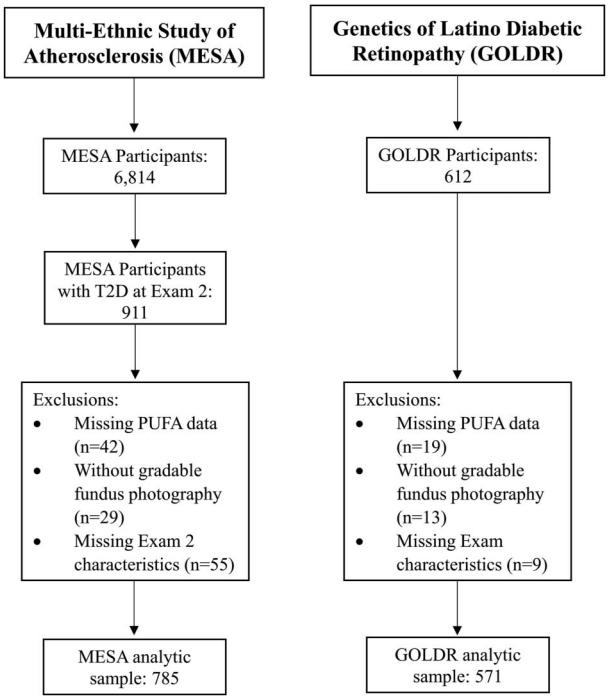

Fig. 1. Inclusion/exclusion criteria for MESA and GOLDR study participants.

participants received dilated ophthalmic eye examinations with seven standard 30° fields using digital stereoscopic fundus photographs (Topcon TRC-50DX, Tokyo, Japan). Standard software was used for image acquisition and archiving (Eye QSL; Digital Healthcare, Inc, Cambridge, England). Images were sent from each field center from both MESA and GOLDR studies to the Ocular Epidemiology Reading Center at the University of Wisconsin, Madison, for assessment of retinopathy and other retinal diseases.[15,16] For the purpose of these studies, participants were grouped into four classes of increasing severity according to the modified Arlie House Classification Scheme and Early Treatment Diabetic Retinopathy Study severity scale: no retinopathy (Levels 10–13), mild nonproliferative DR (Levels 14–31), moderate or severe nonproliferative DR (Levels 37–53), and proliferative DR (Levels 60–85).[17]

Phospholipid Fatty Acid Profiles

Twelve-hour fasting blood was drawn, and EDTA anticoagulant tubes were collected and stored at −70° C using a standardized protocol.[14] Measurement of phospholipid fatty acids was performed at the University of Minnesota for both MESA (Examination 1) and GOLDR populations. MESA participant samples were measured in three batches: Batch 1 (n = 1,000) in 2005, Batch 2 (n = 1,880) in 2008, and Batch 3 (n = 3,900) in 2012. GOLDR participant samples were measured in 2019. All samples were measured using the same method and instrumentation. Phospholipid fatty acid profiles were extracted from EDTA plasma using a chloroform/methanol method.[18] Lipids are extracted with a mixture of chloroform and methanol (2:1, volume for volume), and fractions are separated using thin-layer chromatography. The phospholipid band is harvested and derivatized to methyl esters. The final product is dissolved in heptane and injected onto a single capillary Varian CP7420 100-m column with a Hewlet Packard 5890 gas chromatograph and a flame ionization detector. The system is interphased with HP Chemstation software. Fatty acids were expressed as a percent of total phospholipid fatty acids. The following representative coefficients of variation were obtained for the relevant PUFAs (n = 100): EPA = 7.2% and DHA = 7.9%.

Covariates and Demographic Characteristics

Blood samples were assayed for covariates and biochemical risk factors, including insulin, glucose, hemoglobin A1c (HbA1c), albumin, and cholesterol levels, and urine was assayed for albumin and creatinine. For MESA participants, analyses were performed at a central site at the Advanced Research and Diagnostics Laboratory at University of Minnesota (Minneapolis, MN) using standardized methods previously described.[19,20] For GOLDR participants, standard clinical and urinary assays were performed in the general clinical laboratory at Harbor-UCLA Medical Center, and investigative biochemical assays were performed at the biochemistry laboratories at Lundquist Institute using standardized methods previously described.[18] Information regarding age, sex, race/ethnicity, education, and medication and lifestyle factors was obtained by questionnaires for both MESA and GOLDR cohorts. Anthropometric measurements (height [in meters], weight [in kilograms], and waist circumference) and vital signs (blood pressure and pulse) were collected at baseline examinations.

Statistical Methods

Statistical analysis was conducted using Stata (version 16.1; Stata Corp, College Station, TX) for analysis of MESA data. Baseline characteristics were presented as median (interquartile range) for continuous variables and frequency (%) for categorical variables. Missing data were excluded when calculating frequencies. Fatty acids were divided into quartiles, and logistic regression was used to estimate odds ratios of quartiles of fatty acids on the presence of diabetic retinopathy, with a 95% confidence interval

calculated. Statistical adjustments were made for age, sex, hypertension medication, HbA1c, urine albumin, and racial/ethnic group. Other covariates, including BMI, smoking and drinking status, education, chronic kidney disease, physical activity, CRP, systolic and diastolic blood pressure, and batch of fatty acid measures, were also considered but were not statistically significant in the multivariate model (using MESA data) and therefore were not adjusted. The GOLDR participants are clustered by families. A generalized estimating equation model was used with binomial distribution and logit link function, using SAS (version 9.4; SAS Institute, Inc, Cary, NC). MESA and GOLDR results were combined using a fixed-effect meta-analysis. Heterogeneity I^2 was calculated to assess potential heterogeneity between the two studies. An I^2 >30% was considered as evidence for heterogeneous results.

In a secondary analysis, severity of retinopathy (no retinopathy, mild nonproliferative, moderate or severe nonproliferative, and proliferative) was analyzed as an ordinal outcome using proportional odds logistic regression. The covariates were the same as described above. The proportional odds assumption was assessed using a score test. Because the samples in GOLDR are related, a generalized estimating equation model was used to analyze GOLDR data, using a R package "multigee." Results from MESA and GOLDR were combined using a fixed-effect meta-analysis.

Results

Among the 1,356 participants included in this study, there were 253 MESA participants at Exam 2 and 318 GOLDR participants with retinopathy. Baseline demographic and biomarker characteristics categorized by the presence of retinopathy are shown in Table 1 and **Supplemental Digital Content 1** (see **Table 1**, http://links.lww.com/IAE/B923). Individuals with retinopathy were statistically more likely to be Black or Hispanic ($P = 0.003$), have higher systolic blood pressure ($P = 0.03$), have a higher HbA1c ($P < 0.001$), and have urine albumin/creatinine levels >30 ($P < 0.001$) compared with those without retinopathy. There were no significant differences for the MESA cohort in age, sex, education level, smoking status, hypertension medication use, BMI, diastolic blood pressure levels, self-reported kidney disease, physical activity, fatty acid batch, and levels of EPA or DHA between those with and without retinopathy. Cases in the GOLDR study were more likely to be male, have higher systolic blood pressure levels ($P < 0.001$), exhibit a higher level of HbA1c ($P < 0.001$), have self-reported kidney disease ($P = 0.006$), have urine albumin/creatinine levels >30 ($P < 0.001$), but have a lower BMI ($P = 0.01$) and lower levels of EPA ($P = 0.03$). No significant differences for the GOLDR cohort were observed in age, smoking status, hypertension medication use, diastolic blood pressure, or alcohol use between those with and without retinopathy.

Individual and combined omega-3 PUFA levels with the presence of retinopathy are presented in Table 2. Adjustments for age, sex, race/ethnicity, hypertension medication use, HbA1c, systolic and diastolic blood pressure, and urinary albumin/creatinine were performed. Significant associations were observed with DHA in both cohorts when comparing fourth and first quartiles ($P = 0.018$) for MESA participants and third and first quartiles ($P = 0.01$) for GOLDR participants after multivariable adjustments. Similar associations were observed with combined omega-3s, EPA + DHA, when comparing fourth and first quartiles for both MESA participants ($P = 0.025$) and GOLDR participants ($P = 0.04$) after multivariable adjustments. No significant associations were observed with EPA for either of the cohorts. In supplementary analysis of Hispanic participants only, comparable results were observed and shown in Supplemental Digital Content 1 (see Table 2, http://links.lww.com/IAE/B924).

Fixed-effect meta-analysis revealed strong inverse associations with DHA and combined EPA + DHA when comparing fourth and first quartiles ($P = 0.009$ and $P = 0.004$, respectively) (Table 2). Individuals in the highest quartile of DHA were 17% less likely to have diabetic retinopathy (OR = 0.83, $P = 0.009$). A moderate heterogeneity was observed between the two studies ($I^2 = 36\%$). We observed a slightly larger reduction in the presence of DR between the first and third quartiles (OR = 0.73, $P < 0.001$). In contrast, EPA only showed marginal significance in association with prevalence of DR (OR = 0.87, $P = 0.07$) in the meta-analysis. When EPA and DHA were combined, individuals in the highest quartile were also 19% less likely to have diabetic retinopathy than those in the first quartile (OR = 0.81, $P = 0.004$). Again, a marginally larger reduction in prevalent DR was observed between the first and third quartiles (OR = 0.75, $P < 0.001$).

In a secondary analysis, we analyzed the severity of DR as an ordinal outcome, adjusting for the same set of covariates (Table 3). Using a proportional odds model, we observed significant associations between quartiles of DHA and severity levels of DR (fourth vs. first quartile: OR = 0.62, $P = 0.006$ in meta-analysis), and between quartiles of DHA + EPA and severity of DR (fourth vs. first quartile: OR = 0.61, $P = 0.004$),

Table 1. Baseline Characteristics for MESA (n = 785) and GOLDR (n = 571) Populations

Demographics	MESA N = 785			GOLDR N = 571		
	Controls (No DR)	Cases (DR)	*P*	Controls (No DR)	Cases (DR)	*P*
n (%)	532 (67.8)	253 (32.2)		253 (44.3)	318 (55.7)	
Age, mean (SD)*	65.5 (9.3)	64.9 (9.4)	0.37	54.1 (10.7)	53.2 (10.2)	0.28
Sex, n (% male)	273 (51.3%)	132 (52.2%)	0.82	85 (33.6%)	136 (42.8%)	**0.03**
Race			**0.003**			NA
White, Caucasian	136 (25.6%)	37 (14.6%)		—	—	
Chinese-American	67 (12.6%)	28 (11.1%)		—	—	
Black, African American	175 (32.9%)	104 (41.1%)		—	—	
Hispanic	154 (28.9%)	84 (33.2%)		253 (100%)	318 (100%)	
Hypertension medication use (yes/no)	366 (68.8%)	183 (72.3%)	0.31	153 (60.5%)	217 (68.2%)	0.07
BMI (kg/m^2), mean (SD)	30.95 (6.04)	30.30 (5.94)	0.16	33.13 (6.54)	31.71 (6.95)	**0.01**
Systolic blood pressure (mmHg), mean (SD)	129.3 (20.3)	134.4 (25.3)	**0.03**	127.1 (16.3)	132.24 (19.3)	<**0.001**
HbA1c, mean (SD)	7.07 (1.49)	7.82 (1.84)	<**0.001**	7.88 (1.85)	8.92 (2.01)	<**0.001**
Kidney disease (self-reported)			0.93			**0.006**
No	512 (96.2%)	243 (96.0%)		243 (96.0%)	290 (91.2%)	
Yes	17 (3.2%)	8 (3.2%)		4 (1.6%)	23 (7.2%)	
Do not know	3 (0.6%)	2 (0.8%)		6 (2.4%)	5 (1.6%)	
Urine albumin/creatinine			<**0.001**			<**0.001**
Normal (<30 mg/g creatinine)	411 (77.3%)	159 (62.8%)		217 (85.8%)	198 (62.3%)	
30–299 mg/g creatinine	101 (19.0%)	76 (30.0%)		3 (1.2%)	61 (19.2%)	
≥300 mg/g creatinine	20 (3.8%)	18 (7.1%)		33 (13.0%)	59 (18.6%)	
Alcohol use, current use	192 (36.1%)	92 (36.4%)	0.94	53 (20.9%)	75 (23.6%)	0.68
Area % 20:5n3 (EPA)	0.88 (0.77)	0.81 (0.62)	0.22	0.64 (0.48)	0.56 (0.31)	**0.03**
Area % 22:6n3 (DHA)	3.85 (1.40)	3.73 (1.49)	0.24	3.11 (1.07)	2.97 (1.01)	0.11
Area % EPA + DHA, mean (SD)	4.73 (2.01)	4.53 (1.95)	0.20	3.75 (1.38)	3.53 (1.17)	**0.04**

Bold font indicates significance.
BMI, body mass index.
*Age at Exam 2 for MESA.

but not for EPA alone (fourth vs. first quantile OR = 0.75, $P = 0.096$). Results from MESA and GOLDR studies are mostly consistent ($I^2 = 0\%$ in all but two comparisons). The proportional odds assumption was not rejected in MESA data ($P > 0.10$ for all analyses). A similar test cannot be done in GOLDR because of related samples, and a test ignoring the relatedness showed mostly nonsignificant *P*-values in GOLDR (except for EPA, $P = 0.028$).

Discussion

In a cross-sectional fixed-effect meta-analysis from a subcohort of 785 MESA and 571 GOLDR participants with type 2 diabetes, higher omega-3 PUFAs, DHA and EPA + DHA combined, were significantly associated with lower prevalence of diabetic retinopathy. Additionally, an inverse association with severity of retinopathy was also observed with DHA and EPA + DHA combined. No significant associations were observed with the prevalence or severity of retinopathy and EPA alone. These data suggest that DHA, but not EPA, may exert a protective effect on diabetic retinopathy in participants with type 2 diabetes.

Currently, there is a paucity of studies examining the effects of fatty acids on retinopathy in human populations. To our knowledge, this is the first study to examine circulating long-chain omega-3 fatty acids, both individually and combined, with the presence and severity of retinopathy in individuals with T2D. Overall, our results are in line with the findings from the PREDIMED trial, wherein Sala-Vila et al[21] prospectively evaluated incident sight-threatening DR in 3,614 individuals with diabetes. Using food frequency questionnaires, consumption of fish and omega-3 PUFA intake was used to stratify participants based on whether they met (yes/no) the recommendation of International Society for the Study of Fatty Acids and Lipids (ISSFAL) to consume at least 500 mg per day of long-chain omega-3 PUFAs (EPA and DHA). Individuals who met the ISSFAL recommendation showed a 46% decrease risk ($P = 0.001$) of sight-threatening DR compared with those who did not meet

Table 2. Cross-sectional Association Between n-3 Fatty Acids and Presence of Diabetic Retinopathy (Yes/No) in GOLDR and MESA Participants

	MESA N = 785		GOLDR N = 571		Meta-analysis N = 1,356		Heterogeneity I^2
	OR (95% CI)	*P*	OR (95% CI)	*P*	OR (95% CI)	*P*	%
EPA							
Quartile 1	Ref		Ref		Ref		
Quartile 2	0.98 (0.74, 1.31)	0.89	0.94 (0.81, 1.11)	0.46	0.95 (0.82, 1.10)	0.48	0
Quartile 3	1.13 (0.87, 1.47)	0.37	0.96 (0.83, 1.11)	0.62	1.00 (0.88, 1.13)	0.83	9.9
Quartile 4	0.93 (0.69, 1.26)	0.67	0.85 (0.71, 1.01)	0.07	0.87 (0.75, 1.01)	0.07	0
DHA							
Quartile 1	Ref		Ref		Ref		
Quartile 2	0.75 (0.57, 0.99)	**0.042**	0.92 (0.80, 1.05)	0.21	0.88 (0.78, 1.00)	**0.049**	41
Quartile 3	0.61 (0.44, 0.83)	**0.0021**	0.78 (0.65, 0.94)	**0.01**	0.73 (0.62, 0.86)	<**0.001**	44
Quartile 4	0.70 (0.53, 0.94)	**0.018**	0.87 (0.74, 1.03)	0.10	0.83 (0.72, 0.95)	**0.009**	36
EPA + DHA							
Quartile 1	Ref		Ref		Ref		
Quartile 2	0.68 (0.51, 0.89)	**0.0062**	0.90 (0.78, 1.05)	0.18	0.84 (0.74, 0.96)	**0.012**	68
Quartile 3	0.56 (0.42, 0.76)	<**0.001**	0.81 (0.69, 0.95)	**0.01**	0.75 (0.65, 0.86)	<**0.001**	77
Quartile 4	0.72 (0.53, 0.96)	**0.025**	0.84 (0.72, 1.00)	**0.04**	0.81 (0.70, 0.93)	**0.004**	0

Covariate adjustments were age, sex, race/ethnicity, hypertension medication use, systolic blood pressure, diastolic blood pressure, HbA1c, and urinary albumin/creatinine.

Quartile ranges for MESA were defined as EPA: Q1, 0.13 to 0.47, n = 194; Q2, 0.47 to 0.65, n = 191; Q3, 0.65 to 0.92, n = 203; Q4, 0.92 to 8.89, n = 197. DHA: Q1, 0.85 to 2.74, n = 198; Q2, 2.75 to 3.57, n = 190; Q3, 3.57 to 4.62, n = 199; Q4, 4.63 to 10.07, n = 198. EPA + DHA: Q1, 0.99 to 3.32, n = 194; Q2, 3.33 to 4.22, n = 193; Q3, 4.22 to 5.49, n = 199; Q4, 5.50 to 17.49, n = 199.

Quartile ranges for GOLDR were defined as EPA: Q1, 0.04 to 0.36, n = 142; Q2, 0.36 to 0.51, n = 143; Q3, 0.51 to 0.71, n = 143; Q4, 0.71 to 5.34, n = 142. DHA: Q1, 0.80 to 2.30, n = 142; Q2, 2.30 to 2.91, n = 143; Q3, 2.91 to 3.58, n = 143; Q4, 3.59 to 7.58, n = 142. EPA + DHA: Q1, 1.02 to 2.74, n = 142; Q2, 2.74 to 342, n = 143; Q3, 3.42 to 4.23, n = 143; Q4, 4.24 to 12.55, n = 142.

Bold font indicates significance.

Table 3. Association Between n-3 Fatty Acids and Severity of Retinopathy (No Retinopathy, Mild Nonproliferative, Moderate or Severe Nonproliferative, Proliferative) in GOLDR and MESA Studies

	MESA N = 785		GOLDR N = 571		Meta-analysis N = 1,356		Heterogeneity I^2
	OR (95% CI)	*P*	OR (95% CI)	*P*	OR (95% CI)	*P*	%
EPA							
Quartile 1	Ref		Ref		Ref		
Quartile 2	0.83 (0.53, 1.30)	0.42	0.88 (0.56, 1.38)	0.58	0.86 (0.63, 1.17)	0.33	0
Quartile 3	0.87 (0.56, 1.34)	0.52	0.80 (0.51, 1.25)	0.33	0.83 (0.61, 1.14)	0.26	0
Quartile 4	0.76 (0.48, 1.21)	0.24	0.74 (0.45, 1.21)	0.23	0.75 (0.54, 1.05)	0.096	0
DHA							
Quartile 1	Ref		Ref		Ref		
Quartile 2	0.63 (0.41, 0.98)	**0.039**	0.79 (0.52, 1.22)	0.29	0.71 (0.52, 0.96)	**0.027**	0
Quartile 3	0.47 (0.29, 0.76)	**0.0019**	0.64 (0.40, 1.04)	0.07	0.55 (0.39, 0.77)	<**0.001**	0
Quartile 4	0.49 (0.30, 0.79)	**0.0032**	0.79 (0.48, 1.28)	0.33	0.62 (0.44, 0.87)	**0.006**	48
EPA + DHA							
Quartile 1	Ref		Ref		Ref		
Quartile 2	0.52 (0.34, 0.82)	**0.004**	0.69 (0.45, 1.05)	0.09	0.60 (0.44, 0.82)	**0.001**	0
Quartile 3	0.38 (0.24, 0.62)	<**0.001**	0.65 (0.49, 1.02)	0.06	0.51 (0.36, 0.70)	<**0.001**	59
Quartile 4	0.52 (0.33, 0.84)	**0.0068**	0.71 (0.44, 1.14)	0.15	0.61 (0.44, 0.85)	**0.004**	0

Results are based on proportional odds logistic model.

Covariate adjustments were age, sex, race/ethnicity, hypertension medication use, HbA1c, and urinary albumin/creatinine.

Quartile ranges for MESA were defined as EPA: Q1, 0.13 to 0.47, n = 194; Q2, 0.47 to 0.65, n = 191; Q3, 0.65 to 0.92, n = 203; Q4, 0.92 to 8.89, n = 197. DHA: Q1, 0.85 to 2.74, n = 198; Q2, 2.75 to 3.57, n = 190; Q3, 3.57 to 4.62, n = 199; Q4, 4.63 to 10.07, n = 198. EPA + DHA: Q1, 0.99 to 3.32, n = 194; Q2, 3.33 to 4.22, n = 193; Q3, 4.22 to 5.49, n = 199; Q4, 5.50 to 17.49, n = 199.

Quartile ranges for GOLDR were defined as EPA: Q1, 0.04 to 0.36, n = 142; Q2, 0.36 to 0.51, n = 143; Q3, 0.51 to 0.71, n = 143; Q4, 0.71 to 5.34, n = 142. DHA: Q1, 0.80 to 2.30, n = 142; Q2, 2.30 to 2.91, n = 143; Q3, 2.91 to 3.58, n = 143; Q4, 3.59 to 7.58, n = 142. EPA + DHA: Q1, 1.02 to 2.74, n = 142; Q2, 2.74 to 342, n = 143; Q3, 3.42 to 4.23, n = 143; Q4, 4.24 to 12.55, n = 142.

Bold font indicates significance.

the recommendation after multivariate adjustment for classic risk factors. Thus, the results from the present study in which DHA and combined EPA and DHA were inversely associated with prevalent retinopathy may provide an explanation for the findings from PREDIMED. Furthermore, our results suggest that the potential beneficial effect of omega-3 PUFAs on diabetic retinopathy is due to mostly, if not exclusively, the intake of DHA. In addition, our findings from both the MESA and GOLDR cohorts indicate the beneficial effect of DHA plateaus at or around the median value (3%), suggesting that there is a diminishing return of the protective effect of DHA against retinopathy above that level.

Two other studies have evaluated similar outcomes with PUFAs, but comparability to our study is difficult because of the nature of the exposure variable and the participant characteristics. Sasaki et al[22] found reduced odds and severity of DR with increased dietary intake of total PUFAs among 379 participants with diabetes in a multivariate analysis. Significant associations were only observed for the subset of well-controlled diabetic participants. However, this study evaluated total PUFA intake rather than either omega-3 PUFAs or omega-6 PUFAs, making the results difficult to interpret. Alternatively, Kaushik et al[23] reported borderline beneficial effects from fish oil consumption (consumption of fish twice per week vs. less than once per week) in individuals with normal fasting glucose in an Australian cohort study. Although the results are in line with our study, it must be noted that one of the end points used in that study, arteriovenous nicking, is primarily the result of hypertension rather than diabetes. Additionally, the majority of that study population (93%) did not have diabetes.

The present results align with findings from animal models of diabetes and retinopathy and also corroborate our results. Sapieha et al[24] demonstrated that diabetic mice fed omega-3-enriched diets had significantly less retinal deterioration compared with diabetic mice on normal chow diets. Tikhonenko et al[25] similarly showed that DHA-rich diets prevented type 2 diabetic rats from developing retinal acellular capillaries and blocked upregulation of inflammatory compounds. Connor et al[7] showed that mice with oxygen-induced retinopathy subjected to increased omega-3 PUFA intake had increased regrowth of vessels and decreased expression of inflammatory markers.

The strengths of the present study include the use of blood fatty acid analysis allowing for a more specific analysis of each individual omega-3 PUFAs as compared with fatty acids assessed through food frequency questionnaires and dietary recall methods, an ethnically/racially diverse population of individuals with type 2 diabetes, and two separate cohorts allowing for fixed-effect analysis and confirmation. However, there are some limitations that need to be highlighted. First, in the MESA population, phospholipid fatty acids were measured at the first examination, whereas retinal fundus photography was analyzed at the second examination. The difference of approximately 2 years between the main effect and outcome could account for some variation in the analysis. However, we previously reported that repeated measurement of fatty acids over time is modestly correlated, and thus, one measurement is sufficient for long-term follow-up studies.[26] Alternatively, as the disease may not have developed until after Exam 1, a temporal association may be supported with this analysis, but the true role is unknown. Additionally, the inclusion of the GOLDR cohort, a separate cohort with blood collection for fatty acids and fundus photography performed concurrently, strengthens the association observed in the MESA cohort. Second, it was not possible for us to assess duration of diabetes for the MESA cohort because of the study not originally designed as a diabetes study. Third, the relatively few participants did not allow for stratified analysis by race/ethnicity or sex. However, a test for interaction with sex was performed, and no significant associations were observed ($P > 0.05$). Fourth, although both MESA and GOLDR used the same ETDRS grading for diabetic retinopathy and levels were grouped together consistently through both cohorts, some variation in severity levels may exist because of GOLDR having more severe cases than MESA. Finally, retinopathy was categorized only as present or absent and did not account for progression or possible regression of retinopathy over time.

In conclusion, the present study demonstrated that higher levels of DHA and combined EPA + DHA are associated with reduced odds of retinopathy in a type 2 diabetic population. Furthermore, reduced severity was also observed with higher levels of DHA and EPA + DHA combined. Collectively, these results suggest that circulating omega-3 PUFAs may exert a beneficial influence on pathophysiology of retinopathy. Further studies are required to determine whether dietary modifications to increase omega-3 fatty acids might reduce the incidence and/or severity of retinopathy in individuals with diabetes, and if so, how these modifications could be tailored to influence cultural dietary norms and/or prevention therapy.[27]

Key words: DHA, diabetic retinopathy, EPA, GOLDR, MESA, omega-3 PUFAs.

References

1. Cheung N, Chee ML, Klein R, et al. Incidence and progression of diabetic retinopathy in a multi-ethnic US cohort: the Multi-Ethnic Study of Atherosclerosis. Br J Ophthalmol 2021;106: 1264–1268.
2. Tang J, Kern TS. Inflammation in diabetic retinopathy. Prog Retin Eye Res 2011;30:343–358.
3. Kern TS. Contributions of inflammatory processes to the development of the early stages of diabetic retinopathy. Exp Diabetes Res. 2007;2007:1–14.
4. Joussen AM, Poulaki V, Le ML, et al. A central role for inflammation in the pathogenesis of diabetic retinopathy. FASEB J 2004;18:1450–1452.
5. Kuo JZ, Guo X, Klein R, et al. Systemic soluble tumor necrosis factor receptors 1 and 2 are associated with severity of diabetic retinopathy in Hispanics. Ophthalmology 2012;119:1041–1046.
6. Calder PC. N-3 Polyunsaturated fatty acids, inflammation, and inflammatory diseases. Am J Clin Nutr 2006;83:1505S–1519S.
7. Connor KM, SanGiovanni JP, Lofqvist C, et al. Increased dietary intake of omega-3-polyunsaturated fatty acids reduces pathological retinal angiogenesis. Nat Med 2007;13:868–873.
8. Schnebelen C, Gregoire S, Pasquis B, et al. Dietary n-3 and n-6 PUFA enhance DHA incorporation in retinal phospholipids without affecting PGE(1) and PGE(2) levels. Lipids 2009;44: 465–470.
9. Chen W, Esselman WJ, Jump DB, Busik JV. Anti-inflammatory effect of docosahexaenoic acid on cytokine-induced adhesion molecule expression in human retinal vascular endothelial cells. Invest Ophthalmol Vis Sci 2005;46:4342–4347.
10. Matesanz N, Park G, McAllister H, et al. Docosahexaenoic acid improves the nitroso-redox balance and reduces VEGF-mediated angiogenic signaling in microvascular endothelial cells. Invest Ophthalmol Vis Sci 2010;51:6815–6825.
11. Morris MC, Evans DA, Bienias JL, et al. Consumption of fish and n-3 fatty acids and risk of incident Alzheimer disease. Arch Neurol 2003;60:940–946.
12. Martins JG. EPA but not DHA appears to be responsible for the efficacy of omega-3 long chain polyunsaturated fatty acid supplementation in depression: evidence from a meta-analysis of randomized controlled trials. J Am Coll Nutr 2009;28:525–542.
13. Djuricic I, Calder PC. Beneficial outcomes of omega-6 and omega-3 polyunsaturated fatty acids on human health: an update for 2021. Nutrients 2021;13:2421.
14. Bild DE, Bluemke DA, Burke GL, et al. Multi-ethnic study of atherosclerosis: objectives and design. Am J Epidemiol 2002; 156:871–881.
15. Kuo JZ, Guo X, Klein R, et al. Association of fasting insulin and C peptide with diabetic retinopathy in Latinos with type 2 diabetes. BMJ Open Diabetes Res Care 2014;2:e000027.
16. Wong TY, Klein R, Islam FA, et al. Diabetic retinopathy in a multi-ethnic cohort in the United States. Am J Ophthalmol 2006;141:446–455.e1.
17. Early Treatment Diabetic Retinopathy Study Research Group. Grading diabetic retinopathy from stereoscopic color fundus photographs–an extension of the modified Airlie House classification. ETDRS report number 10. Ophthalmology 1991;98: 786–806.
18. Cao J, Schwichtenberg KA, Hanson NQ, Tsai MY. Incorporation and clearance of omega-3 fatty acids in erythrocyte membranes and plasma phospholipids. Clin Chem 2006;52:2265–2272.
19. Klein BEK, Knudtson MD, Tsai MY, Klein R. The relation of markers of inflammation and endothelial dysfunction to the prevalence and progression of diabetic retinopathy: Wisconsin epidemiologic study of diabetic retinopathy. Arch Ophthalmol 2009;127:1175–1182.
20. Tsai MY, Johnson C, Kao WL, et al. Cholesteryl ester transfer proteingenetic polymorphisms, HDL cholesterol, and subclinical cardiovascular disease in the Multi-Ethnic Study of Atherosclerosis. Atherosclerosis 2008;200:359–367.
21. Sala-Vila A, Díaz-López A, Valls-Pedret C, et al. Dietary marine ω-3 fatty acids and incident sigh-threatening retinopathy in middle-aged and older individuals with type 2 diabetes: prospective investigation from the PREDIMED trial. JAMA Ophthalmol 2016;134:1142–1149.
22. Sasaki M, Kawasaki R, Rogers S, et al. The associations of dietary intake of polyunsaturated fatty acids with diabetic retinopathy in well-controlled diabetes. Invest Ophthalmol Vis Sci 2015;56:7473–7479.
23. Kaushik S, Wang JJ, Flood V, et al. Frequency of fish consumption, retinal microvascular signs and vascular mortality. Microcirculation 2008;15:27–36.
24. Sapieha P, Chen J, Stahl A, et al. Omega-3 polyunsaturated fatty acids preserve retinal function in type 2 diabetic mice. Nutr Diabetes 2012;2:e36.
25. Tikhonenko M, Lydic TA, Opreanu M, et al. N-3 polyunsaturated fatty acids prevent diabetic retinopathy by inhibition of retinal vascular damage and enhanced endothelial progenitor cell reparative function. PLoS One 2013;8:e55177.
26. Djousse L, Petrone AB, Weir NL, et al. Repeated versus single measurement of plasma omega-3 fatty acids and risk of heart failure. Eur J Nutr 2014;53:1403–1408.
27. Chung H, Nettleton JA, Lemaitre RN, et al. Frequency and type of seafood consumed influence plasma (n-3) fatty acid concentrations. J Nutr 2008;138:2422–2427.

COMPARATIVE ANALYSIS OF OCT AND OCT ANGIOGRAPHY CHARACTERISTICS IN EARLY DIABETIC RETINOPATHY

DAVID LE, BS,* ALBERT DADZIE, OD,* TAEYOON SON, PHD,* JENNIFER I. LIM, MD,† XINCHENG YAO, PHD*†

Purpose: To assess the quantitative characteristics of optical coherence tomography (OCT) and OCT angiography (OCTA) for the objective detection of early diabetic retinopathy (DR).

Methods: This was a retrospective and cross-sectional study, which was carried out at a tertiary academic practice with a subspecialty. Twenty control participants, 15 people with diabetics without retinopathy (NoDR), and 22 people with mild nonproliferative diabetic retinopathy (NPDR) were included in this study. Quantitative OCT characteristics were derived from the photoreceptor hyperreflective bands, i.e., inner segment ellipsoid (ISe) and retinal pigment epithelium (RPE). OCTA characteristics, including vessel diameter index (VDI), vessel perimeter index (VPI), and vessel skeleton density (VSD), were evaluated.

Results: Quantitative OCT analysis indicated that the ISe intensity was significantly trending downward with DR advancement. Comparative OCTA revealed VDI, VPI, and VSD as the most sensitive characteristics of DR. Correlation analysis of OCT and OCTA characteristics revealed weak variable correlation between the two imaging modalities.

Conclusion: Quantitative OCT and OCTA analyses revealed photoreceptor and vascular distortions in early DR. Comparative analysis revealed that the OCT intensity ratio, ISe/RPE, has the best sensitivity for early DR detection. Weak variable correlation of the OCT and OCTA characteristics suggests that OCT and OCTA are providing supplementary information for DR detection and classification.

RETINA 43:992–998, 2023

According to estimates, 45% of patients with DM experience vision impairment linked with DR, yet only 50% are aware of their DR.[1] Nonproliferative diabetic retinopathy (NPDR) is an early stage of DR that is typically asymptomatic in visual function. NPDR is usually detected when vascular distortions occur from macular edema.[2] When vision is damaged, the level of DR is often more advanced, and the impairment may be irrecoverable. Early DR identification is therefore essential for timely intervention to prevent visual impairment. Because the retina is a neurovascular complex made up of several classifications of nerve cells and layers of vascular plexus, DR may accompany both vascular and neural abnormalities.

As a noninvasive imaging modality, optical coherence tomography (OCT) can give micrometer-level resolution to distinguish individual retinal layers. OCT angiography (OCTA), an extension of OCT, can enable capillary-level resolution for a quantitative evaluation of the retinal vasculature. Recent research has shown quantitative OCTA characteristics and verified them for nonproliferative DR (NPDR) staging. Significant differences between NPDR and healthy eyes have been found in quantitative OCTA characteristics, such as blood vessel caliber, tortuosity, and branching geometry.[3–5] Thus, OCTA images contain valuable biomarkers that can be used for early DR detection.

However, OCT has made it possible to see changes in the outer retina in detail, particularly those that

From the *Department of Biomedical Engineering, University of Illinois at Chicago, Chicago, IL; and †Department of Ophthalmology and Visual Sciences, University of Illinois at Chicago, Chicago, IL

National Eye Institute (R01 EY023522, R01 EY029673, R01 EY030101, R01 EY030842, P30EY001792); Research to Prevent Blindness; Richard and Loan Hill Endowment.

Reprint requests: Xincheng Yao, PhD, Richard & Loan Hill Professor, Department of Biomedical Engineering (MC 563), University of Illinois at Chicago (UIC), Clinical Sciences North, Suite W103, Room 164D, 820 South Wood Street, Chicago, IL 60612; e-mail: xcy@uic.edu

affect the external limiting membrane (ELM), photoreceptor inner segment ellipsoid (ISe), and retinal pigment epithelium (RPE), which are valuable indicators of photoreceptor function. In retinal degenerative disorders, ISe integrity and visual acuity (VA) are tightly correlated.[6,7] Recently, the metabolic function of retinal photoreceptors has been explored in stimulus-evoked ISe changes.[8] In a recent study, we explored OCT intensity–based characteristics for different outer retinal bands, e.g., ISe and RPE.[9] It was observed that ISe-based characteristics were most sensitive for differentiating controls, people with diabetes with NoDR, and people with mild NPDR. In this study, we compare OCT and OCTA biomarkers of early DR and determine the correlation between the most sensitive OCT and OCTA characteristics.

Methods

The objective of this study is to assess DR biomarkers in patients with DM. The Institutional Review Board (IRB) at the University of Illinois at Chicago (UIC) granted approval for the study's methodology, which complies with the Declaration of Helsinki's ethical principles. The group of patients with DM and controls were enrolled from the UIC Retinal Clinic. The data acquired in this study includes 30 eyes from 20 control subjects, 21 eyes from 15 patients with NoDR, and 26 eyes from 22 patients with mild NPDR. The diabetic patients are representative of a university population who need imaging for DR management. Subjects who were aged 18 years or older met the inclusion criteria. In addition, patients with a diagnosis of type II diabetes mellitus met the inclusion criteria for our diabetic cohort. Subjects with a history of other ocular disorders other than cataracts or minor refractive error, macular edema, previous vitrectomy surgery, NPDR levels higher than mild NPDR, and ungradable OCT pictures were exclusion criteria. A full anterior segment slit-lamp examination and dilated ophthalmoscopy using both the biomicroscope and indirect ophthalmoscopy were performed on all patients. A retina specialist used the Early Treatment Diabetic Retinopathy Study (ETDRS) staging system to categorize the patients as NoDR or mild NPDR.[10]

The ANGIOVUE spectral-domain OCTA system was used in this study. The system used a wavelength of 850 nm with a scan rate of 70 kHz; the axial and lateral resolutions were 5 and 15 μm, respectively. Each en face OCT or OCTA scan represents a 6 mm × 6-mm region focused on the macula. OCT data with excessive motion or signal loss were removed. OCTA en face images were exported using the ANGIOVUE system's built-in Revue program. For additional outer retinal analysis, OCT data were transferred into a custom-designed MATLAB application. OCT B-scans were used to identify retinal regions for investigation, with sites between 1.25 to 2.5 mm and 2.5 to 5.5 mm diameter from the fovea classified as parafoveal and perifoveal areas, respectively (Figure 1A). ELM, ISE, interdigitation zone (IZ), and RPE peaks were manually measured (Figure 1B) using aligned A-line profiles. We assessed the four retinal reflectance intensities from the parafovea and perifovea retinas in this work. To eliminate noise, the intensity measurements were standardized to the intensity of the inner plexiform layer (IPL). In addition, the ISe/RPE intensity ratio was determined. Our recent OCT investigation demonstrated that rods predominate in photoreceptor degradation in early DR.[9] Cones are known to dominate the central fovea.[11] As a result, normalized intensity characteristics in the central retina were not examined as the IPL cannot be determined. However, the ISe/RPE intensity ratio does not require the IPL intensity and therefore could be determined in the central fovea. For the completeness of this study, we measured the ISe/RPE intensity ratio from the central fovea, parafovea and perifovea retinas. Each quantitative feature was determined from an averaged A-line profile (average of 10 neighboring A-lines) in each retinal area.

For quantitative OCTA analysis, en face projection of the superficial vascular plexus (SVP) and deep capillary plexuses (DCP) centered at the fovea were analyzed. Examples of OCTA image processing are demonstrated in Figure 2. From the OCTA images, the vessel map and the corresponding skeleton and perimeter maps are extracted. Similarly, the FAZ area and perimeter maps were extracted from the OCTA images as well. Quantitative OCTA characteristics, namely, vessel diameter index (VDI), vessel perimeter index (VPI), blood vessel tortuosity (BVT), and vessel complexity index (VCI) were analyzed for the SVP because of the presence of large vessels. On the other hand, vessel area density (VAD), vessel skeleton density (VSD), foveal avascular zone (FAZ) area (FAZ-A), FAZ-perimeter (FAZ-P), and FAZ-contour irregularity (FAZ-CI) were analyzed for both SVP and DCP.[3,12]

Statistical analysis was performed using R version 4.2.0 (R Core Team, Vienna, Austria). Multiple group comparisons were conducted using a one-way analysis of covariance (ANCOVA) test while controlling for covariates, i.e., age and hypertension. For individual pairwise comparisons, a Tukey's honest significance test (HSD) test was used. In this investigation, a P value less than 0.05 was considered statistically significant. Kendall rank correlation was used for nonparametric testing in this study. A correlation coefficient of 0 to

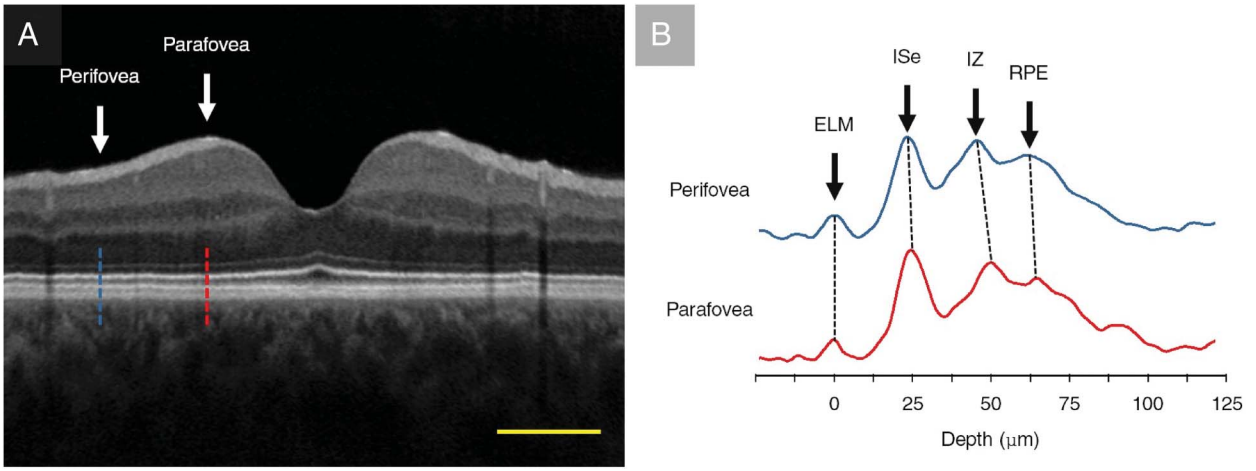

Fig. 1. A. Representative OCT B-scan of controls. **B.** Representative averaged A-line indicating individual retinal layer location. Outer retina characteristics were performed by peak location. The scale bar represents 1 mm.

0.3 (or 0 to −0.3) was considered no correlation. A weak correlation coefficient was defined as 0.3 to 0.7 (or −0.3 to −0.7), and a strong correlation coefficient was defined as 0.7 to 1 (or −0.7 to −1).[13]

Results

30 eyes from 20 control participants, 21 eyes from 15 patients with NoDR, and 26 eyes from 22 patients with mild NPDR were evaluated in this study. No statistically significant differences were found between the cohorts regarding age and sex (analysis of variance [ANOVA], $P = 0.068$, chi-square test, $P = 0.783$). Furthermore, there was no difference in HbA1c and hypertension across diabetes groups (Krusal-Wallis ANOVA [KWANOVA], $P = 0.103$, chi-square test, $P = 0.999$). Between the diabetic groups, there was a significant difference in duration of diabetes (Student's *t*-test, $P = 0.004$). The patients with diabetes in this study were not insulin dependent. Table 1 summarizes all participant demographics and diabetes-related parameters.

In this study, we assessed five OCT characteristics in the parafovea and perifovea: the intensity of the ELM, ISe, IZ, RPE, and ISe/RPE ratio. Statistical examination of the OCT characteristics indicated that statistically significant changes in ELM intensity were identified in the perifovea area between the mild NPDR and NoDR cohorts (Tukey's HSD, $P < 0.01$). In the parafovea and perifovea areas, the IZ intensity indicated statistically significant changes between cohorts, with an overall declining trend with stage progression. The ISe intensity characteristics indicated statistically significant differences between mild NPDR and control eyes (Tukey's HSD, $P < 0.01$), as well as between mild NPDR and NoDR eyes (Tukey's HSD, $P < 0.01$). Overall, the intensity of ISe reduces as the stage progresses. However, RPE intensity characteristics showed a rising tendency as the stage progressed. With retinopathy development, the ISe/RPE ratio showed a declining tendency. Statistically significant differences were observed in the parafovea and perifovea areas, with the perifovea area having statistical differences among the cohorts (Tukey's HSD, $P < 0.05$). Table 2 summarizes all OCT characteristics.

For OCTA analysis, we quantified nine quantitative characteristics to test vascular changes in the SVP and DCP. The statistical analysis suggests significant differences in the VDI between mild NPDR and NoDR eyes (Tukey's HSD, $P < 0.01$) and in the VPI for the superficial layer to differentiate eyes with no retinopathy from diabetic eyes (controls vs. mild NPDR and NoDR vs. mild NPDR, Tukey's HSD, $P < 0.05$). The observed trend suggests in the early stage that, from controls to NoDR, there is an overall narrowing of blood vessels, which is later compensated in the mild NPDR stage. By contrast, VSD in the deep layer suggests significant differences between controls and mild DR eyes (Tukey's HSD, $P < 0.05$). The observed changes in OCTA may suggest that in early DR, there is a level of vascular compensation and remodeling. All quantitative OCTA characteristics are summarized in Table 2.

We found the most sensitive OCT characteristics for differentiating mild NPDR from NoDR and controls were the ISe/RPE peri, ISe/RPE para, and ISe peri. By contrast, we found the most sensitive OCTA characteristics for differentiating mild NPDR from NoDR and controls were VDI sup, VPI sup, and VSD deep. OCT and OCTA contribute different aspects useful for differentiating NPDR from NoDR and from controls. The correlation analysis was performed independently for each cohort. For the control cohort, there is a weak

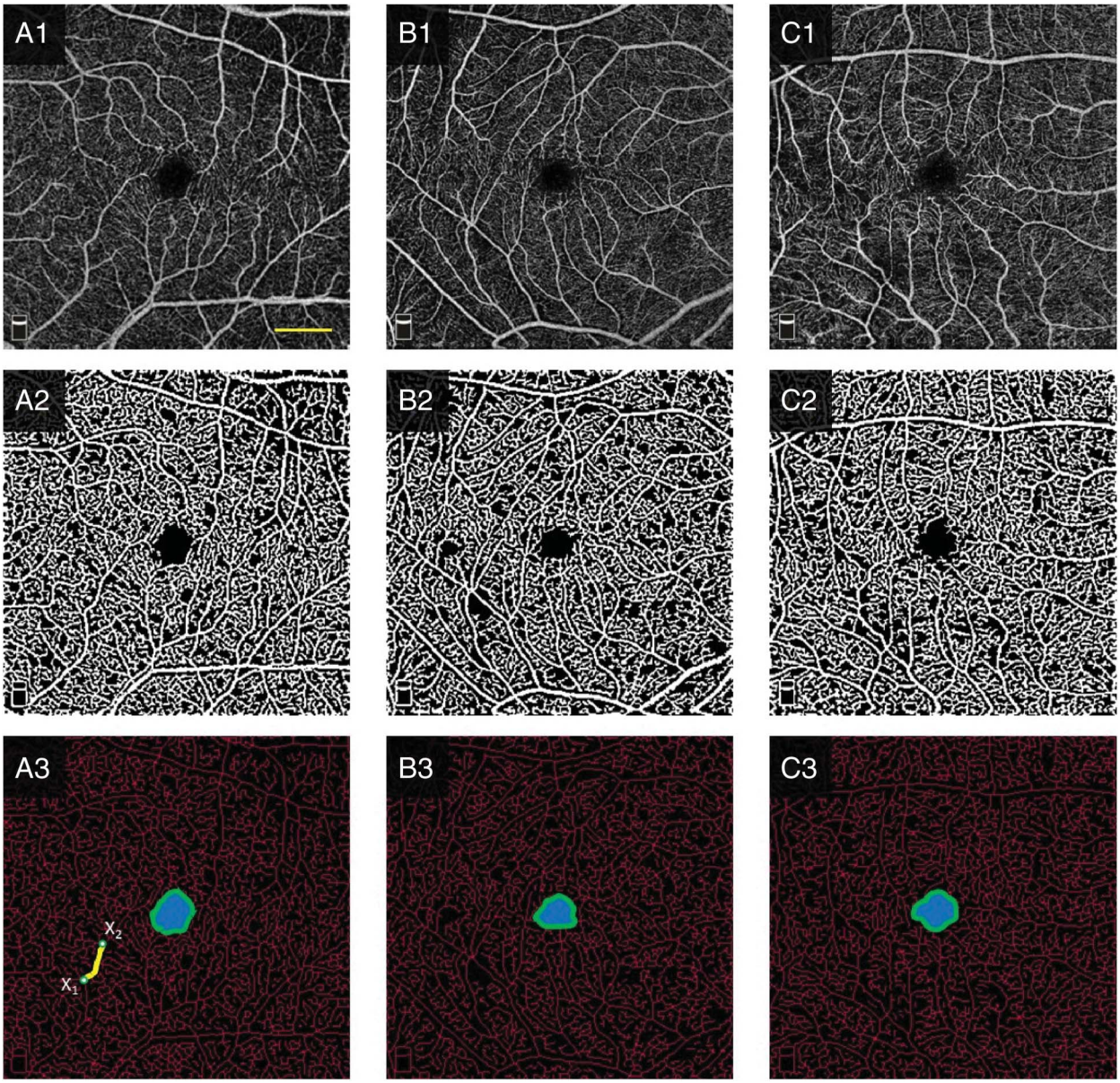

Fig. 2. Representative images of controls **(A)**, NoDR eye **(B)**, and mild NPDR eye **(C)**. The top row represents the OCTA en face images of the superficial layer. The middle row represents the binarized vessel maps. The bottom row represents the binarized vessel skeleton maps. In (A3), the demarcated yellow segment from points $?_1$ to $?_2$ is an illustration of vessel tortuosity measurement, and the blue region is the area of the foveal avascular zone (FAZ), with the green outline for the perimeter of the FAZ. The scale bar represents 1 mm.

Table 1. Demographic of the Healthy Subjects, Patients with NoDR, and Patients with Mild NPDR

	Healthy Subjects	NoDR	Mild NPDR
Number of subjects (n)	20	15	22
Age (years)	52.6 ± 14.57	59.33 ± 11.31	61.73 ± 11.83
Age range	35–80	40–80	24–78
Sex (male/female)	13/7	5/10	9/13
Duration of diabetes (years)	—	11.10 ± 5.17	18.55 ± 5.26
Diabetes type	—	Type II	Type II
HbA1c (%)	—	7.33 ± 1.81	8.52 ± 2.41
HTN prevalence, %	0	80	81

HbA1c = glycated hemoglobin; HTN = hypertension.

Table 2. Differences in OCT and OCTA Features Between Healthy Subjects, Patients with NoDR, and Patients with Mild NPDR

Feature	Healthy subjects (I)	NoDR (II)	Mild (III)	*P*			
				I Versus II	I Versus III	II versus III	ANCOVA
OCT features							
ELM peri	0.834 ± 0.051	0.866 ± 0.040	0.824 ± 0.039	0.081	0.747	0.001	0.002
ELM para	0.859 ± 0.056	0.873 ± 0.043	0.874 ± 0.042	0.627	0.608	0.999	0.598
ISe Peri	1.390 ± 0.091	1.350 ± 0.070	1.280 ± 0.070	0.402	<0.001	0.002	<0.001
ISe Para	1.410 ± 0.096	1.360 ± 0.074	1.320 ± 0.073	0.089	0.003	0.244	0.005
IZ peri	1.380 ± 0.112	1.300 ± 0.087	1.260 ± 0.086	0.059	0.001	0.197	0.002
IZ para	1.420 ± 0.127	1.340 ± 0.098	1.290 ± 0.097	0.082	0.001	0.152	0.002
RPE peri	1.350 ± 0.080	1.370 ± 0.062	1.340 ± 0.062	0.429	0.997	0.219	0.207
RPE para	1.340 ± 0.081	1.380 ± 0.063	1.390 ± 0.062	0.228	0.067	0.714	0.084
Ise/RPE peri	1.032 ± 0.057	0.987 ± 0.044	0.955 ± 0.043	0.018	<0.001	0.037	<0.001
Ise/RPE para	1.055 ± 0.061	0.985 ± 0.051	0.950 ± 0.051	0.001	<0.001	0.057	<0.001
Ise/RPE fovea	0.850 ± 0.066	0.833 ± 0.050	0.848 ± 0.049	0.657	0.993	0.598	0.546
OCTA features							
VDI sup	2.020 ± 0.060	2.010 ± 0.046	2.060 ± 0.046	0.841	0.088	0.003	0.003
VPI Sup	1.780 ± 0.031	1.790 ± 0.024	1.810 ± 0.024	0.318	0.002	0.020	0.001
BVT sup	1.090 ± 0.012	1.095 ± 0.009	1.093 ± 0.009	0.344	0.648	0.793	0.379
VCI Sup	1288 ± 241	1130 ± 186	1167 ± 185	0.057	0.182	0.765	0.712
VAD sup	0.393 ± 0.040	0.378 ± 0.031	0.373 ± 0.031	0.383	0.205	0.872	0.233
VAD deep	0.419 ± 0.055	0.384 ± 0.043	0.366 ± 0.042	0.066	0.003	0.304	0.004
VSD sup	0.186 ± 0.021	0.179 ± 0.017	0.173 ± 0.016	0.466	0.084	0.425	0.096
VSD deep	0.202 ± 0.029	0.184 ± 0.023	0.171 ± 0.022	0.078	0.001	0.123	0.001
FAZ-A sup	0.284 ± 0.203	0.429 ± 0.157	0.335 ± 0.156	0.035	0.6652	0.097	0.281
FAZ-A deep	0.243 ± 0.150	0.336 ± 0.115	0.302 ± 0.115	0.076	0.348	0.558	0.093
FAZ-P sup	1.720 ± 0.619	2.120 ± 0.481	1.850 ± 0.479	0.062	0.710	0.141	0.045
FAZ-P deep	1.640 ± 0.461	1.910 ± 0.358	1.830 ± 0.356	0.115	0.323	0.748	0.139
FAZ-CI sup	0.924 ± 0.062	0.931 ± 0.048	0.912 ± 0.048	0.921	0.785	0.382	0.415
FAZ-CI deep	0.959 ± 0.053	0.9484 ± 0.041	0.951 ± 0.041	0.736	0.844	0.968	0.758

Columns 2 to 4 are presented as mean ± SD, columns 5 to 7 are pairwise comparisons, and column 8 presents multiple group comparisons. For multiple comparisons, if ANCOVA was used, one-versus-one comparisons were conducted using Tukey's honest significance test. Statistical significance, *P* value <0.05.

negative correlation of the ISe/RPE parafoveal and the VPI superficial region (r = −0.3287) and the VSD deep layer (r = −0.3287). For the NoDR cohorts, the ISe/RPE parafoveal has a weak negative correlation for the VSD deep layer (r = −0.3619). For the mild NPDR cohorts, there is no correlation (−0.3 < r < 0.3) between the characteristics observed. A summary of the correlation analysis is provided in Table 3.

Discussion

Clinical diagnosis has generally focused on the vascular complications, e.g., microaneurysms and venous beading.[14] As a result, current attempts for early identification of DR have mostly focused on vascular-based quantitative characteristics for early detection of DR employing OCTA.[3,4,15,16] However,

Table 3. Correlation Coefficients of OCT and OCTA Parameters in Healthy Subjects, Patients with NoDR, and Patients with Mild NPDR

	Healthy Subjects			NoDR			Mild NPDR		
	ISe/RPE peri	ISe/RPE para	ISe peri	ISe/RPE peri	ISe/RPE para	ISe peri	ISe/RPE peri	ISe/RPE para	ISe peri
VDI									0.2421
Sup	0.0023	−0.1356	0.0851	−0.0191	0.0095	0.1714	0.0632	0.0316	
VPI									0.0316
Sup	−0.2000	−0.3287*	−0.0621	−0.2000	−0.2667	−0.0286	−0.1684	−0.1790	
VSD									0.0105
Deep	0.2276	0.3287*	0.0805	0.2952	0.3619*	0.0476	0.0632	0.2842	

All values are presented as the Kendall correlation coefficient for each cohort separately. *Statistically significant correlation.

recent models describing the pathophysiology of DR attribute a variety of factors affected by hyperglycemia, such as oxidative stress, inflammation, and neuronal dysfunction, to the ultimate change of the retinal vasculature.[17] A rodent study suggests that a large supply of reactive oxygen species is obtained from photoreceptors, particularly rods, because of light/dark variations in rod energy exacerbating superoxide formation.[18] However, the exact sequence of alterations, whether disruptions to the photoreceptors occur before the onset of vascular distortions or vice versa, remains to be further elucidated. Therefore, to assess the function in the diabetic retina, it is necessary to quantify the changes of both the photoreceptors and retinal vasculature.

This study collected OCT and OCTA data using a commercially accessible OCTA device for custom digital image processing and feature quantification in eyes of patients with DM with no retinopathy and mild NPDR compared with controls. The characteristics quantified are broadly divided into two categories: vascular characteristics from OCTA and photoreceptor characteristics from OCT. The vascular characteristics quantified in this study were derived from OCTA en face projections of the SVP and DCP, whereas the photoreceptor characteristics were derived from OCT A-line profiles from the parafovea and perifovea.

We observed that there were both vascular distortions and photoreceptor abnormalities in the early stages of DR. However, we observed weak variable correlations between the OCTA and OCT features. After controlling the features for both age and hypertension, for the microvascular complications, the VDI and VPI in the SVP showed a significant increase between the patients with mild NPDR compared with controls and patients with NoDR. We also observe a decreasing trend for the VSD in the DVP; however, post hoc analysis revealed only significant differences between controls and patients with mild NPDR. These results are consistent with previous studies that observed decreasing vessel density from healthy to mild NPDR eyes.[19] For the photoreceptor abnormalities, the ISe intensity in the perifovea region showed significant decrease from the mild NPDR from the controls and patients with NoDR. This observation is similar to a previous study that also compared the ISe intensity differences between mild NPDR eyes and healthy subjects.[20] The ISe/RPE intensity ratio in the parafovea, similarly, revealed the differences among the patients with mild NPDR, controls, and patients with NoDR, whereas the ISe/RPE ratio in the perifovea revealed the significant differences among all three cohorts. The ISe has the highest proportion of photoreceptor mitochondria, and the photoreceptor constitutes roughly 70 percent of the retinal mitochondria.[21] This therefore suggests that factors such as oxidative stress and other metabolic disruptions might be reflected by changes in the ISe intensity. Furthermore, because the perifovea revealed higher sensitivity, we speculate potential rod photoreceptor degeneration in early DR.

This research has certain drawbacks. First, this study relied on a limited sample size obtained from a single imaging site. Second, signal strength index (SSI) varies across patients with diabetes and controls, which may influence the vascular-based characteristics. To address this issue, new algorithms would need to be developed to limit the impact of tissue reflectance fluctuation on vascular-based measures.[22] Third, because of the nature of a retrospective study, the participants were evaluated at different points in time after the diagnosis of DR. This may affect the study outcomes. There are some advantages to our work, including the use of customizable automated feature quantification in OCTA, which could be applied to a clinical environment. Naturally, comparative OCT and OCTA analysis can be readily performed because they are derived from the same imaging device.

In summary, quantitative OCT and OCTA analyses indicated photoreceptors and vascular abnormalities in diabetics with NoDR and mild NPDR. Among OCT characteristics, the ISe intensity and ISe/RPE intensity ratio have the highest sensitivity for DR identification. For OCTA characteristics, VDI, VPI, and VSD are most sensitive for early DR detection. Correlation analysis between OCT and OCTA characteristics revealed weak variable correlations. This observation suggests that OCT and OCTA characteristics may provide supplementary information for early DR detection. Adoption of comparative OCT and OCTA analyses for clinical practice would be beneficial for early screening of DR and instructive for follow-ups and evaluation of therapeutics.

Key words physiology, neurodegeneration, ophthalmology, optical coherence tomography, diabetic retinopathy, optical coherence tomography angiography, noninvasive imaging, macular, image analysis.

References

1. Beagley J, Guariguata L, Weil C, Motala AA. Global estimates of undiagnosed diabetes in adults. Diabetes Res Clin Pract 2014;103:150–160.
2. Cohen SR, Gardner TW. Diabetic retinopathy and diabetic macular edema. Retin Pharmacotherapeutics 2016;55:137–146.
3. Alam M, Zhang Y, Lim JI, et al. Quantitative optical coherence tomography angiography features for objective classification and staging of diabetic retinopathy. Retina 2020;40:322–332.

4. Hsieh Y-T, Alam MN, Le D, et al. OCT angiography biomarkers for predicting visual outcomes after ranibizumab treatment for diabetic macular edema. Ophthalmol Retina 2019;3:826–834.
5. Le D, Alam M, Miao BA, et al. Fully automated geometric feature analysis in optical coherence tomography angiography for objective classification of diabetic retinopathy. Biomed Opt Express 2019;10:2493–2503.
6. Cheung CM, Saxena S, Srivastav K, et al. Photoreceptor inner segment ellipsoid band integrity on spectral domain optical coherence tomography. Clin Ophthalmol 2014;8:2507–2522.
7. Rangaraju L, Jiang X, McAnany JJ, et al. Association between visual acuity and retinal layer metrics in diabetics with and without macular edema. J Ophthalmol 2018;2018:1–8.
8. Ma G, Son T, Kim TH, Yao X. In vivo optoretinography of phototransduction activation and energy metabolism in retinal photoreceptors. J Biophotonics 2021;14:e202000462.
9. Le D, Son T, Lim JI, Yao X. Quantitative optical coherence tomography reveals rod photoreceptor degeneration in early diabetic retinopathy. Retina 2022;42:1442–1449.
10. Group ETDRSR. Early Treatment Diabetic Retinopathy Study design and baseline patient characteristics: ETDRS report number 7. Ophthalmology 1991;98:741–756.
11. Yao X, Son T, Kim TH, Le D. Interpretation of anatomic correlates of outer retinal bands in optical coherence tomography. Exp Biol Med (Maywood) 2021;246:2140–2150.
12. Yao X, Alam MN, Le D, Toslak D. Quantitative optical coherence tomography angiography: a review. Exp Biol Med 2020; 245:301–312.
13. Ratner B. The correlation coefficient: its values range between+ 1/− 1, or do they? J Target Meas Anal Mark 2009;17:139–142.
14. Kollias AN, Ulbig MW. Diabetic retinopathy: early diagnosis and effective treatment. Deutsches Arzteblatt Int 2010;107:75–83.
15. Alam M, Le D, Lim JI, Yao X. Vascular complexity analysis in optical coherence tomography angiography of diabetic retinopathy. Retina 2021;41:538–545.
16. Dimitrova G, Chihara E, Takahashi H, et al. Quantitative retinal optical coherence tomography angiography in patients with diabetes without diabetic retinopathy. Invest Opthalmology Vis Sci 2017;58:190–196.
17. Shin ES, Sorenson CM, Sheibani N. Diabetes and retinal vascular dysfunction. J Ophthalmic Vis Res 2014;9:362–373.
18. Du Y, Veenstra A, Palczewski K, Kern TS. Photoreceptor cells are major contributors to diabetes-induced oxidative stress and local inflammation in the retina. Proc Natl Acad Sci 2013;110: 16586–16591.
19. Bhanushali D, Anegondi N, Gadde SGK, et al. Linking retinal microvasculature features with severity of diabetic retinopathy using optical coherence tomography angiography. Invest Opthalmology Vis Sci 2016;57:OCT519–OCT525.
20. Toprak I, Yildirim C, Yaylali V. Impaired photoreceptor inner segment ellipsoid layer reflectivity in mild diabetic retinopathy. Can J Ophthalmol 2015;50:438–441.
21. Miller DJ, Cascio MA, Rosca MG. Diabetic retinopathy: the role of mitochondria in the neural retina and microvascular disease. Antioxidants 2020;9:905.
22. Gao SS, Jia Y, Liu L, et al. Compensation for reflectance variation in vessel density quantification by optical coherence tomography angiography. Invest Opthalmology Vis Sci 2016; 57:4485–4492.

MACULAR SENSITIVITY CHANGE AFTER COMPLEMENTARY LASER THERAPY AFTER RANIBIZUMAB INTRAVITREAL INJECTION IN BRANCH RETINAL VEIN OCCLUSION

AKIRA OJIMA, MD, YUTAKA KATO, MD, RYUTARO TOMITA, MD, AKIHITO KASAI, MD, YUKINORI SUGANO, MD, TETSUJU SEKIRYU, MD

Purpose: We examined the effect of ranibizumab with or without laser photocoagulation on retinal sensitivity in eyes with branch retinal vein occlusion.

Methods: Prospective randomized control study. Thirty patients with branch retinal vein occlusion received intravitreal injection of ranibizumab in a monthly pro re nata regimen. Fifteen patients received ranibizumab monotherapy alone (monotherapy group). The remaining 15 patients received rescue laser therapy at 3 or 9 months (combined group). The retinal sensitivity was measured at 32 points within central 8°, and the average of the main occlusion side among the 16 upper or 16 lower points was defined as the affected area sensitivity.

Results: In comparing the monotherapy group and the combined group, the number of injections during the 12 months was 5.4 versus 4.9, the change in retinal thickness (μm) was −254 versus −197, the ETDRS letters of improvement was +18.3 versus +19.6, and the change in the affected area sensitivity (dB) was +7.1 versus +4.6. At 12 months, all these results were significantly improved compared with their respective baselines, but none of the differences between the two groups reached statistical significance.

Conclusion: Retinal sensitivity at 12 months improved in both the monotherapy group and the combined group. The additional laser did not reduce the number of injections or further improve visual acuity nor did it affect retinal sensitivity.

RETINA 43:999–1004, 2023

Branch retinal vein occlusion (BRVO) is a disease in which retinal veins are occluded mainly at the arteriovenous crossing, causing retinal hemorrhage, ischemia, and edema. The main cause of visual loss is macular edema, and although laser treatment has been the conventional treatment, in recent years, anti-vascular endothelial growth factor (VEGF) therapy has become the first-line therapy. Although attempts have been made to further improve visual acuity and reduce the number of injections by combining anti-VEGF therapy with a laser photocoagulation, the results have not yet outperformed anti-VEGF monotherapy.[1,2] In the clinical setting, laser treatment is occasionally applied for patients who did not respond to anti-VEGF therapy. It seems effective and beneficial in some patients. Since laser irradiation can destruct the perifoveal tissue, it may affect vision as well as retinal sensitivity. For these issues, the clinical usefulness of additional laser treatment after anti-VEGF therapy remains on the discussion.

The reliable evaluation of macular sensitivity may be difficult during the course of BRVO because the fixation point was unstable. Microperimetry may have the advantage to measure macular sensitivity during course of BRVO. In this study, we investigated the effect of additional laser treatment after ranibizumab

From the Department of Ophthalmology, Fukushima Medical University School of Medicine, Fukushima, Japan.

This study was financially supported by Novartis Pharma.

None of the authors has any financial/conflicting interests to disclose.

The authors have no proprietary interest in any aspect of this study.

Reprint requests: Tetsuju Sekiryu, MD, Department of Ophthalmology, Fukushima Medical University, 1, Hikarigaoka, Fukushima 960-1247, Japan; e-mail: sekiryu@fmu.ac.jp

injections for macular retinal sensitivity by microperimetry in BRVO.

Methods

Patients

This study was conducted as a single-center prospective study. Thirty eyes of 30 new-onset BRVO cases, mean age 72 years, were enrolled (12 male and 18 female patients; mean age, 71.6 years; age range, 54–87 years). All patients visited the Department of Ophthalmology at Fukushima Medical University Hospital and underwent a comprehensive ophthalmologic examination, including measurement of best-corrected visual acuity (BCVA), slit-lamp biomicroscopy, fundus photography, fluorescein angiography, coherence tomography, and macular sensitivity measurement. Eyes with other retinal diseases causing macular edema, such as central retinal vein occlusion, diabetic macular edema, age-related macular degeneration, macular telangiectasia, and uveitis, were excluded. There were no cases with an enlarged foveal avascular zone on fluorescein angiography at baseline.

Treatment Protocol

The protocol of this study is shown in Table1. All patients underwent intravitreal injection of ranibizumab 0.5 mg as a first treatment, and then, intravitreal injection of ranibizumab was added if they had ME with a central subfield thickness (CST) greater than 300 μm during monthly follow-up. All patients were randomized to two groups using a minimization method based on BCVA and retinal thickness at baseline. Fifteen eyes were assigned to the monotherapy group to receive intravitreal injection of ranibizumab monotherapy. The remaining 15 eyes were assigned to the combined group to receive both injections and laser if they met the retreatment criteria at 3 and 9 months, while receiving the same injection treatment as the intravitreal injection of the ranibizumab group in the other months. At the time of laser treatment, fluorescein angiography was reexamined, and scatter laser photocoagulation to the identified nonperfused areas and direct coagulation to the leaking capillary and microaneurysms were performed.

Macular Sensitivity

A total of 32 points of retinal sensitivity were measured in concentric circles at 3° (8 points), 5° (12 points), and 8° (12 points) from the fovea at baseline and 12 months using MP-3^{-TM} (NIDEK, Gamagori, Japan). We measured the sensitivity within 20° circle area centered at the fovea center. To compare uniformly, the macular area was divided into the upper half and the lower half (Figure 1). The part of each area that contained the main occlusion was assigned to the affected side and the other to the unaffected side. The mean sensitivity of the affected side was set as the affected area sensitivity and the rest as the unaffected area sensitivity (dB). The cases which could not determine the occlusion side, such as a double occlusion case, was excluded from the study at baseline.

We examined the changes in visual acuity, retinal thickness, number of injections, and retinal sensitivity after each treatment in the monotherapy and combined groups.

The study was in compliance with the tenets of the Declaration of Helsinki, and informed consent was obtained from all participating patients. The Institutional Review Board of the Fukushima Medical University, Japan, granted approval for this project.

Statistics

The differences between the two groups at the same time points were tested with the Mann–Whitney *U* test. Differences in logMAR visual acuity and macular

Table 1. Protocol of the Examinations and Treatments

		Baseline	1M	2M	3M	4M	5M	6M	7M	8M	9M	10M	11M	12M
All cases (n = 30)	BCVA	○	○	○	○	○	○	○	○	○	○	○	○	○
	OCT	○	○	○	○	○	○	○	○	○	○	○	○	○
	RS	○												○
	FA	○			☆						☆			
Monotherapy group (n = 15)	IVR	○	△	△	△	△	△	△	△	△	△	△	△	
Combined group (n = 15)	IVR	○	△	△	△	△	△	△	△	△	△	△	△	
	PC				☆						☆			

○:Done in all cases.
△:Done when the retreatment criteria are met.
☆:Perform only for the combined group when they meet the retreatment criteria.
BCVA, best-corrected visual acuity; OCT, optical coherence tomography; RS, retinal sensitivity; FA, fluorescein angiography; IVR, intravitreal ranibizumab injection; PC, laser photocoagulation.

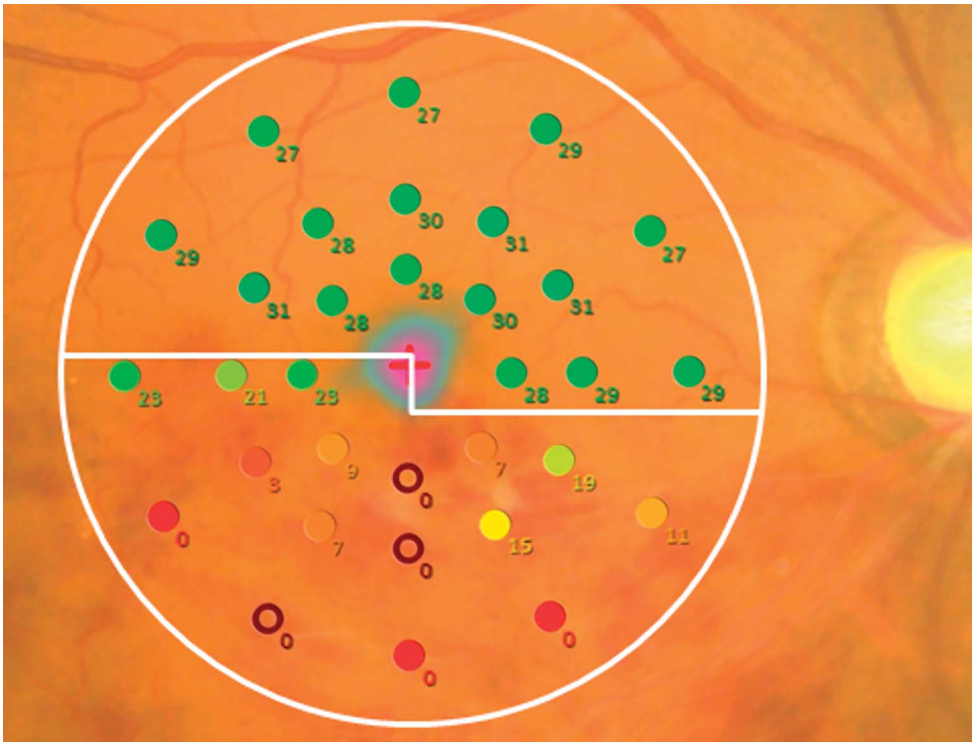

Fig. 1. Layout of the retinal sensitivity measurement points. The inner row is located at 3° (8 points), the middle at 5° (12 points), and the outer row at 8° (12 points). All 32 points are divided above and below, with the three points on the papillomacular bundle included in the upper half. In this example, the mean of the upper 16 points is the normal side sensitivity and the mean of the lower 16 points is the occlusion side sensitivity.

sensitivity between baseline and Month 12 were tested with the Wilcoxon signed-rank sum test. The best-corrected visual acuity was measured in decimal acuity, logMAR values were used for statistical processing, and the results were converted to ETDRS letters.

Results

Baseline Characteristics

Baseline characteristics are shown in Table 2. There was no significant difference between the monotherapy and combined groups at baseline, in a mean age of 73.5 (70.6–77.1) and 69.6 (63.0–75.3) years, a mean CST (μm) of 535 (415–614) and 501 (424–573), an ETDRS letters of 60 and 64, and an affected side sensitivity (dB) of 13.5 (11.2–17.2) and 16.7 (13.5–20.5), respectively. The incidence of the occlusion in the upper area was 13 (87%) of 15 eyes in the monotherapy group and 7 (47%) of 15 eyes in the combination therapy group. Unaffected side sensitivity was significantly lower in the monotherapy group (19.6 dB) than in the combined group (25.3 dB) (P = 0.002, Mann–Whitney U test).

Number of Injections

The mean injection number was 5.1 (range 2–12) in all 30 patients over 12 months, 5.4 (range 2–12) in the monotherapy group and 4.9 (range 3–9) in the combined group. There were no significant differences between the three groups (P = 0.47, Mann–Whitney

Table 2. Baseline Characteristics

	n=	Male	Female	Age	CST (μm)	ETDRS Letters	Occlusion Side Sensitivity (dB)	Normal Side Sensitivity (dB)
All cases	30	12	18	71.6	518 ± 130	62.0 ± 16.0	15.1 ± 6.3	22.5 ± 5.7
Monotherapy group	15	3	12	73.5	535 ± 139	60.0 ± 18.0	13.5 ± 6.5	19.6 ± 5.9
Combined group	15	9	6	69.6	501 ± 122	64.0 ± 14.0	16.7 ± 5.9	25.3 ± 3.9
P = (Mann–Whitney U)				0.24	0.84	0.98	0.19	0.002

CST, central subfield thickness

U test). Nine (60%) of the 15 patients in the combined group also received laser therapy at Month 3 or Month 9. The remaining 6 patients (40%) did not receive laser treatment because they showed macular edema neither at Month 3 nor Month 9.

Visual and Morphological Results

Over 12 months, CST (μm) decreased significantly from 535 ± 139 (415–614) to 281 ± 81 (234–285) in the monotherapy group ($P < 0.001$) and from 501 ± 122 (424–573) to 304 ± 107 (249–292) in the combined group ($P < 0.001$). There was no significant difference in CST between the groups at Month 12 ($P = 0.384$) (Figure 2). Best-corrected visual acuity also improved significantly at 12 months, +18.3 ETDRS letters in the monotherapy group ($P < 0.001$) and +19.6 ETDRS letters in the combined group ($P < 0.001$), but there was no significant difference between groups at 12 months ($P = 0.105$).

Macular Sensitivity

At 12 months, occlusion side sensitivity (dB) improved significantly from 13.5 to 20.6 ($P < 0.01$) in the monotherapy group and from 16.7 to 21.3 in the combined group ($P < 0.01$), but there was no significant difference between the groups ($P > 0.10$). Normal side sensitivity (dB) also improved significantly in the monotherapy group, from 19.6 to 24.71 ($P < 0.01$), and in the combined group, from 25.3 to 27.2 ($P < 0.05$). The larger improvement in the monotherapy group was because many patients had serous retinal detachment extending from the upper occlusion area to the lower portion of the macula at baseline (Table 3).

In comparison with the nine eyes that actually received the laser and the other 21 eyes, the CST(μm) at 12 months was 325 ± 136, 279 ± 69, ETDRS letters score was 81.2 ± 5.9, 80.9 ± 9.3, and the occlusion side sensitivity (dB) was 19.2 ± 8.2, 21.7 ± 5.3, respectively, with no significant difference between the groups ($P = 0.631$, 0.803, 0.472, respectively).

Discussion

Macular edema is the primary cause of vision loss in BRVO, with a visual acuity of less than 20/40 in the natural course of the disease.[3] Although laser photocoagulation[4] and intravitreal injection of triamcinolone acetonide[5] have been tried for macular edema, the current standard care is anti-VEGF treatment with ranibizumab[6] or aflibercept.[7] Although continued anti-VEGF treatment has enabled patients to maintain good

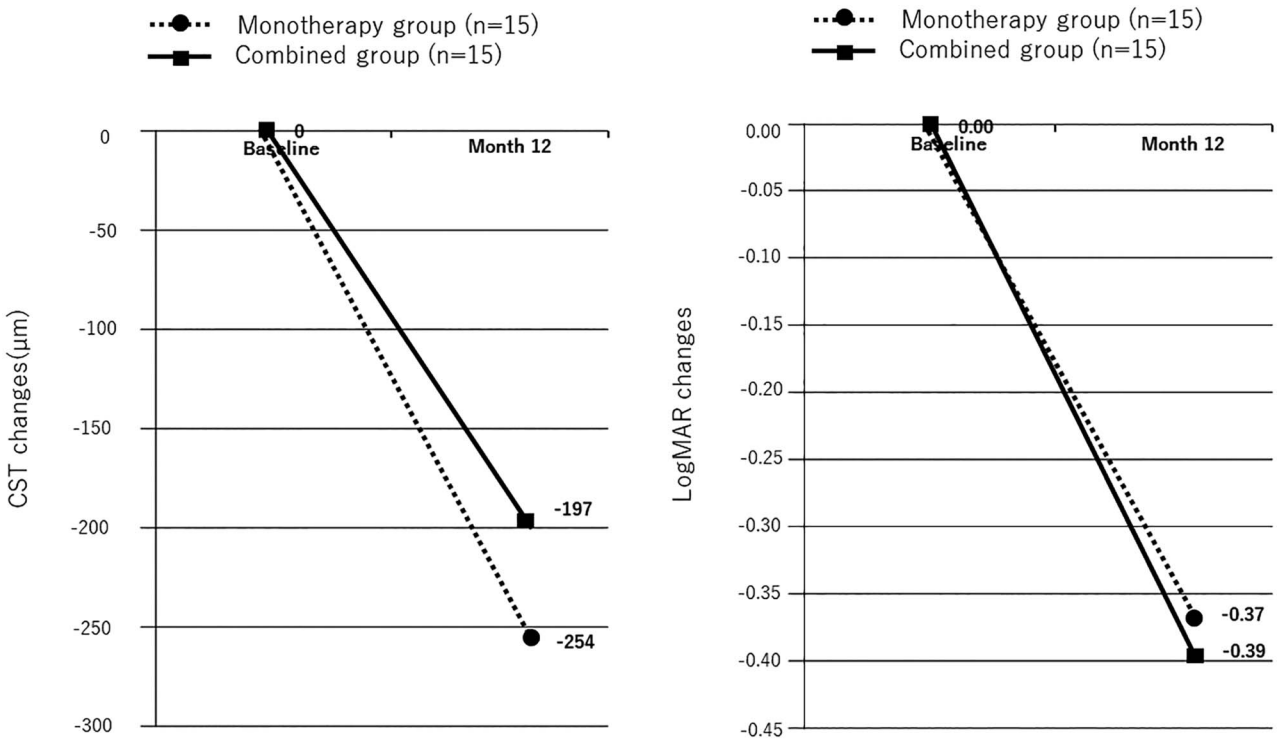

Fig. 2. CST change at 12 months: Both the monotherapy group and the combined group showed significant improvement in CST at 12 months ($P < 0.05$, paired *t* test), but there was no significant difference between the two groups ($P = 0.38$, Mann–Whitney *U* test).

Table 3. Retinal Sensitivity

		Baseline	Month 12	*P*
Occlusion side sensitivity (dB)	Monotherapy	13.5	20.6	<0.05
	Combined	16.7	21.3	<0.05
Normal side sensitivity (dB)	Monotherapy	19.6	24.7	<0.05
	Combined	25.3	27.2	<0.05

vision in BRVO, many patients require long-term treatment due to recurrent macular edema. In a 49-month observation following a large trial of ranibizumab, only 50% of patients with BRVO were able to finish treatment and the remaining 50% were still receiving an average of 3.2 injections in year.[2,6]

A risk factor for prolonged macular edema is microaneurysms that are formed between 3 and 9 months after the onset of BRVO.[8] Direct laser photocoagulation of leaky dilated capillaries and microaneurysms has been reported to reduce edema and improve visual acuity,[9] so laser is effective in the treatment of macular edema in chronic phase BRVO. Therefore, the idea of combining anti-VEGF and laser treatment to achieve better outcomes naturally arises, but unfortunately, there are no reports of it being superior to anti-VEGF treatment alone.

The additional laser photocoagulation to ranibizumab did not further improve visual acuity, reduce macular edema, or reduce the number of injections for recurrent macular edema after 24 weeks of ranibizumab treatment.[10] A 24-month trial comparing a larger number of people with and without the addition of laser to the planned pro re nata administration of ranibizumab did not find any benefit of the addition of laser.[11] However, the laser treatment used in those studies was only for scatter photocoagulation of the nonperfused area, not for coagulation of the leaking capillary or microaneurysms, which are effective in treating recurrent macular edema in chronic phase BRVO.

The additional photocoagulation for leaking lesion and nonperfused area may be applied and provided better results than ranibizumab alone. Conversely, laser treatment near the fovea would have an adverse effect on retinal sensitivity. We performed laser treatment on leaky lesions causing macular edema such as microaneurysms inside the arcades as well as nonperfused areas outside the arcades, but the number of injections was not reduced. Although such laser treatment may contribute to the suppression of macular edema in patients not on anti-VEGF therapy,[9] it is hypothesized that the addition of laser treatment may not have any further effect because of the strong suppression of macular edema in patients with as needed dosing of anti-VEGF drugs.

Retinal sensitivity in BRVO eyes is influenced by the state of retinal perfusion and the presence of edema. Within the BRVO region, the retinal sensitivity has been reported to be reduced in the order of perfused area, partially perfused area, and nonperfused area.[12] The sensitivity is also reduced in the macular edema region, but the sensitivity improves when the edema is improved by ranibizumab injection.[13] There have been few reports of retinal sensitivity measured between ranibizumab alone and laser treatment. Kumar et al[14] reported no difference in retinal sensitivity within the center 4° at 6 months between ranibizumab treatment with or without laser. They used the MP-1^{-TM} (NIDEK, Gamagori, Japan) to measure retinal sensitivity, but the background luminance of this device is four asb. The MP-3 we used had a background luminance of 31.4 asb, which allowed us to perform photopic perimetry, and we think it could measure macular retinal sensitivity more accurately. In addition, they only measured the sensitivity within 4 degrees of center, whereas we measured the sensitivity within 8 degrees of center at 32 locations. In general, central sensitivity is strongly correlated with BCVA, so it often shows similar results to visual acuity changes and does not necessarily reflect the function of the entire macula. We measured a wider range within 8° to investigate the effect of the laser on the macula. Our study is the first to report the effect of adding laser to ranibizumab treatment on macular retinal sensitivity as measured by MP-3.

In our study, both the monotherapy and combined groups showed an improvement in retinal sensitivity after 12 months, but there was no further improvement with the addition of laser therapy. We were unable to statistically demonstrate a benefit of adding the laser to ranibizumab for retinal sensitivity as well as visual acuity or number of injections. However, no adverse effect of laser treatment on macular sensitivity was shown, so laser treatment may be an option for recurrent macular edema in cases where adequate anti-VEGF treatment is not available. Laser therapy has been shown to be effective in patients who, for whatever reason, cannot be treated with anti-VEGF therapy at all. Therefore, the lack

of additional benefit to ranibizumab does not mean that laser therapy itself is futile.

A limitation of this study is that not all patients in the combined group received the laser because we limited the timing of the laser to Month 3 and Month 9. If there was no macular edema at that time, the laser would not have been performed, so 9 of 15 eyes actually received the laser. However, a statistical analysis of the nine eyes that received the laser did not show any advantage over the monotherapy group in visual acuity, CST, number of injections, or retinal sensitivity.

In conclusion, retinal sensitivity at 12 months improved in both the monotherapy group and the combined group. The additional laser did not reduce the number of injections or further improve visual acuity nor did it affect retinal sensitivity.

Key words: branch retinal vein occlusion, laser photocoagulation, macular edema, microperimetry, ranibizumab, retinal sensitivity.

References

1. Heier JS, Campochiaro PA, Yau L, et al. Ranibizumab for macular edema due to retinal vein occlusions: long-term follow-up in the HORIZON trial. Ophthalmology 2012;119:802–809.
2. Campochiaro PA, Sophie R, Pearlman J, et al. Long-term outcomes in patients with retinal vein occlusion treated with ranibizumab: the RETAIN study. Ophthalmology 2014;121:209–219.
3. Rogers SL, McIntosh RL, Lim L, et al. Natural history of branch retinal vein occlusion: an evidence-based systematic review. Ophthalmology 2010;117:1094–1101.
4. The Branch Vein Occlusion Study Group. Argon laser photocoagulation for macular edema in branch vein occlusion. Am J Ophthalmol 1984;98:271–282.
5. Scott IU, Ip MS, VanVeldhuisen PC, et al. A randomized trial comparing the efficacy and safety of intravitreal triamcinolone with standard care to treat vision loss associated with macular edema secondary to branch retinal vein occlusion: the standard care vs corticosteroid for retinal vein occlusion (SCORE) study report 6. Arch Ophthalmol 2009;127:1115–1128.
6. Campochiaro PA, Heier JS, Feiner L, et al. Ranibizumab for macular edema following branch retinal vein occlusion: six-month primary end point results of a phase III study. Ophthalmology 2010;117:1102–1112.
7. Campochiaro PA, Clark WL, Boyer DS, et al. Intravitreal aflibercept for macular edema following branch retinal vein occlusion: the 24-week results of the VIBRANT study. Ophthalmology 2015;122:538–544.
8. Tomiyasu T, Hirano Y, Yoshida M, et al. Microaneurysms cause refractory macular edema in branch retinal vein occlusion. Sci Rep 2016;6:29445.
9. Sakimoto S, Kamei M, Sakaguchi H, et al. Direct photocoagulation to leakage points to treat chronic macular edema associated with branch retinal vein occlusion: a pilot study. Clin Ophthalmol 2014;8:2055–2060.
10. Campochiaro PA, Hariz G, Mir TA, et al. Scatter photocoagulation does not reduce macular edema or treatment burden in patients with retinal vein occlusion: the RELATE Trial. Ophthalmology 2015;122:1426–1437.
11. Tadayoni R, Waldstein SM, Boscia F, et al. Sustained benefits of ranibizumab with or without laser in branch retinal vein occlusion: 24-month results of the BRIGHTER study. Ophthalmology 2017;124:1778–1787.
12. Iijima H. Reduced light sensitivity due to impaired retinal perfusion in branch retinal vein occlusion. Jpn J Ophthalmol 2018;62:151–157.
13. Rezar S, Eibenberger K, Bühl W, et al. Anti-VEGF treatment in branch retinal vein occlusion: a real-world experience over 4 years. Acta Ophthalmol 2015;93:719–725.
14. Kumar P, Sharma YR, Chandra P, et al. Comparison of the safety and efficacy of intravitreal ranibizumab with or without laser photocoagulation versus dexamethasone intravitreal implant with or without laser photocoagulation for macular edema secondary to branch retinal vein occlusion. Folia Med (Plovdiv) 2019;61:240–248.

DIAGNOSTIC YIELD OF IN VITRO VITREOUS BIOPSY FOR INTRAOCULAR LYMPHOMA AT VARIABLE VITREOUS CUTTER SPEEDS USING 25-GAUGE VITRECTOMY

SRUTI TEKUMALLA, BA,* DAVID XU, MD,† KATHERINE AWH, BA,‡ NANCY PHILP, PHD,‡ TATYANA MILMAN, MD,‡§ SUNIR GARG, MD†

Purpose: Primary vitreoretinal lymphoma is the most common intraocular lymphoproliferative disorder. We evaluated the diagnostic yield of pars plana vitrectomy, specifically using modern high cut rate dual-cycle cutters, on in vitro cell viability and diagnostic yield.

Methods: Human Burkitt lymphoma cell line *Namalwa* at 2 x 10^5 cells/mL was aspirated by 25-gauge dual-blade guillotine-type vitrectomy at five speeds (500, 1,000, 4,000, 7,500, or 15,000 cuts per minute). Cell viability and diagnostic yield in each subtype group were determined using hemocytometry, viable cell count using Cell Counting Kit-8, and pathologist-guided manual count.

Results: No significant deviation in cell count was identified in any cut rate by ANOVA ($P = 0.61$), and no trends in the number of viable cells were identified across cut rates ($R^2 = 0.188$, $P = 0.47$). Among histologic cell counts per cut-rate, neither linear regression ($R = 0.531$, $P = 0.16$) nor ANOVA ($P = 0.096$) were statistically significant.

Conclusion: There was no significant degradation in the number of viable cells with increasing cut speed. These results suggest that in contrast to previous findings using 20g or 23g vitrectomy for diagnostic vitrectomy, modern vitrectomy systems may be used at up to 15,000 cpm without compromising the viability of lymphoma cells.

RETINA 43:1005–1009, 2023

The incidence of primary vitreoretinal lymphoma (PVRL), the most common intraocular lymphoproliferative disorder, has been increasing.[1] Among PVRL subtypes, diffuse large B-cell–type lymphoma is most common.[2] Diagnosis remains challenging. Early diagnosis may improve otherwise poor outcomes including loss of vision and central nervous system involvement, which has significant mortality.[3] Although flow cytometry, immunohistochemistry, cytokine levels, and molecular genetic studies have gained importance as ancillary diagnostic methods, cytologic evaluation by an experienced ocular pathologist remains critical[4]; however, the fragile lymphoma cells degrade rapidly after being obtained from the eye with pars plana vitrectomy, and the quality of the specimen may be affected by the transition to smaller gauge and very high cut rate vitrectomy.

Microincision vitrectomy surgery has enabled faster recovery for patients.[5] The increased efficiency of microincision vitrectomy surgery is partly because of dual-cycle vitrectomy cutters. Over the past 10 to 15 years, cutters went from 2,500 cpm to 15,000 cpm and getting closer to 30,000 cpm with the newest hypersonic vitrectomy models. Previous in vitro studies on

From the *Thomas Jefferson University Sidney Kimmel Medical College; †MidAtlantic Retina, the Retina Service of Wills Eye Hospital; ‡Department of Pathology, Anatomy, & Cell Biology, Thomas Jefferson University; and §Wills Eye Hospital Department of Pathology, Philadelphia, Pennsylvania.

Association for Research in Vision and Ophthalmology (ARVO), Denver, CO, May 11-12, 2022.

Funding was provided by the J. Arch McNamara, MD, Fund for Retina Research and Education and supported, in part, by Eye Pathology Education and Research Fund, LLC, Jenkintown PA.

None of the authors has any financial/conflicting interests to disclose.

Reprint requests: Sruti Tekumalla, BA, Sidney Kimmel Medical College at Thomas Jefferson University, 1025 Walnut St #100, Philadelphia, PA 19107; e-mail: sruti.tekumalla@jefferson.edu

the yield of diagnostic 20-gauge (20g) vitrectomy for patients with PVRL have demonstrated lower sensitivity with cut rates above 1,000 cpm, because of mechanical degradation of lymphoid cells.[2] Another in vitro study assessing biopsy yield in 20g versus 25g vitrectomy documented that 25g diagnostic vitrectomy yields an adequate sample for diagnosis of intraocular lymphoma.[6] The diagnostic results of the sample obtained with 25g vitrectomy were superior to those reported for 20g vitrectomy.

The older vitrectomy systems lacked advanced fluidic and intraocular pressure control mechanisms, which may have contributed to the mechanical stresses influencing cellular integrity. The effect of a high cut rate using a modern 25g vitrector on PVRL cytology has not been formally explored. In addition, previous investigations used limited methods to assess cell count and viability.[7–9]

We modeled our investigation on a previous in vitro vitrectomy cytology study using the *Namalwa* human Burkitt lymphoma cell line.[2] The goal of our study was to assess the effect of modern 25g high cut rate dual-cycle vitrectomy cutters at six different cut speeds on cellular integrity and in vitro cell viability.

Methods

This in vitro study not involving human subjects was exempt from the Wills Eye Hospital Institutional Review Board. The *Namwala* human Burkitt lymphoma cell line was used in this experiment. It closely resembles and has similar characteristics to PVRL. It has been used in several lymphoma apoptotic studies in the past and materials for the line were readily accessible for cell culture and experimental use.[10]

Cell Line

Human Burkitt lymphoma cell line *Namalwa* was obtained and grown in culture media containing Roswell Park Memorial Institute 1,640 media with 2 mM L-glutamine adjusted to contain 1.5 g/L sodium bicarbonate; 4.5 g/L glucose; 10 mM HEPES; and 1.0 mM sodium pyruvate, 92.5% with fetal bovine serum, 7.5%. Fresh medium (20% to 30% by volume) was changed every 2 to 3 days. We used cells in a logarithmic growth phase for experiments.

Vitrectomy Biopsy

Cells were obtained using 25g dual blade guillotine vitrectomy probe (Bausch and Lomb Stellaris Elite, Vaughn, ON, Canada) at five different cut rates (500, 1,000, 4,000, 7,500, or 15,000 cpm) at a cell concentration of 2 x 10^5 cells/mL suspended in balanced salt solution (BSS). All samples were acquired with manual aspiration of 1cc/minute. Control samples were obtained by aspirating the sample into the specimen syringe without cutting. Three samples were processed at each cut rate for cytopathology analysis. Two samples at each cut rate were processed using Cell Counting Kit-8 (CCK-8, APE x BIO, Boston, MA)/WST-8 tetrazolium salt colorimetric for viability analysis. Samples were placed in an ice bath between transports from vitrectomy to the assaying lab. For the vitrectomy protocol, we positioned the tip of the vitrectomy cutter in the middle of the cell suspension and collected 2.5 mL for each specimen at its designated cut rate manually using a syringe. Before collecting samples for different cut rates, we thoroughly cleaned the vitrectomy instruments and tubing.

Viability Testing

We determined cell viability and diagnostic yield in each group using hemocytometry with trypan blue staining and viable cell count using CCK-8. We used the manufacturer's protocol for CCK-8. To confirm that time spent on ice did not affect cell viability, we used two different culture plates. Cells obtained directly from the incubator were placed on one plate, and specimens from the vitrectomy aspiration were placed on the second plate. Two rows of 100 μL control (2 x 10^5 cells/mL suspended in BSS) obtained directly from the cell culture incubator were plated on the first 96-well plate. We performed serial dilution with prewarmed Roswell Park Memorial Institute 1640 at 37°C, and 10 μL of CCK-8 solution was added to all dilution and vitrectomy samples and mixed using a micropipette. The plate was then incubated for 1.5 hours and transferred to an absorbance microplate reader. Absorbance was measured at 450 nm. The second 96-well plate, used for control samples and vitrectomized samples, was similarly processed. Two rows of 100 μL control (2 x 10^5 cells/mL suspended in BSS) that were placed on ice and brought to the vitrectomy lab for the duration of cell processing were plated, and serial dilution was performed using prewarmed Roswell Park Memorial Institute 1640 at 37°C. Two rows for each cut rate suspension were serially diluted with prewarmed Roswell Park Memorial Institute 1640, and 10 μL of CCK-8 solution was added to all filled wells and mixed using a micropipette. Absorbance data were converted into cell concentrations based on the dilution curve.

Cytopathology Analysis

Cytopathologic analysis of the samples was performed using Cytospin preparations. We combined 0.2 cc from each sample with 0.2 cc of Epredia Cytospin collection fluid (Portsmouth, NH), centrifuged at 2,000 revolutions per minute for 10 minutes. After centrifugation, Cytospin preparations were fixed for 2 minutes in 95% alcohol and stained with hematoxylin-eosin stain. Slides were scanned at 40× using Ventana DP 200 slide scanner (Roche Diagnostics, Basel, Switzerland) and viewed with Ventana Image Viewer version 3.1.4 (Ventana Medical Systems Inc, Tucson, AZ). Intact cells were manually counted by an experienced ophthalmic pathologist (TM), who was masked to the cell collection protocol and the cut rate. Cells with stripped cytoplasm, cell fragments, and apoptotic cells were excluded from the count (Figure 3A).

Statistical Analysis

The yield of vitreous biopsy by hemocytometry, cytopathology cell count, and cell viability assay was evaluated by ANOVA between the different vitrector cut rates. We assessed linear variation of cellular yield with linear regression. A P value less than 0.05 was considered statistically significant. We repeated experimental quantification tests three times for each specimen and calculated mean values using Excel (Microsoft Corporation, Redmond, WA).

Results

Lymphoma cell biopsy was successful at all cut rates and analyzed by viable cell analysis, hemocytometry, and cytopathology.

Viable Cell Analysis

The mean ± SD viable cell concentration for all samples was 58,481±18,942 cells/mL. Figure 1 plots the viable cell concentration at vitrector cut rates of 500, 1,000, 4,000, 7,500, and 15,000 cpm. No statistically significant deviation in cell count was identified in any cut rate by ANOVA (P = 0.61), and no trends in the number of viable cells were identified across cut rates (R^2 = 0.188, P = 0.47). Lymphoma cell samples were on ice for a mean (SD) of 140.5 (39.23) minutes, including the duration of vitrectomy and the time to transfer for incubation for CCK-8 analysis and Cytospin with ocular pathology. No significant differences in CCK-8 absorbance were noted between the first 96-well plate controls with cells directly from the incubator and the second 96-well plate controls, which were on ice for the duration of experimentation.

Cytologic Cell Count

We analyzed cell concentration by Trypan blue staining and hemocytometry. Figure 2 plots the cell counts as a function of cut rate. Linear regression found no statistically significant linear trend (R^2 = 0.531, P = 0.16). ANOVA found no statistically significant difference between the groups (P = 0.096). Additional post hoc analysis using Tukey HSD comparison of treatments did not yield differences between pairs of individual cut rates.

Cytomorphology

We reviewed the cytopathology of all samples to assess diagnostic sensitivity for lymphoma analysis. All Cytospin preparations had a mixture of intact cells and degenerated cells. The intact cells had ovoid nuclei, prominent nucleoli, and basophilic vacuolated cytoplasm. The degenerated cells included apoptotic cells, cell fragments, and cells that were partially or completely devoid of cytoplasm (Figure 3). Linear regression found no statistically significant linear trend (R^2= 0.0968, P = 0.86). ANOVA found no cytomorphologic difference between the control samples and samples obtained with various cut rates (P = 0.110).

Discussion

Several previous in vitro studies using 20g and 25g vitrectors demonstrated possible diagnostic yield reduction of lymphoma cells at higher cut speeds. Evaluation of cells at speeds greater than 600 cpm revealed decreased cellularity, increased cell fragmentation, and damaged cell morphology and viability using immunohistology and cytopathology.[2,11,12] These studies suggest that more rapid speeds, such

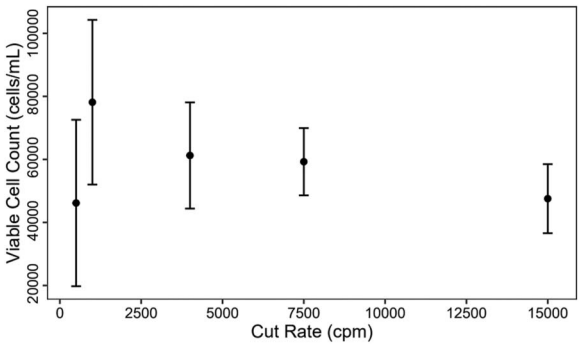

Fig. 1. Viable cell concentration via CCK-8 assay of lymphoma vitrectomy samples from cut rates 500 through 15,000 cuts/minute.

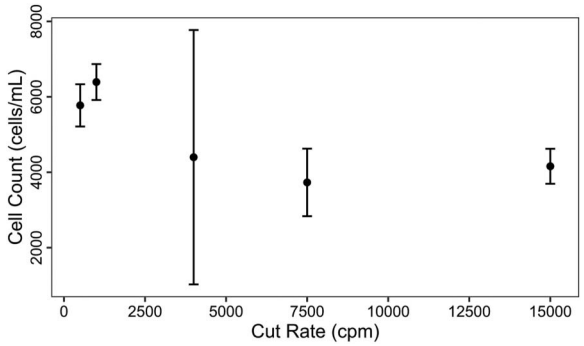

Fig. 2. Cell concentration by hemocytometry as a function of cut rates 500 through 15,000 cuts/minute.

as the cut rates tested in the current study, would cause a high shear force over a large enough zone to disrupt a significant portion of cells. For several years, clinicians were given the cut rate recommendation of 600 cpm or less while performing vitreous biopsy to preserve diagnostic yield for PVRL. The current study suggests this may not be correct. Our study combined cytopathologic assessment by an experienced ophthalmic pathologist with other methods to evaluate cell integrity and viability, including viable cell count with CCK-8 and Trypan blue assays and hemocytometry. We found that high cut rates up to 15,000 cpm with modern 25g vitrectomy probe did not significantly affect cell morphology or counts compared with the control in our in vitro model of PVRL.

There are several advantages to our study. Results from past studies using comparatively low-cut rates and larger gauge vitrectomy instruments do not compare with modern vitrectomy systems because of the decreased flow rate and particle acceleration characteristics with optimized port geometries in modern 25g cutters[13]. Ratanapojnard et al[12] evaluated the effect of cut rates up to 1,500 cpm on microbial and myeloid leukocyte viability using a guillotine mechanism. The authors found that although the high cut rate did not significantly alter culture yield of bacterial and fungal organisms, there was a significant difference in the myeloid leukocyte viability at the cutting rate of 1,500 cpm. Although this study evaluated fast cut rates, it did not closely replicate the cytologic features of PVRL. In our study, we used human Burkitt lymphoma cells, which closely resemble DLBCL regarding morphology, propensity for apoptosis/necrosis, and fragility. To account for the loss of cell viability because of time after acquisition, a control of the CCK-8 viability experiment was performed with cells that were drawn immediately after being collected and those that were on ice for the duration of the experiment.

The current study does have limitations, which primarily stem from its in vitro design. Without a standard vitreous substitute, cell morphology and viability in vivo may differ from cells grown in culture media and may not accurately reflect the viscosity of human vitreous humor. Hydrodynamic differences may exist that are not accounted for when comparing our aqueous medium to the gel-like medium of human vitreous. However, our study standardized cell counts and used varied assays to assess cell viability, which was consistent among all cell counts and with the control group. Although Burkitt lymphoma closely resembles DLBCL cytomorphologically, the two lymphomas are not identical. Additional cell lines, including those that are more often causative of PVRL such as B cell lymphoma, could be tested in future studies. Differences also exist between cultured lymphoma cells and in vivo lymphoma cells; in the human eye, vitreous specimens contain varying amounts of lymphoma cells that may not be evenly distributed. Unlike our study's comparatively high lymphoma cell counts, a patient vitrectomy sample may be mixed with necrotic cells, fibrin, debris, and reactive lymphocytes, contributing to diagnostic challenges.[14] Clumping of lymphoma cells may introduce between-sample variability, which could limit the statistical results;

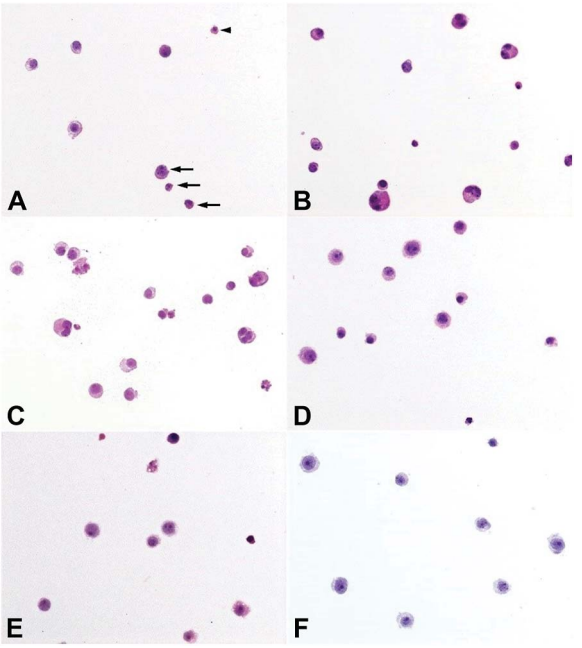

Fig. 3. Representative cytopathology images of human Burkitt lymphoma samples. Intact human Burkitt lymphoma cells feature ovoid nuclei, prominent nucleoli, and scant-to-moderate amounts of basophilic, focally vacuolated cytoplasm. Cell fragments (arrows) and apoptotic cells (arrowheads) were excluded from the cell count. Samples were obtained at control (**A**), 500 (**B**), 1,000 (**C**), 4,000 (**D**), 7,500 (**E**), and 15,000 (**F**) cut rates. [All images: Hematoxylin-eosin stain, 400×].

however, this occurs with in vivo vitreous biopsy as well. In our methodology, three independent vitrectomy specimens were obtained for each cut rate. We found significant variability in the diagnostic yield at each cut rate, which we believe reflects the underlying heterogeneity inherent to vitreous biopsy in in vitro and real-world environments. This variability may limit statistical strength in identifying cut rate differences, thus future efforts should aim to repeat and confirm these findings with a greater sample size.

Our study's main focus was on the viability and integrity of PVRL cells with 25g vitrectomy at various cut rates. Although cytologic assessment remains the cornerstone of PVRL diagnosis, ancillary methods such as immunohistochemistry, *MYD88* mutation studies, immunoglobulin gene rearrangement studies, interleukin levels, and flow cytometry have gained increasing importance in PVRL diagnosis.[15] Except for flow cytometry, cellular viability and integrity are not as vital for diagnostic yield and accuracy of these other ancillary methods.

Our results suggest that 25g vitrectomy systems can be employed using 15,000 cpm without compromising the viability and integrity of lymphoma cells or PVRL diagnosis. In vivo study design and in vitro studies recreating a closer representation of an ocular environment will be crucial to better understand the possible implications of using a high vitrectomy cut rate on cell viability and morphology. Studies evaluating the effect of various vitrectomy protocols on the diagnostic yield of ancillary methods used in PVRL diagnosis will also provide valuable information.

Key words: retina, primary vitreoretinal lymphoma, diagnosis, biopsy, vitrectomy, ocular pathology, cytology.

References

1. Levasseur SD, Wittenberg LA, White VA. Vitreoretinal lymphoma: a 20-year review of incidence, clinical and cytologic features, treatment, and outcomes. JAMA Ophthalmol 2013;131:50.
2. Jiang T, Zhao Z, Chang Q. Evaluation of cytologic specimens obtained during experimental vitreous biopsy using B-cell lymphoma line. Eur J Ophthalmol 2014;24:911–917. doi.
3. Cassoux N, Merle-Beral H, Leblond V, et al. Ocular and central nervous system lymphoma: clinical features and diagnosis. Ocul Immunol Inflamm 2000;8:243–250. doi.
4. Rodriguez EF, Sepah YJ, Jang HS, et al. Cytologic features in vitreous preparations of patients with suspicion of intraocular lymphoma. Diagn Cytopathology 2014;42:37–44.
5. Sato T, Emi K, Bando H, Ikeda T. Faster recovery after 25-gauge microincision vitrectomy surgery than after 20-gauge vitrectomy in patients with proliferative diabetic retinopathy. Clin Ophthalmol 2012;6:1925–1930.
6. Kanavi MR, Soheilian M, Hosseini SB, Azari AA. 25-gauge transconjunctival diagnostic vitrectomy in suspected cases of intraocular lymphoma: a case series and review of the literature. Int J Ophthalmol 2014;7:577–581.
7. Teixeira A, Chong L, Matsuoka N, et al. Novel method to quantify traction in a vitrectomy procedure. Br J Ophthalmol 2010;94:1226–1229.
8. Teixeira A, Chong LP, Matsuoka N, et al. Vitreoretinal traction created by conventional cutters during vitrectomy. Ophthalmology 2010;117:1387–1392.e2.
9. Chen PL, Chen YT, Chen SN. Comparison of 27-gauge and 25-gauge vitrectomy in the management of tractional retinal detachment secondary to proliferative diabetic retinopathy. PLoS One 2021;16:1–2. doi.
10. Shahzidi S, Čunderlíková B, Więdłocha A, et al. Simultaneously targeting mitochondria and endoplasmic reticulum by photodynamic therapy induces apoptosis in human lymphoma cells. Photochem Photobiol Sci 2011;10:1773–1782.
11. Char DH, Ljung BM, Deschênes J, Miller TR. Intraocular lymphoma: immunological and cytological analysis. Br J Ophthalmol 1988;72:905–911. doi.
12. Ratanapojnard T, Roy CR, Gariano RF. Effect of vitrector cutting rate on vitreous biopsy yield. Retina 2005;25:795–797. doi.
13. de Oliveira PRC, Berger AR, Chow DR. Vitreoretinal instruments: vitrectomy cutters, endoillumination and wide-angle viewing systems. Int J Retin Vitr 2016;2:28.
14. Freeman LN, Schachat AP, Knox DL, et al . Clinical features, laboratory investigations, and survival in ocular reticulum cell sarcoma. Ophthalmology 1987;94:1631–1639. doi.
15. Sehgal A, Pulido JS, Mashayekhi A, et al . Diagnosing vitreoretinal lymphomas—an analysis of the sensitivity of existing tools. Cancers 2022;14:598Cancers.

SDC

THREE-DIMENSIONAL HEADS-UP VITRECTOMY VERSUS CONVENTIONAL MICROSCOPIC VITRECTOMY FOR PATIENTS WITH EPIRETINAL MEMBRANE

DONG JU KIM, MD,* DONG GEUN KIM, MD,‡ KYU HYUNG PARK, MD, PHD*†

Purpose: To investigate the efficacy and safety of 3D heads-up display (3D-HUD) vitrectomy compared with conventional microscopy (CM) vitrectomy in epiretinal membrane (ERM) surgery.

Methods: Epiretinal membrane removal with or without internal limiting membrane (ILM) peeling was performed using a 3D-HUD or CM system. The mean changes in best-corrected visual acuity (BCVA) and in central macular thickness (CMT) and postoperative complications were assessed.

Results: Baseline demographics were comparable except for the follow-up period. Both BCVA and CMT improved at the final visit (all $P < 0.05$). The ERM recurrence and dissociated optic nerve fiber layer (DONFL) rates were lower in the 3D group (both $P < 0.05$). conventional microscopic vitrectomy (odds ratio [OR] = 12.86, $P = 0.02$) and absence of ILM peeling (OR = 45.25, $P < 0.05$) were associated with ERM recurrence. In the DONFL, CM vitrectomy (OR = 1.98, <0.05) and combined phacovitrectomy (OR = 2.33, $P = 0.03$) were analyzed as risk factors for DONFL.

Conclusion: The improvement in BCVA and CMT in ERM surgery using a 3D-HUD is comparable with that of CM vitrectomy, with a significantly low rate of ERM recurrence and DONFL occurrence. Therefore, 3D vitrectomy might have an advantage for ERM surgery.

RETINA 43:1010–1018, 2023

The latest advances in vitrectomy platforms provide a remarkable level of performance through their technologies, leading vitreoretinal surgeons to achieve successful vitreoretinal surgery.[1–3] Technology development has been performed in various surgical systems, including small-gauge (G) sclerotomy, high-speed vitreous cutter, intraoperative optical coherence tomography (OCT), and three-dimensional heads-up display (3D-HUD) systems. Among these advanced technologies, 3D-HUD has led to a drastic change in the visualization of intraocular surgery compared with conventional microscopy (CM). The image displayed on a high-definition monitor through a high dynamic range camera observed with passive polarized 3D glasses enables a stereoscopic surgical view with greater sharpness and contrast.[4,5] Improved magnification and extended depth of field allow for specific distinction of the complex posterior anatomy of the eyeball, which eventually leads to minimal tissue manipulation. By digital amplification of a high dynamic range camera and providing personalized color and light temperature, only a minimal endoillumination level is required during surgery.[6] Because the endoilluminator light is directed to the retina without a natural barrier of the anterior ocular structures, minimal endoillumination of 3D-HUD can potentially reduce the risk of phototoxicity.[7] Considering the above strengths

From the *Department of Ophthalmology, Seoul National University Bundang Hospital, Seongnam, South Korea; †Department of Ophthalmology, Seoul National University College of Medicine, Seoul National University Hospital, Seoul, South Korea; and ‡Department of Ophthalmology, Inje University College of Medicine, Inje University Busan Paik Hospital, Busan, South Korea.

This study was supported by the National Research Foundation of Korea (NRF) grant funded by the Korean government (MSIP) (No. 2020R1A2C2011189). The funding organization had no role in the design or performance of this study.

The authors have no proprietary interest in the materials presented herein. All authors attest that they meet the current ICMJE criteria for authorship.

Supplemental digital content is available for this article. Direct URL citations appear in the printed text and are provided in the HTML and PDF versions of this article on the journal's Web site (www.retinajournal.com).

Reprint requests: Kyu Hyung Park, Department of Ophthalmology, Seoul National University Hospital, Seoul National University College of Medicine, 101, Daehak-ro Jongno-gu, Seoul, 03080, South Korea; e-mail: jiani4@snu.ac.kr

of 3D-HUD, it has become more popular as a treatment option for various vitreoretinal diseases.[8,9] Several studies have investigated the surgical outcomes and complications after 3D-HUD vitrectomy compared with CM vitrectomy.[10–12] However, most previous studies were targeting only a small number of population or comparing various vitreoretinal diseases at once, which might be unable to show the actual benefit of 3D-HUD vitrectomy over CM vitrectomy. This study aimed to compare the clinical outcomes and postoperative complications between 3D-HUD vitrectomy and CM vitrectomy for epiretinal membrane (ERM) surgery in a relatively large population.

Materials and Methods

Patient Consent and Clinical Data Collection

A retrospective chart review was performed on 839 consecutive patients with ERM who underwent ERM surgery by a single experienced vitreoretinal surgeon (K.H.P.) between January 1, 2015, and November 30, 2021, at Seoul National University Bundang Hospital (SNUBH). Since the introduction of the NGENUITY 3D visualization system (Alcon Laboratories, Fort Worth, TX) to SNUBH in January 2018, almost all vitrectomies have been performed using a 3D visualization system. A total of 534 eyes of 513 patients with idiopathic ERM with follow-up periods longer than 3 months were enrolled in this study. Patients were excluded if any evidence suggested secondary ERM, high myopia (spherical equivalent ≥ -6.00 D or axial length ≥ 26 mm), a coexisting ocular disease affecting visual or anatomical function, and a history of intraocular surgery except cataract surgery. The details of the patient selection process are shown in Figure 1. This study was approved by the Institutional Review Board of SNUBH (IRB No.: B-2202-736-102) and conducted in accordance with the tenets of the Declaration of Helsinki.

Surgical Procedures

All ERM surgeries were performed by a single experienced vitreoretinal surgeon (K.H.P.) using a 25-G transconjunctival sutureless pars plana vitrectomy (PPV) platform (Constellation, Alcon Laboratories, Fort Worth, TX) and the contact lens system (Hoya Corp, Tokyo, Japan). Phacoemulsification with intraocular lens implantation was performed before vitrectomy in patients with visually disturbing cataracts. End-grip forceps (GRIESHABER; Alcon Inc, Fort Worth, TX) were used to remove the membrane. Internal limiting membrane (ILM) peeling was performed using preservative-free triamcinolone acetonide (Maqaid, Wakamoto Pharmaceutical Co, Ltd, Tokyo, Japan) to enhance the visualization of ILM. If necessary, triamcinolone acetonide was used several times to identify the layer of membrane. Topical antibiotics (0.5% levofloxacin, Culevox; Taejoon, Seoul, South Korea), antiinflammatory drops (prednisolone acetate, Pred Forte; Allergan Inc, Irvine, CA), and cycloplegic drops (homatropine, Homapine; Hanlim Pharm, Seoul, South Korea) were administered postoperatively. The surgical procedure was the same for each system except for the surgical settings. For the 3D-HUD group, the NGENUITY 3D visualization system was used as the surgical viewing platform. A 3D surgical camera was connected to a surgical microscope (OPMI LUMERA 700 surgical microscope, Carl Zeiss Ag, Jena, Germany), and the camera was set at 40% of its iris aperture (ICM5 A; Alcon Laboratories, Fort Worth, TX). The surgeon and his assistants wore passive 3D polarized glasses, and 3D OLED displays (55 inches, 3840 × 2160 resolution, OLED55E6P, LG Ltd, Seoul, South Korea) were positioned at approximately 1.0 to 1.2 m from the surgeon. The endoillumination level was set to 10% for ERM surgery. For the CM group, all the surgical procedures were performed under the same vitrectomy platform and surgical microscope, looking through the ocularis of the microscope. The endoillumination intensity of the CM group was set to 30% in all surgeries.

Ophthalmic Examination

After ERM surgery, patient visits were scheduled regularly at 1 day, 1 week, and 1, 4, 10, and 22 months. All patients underwent complete ophthalmologic examinations during the preoperative and postoperative visits. Ophthalmic examinations included best-corrected visual acuity (BCVA) measurement using the Snellen chart, slit-lamp examination, intraocular pressure measurement with a noncontact tonometer (KT-500 automated tonometer, Kowa Co, Ltd, Tokyo, Japan), and indirect ophthalmoscopy. The axial length was measured in all patients with the IOL master 500 or IOL master 700 (Carl Zeiss Meditec Inc, Jena, Germany). For comparison before and after ERM surgery, fundus photographs and OCT images were obtained from all patients for each follow-up. Spectral domain OCT (SD-OCT) (SPECTRALIS; Heidelberg Engineering, Heidelberg, Germany) with an eye-tracking system and automatic software was used to scan the same location for each follow-up. A 25-line raster scan of the SPECTRALIS was included in the analysis. Infrared reflectance images were simultaneously evaluated to confirm the

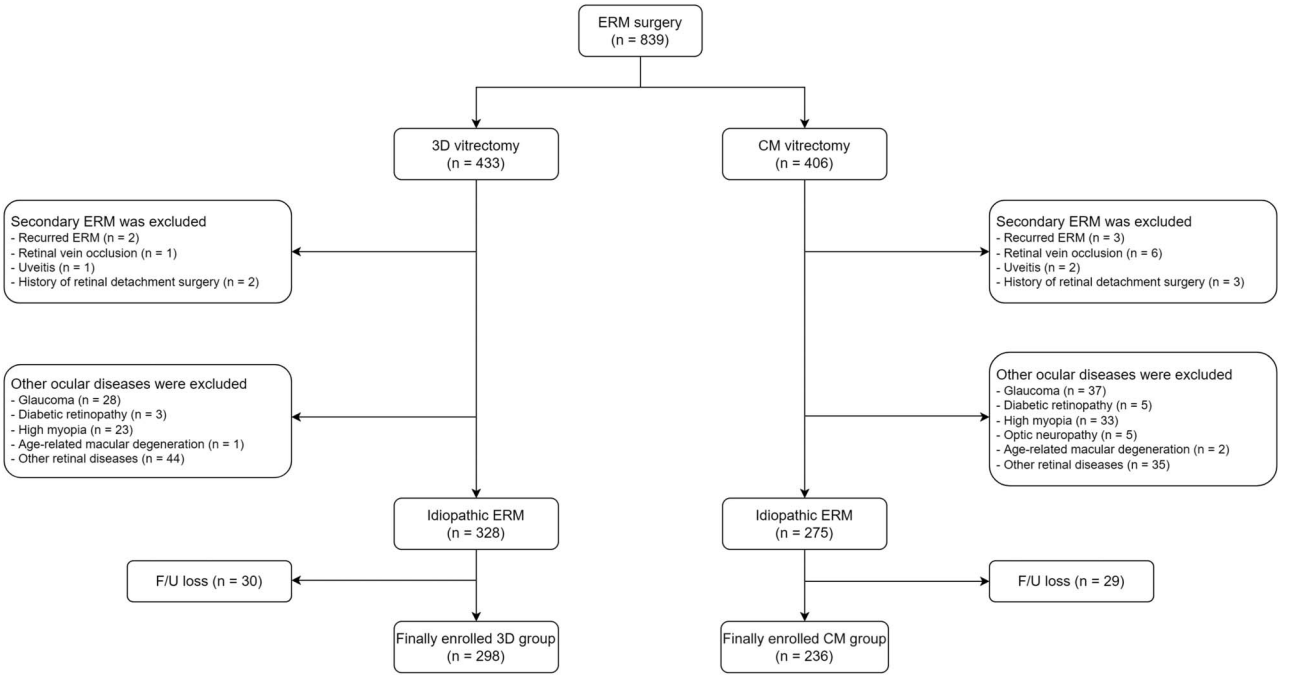

Fig. 1. Flowchart of the study population selection showing the inclusion and exclusion criteria used for patient selection. The number of enrolled patients was described through the process.

location and position of the 25-line raster scans. The central macula was measured using a circular map analysis protocol.

Epiretinal membrane evaluation was performed based on fundus photographs and OCT images at each follow-up. Baseline ERM severity was graded according to OCT images based on Govetto et al.[13] ERM recurrence, dissociated optic nerve fiber layer (DONFL), and swelling of the arcuate nerve fiber layer (SANFL) were assessed independently using fundus photographs and OCT images. Epiretinal membrane recurrence was defined as the reappearance of the removed membrane after ERM surgery or the proliferation of residual ERM.[14–16] Appearance of DONFL was measured with photographs and OCT images acquired at 4 months postoperatively. A DONFL appearance was observed as numerous arcuate retinal striae running along the optic nerve fibers in the macular area on fundus photograph, which correlated with the number of focal dimples on the retinal surface on OCT.[17,18] The presence of SANFL was determined in the infrared image 1 week after ERM surgery. Swelling of the arcuate nerve fiber layer is characterized by transient dark arcuate striae radiating from the optic nerve after ILM peeling (Figure 2).[19] All images were evaluated by two independent observers (D.J.K. and D.G.K.) with blinded clinical information, and the senior supervisor (K.H.P.) adjudicated the discrepancy between the two observers. The Cohen kappa coefficient was used to measure the agreement between the interobservers (D.J.K. and D.G.K.) in SANFL, DONFL, and ERM recurrence. There was high concordance between the two observers with a correlation coefficient ($\kappa = 0.93$ for SANFL, $\kappa = 0.88$ for DONFL, and $\kappa = 0.87$ for ERM recurrence). Microstructural integrity of the outer retina including the external limiting membrane (ELM), interdigitation zone (IZ), and ellipsoid zone (EZ) was also assessed based on the SD-OCT images. Outer retinal defect was defined if there was a defect in each layer within 1,000 μm of the central fovea on horizontal or vertical OCT images taken within 4 months postoperatively (Supplementary Figure 1, http://links.lww.com/IAE/B926).

Evaluation of Efficacy and Safety

The primary outcome used for evaluating efficacy was based on changes in the mean BCVA and improvement in central macular thickness after surgery. The secondary outcome was to analyze surgical complications to ensure safety. The factors associated with postoperative complications were ERM recurrence, SANFL, DONFL, endophthalmitis, rhegmatogenous retinal detachment, postoperative hidden retinal tears, ocular hypertension, cystoid macular edema (CME), iatrogenic macular hole or retinoschisis, sterile inflammation, and defect of outer retinal layer.

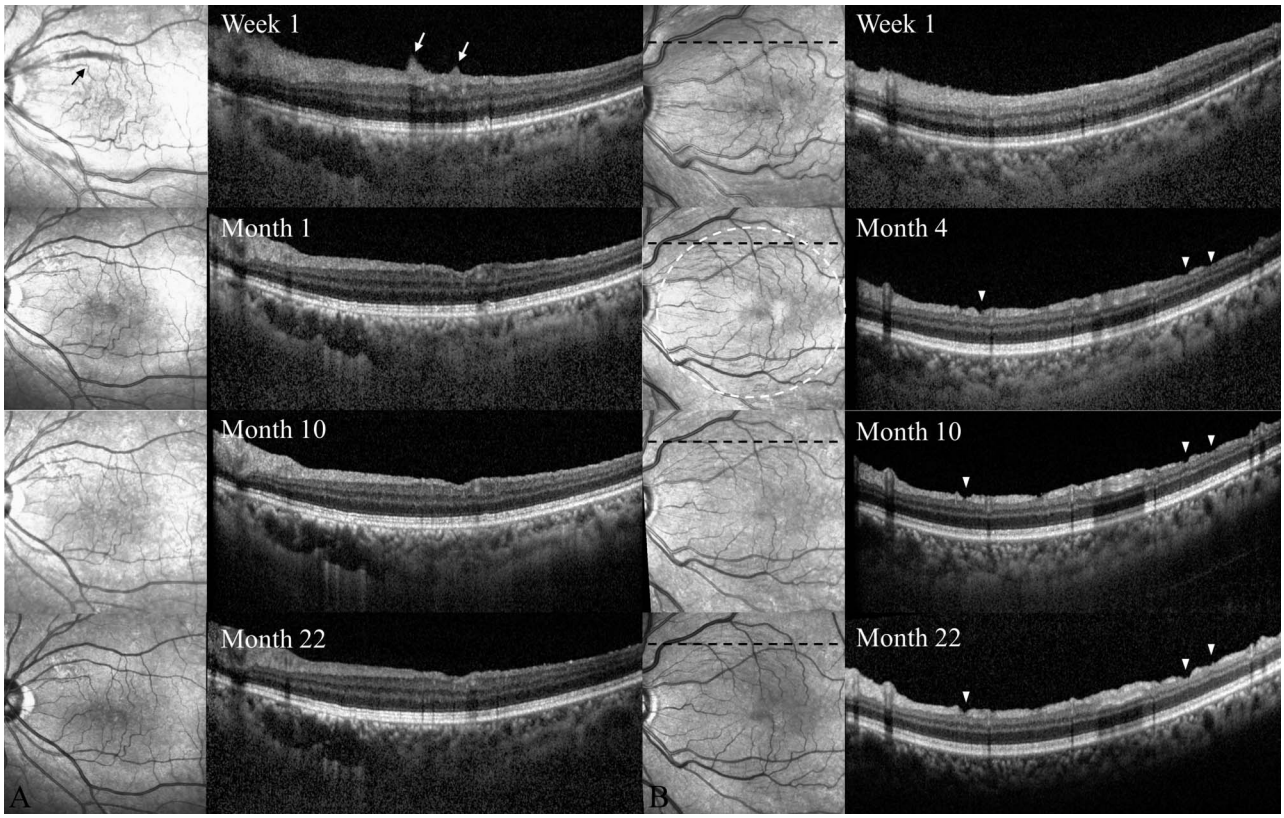

Fig. 2. Representative case of SANFL and DONFL appearance on infrared (IR) and OCT images. **A.** Representative case of SANFL; IR image represented multiple dark striae along with nerve fiber layer (black arrow), and corresponding OCT showed edema of nerve fiber layer at week 1 (white arrows). After 1 month of ERM surgery, multiple dark striae on the IR image and edema of the nerve fiber layer on the OCT image totally disappeared. **B.** Representative case of DONFL; IR and OCT image 1 week after ERM surgery showed no definite arcuate retinal striae and focal dehiscence. IR image 4 months after surgery showed numerous arcuate retinal striae running along the nerve fibers in the macular area (white dotted circle), which is consistent with focal dehiscence (white arrowheads) on corresponding OCT. These new findings remained until 22 months after surgery.ERM, epiretinal membrane; DONFL, dissociated optic nerve fiber layer; SANFL, swelling of the arcuate nerve fiber layer.

Statistical Analyses

Descriptive statistics were calculated for patient demographics and clinical characteristics. Continuous data are described as mean ± SD, and categorical data are reported as frequencies and percentages. All statistical analyses were performed using SPSS Statistics for Windows, version 23 (SPSS Inc, Chicago, IL). Before statistical analysis, the normality of the distribution of data was assessed using the Kolmogorov–Smirnov test or Shapiro–Wilk test. An independent *t*-test was used to compare parametric data. For nonparametric data, the Mann–Whitney *U* test was used. Categorical data were analyzed using chi-squared tests and linear-by-linear association or Fisher exact tests. The Wilcoxon signed-rank test was performed to compare various parameters before and after surgery. Linear mixed models were applied to investigate the difference in longitudinal trends in BCVA, CMT, intraocular pressure (IOP), and spherical equivalent (SE) between the two groups, where group, time, and group × time were included as fixed factors. Logistic regression analysis was performed to identify the factors related to postoperative complications. Statistical significance was set at $P < 0.05$.

Results

Demographics and Clinical Characteristics

The clinical characteristics of the patients, including 298 eyes of 290 patients in the 3D vitrectomy group and 236 eyes of 223 patients in the conventional microscopy (CM) group, are summarized in Table 1. The mean follow-up period was significantly longer in the CM group than in the 3D group. Except for the follow-up period, baseline characteristics were not different between the two groups, including male/female ratio, laterality, age, initial visual acuity, initial IOP, initial SE, axial length, lens status, and prevalence of underlying disease (hypertension and diabetes mellitus). The baseline characteristics of the ERM and

Table 1. Demographics and Baseline Characteristics

Variable	3D Vitrectomy (n = 298)	Conventional Vitrectomy (n = 236)	*P*
Age	63.48 ± 10.14	64.87 ± 8.38	0.09*
Sex (male:female)	102:196	82:154	0.90†
Laterality (right:left)	160:138	120:116	0.51†
Initial VA (logMAR)	0.22 ± 0.23 [approximate Snellen equivalent 20/33]	0.24 ± 0.23 [approximate Snellen equivalent 20/34]	0.76*
Initial IOP	10.51 ± 2.66	10.55 ± 2.71	0.86*
Initial SE (Diopter)	0.26 ± 1.89	0.34 ± 1.80	0.61*
Axial length (mm)	23.59 ± 0.90	23.56 ± 0.89	0.67*
Diabetes (%)	34 (11.4%)	19 (8.1%)	0.19†
Hypertension (%)	101 (33.9%)	74 (31.4%)	0.54†
Lens status (phakia:pseudophakia)	267:31	203:33	0.21†
Follow-up period (month)	14.47 ± 9.03	18.34 ± 8.49	0.00*

Values are described as mean ± SD unless otherwise indicated.
*Independent *t*-test.
†Chi-square test; *P* value <0.05 was considered significant.
VA, visual acuity; IOP, intraocular pressure; SE, spherical equivalent.

surgical factors are summarized in Table 2. Baseline central macular thickness, operation time (PPV only and combined phacovitrectomy), ERM stage, outer retinal defect, and type of surgery were balanced between the two groups. The incidence of ILM peeling was significantly higher in the 3D vitrectomy group ($P < 0.05$).

Postoperative Outcomes

All surgeries were successfully performed without intraoperative complications. Postoperative BCVA at each follow-up period was improved compared with baseline in both groups (all $P < 0.05$) (Figure 3). No significant difference was observed in BCVA between the two groups during the follow-up (all $P > 0.05$). To exclude the effect of cataracts on postoperative visual outcomes, we additionally analyzed only patients with pseudophakia to investigate changes in visual acuity. No significant differences were observed between the 3D and CM groups during the follow-up period (all $P > 0.05$) (Supplementary Figure 2, http://links.lww.com/IAE/B927). The postoperative CMTs significantly decreased at each visit compared with baseline (all $P < 0.05$) in both groups, and the CMTs were not significantly different between the groups at any period (all $P > 0.05$, Figure 4).

Table 2. Baseline Characteristics of ERM and Surgical Factors

Variable	3D Vitrectomy (n = 298)	Conventional Vitrectomy (n = 236)	*P*
Central macular thickness	448.54 ± 91.69	434.87 ± 77.43	0.73*
PPV:combined surgery	157:141	134:102	0.35†
Operation time (min)			
PPV only	30.70 ± 6.56	29.55 ± 6.44	0.99*
Combined surgery	45.79 ± 9.25	46.47 ± 7.23	0.65*
ILM peeling	285 (95.6%)	193 (81.8%)	0.00†
ERM stage			0.05‡
1	4 (1.3%)	6 (2.5%)	
2	22 (7.4%)	33 (14.0%)	
3	174 (58.4%)	131 (55.5%)	
4	38 (12.8%)	24 (10.2%)	
Lamellar hole	60 (20.1%)	42 (17.8%)	
Outer retinal defect			
ELM defect	4 (1.3%)	1 (0.4%)	0.27†
EZ defect	6 (2.0%)	11 (4.7%)	0.08†
IZ defect	24 (8.1%)	17 (7.2%)	0.71†

Values are described as mean ± SD unless otherwise indicated.
*Independent *t*-test.
†Chi-square test.
‡Linear-by-linear association; *P* value <0.05 was considered statistically significant.
ELM, external limiting membrane; ERM, epiretinal membrane; EZ, ellipsoid zone; ILM, internal limiting membrane; IZ, interdigitation zone; PPV, pars plana vitrectomy.

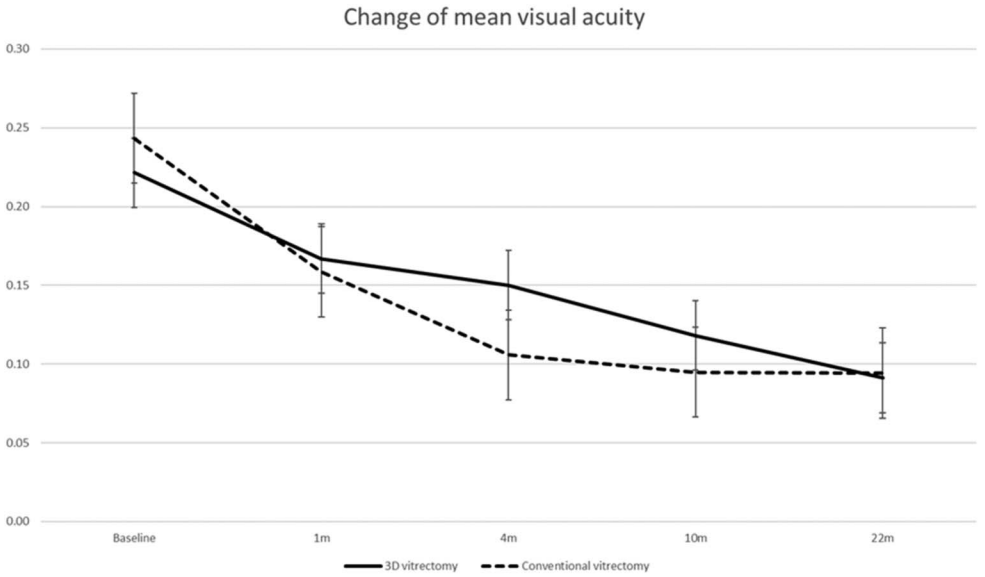

Fig. 3. Changes in mean visual acuity after epiretinal membrane surgery in both groups.

The incidence of postoperative complications, except DONFL and ERM recurrence, was not significantly different between the two groups (Supplementary Table 2, http://links.lww.com/IAE/B931). The incidence of DONFL and recurrence rate 1 year after surgery were significantly higher in the CM group (both, $P < 0.05$) (Supplementary Table 2, http://links.lww.com/IAE/B927). The recurrence rate of ERM was analyzed 1 year after surgery because of the difference in the follow-up period between the two groups. The recurrence rate of ERM for 1 year after surgery was higher in the CM group than in the 3D group [61 (31.8%) vs 14 (7.9%), $P < 0.05$].

Owing to the differences in the frequencies of ILM peeling, a subanalysis was performed in patients who performed ILM peeling in both groups (Supplementary Table 1, http://links.lww.com/IAE/B930). The incidence of DONFL and ERM recurrence was also significantly higher in the CM group than in the 3D vitrectomy group ($P < 0.05$ and $P < 0.05$, respectively). Logistic regression analyses were performed to identify surgical and demographic factors associated with the development of DONFL and ERM recurrence. Factors associated with ERM recurrence were identified using a conventional microscope (OR = 12.86, $P = 0.02$) and the absence of ILM peeling (OR =

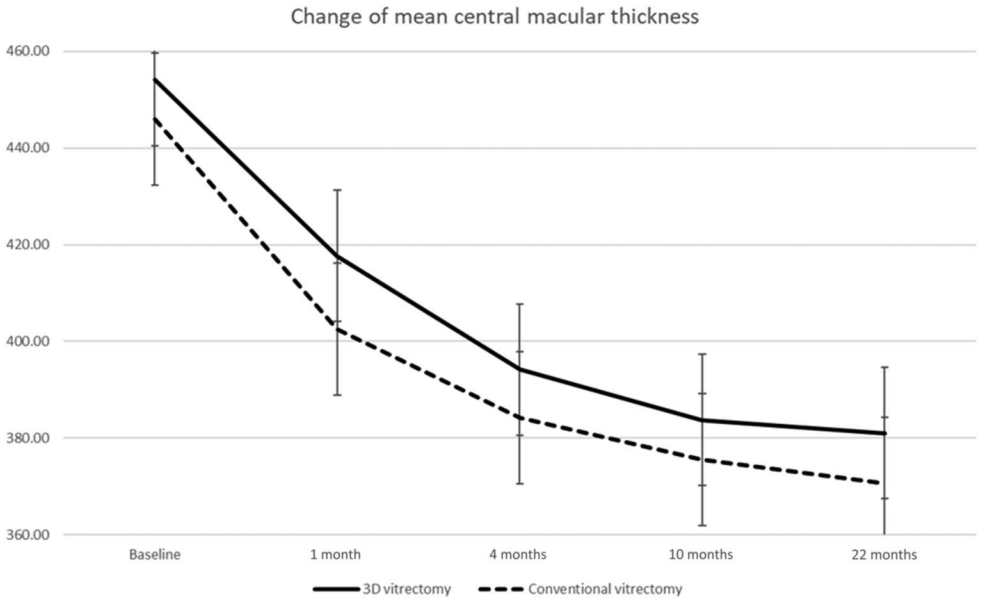

Fig. 4. Changes in central macular thickness after epiretinal membrane surgery in both groups.

Table 3. Logistic Regression Analysis of Risk Factors for ERM Recurrence

Variable	Adjusted OR	95% CI	P*
SANFL	0.30	0.07–4.46	0.14
DONFL	0.56	0.07–4.46	0.58
Device (conventional vitrectomy)	12.86	1.60–103.14	0.02
Sex (male)	0.47	0.14–1.51	0.20
Age	1.03	0.94–1.13	0.47
Diabetes	0.71	0.11–4.50	0.72
Hypertension	0.71	0.18–2.71	0.61
Laterality (right)	0.66	0.21–2.13	0.49
Best-corrected VA	1.91	0.14–26.64	0.63
Intraocular pressure	1.06	0.84–1.33	0.65
Spherical equivalent	0.80	0.57–1.13	0.21
Central macular thickness	0.99	0.99–1.00	0.29
ERM Grade 1	1.00 (ref)		
ERM Grade 2	1.21	0.03–53.62	0.92
ERM Grade 3	0.81	0.02–41.37	0.92
ERM Grade 4	0.43	0.00–69.23	0.74
Lamellar hole	0.17	0.00–11.24	0.41
Axial length	0.66	0.29–1.49	0.32
PPV or combined PPV (PPV)	0.95	0.12–7.49	0.96
Operation time	0.99	0.92–1.09	0.96
Follow-up period	1.08	0.99–1.09	0.21
Lens status (phakia)	0.29	0.03–2.55	0.23
ELM defect	0.00	0.00	1.00
EZ defect	0.31	0.05–1.81	0.19
IZ defect	0.59	0.15–2.44	0.47
ILM peeling (ILM peeling [-])	45.25	16.36–125.17	0.00

*Logistic regression analysis; *P* value <0.05, considered statistically significant.

DONFL, dissociated optic nerve fiber layer; ELM, external limiting membrane; ERM, epiretinal membrane; EZ, ellipsoid zone; ILM, internal limiting membrane; ; IZ, interdigitation zone; PPV, pars plana vitrectomy; SANFL, swelling of arcuate nerve fiber layer; VA, visual acuity.

45.25, $P < 0.05$) (Table 3). The development of DONFL correlated with the use of CM (OR = 1.98, $P < 0.05$) and combined phacovitrectomy (OR = 2.33, $P = 0.03$) (Table 4).

Discussion

This study demonstrated that clinical outcomes, including improvement in visual acuity and retinal thickness, were comparable between 3D-HUD vitrectomy and CM vitrectomy for ERM in a cohort of 534 eyes. One interesting finding of postoperative complications was that the recurrence rate and incidence of DONFL were significantly lower in the 3D-HUD group. The recurrence rate of ERM could vary depending on how the study defines ERM recurrence due to the ability of imaging modalities for ERM. This study adopted the definition of ERM recurrence based on SD-OCT images, which are more sensitive in detecting ERM recurrence than fundus photography.[14] Based on SD-OCT for ERM recurrence, the recurrence rate at 1 year was 14 (7.9%) in the 3D-HUD group and 61 (31.8%) in the CM group. Because of the discrepancy in ERM recurrence between the two groups, we aimed to identify the factors associated with ERM recurrence. Logistic regression analysis showed that CM and the absence of ILM peeling were associated with ERM recurrence. Even in the subanalysis including only patients who underwent ILM peeling, the recurrence rate was significantly lower in the 3D group than in the CM group [10 (5.9%) vs. 40 (25.2%), $P < 0.05$]. According to previous studies on ERM recurrence, ERM recurrence is related to factors such as residual ERM (or incomplete ERM removal), absence of ILM peeling, and surgical trauma, which could be potential sources of fibrocellular proliferation.[20–22] The digital image processing of a 3D-HUD system delivers enhanced visualization and magnification without loss of resolution. This improved surgical view may have enabled the surgeon to perform a less traumatic and more complete removal of the ERM, resulting in a difference in ERM recurrence. We also found that 3D-HUD reduces the incidence of not SANFL but DONFL. Swelling of the arcuate nerve fiber layer is the earliest and transient postoperative inner retinal alteration,[19] whereas DONFL is relatively late onset (approximately 1 month after surgery) and appears as multiple striae or dimples on the inner

Table 4. Logistic Regression Analysis of Risk Factors for Development of DONFL

Variable	Adjusted OR	95% CI	P*
Recurrence	0.84	0.12–5.59	0.86
SANFL	6.39	0.04–10.98	0.99
Device (conventional vitrectomy)	1.98	1.25–3.14	0.00
Sex (male)	1.12	0.66–1.89	0.68
Age	1.01	0.98–1.04	0.38
Diabetes	0.94	0.38–2.34	0.89
Hypertension	0.70	0.40–1.22	0.21
Laterality (right)	1.28	0.79–2.06	0.30
Best-corrected VA	1.76	0.60–5.12	0.30
Intraocular pressure	0.97	0.88–1.06	0.46
Spherical equivalent	0.95	0.81–1.12	0.56
Central macular thickness	0.99	0.99–1.00	0.35
ERM Grade 1	1.00 (ref)		
ERM Grade 2	1.33	0.23–7.74	0.75
ERM Grade 3	1.29	0.25–6.55	0.76
ERM Grade 4	1.79	0.27–11.91	0.54
Lamellar hole	2.24	0.43–11.68	0.34
Axial length	0.78	0.61–1.00	0.05
PPV or combined PPV (combined PPV)	2.33	1.11–4.89	0.03
Operation time	0.96	0.93–1.00	0.05
ILM peeling (ILM peeling [-])	0.51	0.08–3.20	0.47
Lens status	0.74	0.29–1.85	0.52
ELM defect	0.00	0.00	0.99
EZ defect	1.23	0.54–2.78	0.62
IZ defect	0.59	0.34–1.04	0.07
Follow-up period	0.97	0.94–1.00	0.13

*Logistic regression analysis; *P*-value <0.05, considered statistically significant.

DONFL, dissociated optic nerve fiber layer; ELM, external limiting membrane; ERM, epiretinal membrane; EZ, ellipsoid zone; ILM, internal limiting membrane; IZ, interdigitation zone; PPV, pars plana vitrectomy; SANFL, swelling of the arcuate nerve fiber layerVA, visual acuity.

retinal surface.[23] However, the pathogenesis of SANFL and DONFL seems related to Müller cell footplate trauma during ILM peeling.[18,24] Nevertheless, SANFL is likely to occur because of direct surgical trauma to the retinal nerve fiber layer during ILM peeling, and unlike SANFL, trauma to the end plates of Müller cells could change the arrangement of the nerve fiber layer, resulting in DONFL. In this study, ILM peeling was performed more frequently in the 3D vitrectomy group, but no statistically significant difference was observed in the incidence of SANFL between the two groups. However, the incidence of DONFL was much higher in the CM group than in the 3D-HUD group [62 (26.3%) vs 54 (18.1%), $P = 0.02$]. The discrepancies in postoperative ERM and DONFL occurrence rates between the two groups might be because less traumatic surgery was attributed to the 3D-HUD system. Moreover, CM vitrectomy, a risk factor associated with the incidence of DONFL, supports this suggestion. However, there was no difference in postoperative photoreceptor integrity, including ELM, EZ, and IZ, depending on the viewing system.

In all 3D cases, ERM surgery was successfully performed at a 10% endoillumination level. Power, duration of exposure, and proximity are known to be associated with the risk of retinal phototoxicity.[7,25,26] The operative time was comparable between the two groups in this study. Thus, low endoillumination levels could reduce the thermal and chemical injuries caused by phototoxicity. Several studies have also reported a similar possibility of reducing phototoxicity using 3D-HUD.[7,11,27] In addition to the advantage of visualization of the 3D-HUD, improved surgical ergonomics might also contribute to reducing surgical trauma and later complications.[9,11]

This study had several limitations that need to be addressed in future studies. First, the retrospective study design had an inborn possibility of selection bias that might affect the results of this study. Second, there was a discrepancy in the timing of surgery between the two groups. Before January 2018, all ERM surgeries were performed using a conventional microscope. After the introduction of NGENUITY in January 2018, almost all ERM surgeries have been performed using NGENUITY. The learning curves may have

affected the surgical outcomes; however, these seemed to be minimal because the surgical procedure of a single experienced surgeon (K.H.P.) for ERM surgery has not changed over the past 10 years. This is the first study to show the potential surgical benefit of the 3D visualization system compared with CM in ERM surgery with the largest sample sizes to date.

In conclusion, the visual outcome and improved central macular thickness were comparable between 3D-HUD and CM for ERM surgery. For postoperative complications, ERM recurrence and incidence of DONFL were significantly higher in the CM group. The benefits of the 3D-HUD system, such as lower endoillumination, higher magnification, and resolution, may reduce these postoperative complications. Therefore, vitrectomy with a 3D-HUD for ERM surgery may have advantages relative to conventional microscopic vitrectomy.

Data Statement

The data sets generated and/or analyzed during this study are available from the corresponding author on reasonable request.

Key words: 3D heads-up display, epiretinal membrane, macular surgery, operating microscope.

Acknowledgments

Evaluation of outer retinal layer was performed by Seung Woo Choi, Young Hoon Jung, Seok Hyun Bae, and Dong Ju Kim.

References

1. Oravecz R, Uthoff D, Schrage N, Dutescu RM. Comparison of modern high-speed vitrectomy systems and the advantages of using dual-bladed probes. Int J Retin Vitr 2021;7:8–12.
2. Murray TG, Layton AJ, Tong KB, et al. Transition to a novel advanced integrated vitrectomy platform: comparison of the surgical impact of moving from the Accurus vitrectomy platform to the Constellation Vision System for microincisional vitrectomy surgery. Clin Ophthalmol 2013;7:367–377.
3. Lin X, Apple D, Hu J, Tewari A. Advancements of vitreoretinal surgical machines. Curr Opin Ophthalmol 2017;28:242–245.
4. Freeman WR, Chen KC, Ho J, et al. Resolution, depth of field, and physician satisfaction during digitally assisted vitreoretinal surgery. Retina 2019;39:1768–1771.
5. Ehlers JP, Uchida A, Srivastava SK. The integrative surgical theater combining intraoperative optical coherence tomography and 3d digital visualization for vitreoretinal surgery in the discover study. Retina 2018;38:S88–S96.
6. Agranat JS, Miller JB, Douglas VP, et al. The scope of three-dimensional digital visualization systems in vitreoretinal surgery. Clin Ophthalmol 2019;13:2093–2096.
7. Adam MK, Thornton S, Regillo CD, et al. Minimal endoillumination levels and display luminous emittance during three-dimensional heads-up vitreoretinal surgery. Retina 2017; 37: 1746–1749.
8. Eckardt C, Paulo EB. Heads-up surgery for vitreoretinal procedures an experimental and clinical study. Retina 2016; 36:137–147.
9. Romano MR, Cennamo G, Comune C, et al. Evaluation of 3D heads-up vitrectomy: outcomes of psychometric skills testing and surgeon satisfaction. Eye 2018;32:1093–1098.
10. Asani B, Siedlecki J, Schworm B, et al. 3D heads-up display vs. Standard operating microscope vitrectomy for rhegmatogenous retinal detachment. Front Med 2020;7:615515.
11. Kantor P, Matonti F, Varenne F, et al. Use of the heads-up NGENUITY 3D visualization system for vitreoretinal surgery: a retrospective evaluation of outcomes in a French tertiary center. Sci Rep 2021;11:10031–10111.
12. Zhang T, Tang W, Xu G. Comparative analysis of three-dimensional heads-up vitrectomy and traditional microscopic vitrectomy for vitreoretinal diseases. Curr Eye Res 2019;44: 1080–1086.
13. Govetto A, Lalane RA, Sarraf D, et al. Insights into epiretinal membranes: presence of ectopic inner foveal layers and a new optical coherence tomography staging scheme. Am J Ophthalmol 2017;175:99–113.
14. Joon Ahn S, Joon Woo S, Hyung Park K. Recurrence of idiopathic epiretinal membrane and its predisposing factors an optical coherence tomography study. Retina 2021;41:516–524.
15. Sandali O, El Sanharawi M, Basli E, et al. Epiretinal membrane recurrence. Retina 2013;33:2032–2038.
16. Fleissig E, Zur D, Moisseiev E, et al. Five-year follow-up after epiretinal membrane surgery. Retina 2018;38:1415–1419.
17. Steel DHW, Dinah C, White K, Avery PJ. The relationship between a dissociated optic nerve fibre layer appearance after macular hole surgery and Muller cell debris on peeled internal limiting membrane. Acta Ophthalmol 2017;95:153–157.
18. Tadayoni R, Paques M, Massin P, et al. Dissociated optic nerve fiber layer appearance of the fundus after idiopathic epiretinal membrane removal. Ophthalmology 2001;108:2279–2283.
19. Clark A, Balducci N, Pichi F, et al. Swelling of the arcuate nerve fiber layer after internal limiting membrane peeling. Retina 2012;32:1608–1613.
20. Gandorfer A, Haritoglou C, Scheler R, et al. Residual cellular proliferation on the internal limiting membrane in macular pucker surgery. Retina 2012;32:477–485.
21. Schechet SA, DeVience E, Thompson JT. The effect of internal limiting membrane peeling on idiopathic epiretinal membrane surgery, with a review of the literature. Retina 2017;37:873–880.
22. Azuma K, Ueta T, Eguchi S, Aihara M. Effects of internal limiting membrane peeling combined with removal of idiopathic epiretinal membrane. Retina 2017;37:1813–1819.
23. Ito Y, Terasaki H, Takahashi A, et al. Dissociated optic nerve fiber layer appearance after internal limiting membrane peeling for idiopathic macular holes. Ophthalmology 2005;112:1415–1420.
24. Spaide RF. Dissociated optic nerve fiber layer appearance" after internal limiting membrane removal IS inner retinal dimpling. Retina 2012;32:1719–1726.
25. van den Biesen PR. Endoillumination during vitrectomy and phototoxicity thresholds. Br J Ophthalmol 2000;84:1372–1375.
26. Youssef PN, Sheibani N, Albert DM. Retinal light toxicity. Eye 2011;25:1–14.
27. Talcott KE, Adam MK, Sioufi K, et al. Comparison of a three-dimensional heads-up display surgical platform with a standard operating microscope for macular surgery. Ophthalmol Retina 2019;3:244–251.

Modified Intrascleral Fixation for Repositioning the Dislocated Single-Piece, Rigid PMMA Intraocular Lens

Purpose: To describe a modified intrascleral fixation technique for repositioning single-piece rigid polymethyl methacrylate intraocular lenses (IOLs).

Methods: Four patients with dislocated IOLs were enrolled. Surgical modifications included using ≤1-mm scleral incision for haptic externalization, placing the IOL haptic placement in scleral tunnels, and using 8-0 absorbable sutures. Patients were followed up for 6 months with routine ophthalmic examinations, corneal endothelial cell counts, and ultrasound biomicroscopy (UBM).

Results: The mean follow-up time was 13.5 ± 5.45 months. The IOL was well centered and the spherical refraction improved (+10.25 ± 2.21 vs. −0.81 ± 1.59 D, $P < 0.05$), whereas the best-corrected visual acuity (pre 20/43 Snellen, 0.42 ± 0.33 logarithm of the minimum angle of resolution equivalent and post 20/36 Snellen, 0.31 ± 0.22 logarithm of the minimum angle of resolution equivalent; $P = 0.235$), intraocular pressure (pre 13.8 ± 3.21, post 13.55 ± 5.14 mmHg), corneal endothelium density (pre 2,423.8 ± 279.6/mm^2, post 2,280.25 ± 350.7/mm^2), and total astigmatism (pre −1.94 ± 0.43, post −1.69 ± 0.59 D) remained unchanged. The average horizontal and vertical IOL tilt was 0.33 ± 0.22° and 0.81 ± 0.38°, respectively. Intraocular lens decentration was 0.10 ± 0.03 mm horizontally and 0.13 ± 0.06 mm vertically.

Conclusion: The modified intrascleral fixation technique shows encouraging midterm results in patients with dislocated single-piece, rigid polymethyl methacrylate IOLs. Larger samples and longer follow-up are required to confirm the outcomes of this technique.

RETINA 43:1019–1023, 2023

Intraocular lens (IOL) dislocations induce severe visual disturbances in patients and pose management challenges for ophthalmologists.[1] Single-piece, rigid polymethyl methacrylate (PMMA) IOLs have been used in cataract surgery for decades, and their dislocation is reported in ophthalmic practice.[2] Many techniques have been developed to reposition dislocated IOLs, but few are applicable to one-piece rigid IOLs. Lyu J et al described an ab externo scleral suture fixation technique using a single-armed 10-0 polypropylene suture to reposition the dislocated one-piece rigid IOL.[2] However, suture breakdown or erosion remains concerning.[3] This study proposes a modified intrascleral fixation technique for repositioning single-piece, rigid PMMA IOLs and demonstrates surgical success in four patients.

Methods

Four patients were consecutively enrolled and treated by a single retina specialist (C.H.J.) between July 2018 and February 2019. Best-corrected visual

From the *Department of Ophthalmology and Vision Science, Eye and ENT Hospital, Fudan University, Shanghai, People's Republic of China; and †Key Laboratory of Myopia of State Health Ministry, and Key Laboratory of Visual Impairment and Restoration of Shanghai, Shanghai, People's Republic of China.

Publication of this article was supported, in part, by research grants from the National Key R&D Program of China (2017YFC0108200) and the Shanghai Committee of Science and Technology (16140901000, 13430710500 and 15DZ1942204).

None of the authors have any conflicting interests to disclose.

Y. Zong and K. Wu contributed equally to the work presented here.

Supplemental digital content is available for this article. Direct URL citations appear in the printed text and are provided in the HTML and PDF versions of this article on the journal's Web site (www.retinajournal.com).

Reprint requests: Chunhui Jiang, PhD, Department of Ophthalmology and Vision Science, Eye and ENT Hospital, Fudan University, 83 Fenyang Road, Shanghai 200031, People's Republic of China; e-mail: chhjiang70@163.com

acuity, slit-lamp biomicroscopy, dilated fundus examination by indirect ophthalmoscopy, refraction by a autorefractor, intraocular pressure (IOP) by a noncontact tonometer; axial length by IOLMaster (version 3.01; Carl Zeiss Meditec, Jena, Germany), and corneal endothelial density by a noncontact specular microscope (Topcon America Corp, Paramus, NJ) were performed preoperation and postoperation. Spherical equivalent was calculated as the spherical diopter (D) plus one-half of the cylindrical dioptric power. Relevant ocular and systemic history was collected.

Postoperatively, the patients were examined at 1 day, 1 week, 1 month, 3 months, and 6 months, and the following data were recorded. IOL decentration and tilt were measured using Pentacam HR (Oculus Optikgeräte GmbH, Wetzlar, Germany) by one of the coauthors (K.C.W.) according to the method previously described.[4] Intraoperative and postoperative complications were also documented.

Surgical Technique

After a retrobulbar block, the pupil was dilated, and standard three-port 23-gauge (23 G) pars plana incisions were made. Subsequently, nasal and temporal limbal peritomies, as well as limbal incisions at the superior nasal and temporal quadrants were made, and the anterior chamber was filled with viscoelastic (DisCoVisc; Alcon Laboratories, Inc, Fort Worth, TX). The haptic floating in the vitreous cavity was freed from vitreous traction by vitreous cutter (Figure 1A) and was externalized through the limbal incision using a 23 G vitreous forceps. Thus, the IOL was stabilized. With deep scleral indentation, peripheral vitrectomy was performed, and the other haptic—often attached to the vitreous base around the inferior pars plana—was assessed for integrity and was fully mobilized. Using a 500 μm accurate depth knife (BD Atomic Edge, Dickinson and Co, Inc, Franklin Lakes, NJ), two 5 mm long grooves were made 3 mm from and parallel to the nasal and temporal limbus. These grooves were then extended toward the limbus for approximately 1 mm, and two slim scleral flaps were made using a crescent-shaped knife (Beaver Xstar; Dickinson and Company, Inc, Franklin Lakes, NJ) (Figure 1B). Two 23 G scleral incisions placed 180° apart were made under the flaps approximately 2 mm from the limbus. Both haptics was then externalized through these incisions using two vitreous forceps and the hand-shaking technique (Figure 1, C and D). With a banded 25 G needle, two scleral tunnels parallel to the limbus and away from the 23 G scleral incision were also made at the other end of the flap, approximately 3-4 mm apart from the incision (Figure 1E). The two haptics were placed into these tunnels and care was taken to achieve IOL centration. Using 8-0 suture (Vicryl; Ethicon Inc, Somerville, NJ) and deep bite beneath the haptics, the scleral flap was closed, and the haptics were fixed with two separate sutures (Figure 1F). After fundus examination, conjunctival incisions were closed with 8-0 sutures (see **Video**, **Supplemental Digital Content 1**, http://links.lww.com/IAE/B251). Postoperatively, topical prednisolone acetate, levofloxacin, and pranoprofen were used for a month.

Results

Four patients (mean age: 48.0 ± 12.03 years) were enrolled, and the mean time since IOL implantation was 14.0 ± 8.29 years. The mean follow-up time was 13.5 ± 5.45 months. Two patients had ocular trauma, and one patient had secondary glaucoma that was controlled with four antiglaucoma eye drops. The mean axial length was 24.44 ± 1.04 mm (Table 1).

The average operative time for IOL repositioning was 27.88 ± 10.22 minutes. The patients' uncorrected visual acuity improved, pre 20/286 Snellen (1.36 ± 0.48 logarithm of the minimum angle of resolution [logMAR] equivalent) to post 20/87 Snellen (0.66 ± 0.13 logMAR equivalent; $P < 0.05$), equal to 35 Early Treatment Diabetic Retinopathy Study letters. Throughout the follow-up period, the glaucoma patient maintained his IOP with four topical antiglaucoma medications. In addition, one case had transient corneal edema that subsided with one-week topical prednisolone use, whereas another case experienced pupillary capture of IOL optic one week after the repositioning surgery; this was successfully treated with pupillary dilation and supine positioning. No other complications were recorded intraoperatively or postoperatively.

The spherical refraction improved from +10.25 ± 2.21 D at baseline to −0.81 ± 1.59 D at the last follow-up time ($P < 0.05$), whereas the best-corrected visual acuity (pre 20/43 Snellen, 0.42 ± 0.33 logMAR equivalent and post 20/36 Snellen, 0.31 ± 0.22 logMAR equivalent; $P = 0.235$), IOP (pre 13.8 ± 3.21 mmHg, post 13.55 ± 5.14 mmHg; $P = 0.181$), corneal endothelial density (pre 2,423.8 ± 279.6/mm^2, post 2,280.25 ± 350.7/mm^2; $P = 0.212$), and total astigmatism (pre −1.94 ± 0.43 D, post −1.69 ± 0.59 D; $P = 0.353$) remained unchanged (Table 2). The IOL was well positioned at the last follow-up time (see **Figure 2A**, **Supplemental Digital Content 2**, http://links.lww.com/IAE/B252, Table 3). The average horizontal and vertical IOL tilt was 0.32 ± 0.22° and 0.

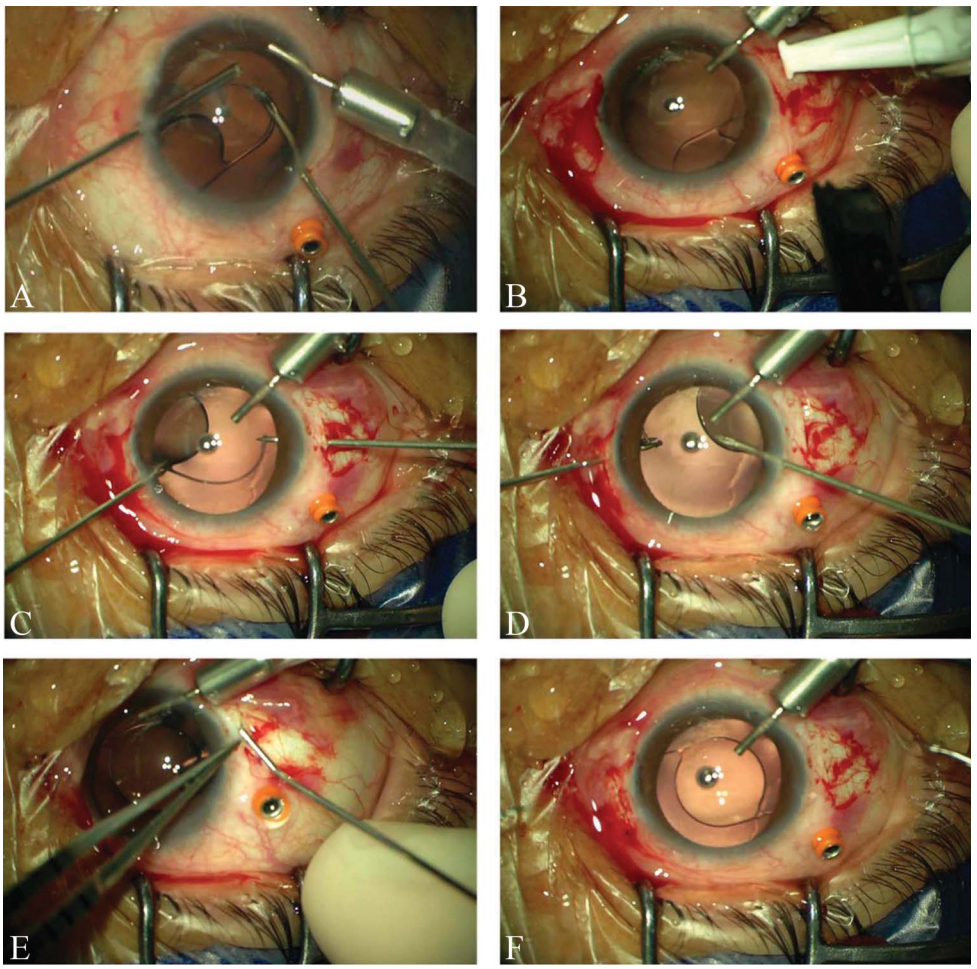

Fig. 1. Surgical steps. **A.** After vitreous removal, the haptic floating in the vitreous was released from traction. **B.** Using a 500 μm accurate depth knife (BD atomic Edge, Dickinson and Company, Franklin Lakes, NJ), two 5 mm long grooves, 3 mm from and parallel to the limbus were made in the nasal and temporal sclera. **C** and **D.** Both haptics were externalized through the 23 G scleral incision under the flap with two vitreous forceps using the hand-shaking technique. **E.** With a banded 25 G needle, two scleral tunnels were made under the other end of the flap, parallel to the limbus. **F.** Both haptics were placed into scleral tunnels, and care was taken to achieve IOL centration.

81 ± 0.38°, respectively. IOL decentration was 0.10 ± 0.03 mm horizontally and 0.13 ± 0.06 mm vertically. Ultrasound biomicroscopy confirmed that the haptics were well positioned in the sclera (see **Figures 2B and 2C**, **Supplemental Digital Contents 2**, http://links.lww.com/IAE/B252).

Discussion

We describe a modified surgical technique for the treatment of dislocated single-piece PMMA IOLs. The procedure is efficacious with reduced incision size, intraocular maneuvers, and less surgical trauma. At the 6-month follow-up, all patients had a quiet , with no increase in baseline IOP, and the IOLs were well positioned.

Management of the posteriorly dislocated IOL was first described by Stark et al,[5] and since then, many surgical techniques have been proposed. The current surgical technique has several advantages. First, it requires a small surgical incision (≤1 mm) consisting of a limbal side port and a 23 G scleral incision. Whereas with other techniques, the IOL extraction or haptic externalization requires a larger incision.[6] The disadvantage of large incisions include increased surgical astigmatism,[7] endothelial cell loss, and intraocular tissue prolapse.[8] In our cases, the mean corneal astigmatism did not change significantly after the procedure, and the average corneal endothelium cell loss was approximately 9.17%.

Second, we adopted intrascleral fixation. This technique was proposed by Gabor SG and others,[9] whereas Agarwal introduced a similar surgical procedure, the glued IOL.[10] Both techniques demonstrated safety and have gained global popularity. A well-recognized advantage of this present technique is optimal IOL positioning.[11] During surgery, the IOL position could be adjusted by pulling the two haptics out or inserting them into the scleral tunnels. Thus, the IOL position is determined by the two intrascleral haptic fragments along a plane, rather than the two suture points used in the traditional scleral suture fixation technique. In geometry, two points determine a line,

Table 1. Individual Patient Characteristics

Patient	Age, years	Gender	Laterality	Axial Length, mm	IOL Implantation to Repositioning, years	Follow-up Time, months	Risk Factor for Zonular Defect
Case 1	63	Male	Left	23.48	10	6	Unknown
Case 2	41	Female	Left	25.89	24	17	Trauma
Case 3	36	Male	Left	24.00	17	18	Trauma
Case 4	52	Male	Right	24.38	5	13	Unknown

and a minimum of three points determine a plane. Scharioth et al[12] and Teichmann[13] had suggested that incarcerating a longer part of the haptic should stabilize the axial position of the posterior chamber IOL and decrease the incidence of IOL tilt. Our results also support the theory. The scleral suture fixation technique of IOL or haptics externalization with encircling suture placement is a more complex surgical maneuver. Technically, intrascleral fixation is less time demanding, and the average surgical time (27.8 minutes) supports the efficiency of the modified technique.

We used intrascleral fixation for single-piece, rigid PMMA IOL dislocation in contrast to the previously reported three-piece IOL procedures. Therefore, specific techniques were modified. First, we externalized the haptics through the scleral incision and then inserted it in the scleral tunnel, which was 3-4 mm away from the externalization incision. In the laboratory, we also used single-piece, rigid PMMA IOLs (EZE-55, Bausch & Lomb, Rochester, NY) for testing this step, during which the haptic tip was bent slightly. However, bending the very tip of the haptic increased the chances of haptic fracture (see **Video**, **Supplemental Digital Content 3**, http://links.lww.com/IAE/B253). Therefore, we modified the scleral tunnel placement 3-4 mm away from the haptic externalization incision. Maher Saleh et al[14] reported such haptic breakage of three-piece IOLs during intrascleral implantation. Thus, haptic externalization and its insertion into the scleral tunnel require caution. Alternatively, the haptics can be placed under the flap and fixed with a proline suture, but suture-related complications may arise. In this study, we used absorbable 8-0 sutures; thus, no suture-related complications (erosion and exposure) occurred. The suture is absorbed within 56 to 70 days[15]; by then, the scleral flap and tunnel scars could hold the haptics in place. This was supported by the stable IOL positioning found by UBM during follow-up. In our cases, the position of the IOL was stable during the follow-up (all $P > 0.05$, see **Table 3**, **Supplemental Digital Content 4**, http://links.lww.com/IAE/B254). Thus, spontaneous IOL dislocation that commonly happens within the first month of intrascleral fixation[12] could be reduced by the modified suturing technique. On the other hand, complications such as conjunctival erosion and haptic exposures are reported with intrascleral fixation of three-piece IOLs. To reduce such complications, we used a 500 μm accurate depth knife to achieve a scleral flap of appropriate thickness and the combination of scleral flap and tunnel.

Many one-piece PMMA IOLs have almost identical designs; hence, we are unable to comment on the exact type of PMMA IOLs in our cases. However, because these IOLs are made of the same material and have a similar design, the technique described here may be generalized to most patients with dislocated single-piece PMMA IOLs. We also used this technique to reposition single-piece, rigid PMMA IOLs with eyelets (Alcon CZ70BD). With this technique, although the primary results were good, only one case has data with follow-up longer than 6 months. Therefore, more

Table 2. Comparison of Ocular Parameters Before Surgery and at the Last Follow-up Time After Surgery

	BCVA (Snellen)		BCVA (LogMAR)		Refraction (D)		IOP (mmHg)		ECD (Cells/mm^2)	
Case	Pre	Post	Pre	Post	Pre	Post	Pre	Post	Pre	Post
1	20/22	20/20	0.05	0	+9.75 DS −1.50 DC*75	−1.250 DS −1.75 DC*85	15	11.4	2,145	2,146
2	20/40	20/40	0.3	0.3	+8.75 DS −1.75 DC*80	−2.75 DS −1.25DC*80	17.1	21.0	2,732	2,794
3	20/133	20/50	0.8	0.4	+13.5 DS −2.00*85 DC	1.0 DS −1.25 DC*80	9.5	9.3	2,584	2,177
4	20/67	20/67	0.5	0.5	+9.00 DS −2.50 DC*10	−0.25 DS −2.50 DC*25	13.6	12.5	2,234	2,004

BCVA, best-corrected visual acuity; D, diopters; DS, diopter sphere; DC, diopter cylinder; ECD, endothelial cell density.

Table 3. Parameters of Intraocular Lens Position at the Last Follow-up Time

Case	H-IOL Decentration, mm	V-IOL Decentration, mm	H-IOL Tilt, Degree	V-IOL Tilt, Degree
1	0.1	0.05	0.0753	0.029
2	0.1069	0.1604	0.3774	0.8059
3	0.1444	0.1039	0.59	0.4494
4	0.0607	0.1974	0.2563	0.2346

H, horizontal; V, vertical.

cases and a longer follow-up period are required to determine if this technique could be used for IOLs with eyelets. Overall, the modified intrascleral fixation technique shows encouraging midterm results in patients with a dislocated single-piece, rigid PMMA IOL. However, larger samples and longer follow-up are required to confirm the outcomes of this technique.

Key words: dislocated IOL, IOL repositioning, intrascleral fixation, single-piece PMMA IOL.

YUAN ZONG, PHD†*
KAICHENG WU, MD†*
WANGYI FANG, MD†*
JIAN YU, MD†*
CHUNHUI JIANG, PHD†*
GEZHI XU, PHD†*

References

1. Mamalis N. Intraocular lens dislocation. J Cataract Refract Surg 2013;39:973–974.
2. Lyu J, Zhao PQ. Simplified ab externo fixation technique to treat late dislocation of scleral-sutured polymethyl methacrylate intraocular lenses. Eye 2016;30:668–672.
3. McAllister AS, Hirst LW. Visual outcomes and complications of scleral-fixated posterior chamber intraocular lenses. J Cataract Refract Surg 2011;37:1263–1269.
4. Zong Y, Wu K, Deng G, et al. Management of dislocated crystalline lens with vitrectomy, perfluorocarbon liquid, and phacoemulsification, combined with modified capsular tension ring and in-the-Bag intraocular lens implantation. Retina 2019 Apr 10. doi: 10.1097/IAE.0000000000002536.
5. Stark WJ, Michels RG, Bruner WE. Management of posteriorly dislocated intraocular lenses. Ophthalmic Surg 1980;11:495–497.
6. Kristianslund O, Råen M, Østern AE, et al. Late in-the-bag intraocular lens dislocation: a randomized clinical trial comparing lens repositioning and lens exchange. Ophthalmology 2017;124:151–159.
7. Eum SJ, Kim MJ, Kim HK. A comparison of clinical outcomes of dislocated intraocular lens fixation between in situ refixation and conventional exchange technique combined with vitrectomy. J Ophthalmol 2016;2016:5942687.
8. Gogate PM, Deshpande M, Wormald RP, et al. Extracapsular cataract surgery compared with manual small incision cataract surgery in community eye care setting in western India: a randomised controlled trial. Br J Ophthalmol 2003;87:667–672.
9. Gabor SG, Pavlidis MM. Sutureless intrascleral posterior chamber intraocular lens fixation. J Cataract Refract Surg 2007;33:1851–1854.
10. Agarwal A, Kumar DA, Jacob S, et al. Fibrin glue-assisted sutureless posterior chamber intraocular lens implantation in eyes with deficient posterior capsules. J Cataract Refract Surg 2008;34:1433–1438.
11. Shekhawat N, Goyal K. Sutureless glueless intrascleral fixation of posterior chamber intraocular lens: boon for aphakic. Indian J Ophthalmol 2017;65:1454–1458.
12. Scharioth GB, Prasad S, Georgalas I, et al. Intermediate results of sutureless intrascleral posterior chamber intraocular lens fixation. J Cataract Refract Surg 2010;36:254–259.
13. Teichmann KD, Teichmann IA. The torque and tilt gamble. J Cataract Refract Surg 1997;23:1433–1434.
14. Saleh M, Heitz A, Bourcier T, et al. Sutureless intrascleral intraocular lens implantation after ocular trauma. J Cataract Refract Surg 2013;39:81–86.
15. Al-Mubarak L, Al-Haddab M. Cutaneous wound closure materials: an overview and update. J Cutan Aesthet Surg 2013;6:178–188.

Glycerin-Assisted Vitreoretinal Surgery in Edematous Cornea

Purpose: To describe the use of glycerin in improving media clarity in cases with edematous cornea.

Methods: Retrospective case series including patients with posterior segment pathologies needing surgical invention and having corneal edema. Each case was studied for the role of topical application of glycerin instead of viscoelastic agents and the course of surgery. The cases were followed up for minimum 3 months duration.

Results: Six cases with corneal edema having posterior segment pathology underwent surgery with intraoperative topical application of glycerin. The corneal edema was seen to clear with progression of surgery and was maintained until the end of surgery. Procedures such as vitreoretinal surgery, identification of break, internal limiting membrane peeling, intraocular lens explantation, scleral indentation, Descemet stripping endothelial keratoplasty graft removal, and subretinal band removal could be performed in these cases.

Conclusion: Intraoperative glycerin use during vitreoretinal surgeries is helpful in improving the corneal clarity and maintaining it till the end of surgery.

RETINA 43:1024–1030, 2023

Visualization is one of the key factors to proceed with vitreoretinal surgery (VRSx). Lens and corneal clarity are important in this concern. Although lenticular involvement is easier to handle with planned or intraoperative cataract extraction, corneal involvement is a matter of concern. Corneal edema is one of the common factors and may be the result of previous surgery, poor endothelial count, inflammation, trauma, or corneal graft failure. It can impair the intraoperative view during VRSx, creating difficulty in surgery and increasing the chances of intraoperative complications. Various management options have its own set of problems and may hamper visual prognosis in long-term. Corneal edema is seen to be responsive to hyperosmolarity agents such as glycerin. Although few studies have demonstrated the efficacy of different strength of glycerol, none of the studies have evaluated the role of hyperosmotic agents intraoperatively.[1–5]

In this article, we describe a novel technique of using glycerin solution as a coupling agent during VRSx in eyes with corneal edema.

Methods

This is a retrospective record review of consecutive cases with posterior segment pathologies needing surgical intervention and having corneal edema causing difficult posterior segment visualization at a tertiary eye care center in North India over a period of 24 months (January 2017 to December 2018). The study is in accordance with the tenets of the Declaration of Helsinki and institutional guidelines for research. Informed consent was obtained from all the patients.

Surgical Technique

All eyes underwent 25-gauge pars plana vitrectomy (PPV) using constellation vision system (Alcon Inc., Fort

From the *Vitreo-retina, Trauma, and Uvea Services, All India Institute of Medical Sciences, New Delhi, India; †Dr. Rajendra Prasad Center for Ophthalmic Sciences, All India Institute of Medical Sciences, New Delhi, India; and ‡Cornea and Refractive Services, All India Institute of Medical Sciences, New Delhi, India.

Video presented at the FLORetina, Florence, Italy, 6th June, 2019.

None of the authors has any financial/conflicting interests to disclose.

Supplemental digital content is available for this article. Direct URL citations appear in the printed text and are provided in the HTML and PDF versions of this article on the journal's Web site (www.retinajournal.com).

The manuscript has been reviewed and approved by all named authors. The criteria for authorship have been met and each author believes that the manuscript represents honest work.

Reprint requests: Abhidnya Surve, MD, Vitreo-retinal, Trauma and Uvea Services, Dr. R.P. Centre for Ophthalmic Sciences, All India Institute of Medical Sciences, Ansari Nagar, New Delhi, India; e-mail: abhidnyasurve@gmail.com

Table 1. Characteristic of Each Case, Maneuvers Performed, and Follow-up

Case No.	Age/Sex	Previous Surgery	Cornea Status	Anterior Segment	Posterior Segment	Surgery	Maneuvers	Postoperative Retina Status (3rd month)	Further Management
1	60, Y/M	LE complicated cataract surgery	Corneal decompensation	Aphakia	Posteriorly dislocated IOL	PPV with IOL explantation	PPV, IOL explantation, and scleral indentation	Retina attached	Referred for optical PK with scleral fixated IOL
2	60, Y/M	RE complicated cataract surgery	Corneal decompensation	Aphakia	Posteriorly dislocated IOL	PPV with IOL explantation	PPV, IOL explantation, and scleral indentation	Retina attached	Referred for keratoplasty with scleral fixated IOL
3	40, Y/M	RE operated PK with cataract surgery with IOL; RE resuturing of posttraumatic graft dehiscence with IOL explantation	Failed graft	Aphakia and temporal peripheral anterior synechiae	Inferior RRD	VRSx	PPV, break identified, and laser barrage	Retina attached	Referred for keratoplasty
4	75, Y/F	RE operated aphakia with DSEK	Corneal decompensation	Pseudophakia	Posteriorly dislocated DSEK lenticule with CD	PPV with DSEK lenticule removal	PPV, DSEK lenticule removal, and scleral indentation	Retina attached	Underwent DSEK surgery
5	80, Y/M	RE cataract surgery; history of trauma	Corneal decompensation	Aphakia	Posteriorly dislocated IOL with RRD with CD	VRSx	PPV, choroidal drainage, IOL explant, break identified, ILM peeling, laser, and silicone oil injection	Retina attached	Silicone oil removal at 3 months. Referred for corneal management
6	61, Y/M	LE operated PK	Failed graft	Aphakia	Total RRD	VRSx	PPV, subretinal bands removal, scleral indentation, laser, and silicone oil injection	Retina attached	Silicone oil removal at 3 months. Referred for corneal management

LE, left eye; PK, penetrating keratoplasty; RE, right eye.

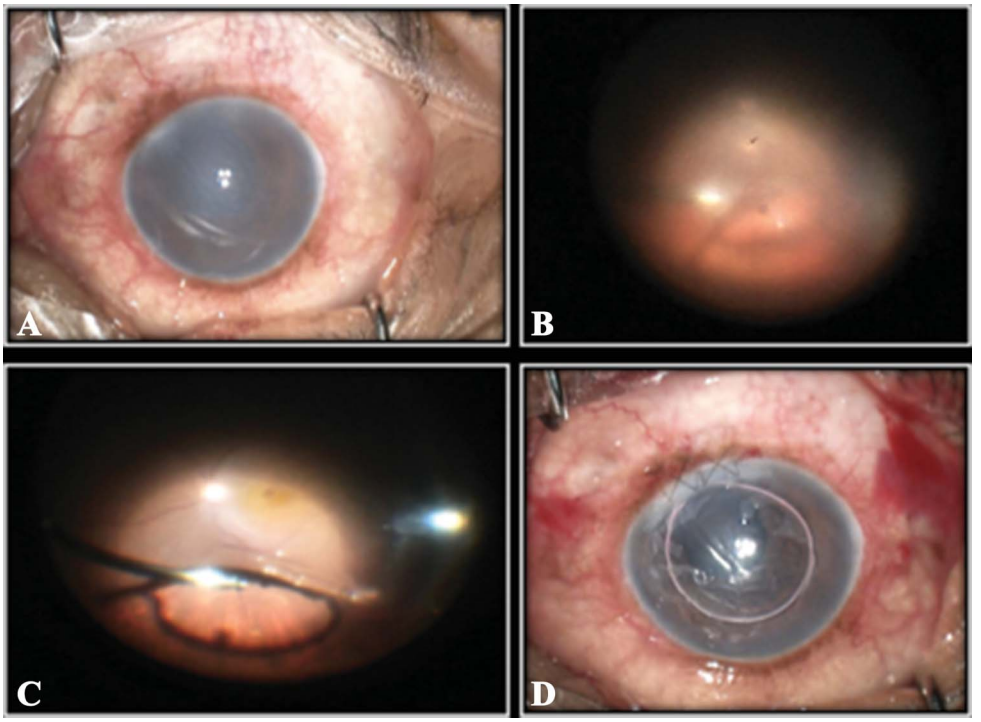

Fig. 1. A 60-year-old man had left eye corneal decompensation with aphakia and posteriorly dislocated IOL. The corneal edema (**A**) led to hazy visualization of the posterior segment (**B**). The epithelium was debrided, and glycerin was used instead of a usual viscoelastic agent leading to improvement in corneal clarity and posterior segment visualization (**C** and **D**). Core vitrectomy and posterior vitreous detachment induction were performed. Superotemporal entangled IOL was freed and removed through corneal incision.

Worth, TX) under peribulbar anesthesia. After sclerotomies were made and infusion was started, the corneal epithelium was debrided using a blunt cotton-tipped instrument. A wide-angle contact viewing system (Mini Quad XL, Volk Inc, United Kingdom) was used in all the surgeries. Instead of a viscoelastic agent (methyl cellulose), 50% glycerin was used as a coupling agent. The retinal view gradually improved in all cases over a period of 3 to 5 minutes, and required steps of posterior segment surgery were performed in each case depending on the pathology. A bandage contact lens was placed on the cornea at the end of surgery. Postoperatively the patients were prescribed topical antibiotic, steroid, and mydriatic-cycloplegic drugs. The patients were followed at day one, 1 week, 1 month, and 3 months after surgery.

Results

Six cases having corneal edema with posterior segment involvement were included in the study. The individual cases are described in detail below (Table 1). Four cases had corneal decompensation while two had a failed graft. Five cases were aphakic while one case was pseudophakic.

Case 1 and 2 had corneal decompensation with posterior dislocated intraocular lens (IOL) for which they underwent glycerin-assisted PPV with IOL explantation. The corneal edema led to hazy visualization of the posterior segment (Figure 1, A and B). The use of glycerin resulted in improvement of corneal clarity as the surgery proceeded and better visualization of the posterior segment (Figure 1, C and D). Core vitrectomy, triamcinolone-assisted posterior vitreous detachment induction, peripheral vitrectomy, and IOL explantation were performed. Scleral depression allowed us to screen for peripheral breaks.

Case 3 had a failed graft, aphakia, and inferior rhegmatogenous retinal detachment (RRD) involving the macula (Figure 2, A and B). After informed consent the patient underwent glycerin-aided VRSx. After vitrectomy, an inferior retinal break was noticed. Fluid–air exchange (FAX) following retinotomy, interface vitrectomy, and laser of break, retinotomy, and 360-degree barrage were performed (Figure 2, B–E). Two milliliters of 100% sulfur hexafluoride was injected in the end. The clarity of cornea had significantly improved by the end of surgery (Figure 2F).

Case 4 had corneal decompensation with aphakia, posteriorly dislocated Descemet stripping endothelial keratoplasty (DSEK) lenticule, and choroidal detachment (CD). She underwent glycerin-aided PPV where posterior segment visualization was initially hazy but had improved during the surgery (Figure 3, A–D). The DSEK lenticule was cut and aspirated with a vitrectomy cutter after vitrectomy (Figure 3B). The patient was subsequently referred back for further management of the cornea.

Case 5 had corneal decompensation with dislocated IOL, RRD, and CD (Figure 4, A and B). The patient underwent glycerin-aided PPV, with choroidal

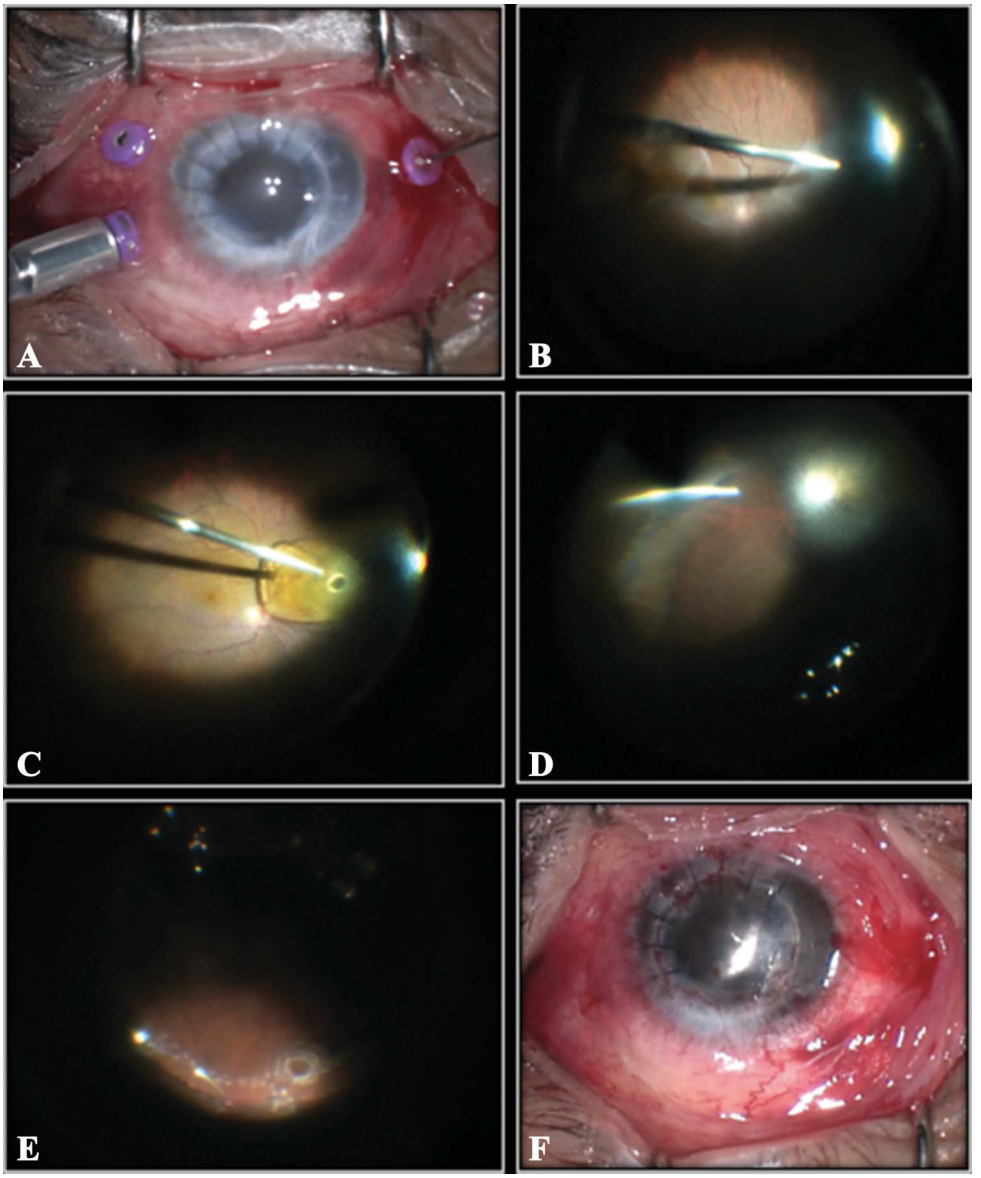

Fig. 2. A 40-year-old man with right eye optical penetrating keratoplasty with edematous cornea, aphakia, and inferior retinal detachment (**A**). Glycerin was applied topically after epithelial debridement. Core and peripheral vitrectomy were performed (**B**). An inferior retinal break was identified. After retinotomy, FAX and interface vitrectomy were performed (**C** and **D**). Break, retinotomy was lasered, and 360-degree laser barrage was performed (**E**). The clarity of cornea had significantly improved by the end of surgery (**F**).

drainage performed in the superotemporal area and IOL explanted through a corneal incision after limited anterior vitrectomy. After core and peripheral vitrectomy, an inferior break was identified (Figure 4, B and C). The internal limiting membrane (ILM) was stained with brilliant blue G and peeled using ILM forceps (Figure 4D). Retinotomy, FAX, and laser were performed (Figure 4E). Silicone oil was injected, and ports were closed. The cornea was remarkably clear at the end of surgery (Figure 4F).

Case 6 had a failed graft, aphakia, and total RRD. The cornea was hazy leading to difficulty in visualization of the posterior segment. The patient underwent glycerin-aided PPV where the corneal clarity improved as surgery proceeded. After core and peripheral vitrectomy, multiple subretinal bands were seen which were removed. On scleral depression, an inferotemporal break was noted. Retinotomy, FAX, and laser photocoagulation were performed. The cornea was significantly clear at the end of surgery. Silicone oil was injected, which was removed after 3 months, and patient was referred for management of the cornea (see **Video 1**, **Supplemental Digital Content 1**, http://links.lww.com/IAE/B267).

Discussion

Corneal clarity is of utmost importance for any VRSx. Corneal edema is one of the most common

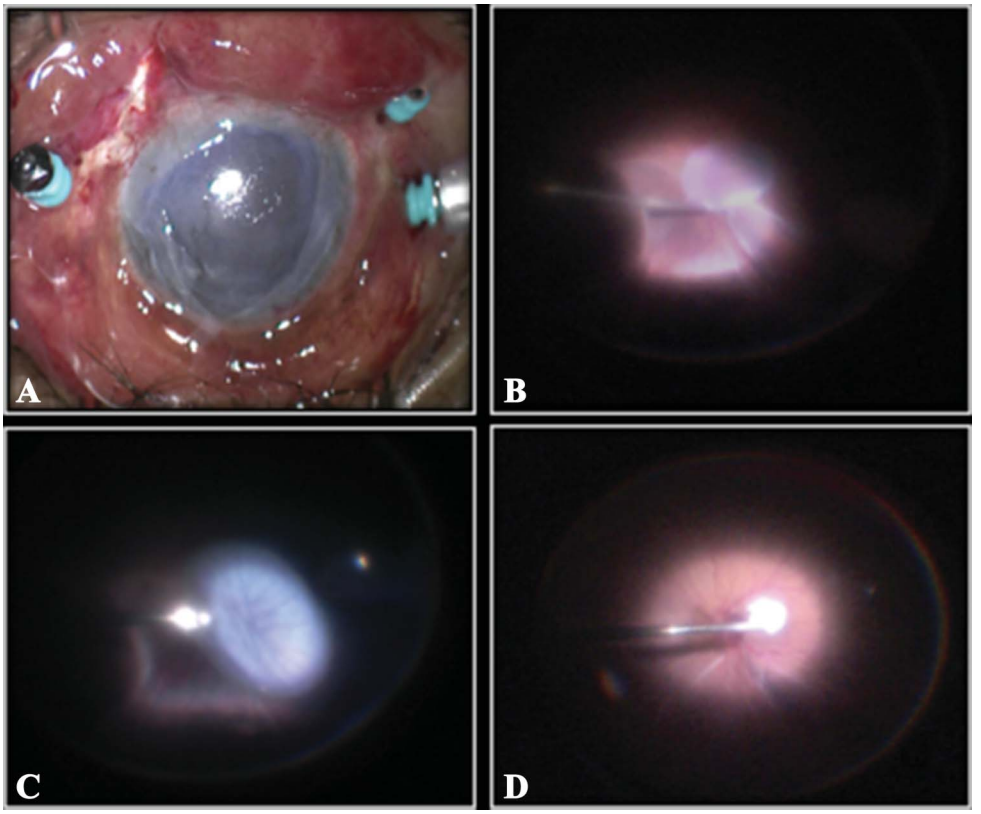

Fig. 3. A 75-year-old woman had right eye edematous cornea with aphakia, a posteriorly dislocated DSEK graft, and CD. The epithelium was debrided and glycerin was applied topically (**A**). The posterior segment visualization was initially hazy but improved during surgery (**B–D**). The DSEK lenticule was cut and aspirated with a vitrectomy cutter (**C**) after complete core and peripheral vitrectomy.

causes affecting it and can result from complicated surgeries, poor endothelial function, inflammation, or trauma. The presence of posterior segment pathologies requiring surgical intervention in such cases is challenging to manage. Management options include stabilization of cornea medically, keratoplasty followed by VRSx, temporary keratoprosthesis–assisted posterior segment surgery, or endoscopy-assisted VRSx. The selection of appropriate management depends on the urgency of posterior segment surgery, prognosis, and the availability of a corneal graft.

Medical treatment using hyperosmolar agents, corticosteroids, decreasing intraocular pressure, and keratoplasty procedures, such as DSAEK, requires time for a graft to clear, which may adversely affect the prognosis of vitreoretinal cases. Open sky vitrectomy, followed by graft placement was performed in the early era but was associated with multiple complications. Vitreoretinal surgery through a new graft also possesses challenges difficult to handle. The graft is rarely completely clear immediately after surgery, and manipulation of the globe during surgery especially passage of band or buckle, cryotherapy, or indentation to check for peripheral breaks may cause breakage of sutures. Also, they may not be able to sustain a high intraocular pressure used to stop intraocular bleeding. Performing peripheral vitrectomy and laser is difficult because of donor–host corneal junction, peripheral sutures, and corneal haze. The refractive error due to sutures could also lead to disturbances in the visualization. Also, performing VRSx within months of keratoplasty is associated with a high risk of graft failure. The surgical trauma, inflammation, and silicone oil–induced damage are the important related factors.[6]

Keratoprosthesis allows better visualization of the posterior segment, is easy to use, and provides good stereopsis but requires the availability of corneal tissue and a corneal surgeon. It is associated with complications, such as poor visual acuity, graft failure, proliferative vitreoretinopathy, and secondary glaucoma. Also, visualization of periphery is limited and requires scleral indentation for the same. The prismatic effect produced by the cylinder of lens, prolonged surgery, and the risk of graft failure are other limitations.[7,8] Endoscopy allows visualization of the posterior segment in cases with poor media. Its flexible probe allows for variable perspective, increased visualization up to anterior zonules, high magnification for better identification of retinal details, and safer globe manipulation. This makes the modality efficacious and safe but do have disadvantages, such as steep learning curve, absence of stereopsis, limited field of view,

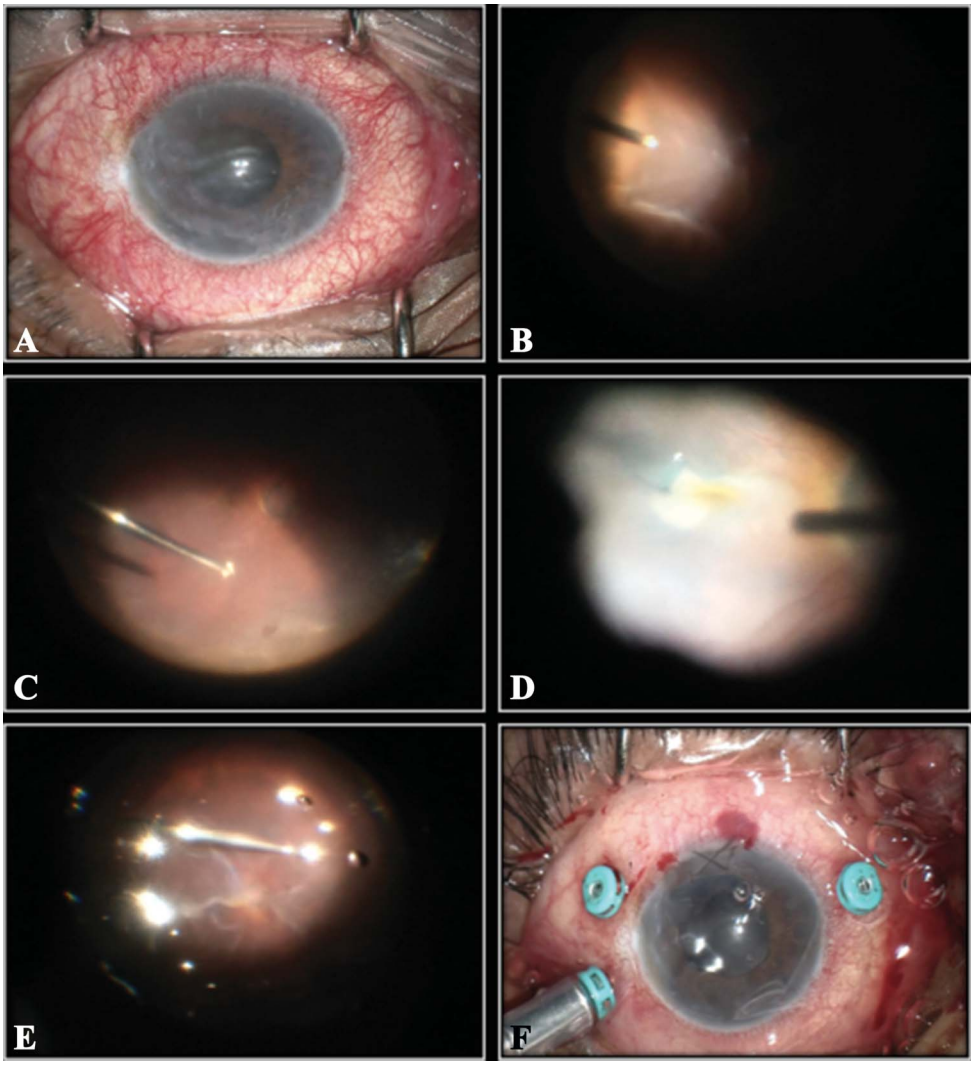

Fig. 4. An 80-year-old man had right eye corneal decompensation with dislocated IOL, retinal detachment, and CD (**A**). After choroidal drainage, limited anterior vitrectomy, and IOL explantation, corneal wound was closed. Core vitrectomy and peripheral vitrectomy were performed, and an inferior break was identified (**B** and **C**). The ILM was stained with brilliant blue G and peeled using ILM forceps (**D**). Retinotomy, FAX, and laser were performed (**E**). Silicone oil was injected at the end. The cornea was remarkably clear at the end of surgery (**F**).

inability to perform bimanual surgeries, and a high cost of system.[9,10]

Hyperosmolar agents, such as glycerin, are seen to be useful in corneal edema because of its osmotic effect. Clearing occurs within 30 to 40 seconds and lasts over several minutes. As it can cause irritation, application is advised after topical anesthesia.[11] It helps to improve corneal clarity in angle closure glaucoma for examination and performing peripheral iridotomy. Few studies have demonstrated the efficacy of different solution strength of glycerol.[1–5] Fifty percent glycerol solution was found to be most effective.[3,4] The application of glycerin over the cornea after epithelium debridement improved the cornea clarity significantly and allowed for posterior segment visualization. In our series, various procedures such as vitrectomy, posterior vitreous detachment induction, identification of breaks, IOL explant, DSEK graft removal, peripheral visualization using scleral indentation, ILM removal, subretinal band removal, and laser photocoagulation could be performed easily. No irritation was noted in any of the cases as the surgeries were performed under peribulbar anesthesia. Postoperatively the epithelial healing was complete in 3 to 5 days in all cases. Other subtle important steps to be considered during surgery include the placement of a wide-angle contact system without any undue pressure to prevent interference due to corneal striae. Keeping infusion pressure on the lower side prevents an increase in corneal edema.

Glycerin-assisted surgery allows vitrectomy and associated complex procedures without any extra cost or equipment. It has an effective action in a short period of time and does not depend on the availability of a corneal surgeon; thus, preventing any delay in the treatment of posterior segment pathology. Procuring cornea tissue is a major limiting factor in many developing nations, and optimum utilization of the available tissue is thus very important. This technique

allows for posterior segment management first, and then the anterior segment surgery can be performed later after stabilization. This reduces the risk of graft failure and may prevent wastage of tissue. The hyperosmolar agents used as topical drops does act through the epithelium and decrease the amount of corneal edema. In our cases, the epithelial removal gives some amount of added clarity, and postoperative epithelialization have occurred within a week in all cases. Hence, we have not tried this technique without epithelial removal. A contact widefield viewing system is used for surgery at our center. However, with intermittent use of glycerin on the cornea in the noncontact system, a similar grade of corneal clarity should be obtained. This technique may not be useful in cases where significant stromal scarring is present. It also requires experience on the part of the surgeon.

To conclude, intraoperative use of glycerin in cases with edematous cornea having posterior segment pathology is a simple and cost-effective method.

Key words: coupling agent, decompensated cornea, glycerin, visualization, vitreoretinal surgery.

VINOD KUMAR, MD†*
ABHIDNYA SURVE, MD†*
SUNEEL KUMAR, MD†*
SHORYA AZAD, MS†*
NAMRATA SHARMA, MD‡†

References

1. Payrau P, Dohlman CH. Medical treatment of corneal edema. Int Ophthalmol Clin 1968;8:601–610.
2. Cogan DG. Clearing of edematous corneas by glycerine. Am J Ophthalmol 1943;26:551.
3. Meyer W, Reinhardt H. Experimental investigations on the effect of glycerine and glucose solutions upon the corneal oedema [in German]. Albrecht Von Graefes Arch Klin Exp Ophthalmol 1971;181:216–227.
4. Bietti GB, Pecori-Giraldi J. Comparative animal experiment studies by means of new technical measuring procedures for the examination of the clearing-up effect of various osmotic substances in corneal edema [in German]. Klin Monbl Augenheilkd 1969;154:662–671.
5. Luxenberg MN, Green K. Reduction of corneal edema with topical hypertonic agents. Am J Ophthalmol 1971;71:847–853.
6. Noorily SW, Foulks GN, McCuen BW. Results of penetrating keratoplasty associated with silicone oil retinal tamponade. Ophthalmology 1991;98:1186–1189.
7. Roters S, Szurman P, Hermes S, et al. Outcome of combined penetrating keratoplasty with vitreoretinal surgery for management of severe ocular injuries. Retina 2003;23:48–56.
8. Garcia-Valenzuela E, Blair NP, Shapiro MJ, et al. Outcome of vitreoretinal surgery and penetrating keratoplasty using temporary keratoprosthesis. Retina 1999;19:424–429.
9. Marra KV, Yonekawa Y, Papakostas TD, Arroyo JG. Indications and techniques of endoscope assisted vitrectomy. J Ophthalmic Vis Res 2013;8:282–290.
10. Sabti KA, Raizada S. Endoscope-assisted pars plana vitrectomy in severe ocular trauma. Br J Ophthalmol 2012;96:1399–1403.
11. Lamberts DW. Topical hyperosmotic agents and secretory stimulants. Int Ophthalmol Clin 1980;20:163–169.

Flapless Intrascleral Knotting Technique for Suture Fixation of Intraocular Implants

Purpose: We will describe a flapless/grooveless/pocketless and minimally invasive technique for scleral suture fixation of intraocular implants.

Methods: After introducing the suture into the eye, the two ends of the suture were left exterior to the globe, the free end and the end connected to a curved needle (the needle side). A back-and-forth intrascleral suture passage was performed with the aid of a curved needle. The suture was thus supported by adequate scleral tissue. The suture was fixated to the sclera by knotting it into the sclerotomy. The ends of the suture were finally anchored intrasclerally with the aid of a 30-gauge needle.

Results: The technique was used in 15 eyes of 15 patients. The mean postoperative follow-up period was 9.1 ± 4.6 months. Postoperatively, the intraoperative lenses of all the eyes remained well-positioned and stable. The postoperative visual acuities for all of the eyes were also improved. No suture erosion, suture loosening, hypotony, scleral atrophy, chronic inflammation, retinal tears, and/or detachments were observed within the follow-up period.

Conclusion: The present technique provides minimal surgical invasion for the scleral suture fixation of intraocular implants.

RETINA 43:1031–1034, 2023

Scleral suture fixation is an important surgical technique for the fixation of various intraocular implants, including posterior chamber intraocular lenses (IOLs), artificial iris prostheses, capsular tension rings or segments, capsular anchors, and dislocated in-the-bag or out-of-the bag IOLs.[1–9] In the most common scleral suture fixation techniques (knotting technique), the suture is secured by tying a knot on the scleral bed. The suture ends and knot are covered by the lamellar scleral tissue to prevent its exposure and late postoperative erosion.[1–5] The creation of large conjunctival openings and scleral flaps, grooves, or pockets are traumatic and time consuming, often resulting in scarring of conjunctiva and sclera and may, therefore, be disadvantageous to potential future surgical procedures. We present a technique that can anchor the fixation sutures and knots intrasclerally under small sutureless conjunctival incisions without the need to create scleral flaps/grooves/pockets.

From the *Department of Ophthalmology, Shanghai Tenth People's Hospital Affiliated to Shanghai Tongji University, School of Medicine, Shanghai, China; and †Department of Ophthalmology, Xinhua Hospital Affiliated to Shanghai Jiaotong University School of Medicine, Shanghai, China.

This study was partially supported by the Shanghai Municipal Health Commission (No. 2019SY031).

None of the authors has any conflicting interests to disclose.

H. Jin and Q. Zhang contributed equally to this research.

Supplemental digital content is available for this article. Direct URL citations appear in the printed text and are provided in the HTML and PDF versions of this article on the journal's Web site (www.retinajournal.com).

Reprint requests: Haiying Jin, MD, Department of Ophthalmology, Shanghai Tenth People's Hospital Affiliated to Shanghai Tongji University, School of Medicine, Yanchangzhong Road, No. 301, Shanghai 200072, China; e-mail: jin_haiying@yahoo.com

Surgical Technique

Surgeries were performed under retrobulbar anesthesia by one of the authors (H.J.). The supplemental video (see **Video, Supplement Digital Content 1**, http://links.lww.com/IAE/B271) and Figure 1 demonstrate the procedures. A twin-armed single 8-0 polypropylene suture (Prolene, Polypropylene Suture; Ethicon, Johnson & Johnson, New Brunswick, NJ) was cut at its middle. The suture was introduced into the eye from the fixation site through a suture-in-needle technique or by an intraocular looping technique advocated in our previous publication.[10,11] The two ends of the suture were left exterior to the eye; the end connected to a curved needle (the needle side) and a free side. The suture inside the eye

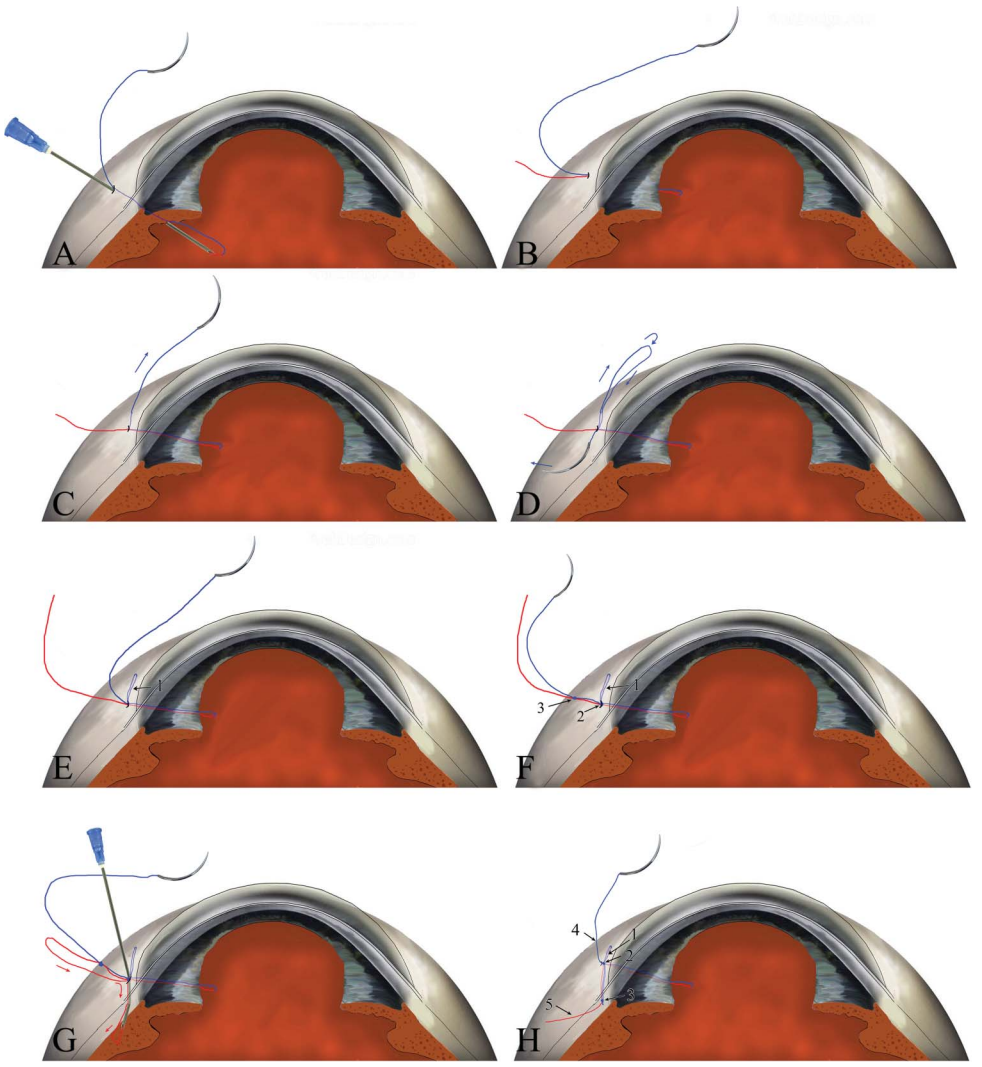

Fig. 1. Schematic figure of the intrascleral knotting technique for the fixation of intraocular implants. **A** and **B.** Introducing the suture into the globe through a suture in needle technique, leaving the free end (red) and the end connected to a curved needle (blue) exterior to the eye. **C.** Perform the intrascleral pass of the suture from the sclerotomy to the adjacent sclera with the aid of a connected curved needle. **D.** Perform the back intrascleral pass to externalize the suture from the sclerotomy. **E.** The suture is supported by the scleral tissue within the back-and-forth passages of the suture (1). **F.** Fixate the suture by knotting the two ends of the suture into the sclerotomy (2). Create another knot approximately 2 mm to 3 mm from the first fixation knot (3). **G.** Perform the intrascleral pass of the free end of the suture from the sclerotomy to the adjacent sclera with the end of a 30-gauge needle. After further pulling the externalized end of the suture, the anchor knot and the two ends of the suture are anchored into the needle track. **H.** After cutting the two exterior ends (4 and 5) of the suture flush to the sclera, all parts of the suture are anchored into the sclera.

was fixated to the implants. For open loop IOLs, a cow hitch technique was used to fixate the suture to the IOL haptics.[12] For dislocated closed loop IOLs or dislocated IOL-capsular bag complexes, the suture was fixated to the IOL haptics through an intraocular looping technique[10] (Case 1 in the see **Video, Supplement Digital Content 1**, http://links.lww.com/IAE/B271). For completely dislocated IOL/IOL-capsular bag complexes, a 25-gauge pars plana vitrectomy was performed to retrieve the IOL. Two of the pars plana sclerotomies were placed 180° apart about 1.5 mm posterior to the limbus. The two sclerotomies were designed as the fixation sites (Case 2 in the **Supplement Digital Content 1** [see **Video**, http://links.lww.com/IAE/B271]). After externalizing the two ends of the suture, the needle side of the external suture was held by a needle holder and was started with an intrascleral pass from the sclerotomy to the adjacent transscleral penetration site, parallel to the limbus. The needle was pulled out transconjunctivally. The needle was then started with an intrascleral pass in an opposite direction and was externalized from the starting sclerotomy of the fixation site. The suture was thus supported by adequate scleral tissue within the back-and-forth suture passages. The same manipulations were performed for the opposite side. After adjusting the suture tensions on both sides for the position of the intraocular implant, the two ends of the suture were separately tied for definitive knotting fixation (the fixation knot) into the sclerotomy. Another overhand knot (anchor knot) was created approximately 2 mm to 3 mm from the first fixation knot. A 30-gauge needle was bent for appropriate curvature. The free end of the suture was then inserted into the lumen of the 30-gauge needle from its tip. The needle was then started with an intrascleral pass from the sclerotomy to the adjacent sclera. When the tip of the 30-gauge needle externalized from the sclera, the end of the suture in the needle tip was pulled out and was then further pulled to lead the ends of the suture and

the anchor knot entering into the intrascleral tunnel. The external ends of the sutures were finally cut by scissors flush to the sclera. In cases where the length between the two knots was longer than the needle track, which could result in the anchor knot being pulled from the scleral tunnel, the anchor knot was cut off, leaving the two ends of the suture anchored intrasclerally (Case 2 in the **Supplement Digital Content 1** [see **Video**, http://links.lww.com/IAE/B271]). The small conjunctival incisions were left sutureless or were closed with one stich of 10-0 nylon suture. The technique can also be performed using a single-armed double polypropylene suture. After externalizing the needle, either end of the suture was cut off from the needle, resulting in the same situation as the needle side and a free end. The following procedures were identical as previously described.

Results

The technique was used in 15 eyes of 15 patients, including six cases of out-of-the bag IOL dislocations, five cases of dislocated IOL-capsular bag complexes and four cases of secondary IOL implantations. No complications were observed except for a transient mild ciliary hemorrhage in two eyes during needle penetration. In all of the patients, the IOLs were well-positioned after a mean follow-up time of 9.1 ± 4.6 months (range 3–18 months). The preoperative logarithm of the minimum angle of resolution visual acuity was 0.96 ± 0.16 (Snellen 20/183). The logarithm of the minimum angle of resolution visual acuity at the final follow-up was 0.32 ± 0.13 (Snellen 20/42). At final examination, there was no evidence of suture erosion, suture loosening, scleral atrophy, chronic inflammation, retinal tear, and/or detachment in any of these patients.

Discussion

Although various modifications of intrascleral haptic fixations for three-piece IOLs have been recently advocated, scleral suture fixation is still an important technique for the fixation of various intraocular implants. Besides in the fixation of a three-piece IOL, suture fixation has wide application in different types of IOLs, modified capsular tension rings/segments, capsular anchor and dislocated IOL-capsular bag complexes, etc. Most suturing techniques involve large conjunctival openings and scleral flaps/grooves/pockets to bury the knots and suture ends to prevent exposure, which are surgically traumatic. There are mainly three types of flapless technique for scleral suture fixations including Z-sutures, friction knot techniques, and modified overhand friction knot techniques.[10,13,14] All of these methods use friction to secure the fixation; however, each technique has its limitations. The Z-suture requires a wide conjunctival opening (3–4 mm) to expose the sclera and repeated zigzagging of the intrascleral suture in five turns. The friction knot technique stabilizes the suture by anchoring a lumpy knot in the needle track and does not require a wide conjunctival dissection. The sliding knot was created by a single thread. The tension of the fixation suture relies on the position of the knot on the suture and its position incarcerated in the sclera. Once the knot enters the scleral tunnel, it is difficult to adjust the position of the intrasclerally fixated knot, and the tension of the suture, because of the distinct frictional force. Therefore, it is difficult to adjust the position of the intraocular implants. The technique has been modified by us to an overhand friction knot technique.[10] Although the position of the knot on the suture can be well controlled by this modification, poor adjustability of the suture tensions remains a problem. To avoid these limitations, we advocate an intrascleral suture knotting fixation technique to anchor the knots and suture ends intrasclerally with minimal surgical invasion. The technique described in this study has several advantages. First, unlike the Z-suture technique and friction knot techniques, the fixation of the present technique is not secured by friction. Fixation is secured using definitive knotting as the widely used in knotting technique. Second, the suture is supported by adequate scleral tissue within the back-and-forth suture passage, which decreases the risk of scleral dehiscence and late dislocation often occurring in the conventional fixation technique. Third, the tension of the suture can be finely adjusted before fastening the fixation knot for good positioning of the intraocular implants. Fourth, the technique is less traumatic because of its minimal conjunctival openings and the avoidance of the creation of scleral flaps/pockets/grooves. Minimal conjunctival dissection is a particular strength of this method and is especially appropriate for patients with glaucoma and patients with severe scaring of the conjunctiva and sclera due to ocular trauma or previous surgeries. Moreover, the technique has a universal applicability for the suture fixation of a variety of implants, including different types of IOLs, IOL-capsular-bag complexes, and capsular tension rings/segments.

A limitation of this study is its small sample size. Nevertheless, our findings suggest that the present technique is an effective alternative, flapless method for the scleral suture fixation of intraocular implants. It provides both reliable suture stability and minimal surgical invasion. A study with a longer follow-up time and more cases is required to confirm the long-term stability of this method and compare it with other methods of fixation.

Key words: intrascleral knotting technique, suture fixation of intraocular implants, surgical technique.

*HAIYING JIN, MD**
QI ZHANG, MD†

References

1. Smiddy WE, Sawusch MR, O'Brien TP, et al. Implantation of scleral-fixated posterior chamber intraocular lenses. J Cataract Refract Surg 1990;16:691–696.
2. Lewis JS. Ab externo sulcus fixation. Ophthalmic Surg 1991; 22:692–695.
3. Lewis JS. Sulcus fixation without flaps. Ophthalmology 1993; 100:1346–1350.
4. Smiddy WE. Modification of scleral suture fixation technique for dislocated posterior chamber intraocular lens implants. Arch Ophthalmol 1998;116:967.
5. Hoffman RS, Fine IH, Packer M. Scleral fixation without conjunctival dissection. J Cataract Refract Surg 2006;32:1907–1912.
6. Gimbel HV, Condon GP, Kohnen T, et al. Late in-the-bag intraocular lens dislocation: incidence, prevention, and management. J Cataract Refract Surg 2005;31:2193–2204.
7. Gimbel HV, Brucks M, Dardzhikova AA, Camoriano GD. Scleral fixation of a subluxated intraocular lens-capsular bag complex through a fibrotic continuous curvilinear capsulorhexis. J Cataract Refract Surg 2011;37:629–632.
8. Spitzer MS, Yoeruek E, Leitritz MA, et al. A new technique for treating posttraumatic aniridia with aphakia: first results of haptic fixation of a foldable intraocular lens on a foldable and custom-tailored iris prosthesis. Arch Ophthalmol 2012; 130:771–775.
9. Li B, Wang Y, Malvankar-Mehta MS, Hutnik CM. Surgical indications, outcomes, and complications with the use of a modified capsular tension ring during cataract surgery. J Cataract Refract Surg 2016;42:1642–1648.
10. Zhang Q, Zhao P, Jin H. Intraocular suture looping and overhand friction knot: a flapless technique to refixate dislocated intraocular lenses. Retina 2019;39:S62–S67.
11. Peden M, Adams S, Huffman B, Kaushal S. Alternative technique for implantation of a scleral-fixated intraocular lens. J Cataract Refract Surg 2009;35:226–229.
12. Hanemoto T, Ideta H, Kawasaki T. Luxated intraocular lens fixation using intravitreal cow hitch (girth) knot. Ophthalmology 2002;109:1118–1122.
13. Szurman P, Petermeier K, Aisenbrey S, et al. Z-suture: a new knotless technique for transscleral suture fixation of intraocular implants. Br J Ophthalmol 2010;94:167–169.
14. Oskala P. Friction knot to fixate scleral sutures. J Cataract Refract Surg 2015;41:497–500.

Scan code to view VIDEO

Surgical Technique

Edited by George A. Williams

Flanged Sutureless Intrascleral Fixation of Dislocated Hard 1-Piece Polymethyl Methacrylate Intraocular Lenses

Purpose: To describe the vitreoretinal surgical technique and report the outcomes of our method of sutureless flanged intrascleral haptic fixation of dislocated 1-piece polymethyl methacrylate intraocular lenses with rigid haptics.

Methods: Ciliary sulcus–based scleral tunnels were created by placing valved 27-gauge (g) trocar cannulas limbus parallel with conjunctival displacement. After complete vitrectomy, the rigid haptics were then externalized using 27g forceps. Cautery was then used to form flanges at the haptic tips. The haptics were then pushed back into the mouths of the scleral tunnels.

Results: Flanged intrascleral fixation was successfully achieved in eight eyes of seven patients. The average age at the time of surgery was 75 ± 13.7 years, with a mean follow-up of 17.9 ± 16.3 months (range 3–42 months). Intraocular lens dislocation/subluxation was the most common indication for surgery. All patients fully recovered to their potential acuity by their third postoperative visit. The most significant complication was erosion of one haptic in one patient, which was successfully managed without requiring intraocular lens exchange. There were no complications of subsequent dislocation, endophthalmitis, retinal detachment, or uveitis–glaucoma–hyphema syndrome.

Conclusion: Flanged sutureless intrascleral fixation of dislocated 1-piece polymethyl methacrylate intraocular lenses with rigid haptics can be safely and successfully performed, avoiding the large wound creation accompanying intraocular lens exchange and the disadvantages of suture-based techniques.

RETINA 43:1035–1038, 2023

Dislocated intraocular lenses (IOLs) present a unique challenge with a variety of management options for the vitreoretinal surgeon, including the more recently described method of flanged sutureless intrascleral haptic fixation.[1,2] This technique has thus far been successfully described primarily with newer 3-piece IOLs.[1,2] If planning flanged sutureless intrascleral IOL fixation in cases where the dislocated IOL is a hard 1-piece polymethyl methacrylate (PMMA) IOL, creation of either a large sclerotomy or corneal wound to remove the IOL and implant a 3-piece IOL for haptic flanging has previously been necessary. Wound creation, especially larger wounds, carries intraoperative and postoperative risks of wound leak, anterior chamber collapse, suprachoroidal hemorrhage, iris prolapse, prolonged recovery, cystoid macular edema, and surgically induced astigmatism, among other potential complications.

One-piece PMMA lenses were the first IOLs implanted in human eyes. Although they are seldom implanted today because of their rigidity and the size of the wound required for implantation, there remains a significant cohort of elderly patients with 1-piece PMMA lenses. A subset of these experience late IOL dislocation. A reliable method of scleral fixation of these older lenses would be advantageous given their rigidity and the wound required for their exchange with a 3-piece IOL.

From the *Department of Ophthalmology and Vision Science, University of Arizona College of Medicine, Tucson, Arizona; and †Retina Associates Southwest, Tucson, Arizona.

None of the authors has any financial/conflicting interests to disclose.

Supplemental digital content is available for this article. Direct URL citations appear in the printed text and are provided in the HTML and PDF versions of this article on the journal's Web site (www.retinajournal.com).

Reprint requests: Mark T. Williams, MD, Department of Ophthalmology and Vision Science, University of Arizona, 655 N. Alvernon Way, Suite 204, Tucson, AZ 85711; e-mail: mtwilli588@gmail.com

We describe here the technique and results of 8 cases of flanged intrascleral fixation performed by the senior author (M.K.W.) between 2016 and 2019, using cautery to form a flange on the haptics in seven 1-piece PMMA lenses with rigid haptics and one older 3-piece silicone lens with clear rigid PMMA haptics.

Technique

The **Supplemental Digital Content 1** (see **Video 1**, http://links.lww.com/IAE/B279) demonstrates key steps of the procedure with emphasis on externalization and flanging of 1-piece PMMA IOL haptics. The initial steps of the technique are similar to what was described in 2017 as a modified flanged IOL fixation technique using trocar-cannulas[2] instead of Yamane and colleagues[1]' double needle haptic fixation. First, three 25 gauge (g) valved cannulas are placed in an oblique fashion so that the wounds are self-sealing 3 mm posterior to the limbus in the superotemporal, superonasal, and inferotemporal quadrants. The 12 and 6 o'clock positions are then marked 14 mm apart, generally resulting in a limbus-to-flange distance of approximately 1.5 mm. Longer distances may preclude proper externalization of the haptics. The ciliary sulcus–based scleral tunnels are then created while the globe is firm before attaching the infusion line by placing valved 27g trocar-cannulas limbus parallel at a ~20° angle after conjunctival displacement. The infusion line is then attached to the inferotemporal 25g valved cannula. A complete vitrectomy is then performed. The IOL is then elevated into the anterior vitreous with a soft tip cannula and aspiration, grasped with 25g broad-platform forceps (Grieshaber-MaxGrip; Alcon, Fort Worth, TX), and then using the vitreous cutter, it is cleaned of any capsular remnants using active cutting and aspiration. One haptic is then elevated into the iris plane, and the haptic tip is grasped with 27g broad platform forceps (MaxGrip; Alcon) placed through one of the 27g cannulas. While still grasping the haptic tip, the 27g cannula is slid up the shaft of the 27g forceps using 0.3 mm toothed forceps, and, then, the 27g forceps still grasping the haptic tip is gently externalized along with the haptic. The haptic tip is melted to form a flange, detailed further below. The second haptic is then externalized using the same method except that this is typically performed posteriorly using the binocular indirect ophthalmomicroscope (Oculus Surgical, Port St. Lucie, FL) and light pipe for easier visualization. One-piece IOL haptics that feature eyelets or notches may be more challenging to externalize. In one patient, externalizing a CZ70BD (Alcon) with eyelets near the haptic tips required small conjunctival incisions over the tunnels for better exposure for flanging (see **Video 2**, **Supplemental Digital Content 2**, http://links.lww.com/IAE/B280). Another lens featured a large notch midway through the inferior haptic. Difficulty pushing the haptic back into the inferior tunnel was overcome using a "pull-and-push" maneuver using forceps to push externally and a Kuglen hook to pull the IOL internally (see **Video 3, Supplemental Digital Content 3**, http://links.lww.com/IAE/B281).

To form the flanges, the haptic is elevated off the surface of the conjunctiva and the distal ~1 mm melted using a fine tip disposable cautery pen (Bovie High-Temperature Cautery Fine Tip, Purchase, NY). This step is performed several minutes after turning off supplemental oxygen to the patient's nasal cannula to minimize the risk of surgical field fire. The material of these 1-piece rigid clear PMMA haptics responds differently to cautery compared with the haptics of 3-piece IOLs (either flexible blue PMMA or flexible polyvinylidene fluoride). Most of these 1-piece PMMA lens haptics will not form bulbs, instead forming flat-edged flanges. The goal is to form a flange twice the diameter of the haptic with soft edges. Flanges that are larger than this can lead to erosion through the conjunctiva, whereas smaller flanges may lead to retraction of the haptic posteriorly into the tunnel. Rarely, the haptic may disintegrate in response to cautery, for which successful flanging requires lowering the heat of the cautery and touching the cautery tip to the haptic. In these cases, the haptic tip can then be angled posteriorly to create an angled flange to reduce the risk of exposure (see **Video 4, Supplemental Digital Content 4**, http://links.lww.com/IAE/B282). With the IOL fixed, gentle 360 scleral depression is performed, and acetylcholine chloride solution (Miochol-E; Novartis, East Hanover, NJ) is then often injected into the anterior chamber to constrict the pupil unless already small. A superior peripheral iridotomy is performed to reduce the risk of reverse pupillary block, and dilation postoperatively is typically avoided to reduce the risk of iris capture. If a sterile air bubble needs to be injected posteriorly to maintain intraocular pressure, then an air bubble is also placed in the anterior chamber to help balance the posterior air bubble's pressure on the IOL.

Results

Flanged intrascleral fixation was successfully achieved in eight eyes of seven patients. The mean age was 75 ± 13.7 years. Patient characteristics and outcomes are summarized in Table 1. Seven IOLs were 1-piece PMMA lenses with rigid haptics and

Table 1. Lists Baseline Characteristics, Intraoperative Features, Visual Outcomes, Complications, and Length of Follow-up of 8 Cases of Flanged Rigid PMMA IOL Fixation Performed by the First Author (M.K.W.)

Patient	Case	Age at Time of Surgery (yr)	Sex	Eye	Notable POHx	Indication	IOL Characteristics
1	1	76	M	OS	Attempted fixation with nonflanged SST prior with subsequent dislocation. Also history of repaired RD, ERM	Dislocation	1-piece PMMA, rigid haptics, Pharmacia 720
2	2	84	M	OS	Glaucoma suspect	Subluxation	1 piece PMMA, rigid haptics, unknown make.
3	3	46	M	OS	Trauma requiring PPV/ Lensectomy. Subsequent scleral sutured IOL dislocated because of breakage of sutures.	Subluxation, lens drops back when the patient lays supine	1 piece PMMA with eyelets on rigid haptics, CZ70BD (Alcon)
4	4	76	M	OS	Subluxed sulcus IOL leading to UGH	UGH	3-piece silicone optic and clear PMMA haptics. Pharmacia 913A
5	5	74		OD	ERM and glaucoma suspect	Dislocation	1 piece PMMA, rigid haptics, unknown make.
6	6	90	F	OD	Repaired RD and AMD	Subluxation	1 piece PMMA, rigid haptics, unknown make.
6	7	90	F	OS	Repaired RD and AMD	Subluxation	1 piece PMMA, rigid haptics, unknown make.
7	8	64	M	OS	ERM	Dislocation	1 piece PMMA, rigid haptics with prominent notch midway on inferior haptic, unknown make.

Patient	Pre-op BCVA	Post-op BCVA	Maximum Time to Full Visual Acuity Recovery	Intraoperative Characteristics	Complications	Follow up Time
1	20/200 − 1	20/30	6 weeks	Flat-edged flanges instead of bulbs.	None.	42 months
2	20/100	20/20	4 weeks	Haptics prone to disintegration. Flanges achieved by lowering the cautery and touching the haptic tips to angle them posteriorly.	Limited intra-op SCH and VH.	39 months
3	20/20 − 1 (supine VA: CF)	20/20	6 weeks	Eyelet haptics required conjunctival incisions to pull haptic sufficiently out of the tunnel to form flange.	None.	12 months
4	20/25 − 2	20/25 + 1 with resolution of UGH	3 weeks	Flat-edged flanges instead of bulbs.	None, no recurrence of UGH.	12 months
5	CF 5 ft	20/20	6 weeks	Flat-edged flanges instead of bulbs.	None.	9 months
6	20/60 − 2	20/40	8 weeks	Inferior flange was initially large and scalloped, required re-melting to form smaller flange.	None.	9 months
6	20/100	20/60 − 2	6 weeks	Flat-edged flanges instead of bulbs.	Erosion of superior haptic 2 weeks post-op, managed by re-melting of both tips to form smaller flanges, each covered with cadaveric sclera (Tutoplast).	7 months
7	20/150 − 1	20/40	4 weeks	Required "pull-and-push" maneuver to position inferior haptic back into the scleral tunnel.	None.	3 months

AMD, age-related macular degeneration; BCVA, best-corrected visual acuity; ERM, epiretinal membrane; OD, right eye; OS, left eye; POHx, past ocular history; RD, retinal detachment; SST, Sutureless scleral tunnel; SCH, suprachoroidal hemorrhage; UGH, uveitis–glaucoma–hyphema syndrome; VH, vitreous hemorrhage.

one an older 3-piece silicone IOL with clear rigid PMMA haptics. One lens was a CZ70BD with haptic eyelets near the tips and another an older 1-piece IOL with an inferior haptic notch. Indications for fixation were IOL dislocation or subluxation in 7 cases and uveitis–glaucoma–hyphema syndrome in one case. The mean follow-up time was 17.9 ± 16.3 months (range: 3–42 months). All patients fully recovered to their potential acuity by their third postoperative visit, which ranged from 3 to 8 weeks.

One patient 2 weeks postoperatively had erosion of the superior haptic. Both haptic tips were remelted to form smaller flanges that were also covered with 5 mm × 5 mm of cadaveric sclera (Tutoplast) to prevent any risk of future erosion, with no further issues at 7 months of follow-up.

Another patient developed a limited suprachoroidal hemorrhage intraoperatively felt to be unrelated to the nature of the IOL being fixated. This did not prevent successful fixation intraoperatively nor full recovery postoperatively.

No complications of subsequent dislocation, endophthalmitis, retinal detachment, or uveitis–glaucoma–hyphema syndrome have been encountered at the latest follow-up in any case.

Discussion

In 2017, Yamane et al[1] described flanged intrascleral fixation using 30g needles to create scleral tunnels and cautery to form bulbs at the haptic ends to achieve more secure haptic fixation compared with previous sutureless scleral tunnel techniques. In 2017, the senior author of this article described a modified version of Yamane et al's flanged intrascleral fixation using 27g trocar-cannulas for scleral tunnel formation and the binocular indirect ophthalmomicroscope for externalization.[2] This approach bypasses the technical challenges of threading the haptic through the needle lumen in the cramped anterior chamber space, instead using forceps to directly pull the haptic through the trocar-cannula created scleral tunnel with most work being performed in the iris plane or more posteriorly. This technique also allows for externalization and flanging of the haptics individually, avoiding the challenges of simultaneous externalization of both haptics. Subsequent data and a force disinsertion study of the 3-piece acrylic MA60AC (Alcon) IOL suggested favorable outcomes and a more secure fixation compared with previous unflanged sutureless scleral tunnel techniques.[3]

The successful application of 27g trocar-cannula based flanged fixation to rigid 1-piece PMMA IOLs is noteworthy given the inherently greater risks large wound creation poses, which is necessary if planning to exchange these rigid IOLs. In addition, flanged scleral fixation of 1-piece PMMA IOLs may be preferable to suture fixation of these IOLs because of well-described suture-failure leading to late dislocation.[4–7]

It is interesting to note that older clear rigid PMMA haptics react differently and less predictably to cautery despite that the haptic material of newer 3-piece IOLs often is also described as PMMA. The term PMMA itself refers to a broad category of acrylic polymers, and their differing behavior likely owe to additives or differences in the polymer chemical structure.

To date, the senior author has performed this technique in eight eyes with excellent outcomes, no instances of dislocation, and one instance of erosion successfully managed without requiring IOL exchange. In our experience, older rigid clear PMMA haptics tend to melt into a flat flanged configuration rather than a bulb. This does not seem to affect the stability of the fixation if the flange is of proper size.

Here, we have described flanged intrascleral fixation of 1-piece PMMA IOLs with rigid haptics with the advantage of avoiding the large wound creation accompanying IOL exchange or suture failure leading to IOL dislocation.

Key words: 1-piece PMMA intraocular lens, flanged intraocular lens fixation, intraocular lens, intraocular lens exchange, dislocation, haptic, sutureless intrascleral fixation, modified Yamane IOL fixation, one-piece rigid polymethyl methacrylate intraocular lens, scleral IOL fixation.

MARK K. WALSH, MD, PHD†*
*MARK T. WILLIAMS, MD**

References

1. Yamane S, Sato S, Maruyama-Inoue M, Kadonosono K. Flanged intrascleral intraocular lens fixation with double-needle technique. Ophthalmology 2017;124:1136–1142.
2. Walsh MK. Sutureless trocar-cannula-based transconjunctival flanged intrascleral intraocular lens fixation. Retina 2017;37:2191–2194.
3. Stem MS, Wa CA, Todorich B, et al. 27-Gauge sutureless intrascleral fixation of intraocular lenses with haptic flanging: short-term clinical outcomes and a disinsertion force study. Retina 2019;39:2149–2154.
4. Solomon K, Gussler JR, Gussler C, Van Meter WS. Incidence and management of complications of transsclerally sutured posterior chamber lenses. J Cataract Refract Surg 1993;19:488–493.
5. Price MO, Price FW Jr, Werner L, et al. Late dislocation of scleral-sutured posterior chamber intraocular lenses. J Cataract Refract Surg 2005;31:1320–1326.
6. Asadi R, Kheirkhah A. Long-term results of scleral fixation of posterior chamber intraocular lenses in children. Ophthalmology 2008;115:67–72.
7. Vote BJ, Tranos P, Bunce C, et al. Long-term outcome of combined pars plana vitrectomy and scleral fixated sutured posterior chamber intraocular lens implantation. Am J Ophthalmol 2006;141:308–312.

Scleral Suture Fixation of Dislocated Posterior Chamber Intraocular Lens: Modification for Tapered Haptics

Purpose: To present a surgical modification to a previously published technique that allows repositioning and scleral fixation of one-piece acrylic intraocular lenses with tapered haptics.

Methods: A retrospective review of three consecutive cases.

Results: Our technique modification enables repositioning using scleral suture fixation of one-piece intraocular lenses with tapered haptics by looping the haptic at its proximal, notched junction to the optic with the polypropylene suture. The suture knot is internalized which effectively suspends the intraocular lens and allows for better adjustment of the intraocular lens centration. Two cases were endocapsular dislocations; the third case was dislocated extracapsularly due through a posterior capsule rupture. All showed adequate lens centration at 3 months of follow-up. One case had suffered a vitreous hemorrhage a month postoperatively that is clearing.

Conclusion: Repositioning using scleral fixation of one-piece intraocular lenses with tapered haptics is possible with a minor technique modification. This offers an alternative to intraocular lens exchange.

RETINA 43:1039–1042, 2023

Intraocular lens (IOL) dislocation or subluxation is often managed surgically, especially when visually symptomatic.[1] Management approaches in the absence of residual capsular support include scleral suture fixation, intrascleral haptic (sutureless) fixation, and IOL exchange for an anterior or posterior chamber IOL (PCIOL) (using various techniques). One-piece PCIOLs are not amenable to intrascleral haptic fixation. Originally described for one-piece polymethylmethacrylate (PMMA) IOLs and, subsequently, for three-piece style IOLs with PMMA or polypropylene haptics,[2] scleral suture repositioning of one-piece acrylic PCIOL that include a haptic design that is thicker distal than it is proximal to the optic.[3] This technique has not been reported with one-piece acrylic IOLs with tapered haptics (e.g., Tecnis AMO ZCB00 aspheric or Symfony style), for fear that the scleral suture would slip off the tapered haptic end, resulting in redislocation; hence, scleral suture techniques have been avoided in favor of IOL exchange techniques. However, IOL exchange techniques may require more time, may result in more postoperative astigmatism, and, most importantly, loss of corneal endothelial cells sufficient to result in corneal decompensation. Moreover, IOL exchange is more complex if there has been previous glaucoma shunts or corneal surgery.

Many one-piece acrylic IOL haptic designs include a notch in the proximal portion of the haptic where it junctures the optic. This notch is suitable for securely looping with a scleral suture (Figure 1). This paper describes our preliminary results with eyes with this sort of PCIOL design repositioned with scleral suture fixation modified to use this haptic design.

From the Department of Ophthalmology, Bascom Palmer Eye Institute, University of Miami Miller School of Medicine, Miami, Florida.

None of the authors has any financial/conflicting interests to disclose.

Supplemental digital content is available for this article. Direct URL citations appear in the printed text and are provided in the HTML and PDF versions of this article on the journal's Web site (www.retinajournal.com).

Reprint requests: William E. Smiddy, MD, Ophthalmology, Bascom Palmer Eye Institute, University of Miami, Miller School of Medicine, 900 NW 17th Street, Miami, FL 33136; e-mail: wsmiddy@med.miami.edu

Surgical Technique

The technique is similar to previous reports.[2,3] Focal conjunctival peritomies are created in preparation of triangular, limbal-based, partial thickness scleral flaps located 180° apart, most conveniently at the 1:30 and

Fig. 1. Representation of a Tecnis-style one-piece acrylic intraocular lens with tapered haptic ends.[4] Note the proximal notched ends on the haptic, where a suture slip knot can be secured for adequate lens suspension.

7:30 meridians. A 23-gauge vitrectomy is performed. The PCIOL is grasped using 23-gauge forceps. A 27 g needle, preloaded with a 9-0 polypropylene suture, is introduced through the base of (first) the more inferior scleral flap bed 1 mm to 3 mm posterior to the limbus. The polypropylene suture loop is advanced toward the proximal end of the haptic, closer to the optic than the usual apogee of the haptic, where a notched contour is found. After pulling the sutures snug, to pull the haptic to the internal eye wall, a square knot is fashioned, leaving the ends untrimmed. Internally, the PCIOL is carefully grasped near the junction of the optic and haptic with intraocular forceps from the opposite side of the eye, to internalize the knot through the needle track. Then, superior (second) haptic is lassoed, tied, and internalized in a similar fashion with assistance of the intraocular forceps. With both haptic suture knots internalized, the polypropylene needle ends are passed along the partial scleral thickness in the base of the scleral flaps and secured initially with the beginning throw of a square knot. The tension on the scleral fixation sutures are adjusted to optimize centration of the optic (without causing torsion by overtightening) in the process of tying the final suture throw. The suture ends are purposely left long (about 4–5 mm), allowing the ends to lay flat on the sclera (mostly under the flap) to minimize suture extrusion through the flap and conjunctiva. The conjunctival incisions are closed using 6-0 plain gut, pulling the conjunctiva snug enough to hold the scleral flaps in place (no sutures are used on the scleral flaps).

Case Series

Case 1

A 60-year-old man had an endocapsular dislocation of an acrylic one-piece IOL, OS, with tapered haptics. Previously, a one-piece acrylic PCIOL designed with a bulb in the distal haptic had been repositioned, right eye, using scleral suture fixation as previously described.[3] Severe glare, left eye, caused difficulty with night driving. Preoperative Snellen best-corrected visual acuity (BCVA) was 20/30 and intraocular pressure (IOP) was 14 mmHg. He underwent repositioning and scleral fixation via the modified loop technique as described above. Postoperative BCVA at 1 month was 20/25. At 3 months, he had developed a vitreous hemorrhage with corresponding BCVA of 20/400 and IOP of 8 mmHg. His IOL remained well-positioned and the scleral flaps were well-apposed (Table 1).

Case 2

A 64-year-old man with a posterior extracapsular dislocation of a one-piece (Tecnis multifocal IOL), left eye, with posterior capsular rupture had BCVA of 20/60 and IOP of 22 mmHg. He underwent repositioning using the above described technique; an epiretinal

Table 1. Clinical Characteristics of Three Cases of Scleral Suture Fixation of Dislocation of One-Piece Acrylic PC IOL With Tapered Haptics and Postoperative Findings

		Preoperative Visit		One-Month Postop Visit		Three-Month Postop Visit	
	Age, Gender	BCVA, IOP	Type of Dislocation	BCVA, IOP	Clinical Findings*	BCVA, IOP	Clinical Findings*
Case 1	60, male	20/30, 14	Endocapsular	20/25, 22	Cells 1+	20/300, 8	VH
Case 2	64, male	20/60, 22	Extracapsular	20/60, 20	Quiet	20/60, 20	Quiet
Case 3	73, female	20/30, 14	Endocapsular	20/60, 14	Cells 1+	20/30, 14	Quiet

*The IOL was centered postoperatively in all cases.
VH, vitreous hemorrhage.

membrane was removed as well. At both his 1-month and 3-month visits, his BCVA remained at 20/60 with a recurrent epiretinal membrane. He had inferior chorioretinal scarring from a regressed choroidal melanocytic tumor. The IOL was centered and well-positioned (Figure 2).

Case 3

A 73-year-old woman presented with inferior endocapsular subluxation of a one-piece acrylic IOL, left eye. Her BCVA was 20/30 and IOP was 14 mmHg. The IOL was centered and well-positioned with BCVA of 20/30 and IOP of 14 one month after scleral suture repositioning using the described technique. This case is illustrated in Figure 3 and a **Video**, **Supplemental Digital Content 1**, http://links.lww.com/IAE/B283.

Discussion

This study reports a modification of a previously reported scleral suture fixation technique for one-piece acrylic PCIOLs[3] that extends its application for use with one-piece acrylic PCIOLs with tapered haptics that hitherto have not been considered amenable to repositioning, and hence required exchange. The key steps involve securing the haptic knot on the proximal, notched end and internalizing the suture which also allows better control in adjusting the suture tension to facilitate optimal centration. This technique offers an alternative to IOL exchange which may increase the risks of severe intraocular hemorrhage, hypotony, corneal endothelial cell loss, and astigmatic changes related to the need for larger or reopened corneal or scleral wounds. Moreover, IOL repositioning may be safer for eyes with concomitant problems, such as glaucoma drainage implants, corneal transplants, corneal edema, or high anterior synechia.

We (and others) have previously reported the applicability of scleral suture fixation techniques for rescuing posteriorly dislocated one-piece acrylic lenses in the absence of capsular support.[3] However, when the design does not include bulbous distal haptic ends to provide a restriction to prevent the suture square knots from slipping off, IOL exchange was the only option. However, an increasingly commonly encountered IOL type (Tecnis-style one-piece acrylic IOLs) lack any distal bulbous ends, but using this technique modification can be rescued for repositioning.

This technique modification seems to have yielded satisfactory anatomic and visual outcomes in the short-term of follow-up that our experience has afforded. As a separate modification, we have inserted the scleral suture slightly more posteriorly, 3 mm from the limbus, where we think it avoids iris rub and induces less refractive change because it approximates the optical location of (originally intended) capsular bag fixation. Although long-term follow-up is warranted, there were no adverse events the initial 3-months postoperatively relatable to this technique modification (although one case had a self-limited vitreous hemorrhage postoperatively).

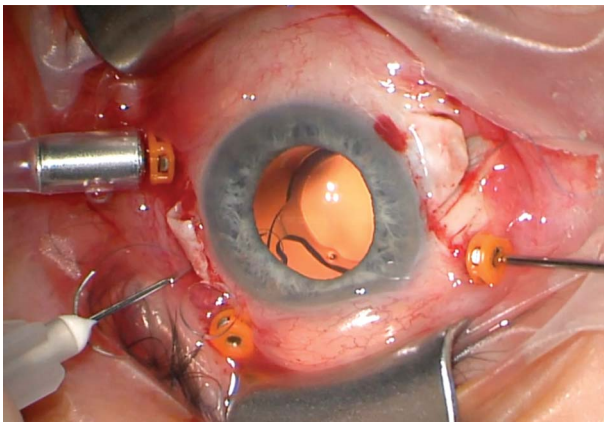

Fig. 2. Postoperative appearance of Case 2, demonstrating centration of the scleral sutured PC IOL 3 months following surgery. The iris pigment attenuation was present before the IOL repositioning surgery.

Conclusion

A modification of an existing scleral suture fixation IOL repositioning technique allow its applicability to one-piece acrylic IOLs lacking the terminal bulbous

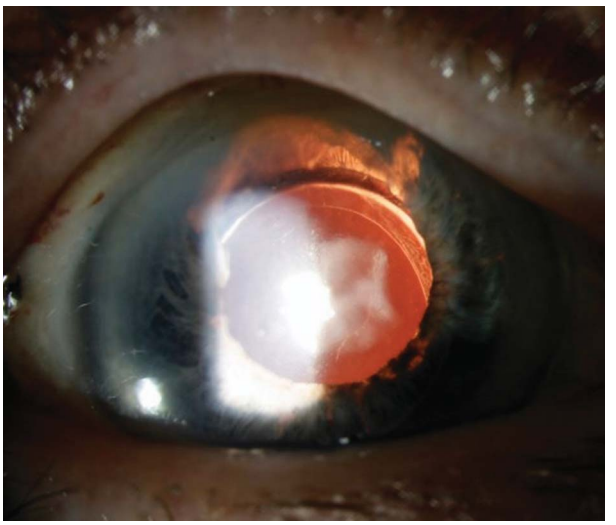

Fig. 3. The polypropylene suture loop is advanced toward the proximal end of the haptic, closer to the optic, where a notched contour is found (Case 3, same as the **Video**, **Supplemental Digital Content 1**, http://links.lww.com/IAE/B283).

haptic end and provides greater control in adjusting IOL position. This procedure offers an alternative to PCIOL exchange.

Key words: intraocular lens dislocation, intraocular lens repositioning, intraocular lens scleral fixation, one-piece acrylic intraocular lens, pars plana vitrectomy.

JOSE J. ECHEGARAY, MD
WILLIAM E. SMIDDY, MD

References

1. Kumar DA, Agarwal A, Jacob S, Agarwal A. Glued trans-scleral intraocular lens exchange for anterior chamber lenses in complicated eyes: analysis of indications and results. Am J Ophthalmol 2013;156:1125–1133 e1122.
2. Kim SS, Smiddy WE, Feuer W, Shi W. Management of dislocated intraocular lenses. Ophthalmology 2008;115:1699–1704.
3. Leung EH, Mohsenin A, Smiddy WE. Scleral suture fixation technique for one-piece acrylic intraocular lens. Retin Cases Brief Rep 2018;12:251–253.
4. Available at: https://www.ophthalmologyweb.com/Featured-Articles/20028-The-Tecnis-1-Piece-Aspheric-IOL/. Accessed July 23, 2020.

Diagnostic and Therapeutic Challenges

Edited by Anita Agarwal

Drs. Apoorva Ayachit, Shrinivas Joshi, Guruprasad Ayachit, and David Sarraf

This case was submitted by Department of Vitreoretina, M M Joshi Eye Institute, Hubballi; commented by Dr. David Sarraf (Los Angeles, California).

Case Report

A 69-year-old gentleman presented with diminished vision in the left eye (LE) for 1 month. He had undergone uneventful cataract surgery with posterior chamber intraocular lens placement in LE 6 weeks prior. There were no systemic complaints, known systemic illnesses, or use of medication.

The best-corrected visual acuity was 6/18, N 18 in LE, and 6/6, N6 in the right eye. The right eye was phakic, and posterior segment was within normal limits (Figure 1A). Left eye fundus examination showed closely arranged yellowish brown pigments straddling the superior arcade that traced downward in a track to straddle the inferior arcade. The pigments

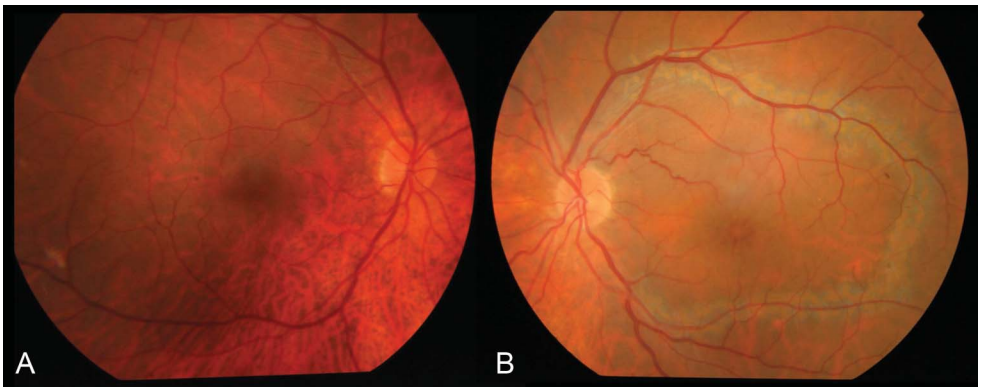

Fig. 1. A. Right eye fundus showing tessellation. **B.** Left eye fundus showing the track of yellowish brown pigmentation with concavity toward disk.

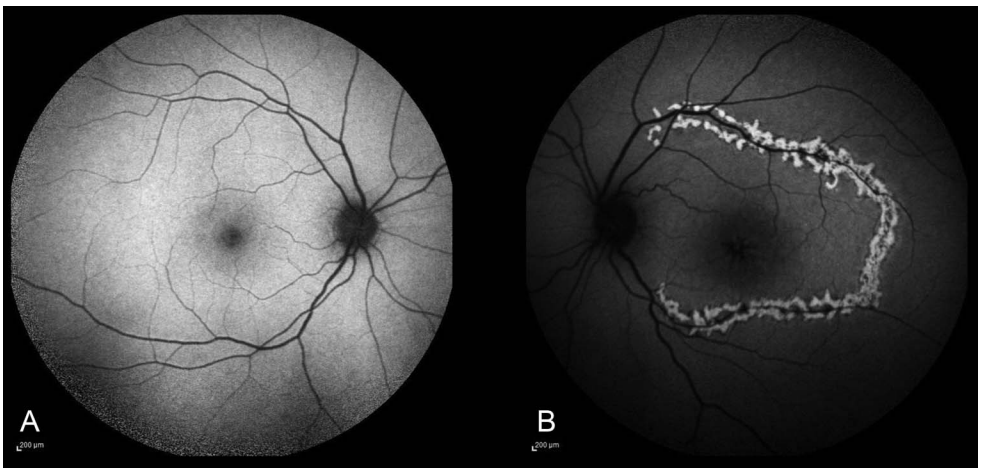

Fig. 2. A. Normal autofluorescence in the right eye. **B.** Left eye showing a speckled pattern in the track with predominantly hyper-AF patches.

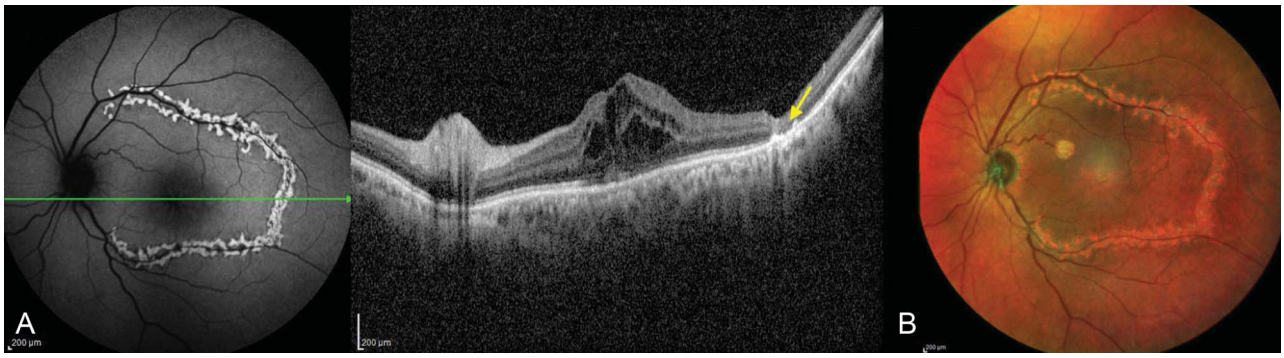

Fig. 3. A. Optical coherence tomography of RE showed cystoid macular edema and RPE clumps at outer retina with outer retinal thinning at the area of pigment (white arrow). **B.** Multicolor image showing reddish brown pigmentation of the track. RE, right eye.

were arranged in a crescentic (necklace) pattern with concavity toward the disk. Cystoid macular edema was present (Figure 1B).

Fundus autofluorescence (AF) of the right eye was normal. LE AF showed a speckled pattern with hyper-AF patches straddling the superior and inferior arcades (Figure 2B). A horizontal line scan on optical coherence tomography showed hyperreflective retinal pigment epithelium (RPE) clumps at the outer retina corresponding to pigment along with outer retinal thinning (Figure 3A). Multicolor image of LE showed brownish red pigments (Figure 3B).

The patient received a posterior segment subtenon triamcinolone acetonide for presumed pseudophakic cystoid macular edema. The edema resolved in four weeks with restoration of the ellipsoid zone (Figure 4).

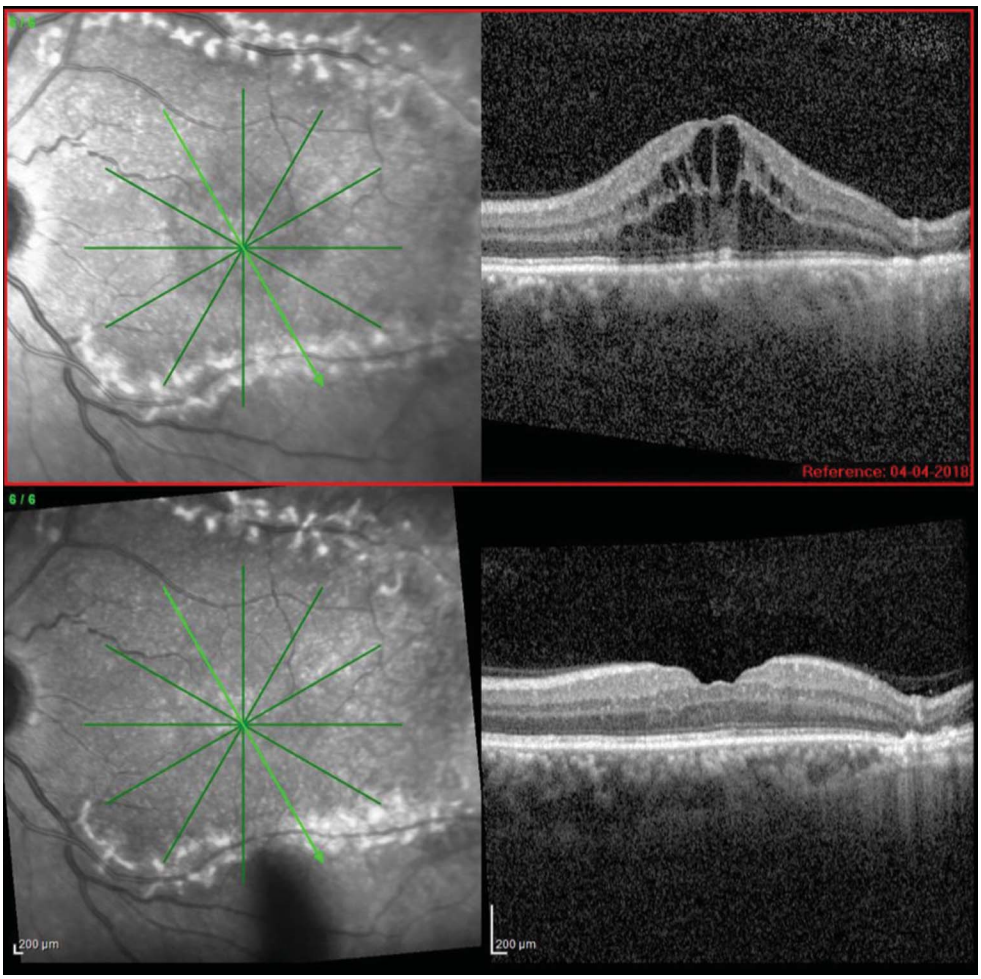

Fig. 4. Resolution of the cystoid macular edema at 1 month after PST- TA.

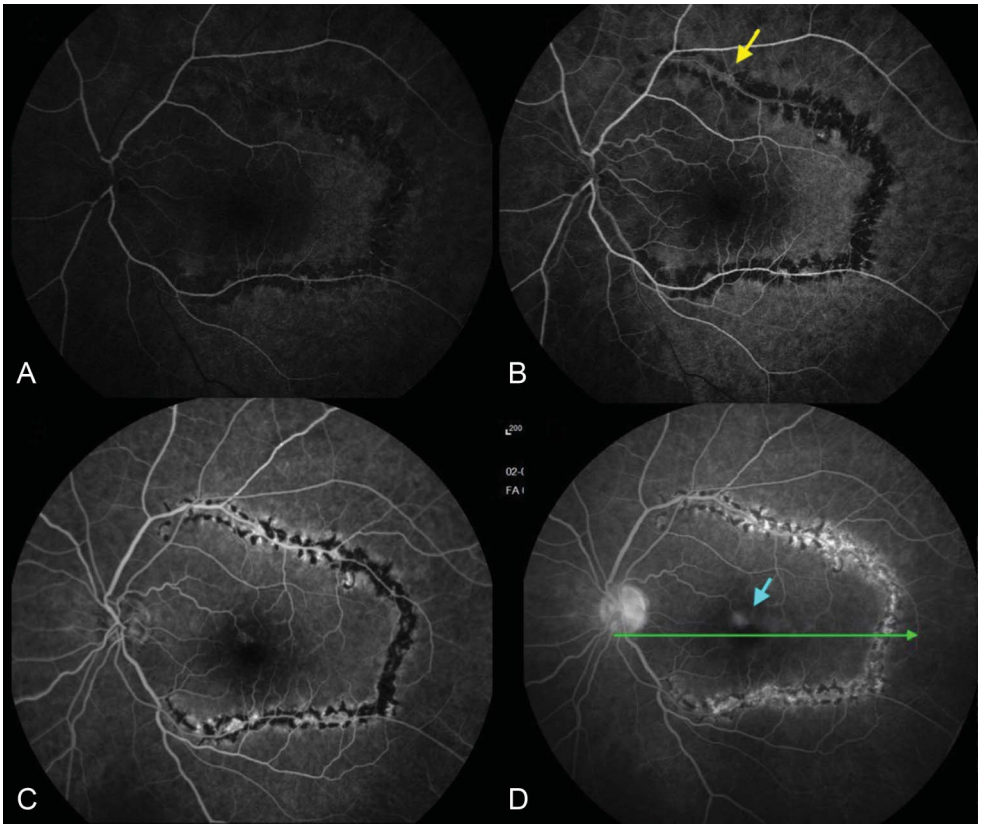

Fig. 5. A. Arterial phase of angiogram showing blocked fluorescence corresponding to the track. **B.** Few hyperfluorescent patches beginning in the superior arcade pigments (yellow arrow). **C.** More hyperfluorescent patches in the arterio-venous phase. **D.** Hyperfluorescence in the superior and temporal parafovea (cyan arrow) and disk hyperfluorescence in addition to increased hyperfluorescence of the track.

At one-month follow-up, fluorescein angiography was performed for further characterization of the crescentic track of pigments. Arterial phase of angiography showed blocked fluorescence (Figure 5A). Mid arterio-venous phase showed few hyperfluorescent areas along the superior arcade (Figure 5B). Late arterio-venous phase showed more hyperfluorescent staining of the patches (Figure 5C)). At 10 minutes, there was hyperfluorescence in the superior and temporal parafovea with disk hyperfluorescence in addition to increased hyperfluorescence of the track (Figure 5D). Systemic workup showed no medical illnesses or evidence of malignancy. This case has been presented for discussion of the possible diagnosis and management.

Dr. David Sarraf (Los Angeles, California): ——

Ayachit et al described a very interesting case of a 69-year-old male patient from India who presented with a 1-month history of vision loss (20/60) in the pseudophakic LE.

Retinal examination in the right eye was entirely within normal limits. However, retinal examination in the LE showed a very remarkable pattern of contiguous whitish lesions, at the level of the retinal pigment epithelium (RPE), forming a circle around the posterior pole.

Multimodal retinal imaging in the left eye showed that the lesions were hyperautofluorescent with FA and corresponded to RPE disruption and outer retinal atrophy with optical coherence tomography. Fluorescein angiography illustrated early hypofluorescence with late staining of the lesions in the left eye.

The diagnosis of this case is challenging, especially because this necklace pattern of RPE alterations is very rare and peculiar. However, the fluorescein angiography highlights an important finding in the LE. The early hypofluorescence with late staining is typical of placoid disease. The hypofluorescence may be the result of inner choroidal ischemia. Therefore, the diagnosis in this case could be serpiginous choroidopathy of the LE. Typically, lesions in serpiginous demonstrate a peripapillary distribution. Although the lesions in this case do not involve the margin of the optic disk, they do extend away from the nerve, albeit in a much wider and more unusual pattern.

Given the presumed Indian demographic of this patient and the endemic nature of tuberculosis in this country, it is important to obtain QuantiFERON Gold testing in this case to rule out tubercular serpiginoid choroiditis which is a treatable condition. Tubercular serpinous is typically associated with multifocal

peripheral lesions, as is illustrated in this case, and therefore, it is essential to determine whether this patient is TB positive so that anti-TB therapy can be promptly initiated.

If TB testing is negative, then an underlying inflammatory disorder causing the placoid lesions may be suspected. While acute posterior multifocal placoid pigment epitheliopathy is in the differential, the circular distribution of the lesions may be more suggestive of serpiginous, although the latter typically demonstrates a recurrent course with new lesions developing contiguous with the old lesions. The time course of placoid disease therefore can be critical to finalize the exact diagnosis and to determine whether immunosuppressive therapy is warranted.

Placoid diseases can be complicated by intraretinal and/or subretinal fluid. Treatment of the underlying inflammation can also address other complications such as macular edema and choroidal neovascularization, although anti-VEGF therapy may also be necessary.

Editor's Note:

Drs. Ayachit, Joshi, and Ayachit have presented a man with unilateral decreased vision and a bewildering appearance of hyperautofluorescent spots after the course of the vascular arcades. Dr. David Sarraf has taken on the impossible mission of discussing this case.

He focuses on the early hypofluorescent, but late staining pattern, of the necklace-like lesions, noting that this is typical of placoid disease. He believes that this finding may indicate inner choroidal ischemia, raising the possibility of serpiginous choroidopathy. Dr. Sarraf recommends QuantiFERON Gold testing to rule out tubercular serpiginous choroiditis.

He also includes acute posterior multifocal placoid pigment epitheliopathy as a possible cause for this necklace-like distribution of lesions.

We thank Drs. Ayachit, Joshi, and Ayachit for this case and Dr. David Sarraf for his discussion. I sent this case out to many, all of whom declined. I have no idea what this is, but someone out there has seen it, or will see it, and they will let us all know. That is how this works.

RETINA®, The Journal of Retinal and Vitreous Diseases, encourages readers to submit **Diagnostic and Therapeutic Challenges** to retina@retinajournal.com. Cases for the Diagnostic and Therapeutic Challenges section should include a detailed history of the patient, the diagnosis, the workup, the management, and finally, the question or questions that the submitter wishes to have answered by the consultants.

New Instruments

A 30 G "POSTERIOR CHAMBER MAINTAINER" FOR PREVENTION OF TRANSIENT HYPOTONY DURING SCLEROTOMY CLOSURE AT THE CONCLUSION OF 3-PORT PARS PLANA VITRECTOMY

Andrew W. Trippiedi, BS*†
Justin Gutman, MD†

*From the *Hackensack Meridian School of Medicine, Nutley, New Jersey †Retina Center of New Jersey, Bloomfield, New Jersey*

At the conclusion of a standard 23- or 25-gauge 3-port pars plana vitrectomy, it is not uncommon for one or more of the sclerotomy sites to leak. Previous studies by Lakhanpal et al,[1] have reported an incidence of 7.1% of small-gauge vitrectomies requiring at least one suture at a single sclerotomy site. The type of wound construction can impact the frequency of incompetent wounds. In addition, trocar size, primary vitrectomy versus a reoperation, high myopia, and the age of the patient can affect the rate of wound leaks encountered. Lin et al[2] observed that leaking wounds are not common, especially in primary vitrectomies, but they are encountered on occasion by every surgeon.

Removal of the infusion trocar cannula from an eye with a wound that does not self-seal, can result in the rapid development of hypotony. Previous reports by Khanduja et al[3] describe hypotony occurring in as many as 25% of the cases of sutureless vitrectomy. This is especially common in patients with a history of previous vitrectomy as described by Mimouni et al.[4]

Surgeons attempt to anticipate and mitigate the extent and duration of hypotony, especially if the surgeon encounters wound leaks from the two instrument trocars that may have required suture closure. When it is believed that the sclerotomy from the infusion trocar will also leak, a suture is simultaneously passed while the infusion trocar is removed. This allows for a rapid closure of the wound and helps the surgeon to place the suture more accurately through the sclerotomy site, because the trocar itself provides a guide for the needle track. When the wound does leak despite the above rapid suturing, the conjunctiva balloons up, making it difficult to see the underlying sclera and difficult to pass the stitch

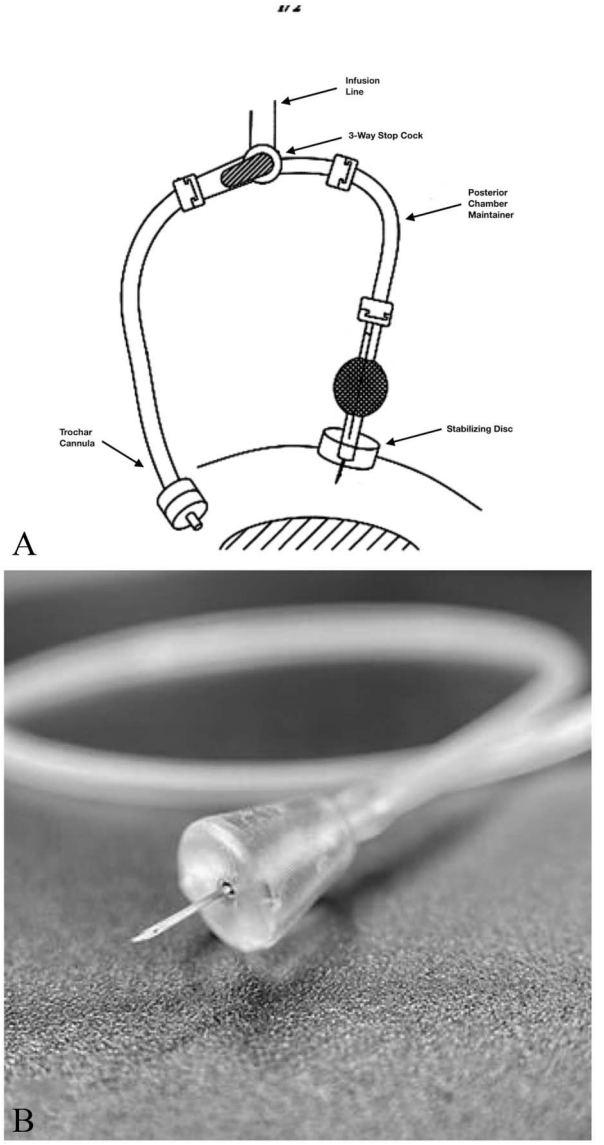

Fig. 1. A. The PC Maintainer is attached to a 3-way stopcock that diverts flow from the 25- gauge infusion trocar. **B.** A closeup of the device showing the stabilizing base from which a 30-gauge needle protrudes.

Justin Gutman, MD holds the patent for the posterior chamber maintainer. None of the other authors have any proprietary interests or conflicts of interest related to this submission.

Supplemental digital content is available for this article. Direct URL citations appear in the printed text and are provided in the HTML and PDF versions of this article on the journal's Web site (www.retinajournal.com).

This submission has not previously submitted and is not being considered for publication in any other journal.

Reprint requests: Justin Gutman, MD, Retina Center of New Jersey, 1255 Broad Street, #104 Bloomfield, NJ 07003; e-mail: justingutman@gmail.com

accurately. Inaccurate needle passes prolong and exacerbate the degree of hypotony. Even in the best scenarios when the stitch is passed perfectly and tied quickly, an unsafe degree of hypotony can still be unavoidable.

When the surgeon determines that the globe is too soft, the remedy is to use a 30-g needle on a syringe filled with BSS or sterile air or gas, and to introduce the needle into the vitreous chamber through the pars plana to reinflate the eye to the appropriate pressure. A 30-g needle puncture is known to reliably self-seal. During those moments before the eye is repressurized, the eye is at risk for rebleeding from vessels that had been ligated during surgery, bleeding from the angle, decompression retinopathy, and choroidal hemorrhage. Mukkamala et al[5] reported that although cases of decompression retinopathy often have favorable outcomes, with visual acuity in as many as 85% of eyes returning to baseline, it may still lead to ocular morbidity.

The 'posterior chamber maintainer' (Vortex Surgical, Saint Charles, MO) seeks to solve these problems by maintaining the intraocular pressure after removal of the infusion trocar, even if that wound is found to be incompetent and leaking rapidly. Instead of reinflating the globe after the eye has lost pressure, this device is preplaced through the pars plana and can be left in place hands-free, providing infusion pressure to the eye as the leaking wound is addressed. This not only will prevent transient hypotony during the surgery, but also may allow for easier closure of the infusion trocar wound site, if necessary. The device has been named the 'posterior chamber maintainer,' but it should be noted that anatomically, the device is placed in the vitreous chamber.

Design of 'Posterior Chamber Maintainer' and Surgical Utility

The 'posterior chamber maintainer' consists of a 30-gauge needle measuring 4 mm in length. The needle is attached to a length of tubing. The tubing has an adapter to hook up to the infusion line via the 3-way stopcock. Most critical to the design is a "stabilizing disk," which helps to keep the needle perpendicular to the eye wall, preventing any tilt or torque of the needle that could threaten the phakic lens or retina. Figure 1.

Before the infusion trocar is removed, the PC maintainer needle is inserted into the vitreous chamber in the inferonasal quadrant of the sclera, 3.5 mm posterior to the limbus. Figure 2A. The tubing is then taped to the drape over the patient's nose. It is then left in place, hands-free as the stabilizing disk prevents movement. The flow of fluid or air is then diverted

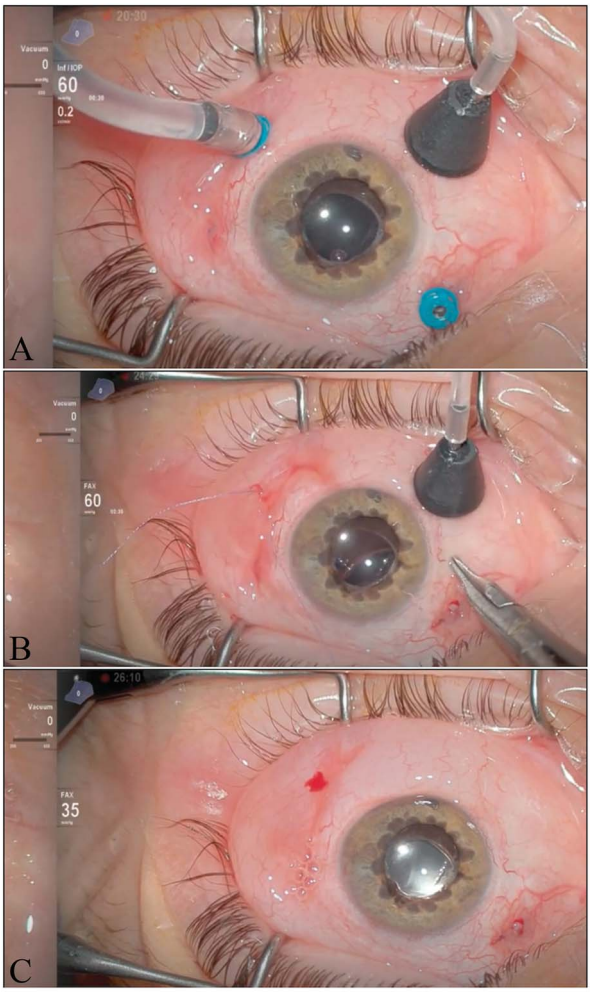

Fig. 2. A. Here is a picture of the device after being inserted, before removal of trocars. **B.** The PC Maintainer assures that there is no transient hypotony after removal of the infusion trocar. **C.** The PC Maintainer uses a 30-gauge needle, which self-seals after removal.

by turning the 3-way stop cock, forcing flow through the PC Maintainer needle. The infusion trocar is then removed and sutured if necessary. Figure 2B. Any fluid that leaks from the wound is compensated for by the flow through the PC maintainer and IOP is never compromised. Once the surgeon is satisfied with the wound closure, the 30-g PC maintainer needle is removed, leaving a self-sealing wound at the conclusion of the case. Figure 2C. See supplemental video for further information (http://links.lww.com/IAE/B965).

Pilot Experiences

We conducted a retrospective review of 50 consecutive total cases. All 50 cases were repeat pars-plana vitrectomies. This study adhered to the guidelines of the Declaration of Helsinki. We contacted WCG IRB

Table 1. Results From Cases With and Without PC Maintainer

	With Posterior Chamber Maintainer	Without Posterior Chamber Maintainer
Transient intraoperative hypotony	0/18	15/17
Cases of intraocular hemorrhage on post-op day 1, endophthalmitis, suprachoroidal hemorrhage or effusion, or postoperative rapid progression of cataract	0	0

and received their approval for a retrospective chart analysis. We compared two separate arms in the study. One arm included 25 cases of repeat vitrectomy, without the 30-g PC maintainer available for use, because they were conducted at the hospital ASC where a consignment for this device has not yet been obtained. The second arm included 25 cases of repeat vitrectomy performed at a private ASC where the 30-g PC Maintainer device was available for use, and is routinely used on every case performed there, including the 25 cases highlighted in this study. Cases of primary vitrectomy, and vitrectomy for retinal detachment when a gas or oil tamponade would be necessary were excluded. All 50 cases used 25-gauge trocars. The intraocular pressure from the infusion source was kept at 35 mmHg when all trocars were removed in both arms. In the PC Maintainer arm, there were 16 cases of silicone oil removal, 6 cases of reoperation for nonclearing vitreous hemorrhage from PDR, 1 reoperation for nonclosure of macular hole, and 2 reoperations to place a secondary IOL for aphakia. The arm with no PC Maintainer included 13 cases of silicone oil removal, 7 reoperations for nonclearing vitreous hemorrhage from PDR, 2 reoperations for recurrent epiretinal membrane, and 3 reoperations to place a secondary IOL for aphakia. As the primary data point, we looked at the incidence of transient hypotony that required the eye to be reinflated after the removal of the infusion trocar. Hypotony was diagnosed by the surgeon intraoperatively by digital palpation. Transient hypotony was recorded if the surgeon determined it was necessary to reinflate the eye, and this reinflation was mentioned in the operative report. We also looked at safety data including the incidence of postoperative intraocular hemorrhage, suprachoroidal effusion or hemorrhage, rapid postoperative progression of cataract, or endophthalmitis. The results of the trial revealed that the rate of leak from the infusion trocar wound was 72% (18/25) in the arm that used the PC Maintainer and 68% (17/25) in the arm where no PC Maintainer was available. In the arm that used the PC Maintainer, 0% (0/18) of the eyes required reinflation, because hypotony was never encountered. In the arm where the PC Maintainer was not available, 88% (15/17) of the cases required the globe to be reinflated because of an unsafe degree of hypotony encountered Table 1.

Conclusion

The 'Posterior Chamber Maintainer' was found in this pilot experience to be safe and effective. It allows for maintenance of intraocular pressure at the conclusion of pars-plana vitrectomy, reliably preventing transient hypotony in these cases. With less hypotony encountered, the chance for ocular morbidity may be reduced, although in this trial, superiority of surgical outcome with our device compared with the standard of care was not demonstrated. Further experience will be needed to determine whether the PC maintainer improves patient safety.

Key words: pars plana vitrectomy, posterior chamber, 3-port pars plana vitrectomy.

References

1. Lakhanpal RR, Humayun MS, de Juan E Jr, et al. Outcomes of 140 consecutive cases of 25-gauge transconjunctival surgery for posterior segment disease. Ophthalmology 2005;112:817–824.
2. Lin AL, Ghate DA, Robertson ZM, et al. Factors affecting wound leakage in 23-gauge sutureless pars plana vitrectomy. Retina 2011;31:1101–1108.
3. Khanduja S, Kakkar A, Majumdar S, et al. Small gauge vitrectomy: recent update. Oman J Ophthalmol 2013;6:3–11. doi.
4. Mimouni M, Abualhasan H, Derman L, et al. Incidence and risk factors for hypotony after 25-GAUGE pars plana vitrectomy with nonexpansile endotamponade. Retina 2020;40:41–46.
5. Mukkamala SK, Patel A, Dorairaj S, et al. Ocular decompression retinopathy: a review. Surv Ophthalmol 2013;58:505–512.

An Unusual Optical Coherence Tomography Appearance in Coats Disease

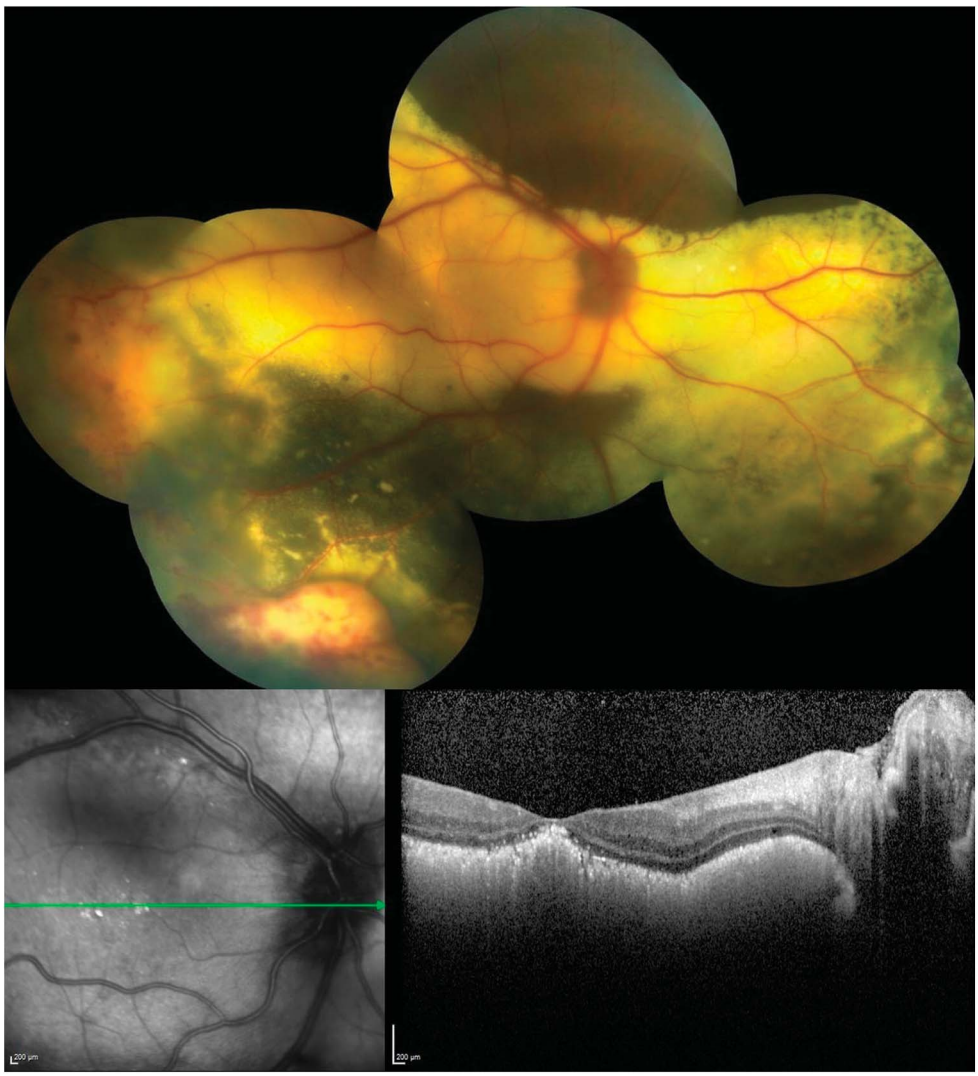

Fig. 1. Colored fundus image of the right eye shows inferior exudative retinal detachment, peripheral retinal telangiectasia, and aneurysms in addition to extensive subretinal lipid deposition (top). Optical coherence tomography B-scan through the fovea of the right eye demonstrates massive subretinal lipid accumulation in the absence of overlying intraretinal fluid (bottom).

In contrast to the traditional en face techniques of fundus imaging including fundus photography and dye angiography, the current optical coherence tomography (OCT) devices enable in vivo visualization of depth-resolved retinal structure resembling that seen histologically with light microscopy.[1] Coats disease is a retinal disorder seen primarily in young male patients presenting with unilateral intraretinal and subretinal exudation originating from telangiectatic and aneurysmal retinal vessels. Herein, the authors present a case of Coats disease with an unusual pattern of lipid deposition revealed with OCT.

A 13-year-old adolescent boy with Coats disease presented with an inferior exudative retinal detachment, peripheral retinal telangiectasia and aneurysms, and extensive subretinal lipid deposition in his right eye (Figure 1, top). Dilated fundus examination of the left

eye was unremarkable. An OCT B-scan scan through the fovea of the right eye showed the unusual finding of massive subretinal lipid accumulation in the absence of overlying intraretinal fluid (Figure 1, bottom).

Histopathological examinations of eyes with Coats disease have revealed retinal thickening because of homogeneous acellular material, typical of lipoproteinaceous exudation. Lipid- and hemosiderin-laden macrophages and cholesterol clefts are present in both the retina and the subretinal fluid.[2]

The authors hypothesize that because of the predominantly peripheral nature of the vascular changes in this patient, the exudation mostly entered the subretinal space. Preserved integrity of tight junctions within the central outer limiting membrane may have provided resistance to the intraretinal accumulation of macular fluid and lipid.[3]

Key words: coats disease, exudation, optical coherence tomography.

*KEMAL TEKIN, MD**
K. BAILEY FREUND, MD†‡
*MEHMET YASIN TEKE, MD**

Acknowledgments

The authors thank for the work supported by The Macula Foundation, Inc., New York, NY.

References

1. Gabriele ML, Wollstein G, Ishikawa H, et al. Optical coherence tomography: history, current status, and laboratory work. Invest Ophthalmol Vis Sci 2011;52:2425–2436.
2. Chang MM, McLean IW, Merritt JC. Coats' disease: a study of 62 histologically confirmed cases. J Pediatr Ophthalmol Strabismus 1984;21:163–168.
3. Omri S, Omri B, Savoldelli M, et al. The outer limiting membrane (OLM) revisited: clinical implications. Clin Ophthalmol 2010;4:183–195.

RETINA® is now accepting manuscripts for consideration for publication in the Photo Essay section. For a manuscript to be considered for publication within this section, the significance of the manuscript should revolve around the photographs. The photographs should convey an important or unique clinical diagnosis, condition, or treatment. The photographs can be a combination of kodachromes, angiograms, histologic sections, or ancillary diagnostic studies (e.g., echograms, radiograms, CT or MRI studies, arteriograms), all of which are imperative in the evaluation, diagnosis, and/or treatment of the condition that is represented. Overall, the Photo Essay manuscript will be limited to 300 words, five photographs, and five references. All figures submitted in color will be published in color at the expense of the authors. Please refer to the Author Instructions for all other general requirements of manuscripts submitted to **RETINA®**.

From the *Ulucanlar Eye Training and Research Hospital, Ophthalmology Department, Ankara, Turkey; †Vitreous Retina Macula Consultants of New York, New York, New York; and ‡Department of Ophthalmology, NYU Grossman School of New York, New York, New York

K. B. Freund is a consultant for Heidelberg Engineering, Zeiss, Genentech, Bayer, Novartis, and Allergan. He receives research support from Genentech/Roche. The remaining authors have no financial disclosures.

The authors declare that there is no conflict of interest regarding the publication of this paper.

Informed consent was obtained from the patient included in the report.

Reprint requests: Kemal Tekin, MD, Kale Street, 59, 06240 Ankara, Turkey; e-mail: drkemaltekin@gmail.com